The bumpy ride to electrification: Knowledge and tools to accelerate the electrification of sub-Saharan Africa's paratransit industry

Christopher Hull

Oriel College

University of Oxford

A thesis submitted for the degree of

Doctor of Philosophy

Michaelmas 2024

Acknowledgements

This thesis is dedicated to my parents, Diana and Richard. You are my every day inspiration, and your love and support make everything in my life possible.

I would like to express heartfelt gratitude to my supervisor Professor Malcolm McCulloch for taking the leap of faith in a bright-eyed and bushy-tailed economics student from 5,000 miles away. Your vision and mentorship have been critical to shaping my thesis and personal development over the past three years, and it has been a privilege of a lifetime working with you.

Thank you to my co-supervisor Dr. Katie Collett. You kept me on track and provided me with invaluable advice and support. Without you I would have gotten nowhere, fast. And thank you for being patient in long meetings with me (even when I was hangry!).

I owe a deep debt of gratitude to Professor Thinus Booysen of Stellenbosch University, without whom most of the work in this thesis would have been impossible. I swear one day I will get you the IPA you've been waiting for from the Fortnum & Mason in Heathrow Terminal 5.

Massive shoutout to my co-authors from the Media Lab at Stellenbosch University: Johan Giliomee and Jacques Wust. You guys made the journey especially fun, and never fail to inspire me with your elite talents and work ethic. You're all going places and I can't wait to see what you do.

Thank you to the whole Energy and Power Group at Oxford for providing a lighthearted atmosphere. Thank you in particular to Alycia and Amelia for helping proofread the thesis.

Thank you to Anthony Kinslow II, who was the role model and catalyst that originally inspired me to apply for this degree in the first place.

Thank you to my girlfriend, Nile. You were the defining feature of my experience at Oxford. Your presence in my life is truly non-fungible and I can't imagine having gone through this DPhil without you.

Thank you to Tim Lann, the co-founder of B&G enterprises. Your insanity keeps me sane, your unequivocal friendship keeps me grounded, and our wacky research endeavors add a unique piquancy and fun to my life which I will always appreciate. I hope I can help you with your DPhil as much as you did with mine.

Finally, thank you to Najars, aka Angry Mike's, for providing me with hundreds of eye-wateringly delicious wraps throughout my DPhil at an unbeatable price. The consistency of your quality of service is inspiring and matched only by the nutritional and financial salubrity of your wraps.

Abstract

Paratransit is the primary mode of road transport in sub-Saharan Africa, accounting for 50 – 98% of trips in many major cities. With global trends in vehicle electrification and Africa's role as a key destination for second-hand vehicles, paratransit electrification is inevitable. However, the scarcity of operational data for paratransit complicates the modeling of electrified transportation, hindering efficient planning and investment.

This thesis develops tools and knowledge aimed at enabling an accelerated transition to electrified paratransit systems in regions that lack electric paratransit vehicles. It first quantifies the intentions of paratransit owners and drivers to adopt electric vehicles. To do so, a structural equation model based on a novel theory of consumer behaviour is applied to a survey of 4,452 respondents. The findings inform an analysis of key technical and financial factors that affect vehicle performance and cost, including energy consumption, battery size, and payback period.

To estimate energy consumption, a methodology is developed to construct representative driving cycles that account for data transients. A kinetic model is applied to the paratransit driving cycle to estimate energy consumption and finds a rate of 0.55 kWh/km, which is validated against raw GPS tracking data. 0.55 kWh/km leads to battery size requirements that are comparable to minibuses in other global markets, and an estimated payback period of eight years.

The thesis also explores the economic potential of hybrid renewable energy systems at paratransit charging stations through a novel technoeconomic optimization model. The model optimally sizes solar-storage investments to maximize net present value while incorporating electricity supply constraints, a crucial feature of regions affected by load shedding. Key findings from a case study show how the model can help fleet owners optimally integrate renewable energy solutions with commercial fleet operations.

Overall, the thesis demonstrates that even in the absence of in-region electric paratransit vehicles, one can model the adoption intention, technical and financial viability of paratransit electrification from the fleet owner perspective. While the thesis focuses on case studies in South Africa, the methods can be applied across developing contexts in sub-Saharan Africa where paratransit dominates.

Contents

List of Figures

Abbreviations

2W . . . . Two-wheeler

4W . . . . Four-wheeler

AADT . . . . . Average annual daily traffic

AC . . . . Alternating current

CA . . . . Clustering analysis

CFI . . . . . . Comparative Fit Index

CLTC . . . . . China Light-Duty Vehicle Test Cycle

COE . . . . . . Cost of electricity

CRF . . . . . . Capital Recovery Factor

CS . . . . Charging station

DTW . . . . . Dynamic time warping

EC . . . . Environmental Considerations

EDR . . . . . . Edit-distance of real number sequences

EV . . . . Electric vehicle

ES . . . . Energy storage

FFT . . . . . . Fast Fourier Transform

FTP . . . . . . Federal Test Procedure

GFI . . . . . . Goodness of Fit Index

GhG . . . . . . Greenhouse Gas

GPS . . . . . . Global Positioning System

ICE . . . . . . Internal combustion engine

INT . . . . . . EV Adoption Intention

KMNDI . . . . Kayamandi, South Africa

LCOE . . . . . Levelized cost of electricity

LCSS . . . . . Longest common Sub-sequence

LS . . . . Load shedding
MCMC . . . . Monte Carlo-Markov Chain
MIP . . . . . . Mixed integer programming
NCA . . . . . . National Credit Act
NAM . . . . . Norm Activation Model
NEDC . . . . . New European Driving Cycle
NFI . . . . . . Normed Fit Index
NPV . . . . . . Net Present Value
OB . . . . Optimization-based
OEM . . . . . Original Equipment Manufacturer
OLS . . . . . . Ordinary Least Squares
OSM . . . . . . Open Street Maps
PAM . . . . . . Perception of Automobile Market Trends
PBC . . . . . . Perceived Behavioral Control
PDC . . . . . . Paratransit Driving Cycle
PIC . . . . . . Perception of ICE Costs
PIR . . . . . . Perception of ICE Reliability
PN . . . . Personal Norms
POC . . . . . . Perception of Costs
PU . . . . Perceived Utility
PV . . . . Photovoltaic
RE . . . . Relative Error
RDC . . . . . . Representative Driving Cycle
RS . . . . Random selection
RMSEA . . . . Root Mean Square Error of Approximation
RP . . . . Risk Perceptions
SB . . . . Segment-based
SDG . . . . . . Sustainable Development Goals
SFTP . . . . . Standard Federal Test Procedure
SSA . . . . . . Sub-Saharan Africa
ST2 . . . . . . Stage 2 load shedding

ST4 . . . . . . Stage 4 load shedding

STB . . . . . . Stellenbosch, South Africa

SUMO . . . . Simulation of Urban MObility

SW . . . . Somerset West, South Africa

TAM . . . . . . Technology Acceptance Model

TC . . . . Trickle charging

TLI . . . . . . Tucker-Lewis Index

TPB . . . . . . Theory of Planned Behavior

UN . . . . United Nations

VoR . . . . . . Value of resiliency

WCSS . . . . . Within-cluster sum of squares

WLTC . . . . . Worldwide Harmonized Light Vehicles Test Cycle

WLTP . . . . . Worldwide Harmonized Light Vehicle Test Procedure

Variables

α . . . . Annual capital payments

a . . . . Acceleration

A . . . . Vehicle frontal surface area

$A_{\mathbf{p \times p}}$ . . . . . . Cluster identification matrix

$B_{\mathbf{t}}$ . . . . Battery replacement cost in time period t

$c_{\mathbf{d}}$ . . . . Roll drag coefficient

$c_{\mathbf{rr}}$ . . . . Rolling resistance coefficient]

$C^{\mathbf{t}}_{\mathbf{base}}$ . . . . . . Energy cost without PV-ES-CS system

$C^{\mathbf{t}}_{\mathbf{sys}}$ . . . . Energy cost with PV-ES-CS system

δ . . . . Discount rate

d . . . . Average deceleration

D . . . . Down payment in year 0

$D_{\mathbf{ES}}(h)$ . . . . . Load served by ES in hour h

$D_{\mathbf{grid}}(h)$ . . . . Load imported from grid in hour h

$D_{\mathbf{load}}(h)$ . . . . Total load at charging station in hour h

$D_{\mathbf{p \times p}}$ . . . . . . Matrix of DTW distances

$D_{\mathbf{PV}}(h)$ . . . . . EV load served by PV in hour h

$D_{\mathbf{sys}}(h)$ . . . . . Load served by PV-ES-CS in hour h

$D_{\mathbf{veh}}(i, h)$ . . . Load from vehicle i in hour h at CS

$\eta^{\mathbf{DC}}_{\mathbf{ES}}$ . . . . Discharge efficiency of ES

η_{EV} . . . . Energy consumption rate of EV in kWh/km

η_{ICE} . . . . . . Fuel efficiency of ICE vehicle in L/km

$\eta_{\mathbf{rg}}$ . . . . Regenerative braking efficiency

$\eta_{\mathbf{v}}$ . . . . Powertrain efficiency

$E(n)$ . . . . . . Energy flow in sample n

$E_0(n)$ . . . . . . Energy used for auxiliary systems in sample n
$E_{\mathbf{ES}}(h)$ . . . . . Energy available in ES in hour h
$E_{\mathbf{kin}}(n)$ . . . . . Kinetic energy in sample n
$E_{\mathbf{LS}}^{\mathbf{t}}$ . . . . Energy lost to load shedding in period t
$E_{\mathbf{prop}}(n)$ . . . . Energy used for propulsion in sample n
$E_{\mathbf{PV}}(h)$ . . . . . Energy output of solar PV in hour h
$E_{\mathbf{rad}}(n)$ . . . . . Energy used to overcome radial drag in sample n
$E_{\mathbf{rot}}(n)$ . . . . . Energy used to overcome rotational inertia in sample n
$E_{\mathbf{regen}}(n)$ . . . . Energy charged into battery during braking in sample n
$E_{\mathbf{trip}}$ . . . . . . Energy consumption for an entire trip
$F_{\mathbf{ad}}(n)$ . . . . . Aerodynamic drag force in sample n
$F_{\mathbf{ext}}(n)$ . . . . . Sum of external forces on vehicle in sample n
$F_{\mathbf{rs}}(n)$ . . . . . Slope drag force in sample n
$F_{\mathbf{rr}}(n)$ . . . . . Rolling resistance in sample n
$F_{\mathbf{t}}$ . . . . Fuel cost in time period t
g . . . . Gravitational acceleration
$h(n)$ . . . . . . Elevation in sample n
h . . . . Hour index
H . . . . Total number of hours per period of analysis
I . . . . Internal moment of inertia of vehicle
$I_{\mathbf{ES}}$ . . . . Investment cost of energy storage
$I_{\mathbf{PV}}$ . . . . Investment cost of PV
$I_{\mathbf{sys}}$ . . . . Investment cost of PV-ES-CS system
k . . . . Number of clusters
$\lambda_{\mathbf{t}}$ . . . . Government incentive for EVs in time period t
Λ^t . . . . Value of resiliency provided by PV-ES system in time period t
$m_{\mathbf{v}}$ . . . . Minibus weight
$M_{\mathbf{t}}$ . . . . Maintenance and repair cost in time period t
$M_{\mathbf{ES}}^{\mathbf{t}}$ . . . . . . Maintenance cost of ES in period t
$M_{\mathbf{PV}}^{\mathbf{t}}$ . . . . . . Maintenance cost of PV in period t
$M_{\mathbf{sys}}^{\mathbf{t}}$ . . . . . . Maintenance cost of PV-ES-CS in period t

$N_{\mathbf{t}}$ . . . . Insurance cost in time period t

ω . . . . Angular velocity

O . . . . Cost of ownership

$OS^{\mathbf{t}}$ . . . . Operational savings in time t

p . . . . Number of micro-trips in dataset

π . . . . Inflation rate

ϕ . . . . Interest rate

p_0 . . . . Power offtake

$P_{\mathbf{a}}$ . . . . Percentage of time spent accelerating

$P_{\mathbf{cr}}$ . . . . Percentage of time spent cruising

$P_{\mathbf{d}}$ . . . . Percentage of time spent decelerating

$P_{\mathbf{grid}}(h)$ . . . . Grid electricity price in hour h

$P_{\mathbf{t}}$ . . . . Loan payment in time period t

$P_{\mathbf{PV\text{-}rated}}$ . . . . Installed PV capacity in kW

ρ . . . . Density of air at 25°C

ϱ^t . . . . Replacement cost of an asset in time period t

$r_{\mathbf{curve}}$ . . . . . . Radius of turning curve

$r_{\mathbf{wheel}}$ . . . . . . Radius of vehicle's wheel

R . . . . Residual value of an asset

$\sigma_{\mathbf{a}}$ . . . . Standard deviation of acceleration

$s(n)$ . . . . Displacement in sample n

$S^{\mathbf{t}}$ . . . . Energy cost savings in period t

τ . . . . Time between samples

$\theta(n)$ . . . . Slope angle in sample n

T . . . . Number of periods in project lifespan

t_{min} . . . . Minimum duration for a single micro-trip

$\chi_{\mathbf{i}}$ . . . . ith cluster

X_j . . . . Distance of data point j from a centroid cluster

$v(n)$ . . . . Velocity in sample n

V . . . . Average velocity

$V_{\mathbf{r}}$ . . . . Average running velocity

$Y_{\mathbf{PV}}(h)$ . . . . . Capacity factor of solar PV in hour h

We propose that with innovative thinking and context-specific approaches and technologies [...] electric vehicles could in fact offer benefits to governments, the power systems, and vehicle owner-operators in Sub-Saharan Africa

— K.A. Collett, S.A. Hirmer, H. Dalkmann, C. Crozier, Y. Mulugetta, M.D. McCulloch [1]

1 Introduction

Contents

The aim of this thesis is to address the research question: *Given the absence of electric paratransit vehicles in sub-Saharan Africa, is it possible to model the market perception, as well as the technical and financial viability, of electrifying the region's paratransit systems from the perspective of fleet owners?* Paratransit accounts for 50 – 98% of passenger trips in sub-Saharan Africa [2] and is one of the world's largest, most complex and poorly documented transportation systems [3]. Through the investigation of the above stated central research question, this thesis provides knowledge and tools to accelerate the electrification of sub-Saharan African paratransit in service of the global march towards sustainable development.

1.1 Context and motivation

Road transport contributes three-quarters of the greenhouse gas (GhG) emissions accounted to the transport sector, which in turn contributes to one-quarter of global emissions [4]. Global decarbonization of road transport is directly instrumental in achieving UN Sustainable Development Goals (SDGs) 7 (affordable and clean energy), 8 (decent work and economic growth), 9 (industry, infrastructure, and innovation), 11 (sustainable cities), and 13 (climate action) [5]. Accordingly, electric vehicles (EVs) are becoming increasingly common in developed countries, especially as more and more governments aim to reduce global carbon emissions. In response, many original equipment manufacturers (OEMs) such as BMW, Ford, and General Motors have stated plans to stop production of new internal combustion engine (ICE) vehicles by 2035 [6].

Conversely, in the Global South, and in sub-Saharan Africa (SSA) in particular, the transition to EVs has been delayed by high upfront costs and low electricity access. SSA is a major destination for old and used vehicles, which typically consume particularly dirty fuel such as diesel with high-sulfur content. Over 40% of used vehicles exported globally end up in SSA, and 80% of 4-wheeler (4W) imports to the region are used vehicles [7]. These inefficient second-hand vehicles not only cause serious air pollution and health problems in African cities, they contribute heavily to greenhouse gas emissions [8]. Their fuel is typically imported as well, leaving these dependent countries vulnerable to issues related to fuel quality, energy security and price fluctuations [8].

In light of these trends, the need for an innovative approach to transport electrification in SSA becomes clear. However, large-scale transport electrification is a massive societal shift, and vehicle and infrastructure requirements must be modelled in order to draw investment, incentivize key stakeholders, and enable efficient transitions. Different sectors of transportation have different technical requirements, financial costs, and operating conditions, and must be modelled on their own basis. The focus of this thesis will be on paratransit, the largely informal sector which provides the bulk of road transport in SSA [2]. Vehicles in the paratransit space are bought by fleet owners [9]. Thus, fleet owners are the principal actors in the paratransit space, and if the adoption of electric vehicles is not viable for them, then the overall transition will falter. The focus of the thesis is on providing knowledge and tools for fleet owners that help determine the technical and financial viability of electrifying paratransit. However, some of the results and modelling in the thesis are also useful to other paratransit industry stakeholders such as grid operators and policymakers.

1.1.1 Background on paratransit

Paratransit in the developed world has a different connotation than it does in the developing world. In the developed world, paratransit refers to a type of demand-responsive transport system that operates alongside (hence "para") standard public transport systems to service trips that the conventional system cannot fulfill. The services are typically for-hire and make up a relatively small percentage of overall road-based market share; for example, the so-called "dial-a-ride" services for people with movement disabilities fall into this category. This service allows individuals with movement disabilities to book a ride on-demand, providing flexible, door-to-door transportation that accommodates their specific mobility needs, which conventional public transport systems cannot fulfill.

In the developing world, paratransit operates on a completely different scale. It is estimated to comprise the largest modal share of public transport in most major African cities [2, 10]. For example, in Kampala, Uganda, Kigali, Rwanda, and Dar es Salaam, Tanzania, paratransit's share of road-based public transport passenger markets exceeds 98% [2, 11]. Its scale, affordability, and accessibility makes it a linchpin in the economies of many low-income and middle-income countries by facilitating access to jobs, goods, and services for a great number of people.

Within African paratransit, there are multiple vehicle modalities, including the minibus taxi in South Africa, Kenya, Nigeria, Ghana, and Uganda, tricycle taxis in Nairobi and single passenger motorcycle taxis in north-east SSA [12, 13, 14]. The focus in this thesis is on the most common paratransit modality, the minibus taxi (Figures 1.1a and 1.1b), which comprises roughly 83% of paratransit trips throughout the region [2, 11, 15, 16]. The critical role paratransit plays in urban road transport means that the minibus taxi industry provides access to many citizens for economic, healthcare, and education opportunities, which tie into UN SDGs 1 (no poverty), 3 (good health and well-being), and 4 (quality

(a) Close up of Toyota Quantum Ses’fikile, the most common minibus taxi in South Africa. [17]

(b) Toyota Quantum Ses’fikile minibus taxis parked at an informal taxi rank in Stellenbosch, South Africa.

Figure 1.1: Typical Minibus taxis in South Africa

education) [5]. In certain areas of SSA, “paratransit" and “minibus taxi" are often used interchangeably, and the same will be done here in this thesis for the sake of brevity.

The popularity of the minibus taxi is due to its size (9 to 16 seats depending on the model, oftentimes with more passengers squeezed in to maximize profit per trip) [2], along with its availability at a low cost as affordable second-hand imports from developed countries [18]. However, these vehicles tend to be old and under-maintained, leading to fuel-inefficiency and high operational costs. A. Mahaputra Kumar et al. [19] found the average age of minibus taxis across 12 African cities to be nearly 15 years old, which means these taxis emit higher levels of greenhouse gas emissions than would be seen in a typical minibus [20]. Moreover, old vehicles are often not covered by emissions regulations, meaning that minibus taxis play a large role in decreasing the air quality across African cities [3]. That the taxis spend much of their time idling in traffic only exacerbates the pollution issue, which is serious in the region. The World Health Organization estimated that along with increasing cardiopulmonary and cardiovascular disease prevalence, ambient air pollution caused 1.1 million deaths in Africa in 2016 [21, 22, 23, 24].

1.1.2 Electrification of paratransit

With 97% of the transport sector's power coming from fossil fuels worldwide, it is the least diverse of all energy end-use sectors [25]. In SSA, in the face of the increasing demand for urban commuting heralded by urbanization and population growth, the electrification of paratransit is a critical opportunity for significant regional transport sector decarbonization. Despite SSA only contributing to 2.3% of global CO2 emissions, of which less than 12% were from transport [25, 26], emissions from transport grew faster than any other sector in the region between 2010 and 2019 [25]. If the status quo of combustion-powered paratransit is maintained, then increasing urban migration, population growth, and an expanding middle class will see these trends move from unsustainable to catastrophic [3, 15, 27]. By the same token, the electrification of paratransit presents an opportunity for significant decarbonization in SSA. Furthermore, the co-benefits of transport and power sector electrification [1] mean the electrification of paratransit could stimulate a similar transition in the power sector. This dual transformation improves the likelihood of efficiently addressing the energy trilemma of affordability, accessibility, and security for millions of people. Figure 1.2, adapted from Fig. 3 in [1], visualizes the opportunities presented by the electrification of road transport in SSA [5].

In addition to local economic and environmental pressures, global economic and supply chain forces are advancing the end of internal combustion engine (ICE) vehicle production. Many large global automobile original equipment manufacturers (OEMs) have committed to stop production of ICE vehicles entirely by 2035 [6], and 130 million EVs are estimated to hit the roads of Europe by 2030 [28]. If the need for transport electrification in SSA wasn't already pressing enough on its own basis, past trends tell us that many of these European vehicles will end up on African roads [2, 29]. One way or another, the region must prepare itself for EV integration.

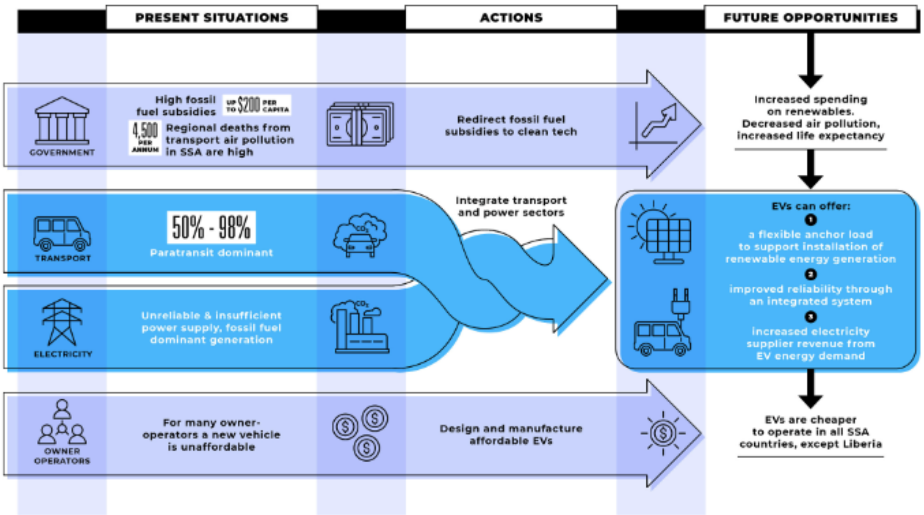

Figure 1.2: Schematic to show the future opportunities offered by electric vehicles in the paratransit sector in SSA, and the actions necessary to transition to this future from the present situation (adapted from Fig. 3 in [1].)

1.1.3 Obstacles to Paratransit Electrification and Decarbonization

Despite the opportunities of paratransit electrification, there are significant challenges associated with a shift to an electrical energy source for transportation in this region. Specifically, these include stakeholder perceptions of EVs, their high cost, and electricity supply constraints [10, 30].

Stakeholder perceptions critically influence the adoption of new technologies like EVs. Previous research has demonstrated that consumer buy-in and perceptions significantly influence the rate of technology adoption [31]. In affluent, developed nations, the push towards EVs has greatly benefited from momentum generated by societal climate movements. In contrast, developing regions lack such momentum due to resource constraints, differing priorities, social climates, and educational levels.

The high capital cost of EVs relative to comparable ICE vehicles may be a greater disincentive in regions where capital availability is limited, even if total cost of ownership is lower [7]. The paratransit industry in particular operates on razor-thin margins [2], so a large, potentially unfamiliar investment that yields returns only in the long run may not be an obvious or financially attractive choice for paratransit vehicle owners.

Electricity supply constraints in SSA will affect the technical feasibility of converting to EVs. In particular, the region's energy-constrained grids may disrupt charging services. This therefore requires capital investment to upgrade local grid infrastructure. The challenge for the fleet owner is that the cost of the EV purchase and the indirect costs of the infrastructure upgrade via increased electricity tariffs may be substantial. This therefore raises the question of whether it will still be financially viable for the fleet owner to electrify their fleet. If it is, then this will enable electricity providers to invest in infrastructure, thus dealing with the conundrum of whether you invest in electric transport infrastructure or vehicles first.

These challenges highlight the narrow margin for error in achieving an economically efficient and timely transition to an electric fuel source. Before committing to substantial investment or policy decisions, thorough modelling and research efforts are needed to understand stakeholders' perceptions of EVs. Methodologies must be devised for modelling various parameters that go into vehicle and infrastructure design and facilitate financial and technical feasibility analyses. Such research must be informed by the context of sub-Saharan African paratransit which includes constraints on electrical and capital resources.

Inadequate planning hamstrings investment and delays the whole electrification and decarbonization process. Without a solid understanding of the perceptions paratransit vehicle owners and drivers hold of EVs, and credible estimates of the technical and financial requirements of electric paratransit vehicles, it becomes extremely challenging to determine the technical and financial viability of electric paratransit vehicles for a vehicle owner. This lack of knowledge leads to significant challenges related to generating investment, promoting policy support, and accelerating consumer adoption.

1.2 Scope of the problem addressed

The above motivation leads to the central research question of the thesis, *Given the absence of electric paratransit vehicles in sub-Saharan Africa, is it possible to model the market perception, as well as the technical and financial viability, of electrifying the region's paratransit systems from the perspective of fleet owners?* Given the potentially broad remit, it is necessary to define the scope of the research inquiry's boundaries.

First, as described in Section 1.1.1, although there are several types of paratransit in the world and several different paratransit modalities in sub-Saharan Africa focus of this thesis is on public transport minibus taxi paratransit. Public transport minibus taxi paratransit is an important sector for the economies of many developing countries.

Secondly, due to data availability, this thesis uses data from only one country, South Africa. Market perception data for Chapter 3 are gathered through surveys in the Western Cape, and mobility data are obtained through GPS tracking data gathered on minibus taxis traveling around the Western Cape province for Chapters 4 and 5, and in Johannesburg for Chapter 6. The limitation to South Africa is an advantage in one sense since minibus taxis, the modality of interest in this thesis, comprise 100% of the paratransit industry in South Africa. However, since vehicle operational conditions and socio-economic environments may vary between countries, the limitation does mean the specific results found in this thesis are geographically limited. Nonetheless, given the similarities between paratransit systems across sub-Saharan Africa and those in South Africa, the knowledge obtained and tools developed in this thesis are still broadly applicable. The knowledge can serve as valuable benchmarks for investment and a foundation for future research on paratransit electrification throughout, and the tools should be able to be applied in other countries throughout the region.

Next, although paratransit is a vast system with a large variety of institutions and actors, the focus of this thesis is primarily to examine the technical and financial feasibility of electrifying paratransit fleets from a fleet owner perspective. A fleet owner is defined as an individual or organization that owns and operates one or more paratransit vehicles for commercial use. This thesis highlights how tools and knowledge developed in the thesis may benefit other stakeholders, but the fleet owner perspective provides the impetus for deeper analysis. The one slight exception to this rule is the inclusion of paratransit drivers in the development of tools and knowledge to model market perceptio, which is a key component of the research question. Drivers are included because they will be the main users of an EV product in this sector.

1.3 Research sub-questions

In this thesis, the central research question is deconstructed into the following sub-questions. Each sub-question, though consisting of multiple components, aligns with a specific chapter of the thesis:

1a. *What are the intentions of paratransit owners and drivers to switch to EVs when they become available?* This first sub-question addresses market perception of electric paratransit, and is approached via a survey which establishes a baseline of interest among relevant constituents

1b. *What are the factors that influence EV adoption intention for paratransit owners and drivers?* A set of nine hypotheses about the relevant factors are tested with a structural equation model. Exploring this sub-question yields a first-order understanding of the tools and knowledge necessary to move the needle on adoption intention. It validates the necessity and usefulness of the research later on in the dissertation.

2a. *How can we construct representative driving cycles for paratransit?* A time series shape-based clustering methodology is developed to construct representative driving cycles from GPS tracking data.

2b. *How well do international driving cycles represent paratransit mobility?* Using a set of standard representative parameters, the capabilities of three standard international driving cycles to represent paratransit mobility are compared with that of the driving cycle constructed to answer sub-question 2a.

3a. *What are the per-distance energy requirements of electric paratransit?* This sub-question addresses the energy consumption (kWh/km) rating for electric paratransit vehicles, which is critical for vehicle battery sizing. A first-principles vehicle electrokinetic model is applied to the representative driving cycles developed to answer the previous sub-question. The driving-cycle based kWh/km results are validated by applying this kinetic model to the entire set of GPS tracking data from which the driving cycles were constructed.

3b. *Can per-minute GPS tracking data reliably determine the energy consumption of paratransit vehicles?* This sub-question validates the need for high-resolution GPS data to estimate paratransit energy requirements. Energy consumption estimates in kWh/km are gathered separately using per-minute and per-second data. A fast fourier transform is implemented to quantify the energy signal captured by the per-minute data as compared to the per-second data and explain discrepancies.

3c. *What is the payback period of an electric minibus taxi?* The total cost of vehicle ownership model for an electric paratransit vehicle is compared with that of an equivalent ICE paratransit vehicle.

4a. *How can we optimize the size of PV and energy storage at paratransit charging stations to maximize economic gain, considering electricity supply constraints?* A techno-economic optimization model which accounts for electricity supply constraints is developed, quantifying the benefits of resiliency provided by hybrid solar-storage systems at charging stations.

4b. *What are the effects of varying electricity demand (as fleet size) on the economic performance of the PV-energy storage-charging station (PV-ES-CS) system?* The techno-economic optimization model is run under a variety of scenarios with differing fleet sizes and rates of electrification. The results yield trends which reveal the financial ramifications of different fleet electrification strategies for fleet owners.

These sub-questions are based on research gaps identified in the literature review in Chapter 2.

1.4 Thesis structure

Figure 1.3 visualizes the structure of the field of literature within which this thesis fits. The framework in this figure facilitates an organized understanding of how various segments within the thesis interconnect and contribute to addressing the central research question.

The framework is structured around three principal domains based on the central research question: market perception modelling, technical modelling, and financial mod-

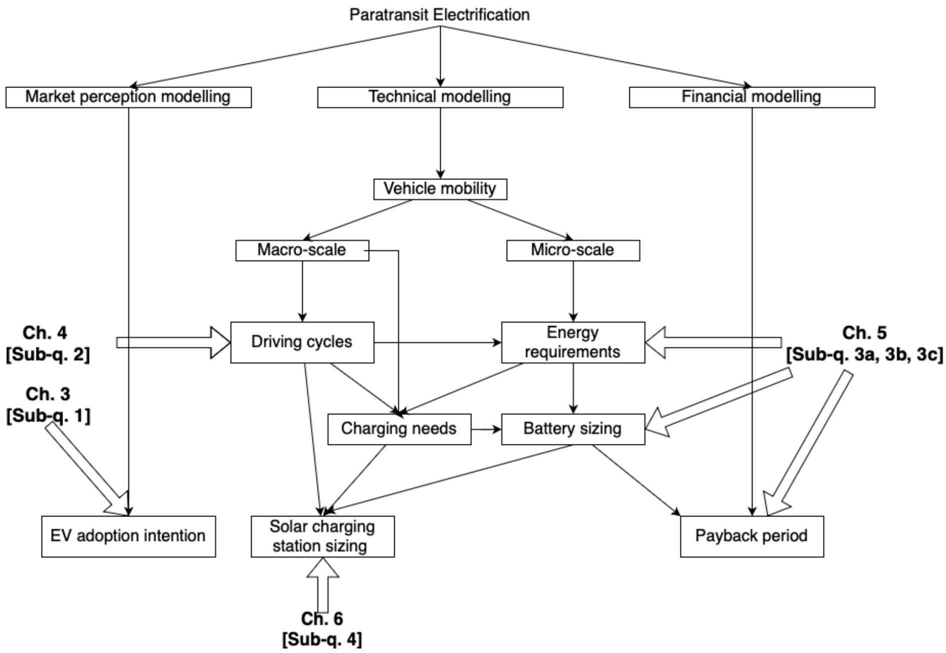

Figure 1.3: Taxonomy of literature on paratransit electrification and outcomes related to the central research question.

elling. The ensuing literature review in Chapter 2 reveals substantial deficiencies within the domains of market perception and financial modeling in paratransit electrification, which this thesis endeavors to address. Although the technical modelling literature is comparatively more mature, it is still a relatively nascent field and presents essential gaps that this dissertation seeks to bridge.

The rest of this section shows how each chapter builds upon the previous to construct a coherent narrative and thorough investigation into the electrification of paratransit. As previously alluded, each research chapter lines up with one of the four research sub-questions detailed in Section 1.3

Chapter 2 lays the groundwork for the thesis by reviewing existing literature on paratransit electrification and identifying the gaps in knowledge which this thesis intends to fill. This process validates the research sub-questions presented earlier. Five gaps are identified, the first three of which align individually with the first three sub-questions and research chapters of the thesis, while the latter two fall under sub-question 4 and are addressed in Chapter 6.

Chapter 3 addresses *sub-questions 1a* and *1b*, focusing on market perception. By surveying paratransit owners and drivers, the chapter delves into their intentions to adopt EVs and the factors that influence these decisions. The findings inform the understanding of what makes electric paratransit viable or attractive for owners and drivers, substantiating the need for the subsequent research in this thesis.

Building on the insights on market perception, **Chapter 4** establishes a foundation for modelling the technical and financial viability of electric paratransit vehicles. It answers *sub-question 2a* by introducing a methodology to construct representative driving cycles for paratransit using 1Hz GPS tracking data gathered on minibus taxis travelling in South Africa. It then answers *sub-question 2b* by constructing a representative driving cycle for paratransit and comparing it against standard international driving cycles. This construction unlocks the analysis in Chapter 5, which focuses on vehicle energy consumption.

Chapter 5 extends the technical analysis in Chapter 4 and answers *sub-question 3a* by using the representative driving cycle developed in Chapter 4 to calculate the energy requirements of electric paratransit vehicles. The results are validated with the first high-fidelity estimates of paratransit energy consumption. The chapter then tackles *sub-question 3b* by using fast fourier transforms to quantify the accuracy of estimating paratransit energy consumption from per-minute GPS tracking data. Finally, it answers *sub-question 3c* by using the energy consumption estimates to develop financial models, calculating the total cost of ownership and payback period for electric minibus taxis on a per-vehicle basis. These estimates are critical inputs for the analysis in Chapter 6.

Chapter 6 shifts the thesis' scope from vehicle-scale to fleet- and infrastructure-scale. It addresses *sub-question 4a* by developing a methodology to techno-economically optimize the size of hybrid renewable energy systems for charging stations with constrained electricity supply and varying demand. *Sub-question 4b* is answered by evaluating system feasibility under varying electricity supply and demand scenarios for a case study paratransit fleet in Johannesburg, South Africa.

Chapter 7 concludes the dissertation by summarizing the main findings and contributions to knowledge, and reflecting the implications of the research. It consolidates the insights gained across the four analysis chapters and indicates potential directions for future research.

Minibus taxi public transport is a seemingly chaotic phenomenon in the developing cities of the Global South with unique mobility and operational characteristics. Eventually this ubiquitous fleet of minibus taxis is expected to transition to electric vehicles.

— C.J. Abraham, A.J. Rix, I. Ndibatya and M.J. Booysen [29]

2 Literature Review

Contents

This chapter provides an overview of the body of academic literature on paratransit electrification and identifies research gaps that motivate this thesis, thereby clarifying how it fits within the field. The overview begins with factors influencing the acceptance and perception of EVs among paratransit fleet owners and drivers, then moves onto paratransit mobility, energy, and infrastructure requirements. Research gaps are highlighted in **bold** and discussed at the end.

Figure 2.1 builds on Figure 1.3 to explicitly display the level of study on each topic within the taxonomy of literature on paratransit electrification. Colored squares and circles attached to each topic indicate the depth of study in the global and sub-Saharan African paratransit bodies of literature respectively. It can be easily seen that compared to the global EV scale, paratransit in SSA remains relatively poorly studied.

Furthermore, the figure shows where the research chapters in this thesis fit into the

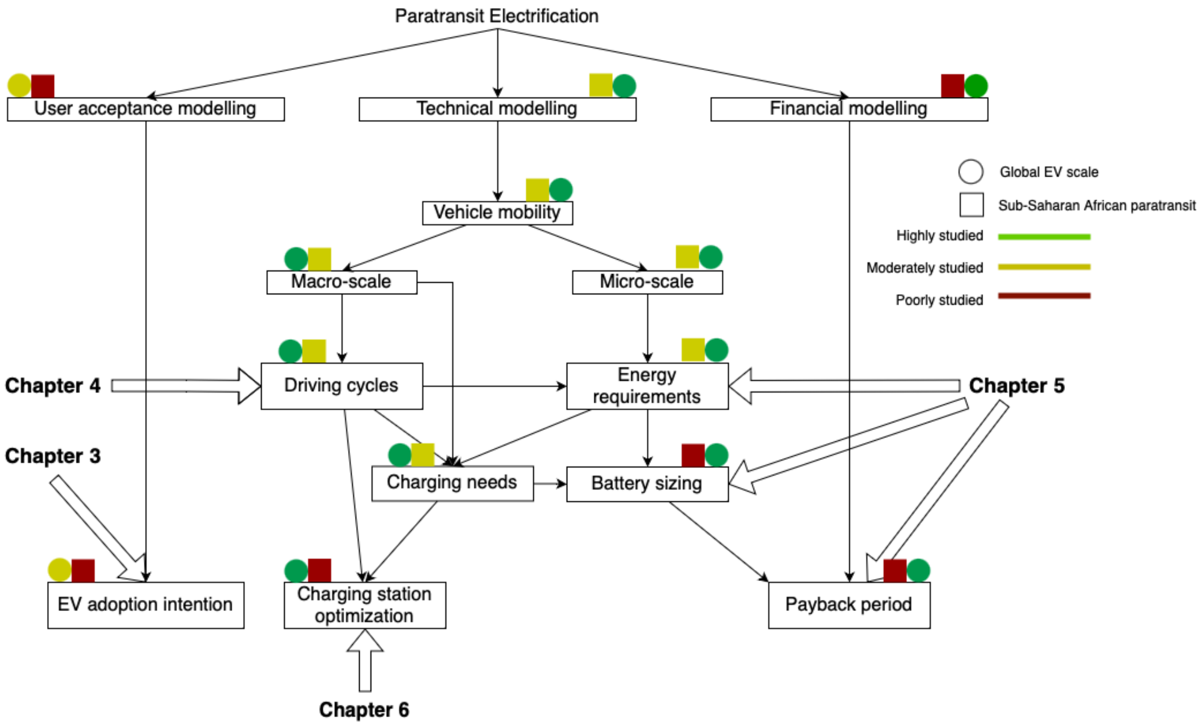

Figure 2.1: Taxonomy of literature on paratransit electrification. Green, yellow, and red outlined shapes denote highly, moderately, and poorly studied areas respectively. The color of the circle indicates the level of study on EVs at a global scale, and the color of the square indicates the level of study on paratransit in SSA. The positioning of the thesis chapters within this literature is also indicated.

taxonomy of literature. It is recognized that the node “charging station design" could encompass a broad variety of topics, so the scope within which it is investigated in the thesis is clarified by the discussion of the research gaps in this chapter.

2.1 Factors influencing market perception and user acceptance of EVs

In order to ensure the successful electrification of the paratransit sector, it is important to delve into the decision-making processes of vehicle owners and drivers, who ultimately drive this transition. Plananska [32] argues that interventions which encourage EV adoption are often hindered by a limited understanding of the factors that influence user readiness and consumer uptake. Minimizing errors is critical, as EV adoption can be limited by consumer reticence even in markets that can overcome material barriers [33]. On the flip side, research has shown that technology adoption can be hastened by pushing an agenda that fits the interests of product users [31].

EVs have only recently been introduced to sub-Saharan Africa, including South Africa, and there are not yet any electric minibuses available on the market [34]. Given the unique socio-economic and political context of developing countries in sub-Saharan Africa such as South Africa, factors such as load shedding, access to electricity and charging infrastructure, cost, perceptions of EV capabilities and perceptions of the global automobile market may differ from those in developed countries which *have* been studied. Thus, efforts should be focused on understanding the perceptions and attitudes of vehicle owners and drivers, as this knowledge can inform the development of targeted and effective policies, incentives, and educational campaigns to drive EV adoption in the paratransit sector in a way that is socially, economically, and environmentally sustainable. The need to understand market perceptions and facilitate an efficient transition to electric paratransit is particularly crucial in the Global South, where limited resources, the pressing urgency to mitigate climate change, and the necessity to prepare for future imports of used electric vehicles create a compelling case for action.

Research into the market perception and user acceptance of electric vehicles (EVs) in paratransit systems offers diverse perspectives on which factors may significantly influence adoption intention. Studies from Malaysia [35, 36], India [37, 38], and Vietnam [39] consistently highlight factors such as perceived cost and infrastructural readiness as pivotal to adoption, and the applicability of these findings to the SSA context is uncertain due to unique regional challenges such as load shedding and the nascent stage of EV market penetration. A recent systematic literature review by Bryła et al. [40] identifies 30 studies done in Asia, 18 in Europe, 12 in USA & Canada, and 1 in Saudi Arabia. The strict exclusion criteria in the review means that some articles may have been missed, but there is clearly a dearth of research in market perception of EVs in sub-Saharan African paratransit. Similarly, despite an increasing number of articles in recent years being published on technical topics related to paratransit electrification, which are discussed further down in this chapter, the literature is missing an understanding of the perspective of paratransit fleet owners and drivers, the critical agents of the sector. This leads to **Research Gap 1: an understanding of the perception paratransit fleet**

owners and drivers have of EVs.

2.2 Paratransit mobility, energy, and infrastructure requirements

The critical role of market perception in the adoption of electric paratransit has been established, along with the recognition of the lack of studies in this area. Next, technical challenges of electric paratransit mobility and accompanying infrastructure requirements will be discussed. These elements are intrinsically linked, as the successful implementation of EV technology depends not only on psychological acceptance but also on the adequacy of the underlying physical and energy infrastructure.

While the driving cycles, energy demands, and infrastructure requirements of EVs in the developed world are well established and deeply analyzed [41, 42, 43], the body of literature on these topics for paratransit in SSA is sparse. Indeed, there are only a handful of studies on paratransit mobility and energy usage in SSA [29, 44, 45, 46, 47, 48] (all discussed further in next section) and none of them relate to representative driving cycles.

Representative driving cycles are vehicle speed-time series that simulate real-world driving conditions. They have a wide range of uses, from determining fuel consumption and emissions profiles [49, 50, 51] to designing traffic control systems [52] and determining the performance of vehicle systems [53, 54]. It has been noted in the literature that driving cycles differ between different driving contexts [55, 56, 57]. However, a multi-continental review of over 100 driving cycles lacked a single drive cycle from the continent of Africa due to lack of data [58]. Given the unique mobility patterns and unconventional driving styles seen in African paratransit systems [59], conventional driving cycles from high-income countries are unlikely to be applicable.

2.2.1 Mobility

Understanding the mobility patterns and operations of current ICE paratransit fleets is crucial for accurately modeling key parameters, such as vehicle energy consumption, for planning the operations of future EV fleets, and for constructing representative driving cycles. Driving cycles are vehicle speed-time series that simulate real-world driving conditions. They have a wide range of uses, from determining fuel consumption and emissions profile, to designing traffic control systems and determining the performance of vehicle systems [49, 52, 53]. While future EV fleets may not exactly mirror the operational patterns of ICE fleets, analyzing the differences between the two will provide valuable insights for modellers and planners. This will enable a more precise assessment of the technical, social, economic, and environmental impacts of fleet electrification, laying the foundation for effective policy and infrastructure planning. Prior to this thesis, the literature addressing paratransit mobility in the context of modeling and planning has included studies such as [29, 44, 45, 46, 47, 48], which are discussed below. Other literature on sub-Saharan African paratransit has focused on regulations and reforms [60, 61], as well as sector governance [62].

Early studies of minibus taxi trajectories in the literature reveal insights about the broader dynamics of minibus taxi operations, but do not turn an eye toward minibus taxi speed-time series' or micro-movements (critical for driving cycles), or energy consumption [45, 46, 47, 59]. Ndibatya et al. [45] uses GPS tracking data to develop a transportation prediction model that helps provide passengers with intelligence to reduce their waiting time for taxis. The data was partitioned into density clusters based on where the taxis stopped, and the common pick up/drop off locations were identified. The data was filtered to select only points with less than 1km/h speed, and no analysis of energy consumption or replicable methodology for driving cycle construction was developed. Ndibatya et al. [47] focus on methodologies to map the geospatial characteristics of the Kamapalan paratransit network with GPS data gathered via smartphone. The goal of that research was to provide travellers with an understanding of the routes taken and stops made by local paratransit vehicles. Ndibatya and Booysen [59] further characterize minibus taxi movement patterns, noting their tortuosity, Lévy walk-like behavior, and changing topology and shape. Lévy walk-like movement patterns are typically observed in the field of animal biology by predators when they are hunting for prey. These trajectories believed to represent an optimally efficient search pattern, and the fact that taxi drivers exhibit this behavior emphasizes the highly competitive and profit-driven nature of the industry. Again, this research was focused on the spatial distribution of minibus taxi movement patterns, so as to help travellers plan their movements and urban planners optimize infrastructure placement. Ndibatya and Booysen [46] use economic metrics such as taxi fares and occupancy, and efficiency metrics such as passenger waiting time and taxi hold-back time, to study the operational economics operations, economics, and efficiency of minibus taxis in Kampala. They find an overall low profitability-index and great economic inefficiencies in the sector, but again address neither energy consumption nor driving cycles.

Later works begin to attempt to address the issue of taxi energy consumption. Abraham et al. [29] and Booysen et al. [48] use per-minute GPS data (Stellenbosch, South Africa, and Kampala, Uganda respectively) in conjunction with a custom built EV fleet simulator based on the micro-traffic simulator SUMO (Simulation of Urban MObility) to analyze minibus taxi spatial mobility patterns – including charging opportunities – taxi energy demand, and required PV area to support the taxis. The purpose of the analysis in both studies to help traffic planners and grid operators plan the roll-out of EV fleets, as well as demonstrate how the usage of the custom EV fleet simulator can help planners and operators in other contexts not captured in the paper. Important parameters for EV fleet planning captured in the papers include vehicle energy efficiency, vehicle temporal mobility analysis throughout the day, charging opportunities, and area of PV solar required to cover EV charging. However, the analysis in these papers is severely limited by the low resolution of GPS data gathered, and several glitches in SUMO's routing algorithm [63], which are discussed further in Section 2.2.2.

Finally, Zeeman and Booysen [44] present a theoretical model to detect reckless driving behavior in minibus taxis, and validate it with GPS data. The frequency of data captured is unspecified, and the model focuses on detection events rather than characterization of mobility patterns.

Overall, these papers provide macro-level mobility and operational analysis, and offer techniques for monitoring driver behavior. However, they lack a reliable methodology for reproducing minibus taxi driving cycles at a high fidelity. The design and operation of paratransit systems can be hindered by a lack of accurate, high-fidelity representative driving cycles that reflect the unique driving conditions of the region [3]. Limitations in SSA for driving cycle development stem primarily from a lack of data on actual driving patterns and a lack of standardized testing procedures. By contrast, the driving cycles of electric passenger vehicles and larger buses in the developed world where data is readily available have been analyzed heavily [41, 42, 64, 65, 66]. The next section explores driving cycle research, with a focus on constructing representative driving cycles for paratransit vehicles, particularly in sub-Saharan Africa, where unique driving patterns pose distinct challenges.

Representative driving cycles

Driving cycles are a foundational element in accurately simulating the real-world energy demands of paratransit vehicles in SSA. As previously alluded, driving cycles are vehicle speed-time series that simulate real-world driving conditions. They are used as the basis for protocols that determine vehicle fuel or electricity consumption and emissions ratings, as well as vehicle sub-system performance evaluation [49, 52, 53]. In practice, this can imply that driving cycles will dictate the procedure a vehicle is run through (often on a machine such as a chassis dynamometer) to measure performance under typical driving conditions. Cycles can also be used by engineers for vehicle technology research and development, or by policymakers and urban planners for transportation planning. Consequently, a detailed understanding of driving cycles can be useful for guiding long term vehicle design [67, 68] such as engine power, fuel type (e.g. diesel or electric), and vehicle size, constructing policies that efficiently manage congestion and transportation emissions [56, 69, 70], and generally understanding transportation system operations.

It is particularly important that driving cycles accurately represent the driving patterns of the target vehicle type in the target region, so that results from performance tests capture realistic vehicle performance. However, well-known standard international driving cycles such as the New European Driving Cycle (NEDC) or Worldwide Harmonised Light Vehicle Procedure (WLTP) have been found in various studies and reviews to insufficiently represent local driving patterns in many developed economies [50, 52, 71, 72, 73]. Unique traffic patterns, road conditions, driver behavior, and the typical vehicle stock seen in traffic tend to differ between developed and developing countries. All of these factors may affect the speed-time relationship in a typical vehicle-trip and thus different driving cycles [74, 75].

Over the last several decades, the development of representative driving cycles has been a focus of transportation research, resulting in established cycles for various global cities as documented by several studies (e.g. [49, 50, 76]). Literature reviews of driving cycle development show that these efforts predominantly concentrate on regions such as the USA, Europe, South America, and Asia [71, 77, 78]. However, the distinctive and often unconventional driving patterns that have been observed in African paratransit systems [44, 59] present unique challenges that standard international driving cycles, typically derived from high-income countries, are unlikely to adequately represent.

Existing literature has attempted to utilize low-resolution data from paratransit systems to estimate energy consumption and infrastructure needs, employing widely available open-source mobility simulation tools Abraham et al. [29] and Booysen et al. [79] However, these simulations often fall short due to the inherent limitations of such tools (discussed in detail in the following subsection), leading to significant inaccuracies in mobility modeling. While open-source simulators offer the flexibility to integrate custom driving cycles, such modifications require a profound understanding of specific vehicular behaviors within the target population—a requirement seldom met in the context of African paratransit.

Research by Zeeman and Booysen [44] and Ndibatya and Booysen [59] provides some insight into the erratic, Lévy walk-like movement patterns of minibuses as they navigate urban landscapes in search of passengers and profit. Yet, these studies do not extend to a comprehensive methodological framework for capturing the nuances of paratransit micro-mobility. This oversight underscores a critical research deficiency, leading to **Research Gap 2: a lack of methodologies to construct representative driving cycles for paratransit**, which is essential for accurate modeling and simulation of these transport systems.

2.2.2 Vehicle energy consumption

The establishment of representative driving cycles is foundational for understanding how vehicles consume energy under realistic operational conditions. As outlined by Collett and Hirmer [3], understanding energy consumption is integral not only to infrastructure plan-

SUSTAINABLE DEVELOPMENT GOALS	1	2	3	4	5	6	7	8	9	10	11	12	13	14	15	16	17
Reduced greenhouse gas emissions			3.4, 3.9								11.6	12.2		14.3	15.3, 15.5		
Reallocated government spending from reduced fossil-fuel subsidies	1.a							8.2				12.c	13.2, 13.a				
Reduced transportation costs from lower energy cost per kilometre	1.4									10.1	11.2						
Investment in green infrastructure electricity generation and EV charging							7.2, 7.a, 7.b	8.4	9.1, 9.2, 9.5, 9.a		11.a		13.2				
Increased energy access through distributed supply	1.4						7.1		9.1	10.1	11.2						
Increased reliability of energy supply							7.1, 7.2, 7.3										
Increased revenue for electricity retailers							7.2	8.2					13.a				17.1
Increased energy efficiency							7.3					12.2					
Increased opportunities for developing low-carbon transport markets, including retrofit							7.3	8.2, 8.3, 8.4	9.4, 9.a			12.5					17.7

Figure 2.2: The potential benefits of EV adoption to achieving UN SDGs. For each SDG, specific targets potentially supported by EV adoption are listed. From [3] (with license and authors permission).

ning and business model development, but also to making informed investment decisions and shaping effective policy research. In other words, it is a key input parameter for many downstream models which are core to understanding the technical and financial viability of paratransit electrification, and for unlocking the benefits visualized in Figure 2.2.

Prior to the work of this thesis, the literature on paratransit energy requirements is limited to Abraham et al. [29] and Booysen et al. [48]. In these studies, the estimates of energy consumption were based on the same per-minute data as the spatial-mobility analyses which motivated the papers. Unfortunately, in part due to the aggressive nature of minibus taxi driving where multiple high acceleration/deceleration maneuvers can occur in a matter of seconds, an infrequent sampling frequency in this setting is liable to inaccurate and highly variant estimates [80]. These previous studies have attempted to work around this hurdle by feeding the per-minute GPS data through a simulation software known as EV-Fleet-Sim [29]. EV-Fleet-Sim takes in low-frequency GPS data (one sample per minute) as input, and uses a micro-traffic simulator known as SUMO (Simulation of Urban MObility) [81, 82] in conjunction with an underlying map representation (OSM – Open Street Maps) to retrieve per-second vehicle mobility patterns.

During the research for this thesis, it was found that the routing algorithm in SUMO does not accurately compute per-second MBT driving behavior. Working with partners at Stellenbosch University who developed EV-Fleet-Sim, it was uncovered that the algorithm in SUMO is subject to several glitches, including the following:

- SUMO's assumed driving style for minibus taxi drivers is not representative of their actual driving style.
- SUMO does not capture pickup/dropoff stops. It only stops for passengers at the beginning and end of the trip.
- OSM, the geographic database used by SUMO, does not satisfactorily capture all routes that vehicles travel in informal settlements.
- SUMO will occasionally route the vehicle on the wrong side of the street, due to GPS spatial errors. This has the effect of making the vehicle complete an impossible U turn and sending it in the wrong direction.

The severity of these errors plus the inherent shortcomings of per-minute data lead to the hypothesis that per-minute data was insufficient for estimating vehicle energy consumption and thus **Research Gap 3: an absence of high-fidelity estimates of energy consumption for minibus taxis in SSA**.

Addressing this gap is crucial as it underpins the modeling of numerous other elements in large-scale paratransit electrification. For example, accurate energy consumption data is essential for effectively determining vehicle battery size, assessing grid impacts, calculating fleet emissions, evaluating vehicle payback periods, and designing charging stations. Although Ndibatya and Booysen [46] use economic metrics to estimate minibus taxi drivers profitability-index and and efficiency metrics, the field is missing an assessment of electric versions of current combustion-powered fleets, with appropriate energy consumption estimates.

2.2.3 Charging infrastructure

With a more refined understanding of vehicle energy consumption, the thesis shifts its focus towards the infrastructural requirements necessary to support an electrified paratransit system. A key challenge in this context is the design of charging stations that are both economically viable and resilient, particularly within the context of SSA's unstable energy landscape. Many locations throughout SSA are plagued by a constrained energy supply and load shedding – conditions that significantly complicate the development of sustainable charging infrastructure. Load shedding refers to power outages during which the grid is unable to supply electricity, which would disable EVs from charging from grid-connected charging stations. The load shedding issue is especially persistent in South Africa, where between September 6, 2022 and September 6, 2023, load shedding occurred on 360 out of 365 days [83]. The phenomenon is not strictly localized to South Africa, however, with other countries across SSA as well as regions such as India, Pakistan, Lebanon, and Sri Lanka also commonly experiencing disruptive power outages [84].

Frequent load shedding can significantly increase the value proposition of PV and ES systems at charging stations, as these systems provide a local energy source that enables fleets – or substantial subsets of fleets – to continue charging during blackouts and thus continue normal operations [85]. As a result, PV-ES systems could be pivotal in enhancing the reliability and attractiveness of electrified paratransit in regions plagued by grid instability. For instance, Collett and Hirmer [3] propose a strategy that involves coordinating investments in PV panels at charging stations with the phased adoption of EVs. Complementing PV installations with ES systems, as suggested by Giliomee and Booysen [85], could further alleviate grid strain. Such integrated PV-ES solutions not only reduce grid dependence, but mitigate environmental impact and lower charging costs, thereby improving the financial sustainability of charging infrastructure. Moreover, they enhance energy resilience, a crucial consideration given the frequency of power outages in the region. Overall, hybrid PV and energy storage (ES) systems at charging stations offer a promising solution to alleviate grid dependence, enhance resilience, and maintain operations during power outages [86, 87]. That said, the literature has as of yet failed to provide methodologies to maximize the economic gain from PV and ES investments at charging stations affected by load shedding.

Several studies have investigated the grid implications of PV-ES-CS systems, each contributing insights into different operational modes but often lacking holistic optimization approaches that account for grid constraints, resilience, and economic feasibility. For instance, Singh et al. [86] examine the potential of a PV-wind hybrid system for powering a small shopping mall with an integrated EV charging station, providing valuable insights into how such systems can reduce grid dependence and supply local energy demand. Their work does not account for how frequent load shedding might necessitate system design adaptations. In this context, PV-ES systems could offer substantial benefits by enabling continuous EV charging during grid outages, which would enhance the reliability and appeal of electrified paratransit systems in SSA.

Similarly, Singh et al. [87] develop a grid-tied PV-ES-diesel generator-CS system, ensuring technical functionality in both islanded and grid-connected modes, but this study stops short of optimizing system size for economic performance. This is a notable limitation, as optimizing system size and resource allocation is critical for achieving long-term financial sustainability, particularly in regions with constrained electricity supply. Additionally, the findings of these studies, while promising, focus on small community use, leaving a gap in how such systems can be scaled and optimized for larger, mobile paratransit fleets

Further, Hassoune et al. [88] propose power management strategies for grid-tied PV-ES-CS systems to reduce grid stress during peak demand. Although these strategies are important for improving grid integration, they do not address the unique challenges posed by unreliable grids or how to optimize system configurations in such environments. This omission underscores the need for a more comprehensive approach that incorporates grid reliability as a factor in system design.

Other studies, such as Amrollahi and Bathaee [89], have explored how demand response can enhance the performance of hybrid renewable systems. While demand response strategies are useful, they are often predicated on stable grid conditions and thus fall short of addressing the more pressing issue of grid instability in developing regions. Similarly, Amry et al. [90] analyze the engineering efficiency of a grid-tied PV-flywheel system but do not extend their analysis to scenarios involving frequent grid disruptions, which limits the applicability of their findings to regions like sub-Saharan Africa.

A further limitation of the existing literature is the lack of attention to system resilience. For example, Bakht et al. [91] model a PV-ES-diesel generator system to mitigate load shedding in Pakistan, but they do not apply their model to an EV charging station context, nor do they consider how the resiliency provided by the system could be optimized. This gap is significant, as load shedding is a widespread issue in both Pakistan and sub-Saharan Africa, where the ability to maintain EV operations during outages could greatly enhance the economic viability of electrified paratransit systems.

Additionally, while Zieba Falama et al. [92] design a PV-ES system to reduce load shedding at households in Cameroon, their study does not extend to EV charging stations. This is a crucial gap, given that charging infrastructure for paratransit systems in developing regions must be resilient not only to power outages but also to fluctuating grid availability. As such, there remains a need for studies that integrate grid constraints into the system capacity optimization process, aiming to maximize economic performance while ensuring operational resilience. This leads to **Research Gap 4: the lack of approaches that incorporate electricity supply constraints, particularly grid instability, into the optimization of PV-ES-CS system capacities.**

Moreover, the literature largely overlooks how varying levels of EV penetration will impact the design and performance of charging stations. Studies by Ullah et al. [93] and Ampah et al. [94] consider fleet mix and EV penetration: Ullah et al. [93] investigate the grid and cost impact of a PV-based highway charging station for a mix of large and small EVs. Ampah et al. [94] do a performance assessment for PV-wind-biomass system to charge fleets of 30 and 70 fuel cell electric vehicles in Ghana, however they consider the same system for both fleets. However, their analyses are limited in scope, often assuming full fleet electrification or static fleet sizes. This assumption does not reflect the realities of partial or staged fleet electrification, particularly in regions where financial and manufacturing constraints limit rapid EV deployment. Consequently, there is a clear need for studies that model different EV penetration scenarios and assess their impact on the optimal configuration of PV-ES-CS systems, leading to **Research Gap 5: the lack of studies to analyze the effects of different degrees of fleet EV penetration on PV-ES-CS system feasibility and techno-economic performance**.

2.3 Research gaps

Collectively, the reviewed literature builds a complex but incomplete picture of paratransit electrification. While studies from developed regions provide a robust foundation of knowledge, their limited applicability to SSA due to contextual differences necessitates targeted research in this region. The integration of findings across studies thus not only maps the current landscape but also sharply delineates the urgent research needed to adapt and optimize paratransit electrification strategies for the unique challenges of sub-Saharan Africa. In particular, the literature review has pinpointed five critical gaps in the research, summarized below, which when tackled will address the four research sub-questions identified in Section 1.2.

1. **Research Gap 1: An understanding of paratransit fleet owner/driver perceptions of EVs.** EV adoption intention has been studied all over the world, and has been identified as an important factor in a speedy transition to electric transport. However, due to the absence of electric minibus taxis in SSA, no attempts have yet been made to understand the decision-making processes of paratransit industry constituents. This gap, which may hinder effective interventions, directly links to research sub-question 1. Chapter 3 answers the sub-questions and addresses the gap using survey responses to characterize paratransit owner and driver intentions to adopt EVs when available and the factors that affect adoption intention.

2. **Research Gap 2: Methodologies to construct representative driving cycles for paratransit.** Representative driving cycles are critical for modelling a number of parameters related to vehicle electrification, including energy consumption. Methodologies to construct driving cycles for transport systems in first world countries are heavily developed, yet unsuitable for modelling the unique operating conditions of paratransit vehicles, which are notoriously aggressive. The lack of appropriate methodologies for constructing representative driving cycles for paratransit leads to sub-question 2. Chapter 4 tackles the gap and answers the sub-question by introducing a methodology for developing representative driving cycles for paratransit that includes data transients, and using it construct the first

real-world representative driving cycles for paratransit.

3. **Research Gap 3: High-fidelity estimates of energy consumption for minibus taxis in SSA.** There are issues with attempting to model vehicle energy consumption with low-resolution data. However, primarily due to a lack of high-resolution data, the energy consumption of minibus taxis in SSA has never been modeled at a high fidelity, leading to research sub-question 3. Chapter 5 fills this gap using 1Hz data gathered on taxis traveling around Stellenbosch, South Africa, and validates the representative driving cycle construction methodology developed in Chapter 4. Filling this gap allows for further analysis in Chapter 5 on battery sizing, emissions and grid impact, and vehicle payback period.

4. **Research Gap 4: Techno-economic optimization model that incorporates electricity supply constraints into photovoltaic-energy storage-charging station (PV-ES-CS) sizing problem given fixed demand.** There are significant concerns for vehicle electrification in SSA due to grid constraints such as load shedding. However, there are a lack of approaches in the PV-ES-CS modelling literature that incorporate grid constraints into system techno-economic optimization and design, thus prompting research sub-question 4a. Chapter 6 develops a technoeconomic model that fills this research gap and answers the question, and applies it to a case study of a minibus taxi fleet operating in Johannesburg, South Africa.

5. **Research Gap 5: Analysis of the effects of varying electricity demand on PV-ES-CS system feasibility and techno-economic performance.** Due to capital constraints, some paratransit fleets may only partially electrify, which may affect system feasibility. The effects of varying electricity demand on system feasibility have not been studied before, thus prompting research sub-question 4b. This gap is tackled alongside research gap 4 in Chapter 6.

Only through a process of inquiry leading to an understanding of the complexities of vehicle purchases [...] can [stakeholders] identify relevant touchpoints and design targeted interventions that will help them overcome the remaining barriers to EV purchasing.

— Jana Plananska [32]

3 The Intentions of Paratransit Owners and Drivers to Adopt Electric Vehicles

Chapter 2 identifies a gap in the understanding of paratransit owners and drivers perception of EVs, and the factors influencing their adoption. This chapter addresses the gap by answering the research questions:

- *What are the intentions of paratransit owners and drivers to switch to EVs when they become available?*
- *What are the factors that influence EV adoption intention for paratransit owners and drivers?*

Investigating these questions will set the stage for determining what knowledge and tools will have the greatest impact on electric paratransit adoption intention, thus validating the need for and utility of the research in this thesis.

To accelerate the electrification of the paratransit sector, it is crucial to explore the decision-making processes of vehicle owners and drivers, as they play a central role in this transition. An inadequate understanding of the factors influencing consumer uptake of EVs can actually hamper efforts to promote technology adoption [32]. Avoiding this pitfall is essential, as EV adoption is often constrained by user readiness or social factors, even in markets capable of overcoming material barriers [33]. Without insights into the current perception of EVs among paratransit owners and drivers, it becomes challenging to model the feasibility of EV adoption for fleet owners. Additionally, time and resources could be wasted on interventions that are poorly designed or contextually irrelevant, which may result in market setbacks with technical, economic, and environmental repercussions, particularly in resource-constrained countries in the Global South where swift action is needed to address climate change.

On the positive side, research indicates that consumers in a market system can accelerate technology adoption by advocating for solutions that align with their interests [31]. Therefore, efforts to expedite the transition should prioritize understanding the attitudes and perceptions of vehicle owners and drivers, as this knowledge can guide the creation of targeted policies, incentives, and educational campaigns that drive EV adoption in the paratransit sector in a socially, economically, and environmentally sustainable manner.

As previously mentioned, paratransit is the dominant road transport modality in sub-Saharan Africa [2], significantly influencing local economies and the environment. Although EVs have only recently entered the region, and electric minibuses are not yet available on the market, any serious large-scale attempts to electrify road transport in this region will heavily involve paratransit. However, perceptions of EV capabilities and the global automobile market may differ from those in developed countries, which have been the focus of most studies. Given the unique socio-economic and political contexts of developing nations like South Africa, factors such as grid limitations, access to electricity and charging infrastructure, and cost are likely to be more prominent. Thus, it is critical to study the specific factors influencing EV adoption intentions among those who will purchase and operate these vehicles to inform contextually appropriate policy interventions that promote EV uptake in similar settings.

In this chapter, eleven hypotheses based on consumer behavior theory literature are developed and tested in a structural equation model. The analysis relies on anonymous secondary survey data gathered from 4,452 paratransit owners and drivers in South Africa. Due to the absence of electric minibuses in South Africa, this study, like other studies on EV adoption in geographies with low EV market penetration, focuses on EV adoption intention rather than actual documented purchase behavior [95]. In turn, adoption intention is modelled via latent constructs that are composed of the measured items in the survey.

More detailed information is required on factors that may affect paratransit owner and driver decision making regarding EV adoption. Consequently, the objective of this chapter is to address **Research Gap 1** identified in Chapter 2 by answering the research questions: *What are the intentions of paratransit owners and drivers to switch to EVs when they become available?* and *What are the factors that influence EV adoption intention for paratransit owners and drivers?*.

EV adoption intention is defined here as the survey respondents' answer to the question "You would buy an electric taxi when available". The factors are explored under a novel integrated framework of consumer behavior which combines three established frameworks and extends them with three additional constructs. These extensions increase the predictive power of the final model and enhance the operability of the insights gleaned from the results. Elevent hypotheses about the influence of these constructs on EV adoption intention are formulated and tested via structural equation modeling. By analyzing and thoroughly understanding the relationships between these constructs and EV adoption intention, potential barriers to EV adoption can be identified and addressed with targeted interventions that facilitate the uptake of electric paratransit vehicles in South Africa and provide a platform for similar interventions to take place around sub-Saharan Africa. The effectiveness of the interventions can be measured in the future based on the benchmark of EV adoption intention provided here.

The rest of the chapter is structured as follows: First, Section 3.1 provides theoretical background and walks the reader through the analytical framework employed in this study. Next, Section 3.2 describes the methodologies used for survey data collection and statistical analysis. Section 3.3 describes the survey sample and presents the results of the structural equation modeling analysis. Section 3.4 discusses key takeaways and implications for promoting the adoption of electric minibus taxis in South Africa. Finally, Section 3.5 concludes with a summary of the main findings and contributions of the chapter and suggests directions for future research.

3.1 Theoretical background and analytical framework

Many theoretical frameworks for modeling consumer behavior related to EV adoption intention are discussed in the literature [40, 96], including the theory of Automobility [97], Actor Network Theory [98], the Motivation Model [99], the Theory of Planned Behavior (TPB) [100], the Norm Activation Model (NAM) [101], the Technology Acceptance Model (TAM) [102], and the Unified Theory of Acceptance and Use of Technology [103]. It is common in consumer behavior literature to select elements from different frameworks and combine them for a more integrated approach. For example, Sovacool [104] proposes a framework for EV adoption that blends aspects of Automobility, Actor Network Theory, and the Unified Theory of Acceptance and Use of Technology, based on expert interviews. The benefit of this integrated approach is that it can bridge gaps where a single theory might fall short.

This analytical framework incorporates elements from the three most common frameworks used to model EV adoption intention: TPB, NAM, and TAM. The following section provides an overview of TPB, NAM, and TAM, and explains the framework and hypothesis development for this study.

TPB is widely used in studies assessing EV adoption intention [38, 105, 106, 107, 108, 109], making it the most frequently employed framework for this purpose [40]. It is also one of the most prominent theories in consumer behavior research overall and is recognized as one of the most comprehensive theories in the study of pro-environmental behavior [36, 110, 111]. TPB posits three psychological predictors of behavioral intention:

1. Attitude: A personal assessment of the behavior.
2. Behavioral control: The individual's ability to perform the behavior.
3. Subjective norms: Beliefs about how reference groups view the behavior.

These predictors are based on personal interest, which positions TPB as an individual rational choice model grounded in consumers' internal cost-benefit analyses [112].

NAM helps explain how social norms and personal values drive pro-social behavior. In modeling EV adoption, NAM is used to assess how personal values (such as environmental concern) and social norms influence attitudes toward EVs and, consequently, EV adoption intention [35, 36, 113, 114, 115].

TAM provides a framework for understanding how individuals perceive and adopt new technologies, and it is widely applied in EV adoption studies [116, 117, 118]. TAM identifies two main determinants of a user's intention to use technology: perceived usefulness (e.g., benefits of an EV over a traditional internal combustion engine vehicle) and perceived ease of use (how easily users believe they can operate an EV).

In summary, TPB emphasizes self-interest, while overlooking morality; NAM focuses on pro-social behavior, neglecting self-interest; and TAM addresses technological factors, disregarding environmental concerns. All three models suggest that intention predicts behavior, meaning that intention mediates the relationship between constructs in each model and the resulting behavior (in this case, EV adoption). While each framework is valuable for modeling EV adoption intention, none are complete. TAM and TPB do not examine the personal standards that drive behavior, which is NAM's strength. However, NAM lacks a consideration of behavioral control factors (present in TPB) that can influence consumer behavior [119].

3.1.1 Hypothesis development

It is proposed that the factors highlighted in the Theory of Planned Behavior (TPB), Norm Activation Model (NAM), and Technology Acceptance Model (TAM) will influence EV adoption intention among paratransit owners and drivers, with two notable exceptions. First, as the sample comes from a market where few, if any, consumers have direct experience with EVs, this study aligns with the approach in [110] by omitting perceived ease of use from TAM. Second, subjective norms from TPB, which refer to perceived social pressure to adopt a behavior, are also excluded. Subjective norms may not always be relevant in the context of technology adoption intent [100], and for paratransit owners and drivers operating in economically constrained conditions, the decision to adopt EVs is likely to be based on personal evaluations of the technology's fit with their individual standards and business needs. As a result, subjective norms are excluded from the modeling in this study.

Along with the exclusion of perceived ease of use and subjective norms, the integrated TPB, NAM, and TAM framework is extended with three additional constructs. Research has shown that additional factors can significantly influence EV adoption intention, making it appropriate to extend existing models to enhance their predictive power [108, 120]. In paratransit, incumbent ICE vehicles often have numerous issues due to being second-hand, aging, heavily used, and poorly maintained. It is therefore hypothesized that both Perception of ICE Costs (PIC) and Perception of ICE Reliability (PIR) will impact EV adoption intention. Furthermore, it is posited that a more positive perception of the availability of EVs, coupled with the decreasing availability of ICE vehicles in the future, would be associated with increased readiness and intention to adopt EVs, as they are seen as not only more accessible but also more viable. This construct is referred to as Perception of Automobile Market Trends (PAM). These additions to the framework are designed to enhance its predictive capabilities, and because they relate to straightforward and relevant knowledge, the insights gained from incorporating them could help guide targeted interventions aimed at promoting EV adoption among paratransit owners and drivers.

In conclusion, this study draws upon constructs from three widely recognized consumer behavior theories—TPB, NAM, and TAM—that have frequently been used to model EV adoption intention. The relevant constructs are Perceived Usefulness (PU) and Perceived Behavioral Control (PBC) from TPB, and Personal Norms (PN) from NAM. In the research framework, PU is modeled as a higher-order factor of Perception of Cost (POC) and Perceived Behavioral Control (PBC), while PN is represented as a higher-order factor of Risk Perceptions (RP) and Environmental Considerations (EC). These constructs are integrated into a single framework and further extended with three additional factors: Perception of ICE Costs (PAC), Perception of ICE Reliability (PIR), and Perception of Automobile Market Trends (PAM). These constructs were chosen to create the most comprehensive model possible, supported by literature, that can be analyzed in a way that yields actionable insights.

The hypotheses regarding these constructs are as follows:

Hypothesis 1 (H1):

Positive impact of Perceived Usefulness (PU) on EV Adoption Intention (INT).

PU relates to an individual's belief that adopting a particular technology will enhance their performance [102]. It has been identified as a key driver of purchase behavior in previous research [121]. Prior studies have consistently demonstrated a positive correlation between PU and INT [117, 122]. This hypothesis is adopted here, especially considering that investment decisions in competitive markets like paratransit naturally prioritize the utility derived from such investments.

In this study, PU is structured as a higher-order construct, incorporating Perception of Cost (POC) and Perceived Behavioral Control (PBC) from TPB. Based on previous findings on factors like cost and range anxiety influencing EV adoption [31, 38, 123], this study proposes that these factors not only indirectly influence EV adoption intention but also have a direct impact, leading to two separate hypotheses for POC and PBC:

Hypothesis 2 (H2):

2a: *Positive impact of Perception of Costs (POC) on PU.*

2b: *Positive impact of POC on INT.*

Cost and pricing are widely acknowledged as barriers to EV adoption [123, 124]. In some cases, a reduction in prices is believed to facilitate mass EV adoption [31]. Since paratransit is a highly competitive industry, cost may be the most critical factor for operators when deciding whether to transition to an electric alternative to their current vehicles.

Hypothesis 3 (H3):

3a: *Positive impact of Perceived Behavioral Control (PBC) on PU.*

3b: *Positive impact of PBC on INT.*

PBC refers to an individual's belief in their ability to control a particular behavior [100]. Concerns about the availability of charging stations are a significant deterrent for potential EV adopters [125, 126], and a paratransit vehicle's usefulness is closely tied to its ability to complete routes efficiently. Many studies have demonstrated that PBC affects INT [38, 105, 106, 107, 108, 109], and in this context, it is hypothesized that PBC's influence on INT is primarily mediated by perceptions of the usefulness EVs can provide.

Hypothesis 4 (H4):

Positive impact of Personal Norms (PN) on INT.

PN refers to an individual's internalized principles that influence behavior in particular situations. These norms play a crucial role in decision-making processes [101]. Previous studies have found a strong positive relationship between PN and INT [35, 36, 127], and it is anticipated that this relationship will hold in this context as well.

Similar to PU, PN is modeled as a higher-order construct, which includes environmental considerations and risk perceptions:

Hypothesis 5 (H5):

Positive impact of Environmental Considerations (EC) on PN.

EC reflects the extent to which awareness of environmental issues elicits concern in individuals regarding the impact of their behavior on the environment. Numerous studies conducted across various countries have examined EC's effect on the public's intention to adopt EVs [128, 129, 130, 131, 132, 133]. While some studies found EC to be a significant factor in predicting purchase intent [130], others did not [106, 134]. Despite this, the consensus in the literature suggests that EC has a positive effect on INT, and this study follows that understanding.

Hypothesis 6 (H6):

Positive impact of Risk Propensity (RP) on PN.

RP refers to an individual's willingness to take risks. Risk aversion to new technologies has been used to model the adoption of EVs [33, 124, 135, 136]. As with EC, there are mixed results, with some studies indicating significant effects [136], while others did not [33]. It is hypothesized that individuals who are more risk-tolerant are more inclined to adopt EVs, as they are still a relatively new technology and may be perceived as riskier than familiar ICE vehicles.

Hypothesis 7 (H7):

Negative impact of Perception of ICE Costs (PIC) on INT.

This hypothesis is analogous to H2 for ICE vehicles. The decision to switch to an electric paratransit vehicle is primarily a business decision, and as highlighted in H1, perceptions of EV costs play a critical role in this decision. However, the costs of new technology are always relative to the costs of the technology being replaced. Several studies have shown that cost savings and fuel efficiency from switching to EVs are significant factors in consumer evaluations [95]. Therefore, this study includes PIC and hypothesizes that a more favorable view of ICE costs will negatively affect INT.

Hypothesis 8 (H8):

Negative impact of Perception of ICE Reliability (PIR) on INT.

PIR refers to how reliable and safe individuals perceive their current ICE-powered vehicles to be. Consumer perceptions of vehicle safety, reliability, and performance have been shown to affect EV adoption [133, 137, 138]. Given the aging and poorly maintained nature of many paratransit vehicles, it is hypothesized that paratransit operators dissatisfied with the reliability of their ICE vehicles will be more inclined to switch to EVs. Conversely, those with positive views of their current vehicles' reliability may be more reluctant to make the switch.

Hypothesis 9 (H9):

Negative impact of Perception of Automobile Market Trends (PAM) on INT.

PAM relates to an individual's view of how quickly EVs will become available and ICE vehicles will become obsolete. It reflects perceptions of current and future market dynamics and consumer preferences. As EVs become more accessible and ICE vehicles less available, consumers may increasingly view EVs as a practical option. It is hypothesized that paratransit operators who are optimistic about the EV market and pessimistic about the ICE market will be more inclined to adopt EVs.

3.1.2 Hypothesized framework of consumer behavior

Based on the preceding literature review and hypothesis development, Figure 3.1 illustrates the structure of the proposed framework or model designed to analyze EV adoption intention among paratransit owners and drivers. In summary, the model incorporates the direct effects of factors such as perception of cost (POC), perceived behavioral control

(PBC), perceived utility (PU), personal norms (PN), perception of ICE costs (PIC), perception of ICE reliability (PIR), and perception of automobile market trends (PAM) on EV adoption intention (INT). It also accounts for the indirect effects of POC and PU on INT through PU, as well as the indirect effects of environmental considerations (EC) and risk perceptions (RP) on INT via PN. Additionally, socio-demographic factors such as gender, age, location, region, education level, and occupation are included in the model as control variables. This comprehensive and extended framework aims to provide a thorough understanding of the various factors that influence EV adoption intention in paratransit operators. Insights derived from the model can serve as valuable guidance for policymakers and researchers working on developing effective strategies to encourage EV adoption within the taxi driver community.

Given that electric paratransit vehicles are currently non-existent in South Africa, it is not feasible to include prior EV experience as a variable in the model at this time. However, prior EV experience has been shown to have a significant impact on EV adoption intention [95, 109, 139], suggesting that studying prior EV experience will be crucial for future growth of the electric paratransit market and the development of targeted interventions for these groups. As such, Figure 3.1 also demonstrates how the proposed framework can evolve in future research, once data on electric paratransit vehicle purchases and usage become available, to evaluate the influence of prior EV experience on adoption intention and behavior within this population.

3.2 Methodology

3.2.1 Measurement and construct development

To obtain feedback from the paratransit industry, an online survey was developed using Microsoft Teams. Initially, it was distributed across various social media platforms, but this approach resulted in limited responses. Consequently, field workers were sent to taxi ranks in and around Cape Town, Western Cape, to gather responses in person. The field workers collected data over a 4-week period. Tablets were used to collect responses, and each survey took about 10 minutes. Incomplete questionnaires were not saved to the database.

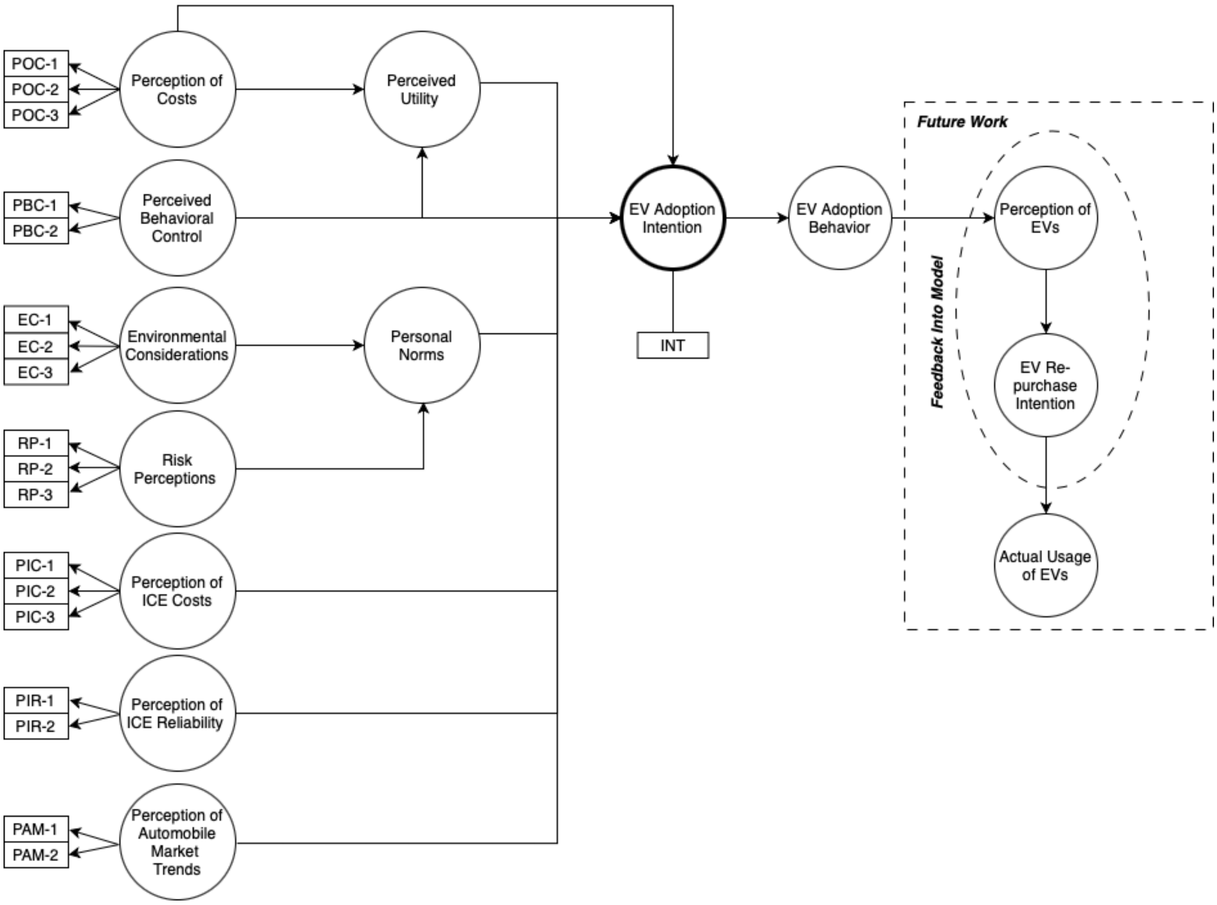

Figure 3.1: Nomological network of the theoretical framework used to model EV adoption intention in this study. Measured items are encapsulated in rectangles and latent constructs in circles. Arrows designate regression pathways. The figure shows how this study sets up future work in a dashed box on the right.

The thesis author's involvement in data collection was limited to abstract conceptualization of questions before there were plans to initiate any surveys. Beyond this, the author of this thesis was not involved in any way with data collection nor questionnaire design. These steps were carried out by the co-authors of Hull et al. [140] at the University of Stellenbosch and University of Cape Town, who shared the data with the thesis author after the fact. Ethics clearance was granted by University of Cape Town, through the Faculty of Commerce, application number REC 2022/10/014. For further details, the author refers the reader to the data-in-brief article published here: `https://www.sciencedirect.com/science/article/pii/S2352340924000982#sec0007` [140].

In the demographic section of the survey, participants were asked about their gender, age, whether they live in an urban or rural setting, their region or province, income level,

Table 3.1: The measurement items composing the constructs of the theoretical framework.

Construct	Code	Question
Perception of Costs	POC-1	To charge an electric taxi will be expensive
	POC-2	To buy an electric taxi will be expensive
	POC-3	To service an electric taxi will be expensive
Perceived Behavioral Control	PBC-1	You are worried that there won't be enough charging stations?
	PBC-2	Load shedding and electricity power outages will impact your operations
Environmental Considerations	EC-1	The taxi industry should reduce its environmental impact
	EC-2	Electric taxis will help lessen the environmental impact caused by the taxi industry
	EC-3	Climate change is a serious issue
Risk Perceptions	RP-1	You describe yourself as someone who has a lot of trust in other people and institutions in general
	RP-2	You describe yourself as someone who generally trusts new technologies
	RP-3	You describe yourself as someone who often takes risks
Perception of ICE Costs	PIC-1	The fuel for petrol and diesel taxis is expensive
	PIC-2	To buy a petrol or diesel taxis is expensive
	PIC-3	To service a petrol or diesel taxis is expensive
Perception of Ice Reliability	PIR-1	Petrol and diesel taxis are safe
	PIR-2	Petrol and diesel taxis are reliable
Perception of Auto. Market	PAM-1	In how many years from now will it be possible to buy an electric vehicle?
	PAM-2	In how many years from now will it no longer be possible to buy a petrol or diesel vehicle?
EV Adoption Intention	INT	You would buy an electric taxi when available

and whether they drive taxis, own them, or both.

To measure the latent constructs within the theoretical framework, respondents provided answers on a Likert scale ranging from 1 (strongly disagree) to 5 (strongly agree), with the exception of the perception of automobile market trends (PAM), which used a numerical scale. The PAM scale was designed to capture participants' estimates of how many years they believe it will take for an EV transition to occur. The measurement items for each construct were consistently scaled to facilitate factor analysis for structural equation modeling. Details of the measurement items for each construct can be found in Table 3.1.

3.2.2 Statistical analysis

After gathering descriptive statistics on the socio-demographic characteristics of the sample (Section 3.3.1), the structural equation model is evaluated. Structural equation modeling follows a two-step process. First, the measurement model for the latent constructs is assessed for reliability and validity (Section 3.3.2.1) using confirmatory factor analysis (CFA). After this, the structural model is estimated based on the model illustrated in Figure 3.1 (Section 3.3.2.2). As previously mentioned, the perceived utility (PU) construct was developed as a higher-order factor, combining perception of cost (POC) and perceived behavioral control (PBC) to capture their shared variance. Similarly, personal norms (PN) were derived from environmental considerations (EC) and risk perceptions (RP). EV adoption intention (INT) was then modeled using POC, PBC, PU, PN, perception of ICE costs (PIC), perception of ICE reliability (PIR), and perception of automobile market trends (PAM).

As noted in a recent literature review by Bryla et al. [40], structural equation modeling and confirmatory factor analysis are the two most commonly employed methods in EV adoption research. Other frequently used approaches include stated preference choice experiments and random utility modeling. Stated preference methods are useful for assessing willingness to pay in new scenarios, while random utility modeling is better suited for modeling discrete choices and preferences. However, structural equation modeling has several advantages over these approaches: 1) it enables the testing of complex theoretical models with multiple pathways and feedback loops, 2) it incorporates multiple measures for each variable within distinct latent constructs, reducing multicollinearity and improving reliability and validity, and 3) it allows for the testing of mediating and moderating effects, which helps to uncover how variables interact to influence outcomes. Additionally, SEM provides an intuitive visual representation, making it easier to convey the model graphically rather than through a series of equations with potentially complex notation. For example, the model in Figure 3.1 represents the mathematical equations used in the modeling process, which are solved simultaneously to fit the model and estimate parameters. These results can be visualized in Figure 3.4.

Despite its advantages, structural equation modeling has some limitations: 1) it assumes that the measured variables follow a multivariate normal distribution, 2) it cannot establish causality and requires supporting evidence for causal claims, 3) careful specification of the model is necessary to avoid biased parameter estimates, and 4) SEM models can be complex, making the interpretation of results more challenging. In other words, while SEM is a powerful tool, its complexity requires that the inquiry be carefully guided by theory [141].

A stepwise hierarchical regression approach was also considered to answer the second research question of this chapter and determine which factors are most predictive of EV adoption intention. Stepwise hierarchical regression is another commonly used method for modeling EV adoption intention in the literature [40, 142], and it could have been used to model variables that were measured on entirely different scales. However, given the complex relationships between predictors and the target variable in this study, a hypothesis-driven approach based on a priori assumptions was preferred. This method involves selecting variables and constructs based on theoretical and empirical considerations, rather than purely on statistical significance, making it more appropriate for hypothesis testing. Stepwise regression is more exploratory in nature and is not ideal for testing complex models like the one used in this study, as it can lead to model overfitting. In contrast, structural equation modeling allows all variables and constructs to be modeled simultaneously, with maximum likelihood estimation techniques used to account for relationships between variables.

After considering the strengths and limitations of different analytical methods commonly employed in EV adoption research to test the eleven research hypotheses, as suggested by Sovacool et al. [141], structural equation modeling was selected. SEM provides a more comprehensive and nuanced understanding of the relationships between constructs and offers more accurate estimates of the effects of various predictors on the outcome of interest.

3.3 Results

In this section, descriptive statistics are presented, starting with an overview of the responses to the question, “You would buy an electric taxi when available," which addresses the first research question of the chapter. Following this, the results from the structural model are analyzed to explore the factors influencing survey respondents' EV adoption intentions, addressing the second research question.

3.3.1 Descriptive statistics

A total of 5,703 respondents participated in the survey. 93 respondents were filtered out either for providing inconsistent answers to questions that were asked twice, or filling out nonsensical responses. Of the 5,610 remaining, 398 did not specify their occupation, and 760 indicated they were not interested in purchasing any taxi, leaving 4,452 eligible respondents for analysis. Table 3.2 provides a breakdown of the respondents' socio-demographic characteristics. The vast majority of drivers were male and from the Western Cape province. Most respondents fell within the 35-44 and 45-54 age groups and had not completed Grade 12 (high school) education. The sample was relatively evenly split between those living in urban and rural environments, with a slight majority from rural areas. Additionally, drivers made up 89.4% of the sample, with owners and driver-owners representing 7.8% and 2.8%, respectively. This is reflective of the high cost of paratransit vehicles, which are a significant business investment typically accessible to wealthier individuals who own multiple taxis, resulting in more drivers than owners in this industry.

One limitation of the study is the homogeneity of the sample, with almost all participants coming from the Western Cape region of South Africa (98%). Therefore, the generalizability of the study's findings may be limited. Future research could investigate factors influencing EV adoption in other regions to assess the transferability of these findings across different contexts.

Figure 3.2 presents the responses to the question, "You would buy an electric taxi when available" (INT). Notably, drivers were the least likely to express interest, while owner-drivers and owners were more neutral on the subject. They seemed more inclined to wait and see whether electric taxis prove to be more profitable than internal combustion engine (ICE) taxis before making a firm decision. This could be attributed to their greater experience as business owners, leading them to approach the transition to EVs as a pragmatic business decision, primarily focused on profitability. On the other hand,

Table 3.2: Descriptive statistics of the sample (n = 4,452).

Variable	Frequency	Percent (%)
Gender		
Male	4417	99.2
Female	35	0.8
Age		
18 - 24	98	2.2
25 - 34	915	20.6
35 - 44	1998	44.9
45 - 54	1231	27.7
55 - 65	187	4.2
65+	23	0.5
Location		
City/Urban	2092	47.0
Rural	2360	53.0
Region		
Western Cape	4376	98.3
Other	76	1.7
Education		
Under Grade 12	2849	64.0
Grade 12	1372	30.8
Any Tertiary	231	5.2
Occupation		
Driver	3978	89.4
Owner	349	7.8
Driver-Owner	125	2.8

drivers may base their decision on factors like vehicle reliability, which directly impacts their personal safety. The results of the structural equation model (Section 3.3.2.2) provide further support for these interpretations.

Overall, the sample was not particularly enthusiastic about EV adoption. While 38% of the respondents strongly agreed or agreed that they would purchase an EV when available, 47% disagreed or strongly disagreed, and 15% were neutral. This places the sample in the “Early Majority" phase of the technology adoption curve [143], suggesting that while the “Early Adopters" stage (around 16% user acceptance) has been surpassed, there is still room for targeted interventions to increase EV adoption among paratransit owners and owner-drivers.

The means, medians, modes, and standard deviations of the explanatory constructs within the research framework are provided in Table 3.3 and visualized in Figure 3.3 for ease of comparison. Although some researchers argue that calculating the mean for ordinal Likert scale values is inappropriate, it can still offer a quick and simple estimate of the

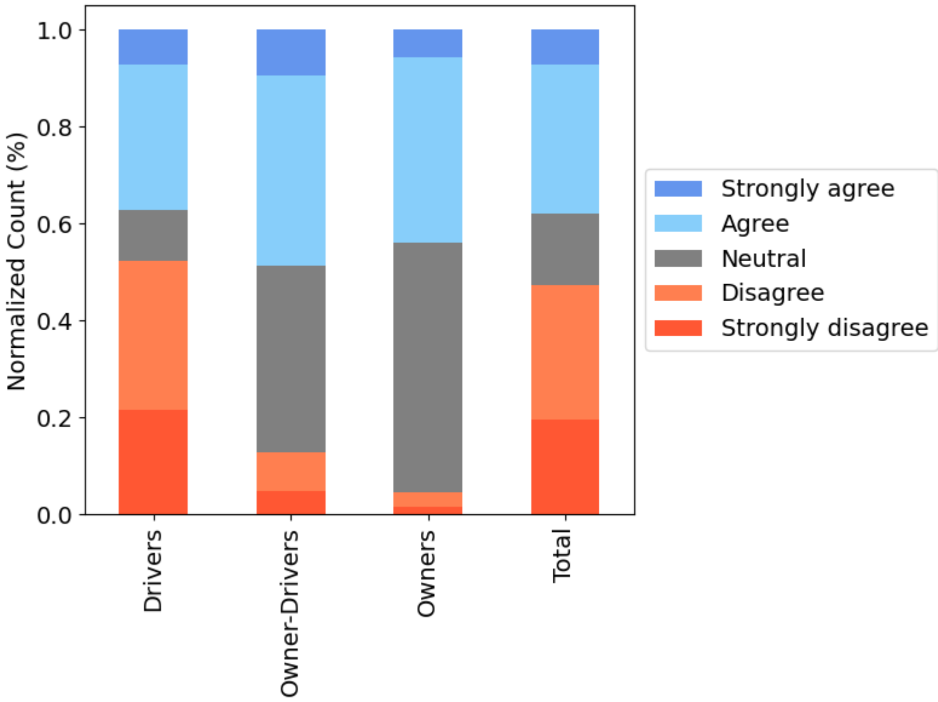

Figure 3.2: Distributions of indications of EV adoption intention by occupation (driver, owner-driver, owner) and the aggregate for the sample (total).

central tendency, which can be helpful in gauging the overall sentiment or attitude within the group of respondents. These preliminary results suggest that negative perceptions of costs (POC) and perceived behavioral control (PBC) may act as barriers to EV adoption, while the generally positive views on ICE reliability and safety, as reflected in the perception of ICE reliability (PIR), may reinforce this reluctance. Both risk perceptions (RP) and environmental considerations (EC)—the constructs that make up the higher-order factor personal norms (PN)—scored relatively high, indicating strong personal norms that could potentially influence respondents' intention to adopt EVs.

Perceptions of automobile market trends (PAM) are not included in Figure 3.3 because, as mentioned in Section 3.2.1, they were measured on a different scale. The mean values for PAM suggest a slightly pessimistic outlook on the global EV market, with respondents predicting that EVs will become widely available in approximately eight years, even though they are likely to be available sooner. Lastly, the relatively high standard deviation for EV adoption intention (INT), compared to its moderately low mean, indicates that there may be considerable potential in identifying factors that account for this variance.

Table 3.3: Means, medians, and standard deviations of the measured items in each construct.

Construct	Item	Mean	Median	Mode	Std. Dev
Perception of Cost	POC-1	2.04	2	2	0.87
	POC-2	1.94	2	2	0.79
	POC-3	2.04	2	2	0.84
Perceived Behavioral Control	PBC-1	1.84	2	2	0.96
	PBC-2	1.79	2	2	1.09
Environmental Considerations	EC-1	3.59	4	4	0.99
	EC-2	3.58	4	4	0.82
	EC-3	3.62	4	4	0.80
Risk Perceptions	RP-1	3.52	4	4	0.85
	RP-2	3.26	4	4	0.87
	RP-3	3.56	4	4	0.84
Perception of ICE Costs	PIC-1	1.87	2	2	0.72
	PIC-2	1.92	2	2	0.71
	PIC-3	2.19	2	2	0.96
Perception of ICE Reliability	PIR-1	4.02	4	4	0.68
	PIR-2	4.10	4	4	0.64
Perception of Auto. Market	PAM-1*	8.24	8	8	4.53
	PAM-2*	10.74	11	11	3.81
EV Adoption Intention	INT	2.78	3	3	1.21

A higher score for each factor indicates the following:
POC: More favorable perception of EV costs
PBC: Greater perceived behavioral control
EC: Greater concern for the environment
*RP:*Greater tolerance for risk
PIC: More favorable perception of ICE costs
PIR: More favorable perception of ICE reliability
PAM: More favorable perception of automobile market trends for EVs
* *PAM* is measured in years whereas other items are measured on a Likert Scale (1-5)

For clarity in the data analysis and presentation of results, the responses for POC and PBC were measured on a negative index, meaning higher scores reflect more favorable perceptions of EV costs and greater perceived behavioral control, respectively. This approach was used to enhance the interpretability of the findings, particularly in relation to the hypotheses discussed in Section 3.1.1. An explanation of the relative index for each construct is provided in the notes of Table 3.3.

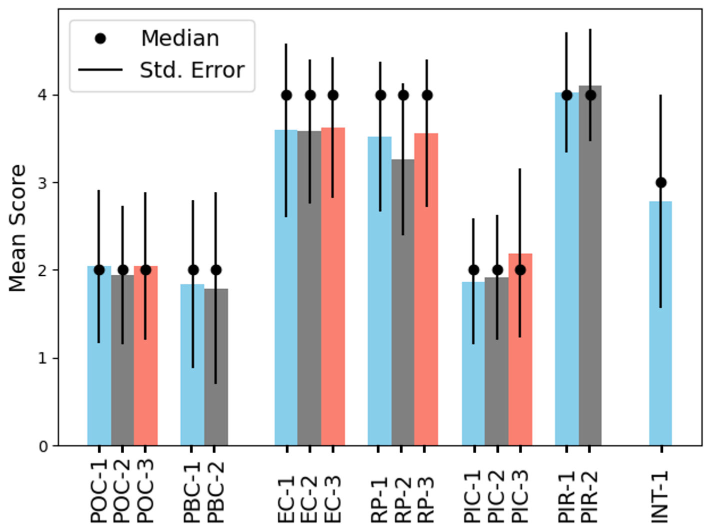

Figure 3.3: A visual representation of Table 3.3 to more easily compare the constructs. Mean (bar), median (dot), and std. deviation (error bar) of the score for each item in each construct in the survey that was measured on the Likert Scale. From left to right: Perception of Costs (POC), Perceived Behavioral Control (PBC), Environmental Considerations (EC), Risk Perceptions (RP), Perception of ICE Costs (PIC), Perception of ICE Reliability (PIR), and EV Adoption Intention (INT). Perception of Automobile Market Trends (PAM) is left out due to different measurement scale

3.3.2 Structural equation modeling

In this section, the results of the structural equation modeling are presented. Structural equation modeling follows a two-step process. First, the reliability and validity of the measurement model are assessed through confirmatory factor analysis (Section 3.3.2.1). Second, the relationships between the constructs in the model and the target variable are estimated using the structural model (Section 3.3.2.2).

3.3.2.1 Measurement model

Before conducting confirmatory factor analysis, it is necessary to ensure that the data is suitable for factor analysis through the Kaiser-Meyer-Olkin (KMO) test and Bartlett's test of sphericity.

The KMO test (eq. 3.1) measures the adequacy of the sampling for factor analysis by assessing the correlation between each variable and the other variables in the dataset. Specifically, the test statistic KMO is computed as the ratio of the sum of squared correlations r_{jk}^2 between pairs of variables j and k to the sum of squared correlations plus the sum of squared partial correlations p_{jk}^2. The test produces a value between 0 and 1, where values closer to 1 indicate that the dataset is appropriate for factor analysis, and values closer to 0 suggest that it is not. The model passes the KMO test with a value of 0.84, exceeding the 0.65 threshold established in the literature [144, 145].

$$KMO = \frac{\sum \sum_{j \neq k} r_{jk}^2}{\sum_{j \neq k} r_{jk}^2 \sum_{j \neq k} p_{jk}^2} \tag{3.1}$$

Bartlett's test of sphericity (eq. 3.2) tests the null hypothesis that the correlation matrix of the variables in the dataset is an identity matrix, meaning the variables are uncorrelated. The test statistic χ^2 is computed using the total sample size N, the number of groups k, the individual sample sizes n_i, and the sample variances S_i^2. The pooled variance estimate S_p^2 is also incorporated to assess the homogeneity of variances across groups.

If the p-value associated with χ_B^2 is below the significance level (e.g., 0.05), the null hypothesis is rejected, indicating that the variables are correlated, making factor analysis appropriate [145]. Bartlett's test of sphericity is passed with a significance level of $p < 0.05$.

$$\chi_B^2 = \frac{(N-k)\ln(S_p^2) - \sum_{i=1}^{k}(n_i - 1)\ln(S_i^2)}{1 + \frac{1}{3(k-1)}\left(\sum_{i=1}^{k}\left(\frac{1}{n_i - 1}\right) - \frac{1}{N-k}\right)} \tag{3.2}$$

Following these preliminary tests, confirmatory factor analysis is carried out to evaluate the overall reliability and validity of the measurement model. This analysis examines the relationships between the measured variables (MVs) and the latent variables (LVs) to determine if the observed data supports the theoretical model. The confirmatory factor analysis focuses on two types of validity: convergent and discriminant validity. Convergent validity assesses the degree to which factors on the same scale measure the same underlying construct, while discriminant validity ensures that a measure captures only what it is intended to, distinguishing itself from unrelated constructs.

The following metrics were used to assess convergent validity: factor loading (λ), Cronbach's alpha, average variance extracted (AVE), and composite reliability. Table 3.4 shows the results of the convergent validity analysis.

Factor loading indicates the strength of the relationship between each observed variable and the corresponding latent variable. A factor loading value above 0.70 is required to confirm internal consistency reliability for the constructs [146]. Factor loadings (λ)

are computed as follows, where ξ is the latent construct, X is the observed variable, and σ_X is the standard deviation of X. In this model, the factor loadings range from 0.83 to 0.95, exceeding the threshold.

$$\lambda = \frac{\mathrm{cov}(\xi, X)}{\sigma_X} \tag{3.3}$$

Cronbach's alpha assesses the degree to which a set of items measures a single underlying construct [147]. The generally accepted threshold is 0.70. However, if Cronbach's alpha is below 0.70 but the average variance extracted (AVE) is greater than 0.50, it is still acceptable to retain the factor in the model [146]. In this case, PAM falls below the Cronbach's alpha threshold but meets the AVE requirement, so it remains in the model. It is calculated with equation 3.4, where k is the number of items, σ_i^2 is the variance of each item, and σ_T^2 is the total variance of the scale.

$$CA = \frac{k}{k-1}\left(1 - \frac{\sum \sigma_i^2}{\sigma_T^2}\right) \tag{3.4}$$

Average variance extracted (AVE) measures the proportion of variance explained by the construct in relation to variance due to measurement error. Values above 0.50 are considered acceptable, as they indicate that the construct explains more variance than can be attributed to measurement error [147]. All items in the model meet the 0.50 AVE threshold. AVE is computed via equation 3.5, where λ_i represents standardized factor loadings, and k is the number of items.

$$AVE = \frac{\sum \lambda_i^2}{k} \tag{3.5}$$

Composite reliability estimates the proportion of true score variance relative to measurement error in a set of items. The threshold for acceptability is 0.70 [148], and all constructs in the model pass this threshold.

Overall, the results from the confirmatory factor analysis indicate that the measurement model is reliable and valid for further assessment. It is given in equation 3.6, where λ_i are the standardized factor loadings, and θ_i denotes the error variances of the items.

Table 3.4: Confirmatory factor analysis of measurement model (CA = Cronbach's Alpha, AVE = Average Variance Extracted, CR = Composite Reliability).

Construct	Item	λ	CA	AVE	CR
Perception of Cost	POC-1	0.89	0.83	0.84	0.94
	POC-2	0.95			
	POC-3	0.91			
Perceived Behavioral Control	PBC-1	0.88	0.78	0.78	0.88
	PBC-2	0.88			
Environmental Considerations	EC-1	0.95	0.84	0.84	0.94
	EC-2	0.91			
	EC-3	0.89			
Risk Perceptions	RP-1	0.91	0.71	0.79	0.92
	RP-2	0.86			
	RP-3	0.90			
Perception of ICE Costs	PIC-1	0.90	0.73	0.81	0.93
	PIC-2	0.95			
	PIC-3	0.84			
Perception of ICE Reliability	PIR-1	0.90	0.85	0.82	0.90
	PIR-2	0.90			
Perception of Automobile Market Trends	PAM-1	0.83	0.36	0.69	0.82
	PAM-2	0.83			

Factor loading (λ) threshold ≥ 0.70. [146]
Cronbach's Alpha threshold ≥ 0.70. [146]
Average Variance Extracted threshold ≥ 0.50. [147]
Composite Reliability threshold ≥ 0.70. [148]

$$CR = \frac{\left(\sum \lambda_i\right)^2}{\left(\sum \lambda_i\right)^2 + \sum \theta_i} \tag{3.6}$$

The Heterotrait-Monotrait (HTMT) ratio is a metric used to evaluate discriminant validity in structural equation modeling. Essentially, it measures the similarity between latent constructs. It is calculated by taking the square root of the average variance extracted (AVE) for each construct and dividing it by the correlation between those constructs. To ensure discriminant validity between any two constructs, HTMT values should be below 0.85 [149]. The results of the HTMT analysis are shown in Table 3.5, confirming that discriminant validity is established for all constructs.

Table 3.5: Discriminant validity test Heterotrait-Monotrait ratio.

Construct	POC	PBC	EC	RP	PIC	PIR	PAM
Perception of Cost	–	–	–	–	–	–	–
Perceived Behavioral Control	0.72	–	–	–	–	–	–
Environmental Considerations	0.17	0.14	–	–	–	–	–
Risk Perceptions	0.12	0.05	0.70	–	–	–	–
Perception of ICE Costs	0.46	0.31	0.41	0.38	–	–	–
Perception of ICE Reliability	0.48	0.16	0.44	0.20	0.62	–	–
Perception of Automobile Market	0.00	0.19	0.08	0.24	0.10	0.10	–

3.3.2.2 Structural model

The structural model was estimated using the *semopy* package in Python [150], utilizing the Sequential Least Squares Programming (SLSQP) solver, which is particularly suited for problems involving many constraints. The Wisehart Maximum Likelihood (MLW) objective function was used. Socio-demographic variables were included to control for their influence on EV adoption intention and to analyze their impact on EV adoption.

Table 3.6 and Figure 3.4 present the standardized parameter coefficient estimates from the model along with the results of the hypothesis testing. The path coefficients show the strength and direction of relationships between the latent constructs and the target variable. Standardized coefficients allow for easier comparison of the relative strengths of these relationships [109].

Unlike traditional statistical methods, structural equation model fit cannot be judged solely by one parameter [151]. Therefore, multiple fit indices were calculated, including the Comparative Fit Index (CFI = 0.92), Goodness of Fit Index (GFI = 0.91), Normed Fit Index (NFI = 0.91), Tucker-Lewis Index (TLI = 0.90), and the root mean square error of approximation (RMSEA = 0.052). All of these fit indices—CFI, GFI, NFI, and TLI—surpass the acceptable threshold of 0.90, while the RMSEA falls well below the threshold of 0.08 [152]. Overall, these indices indicate a satisfactory model fit. The commonly used χ^2 (likelihood ratio) test is not applied here. This test, which examines the difference between the covariance matrices of the sample and the fitted model, tends to favor smaller samples and can be misleading, as it assumes that an exact fit is achievable, even when a model accounts for the primary sources of covariance in the data [151, 153, 154, 155]. Furthermore, small samples tend to yield poor parameter estimates [156, 157],

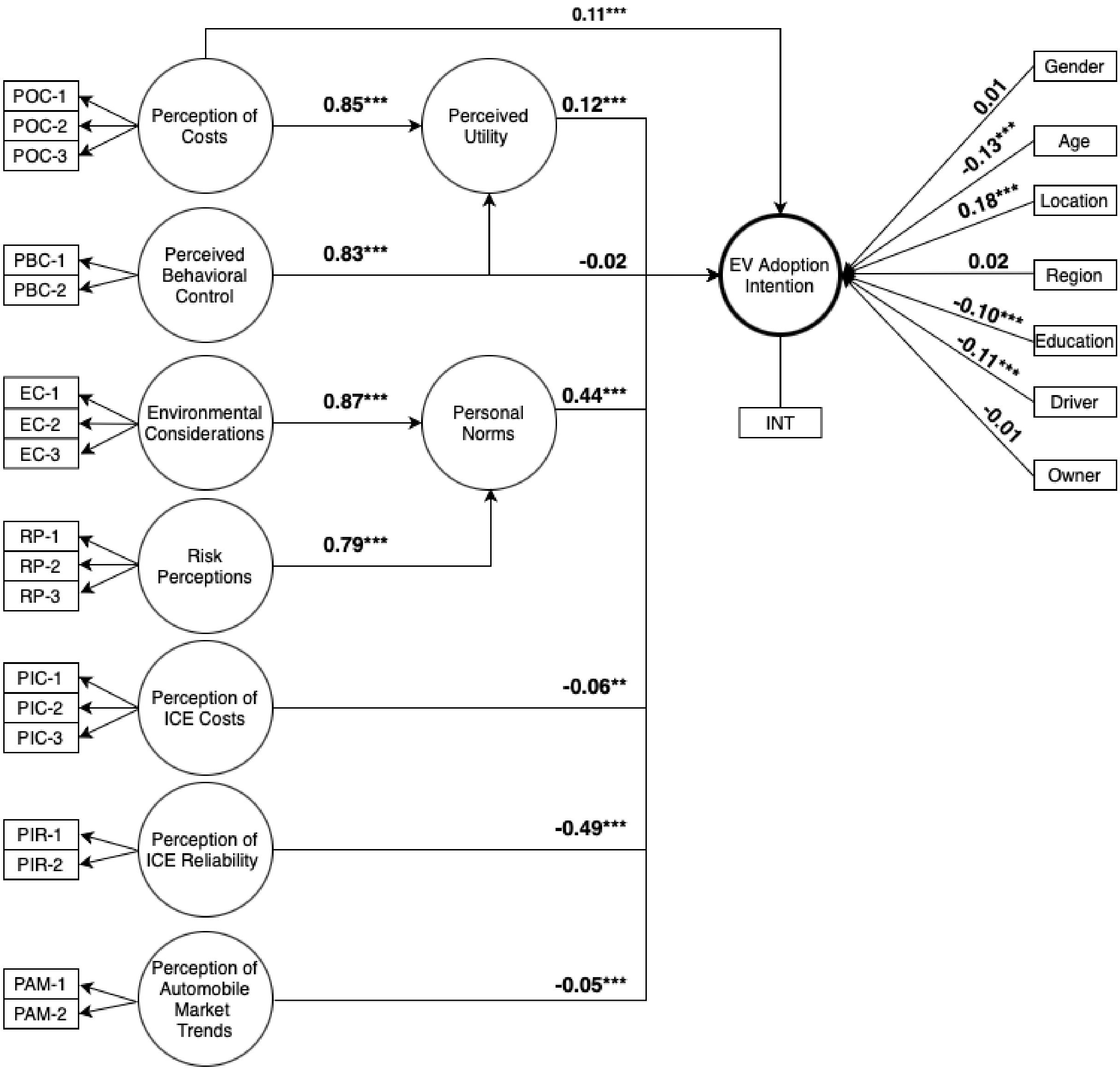

Figure 3.4: Path diagram of structural model results with standardized coefficient estimates.

making χ^2 a limited test. As [151] succinctly stated, “The null hypothesis of overall fit tested by the χ^2 distribution is often not of general interest." Therefore, multiple fit indices were used in this analysis instead.

The results indicate that ten out of the eleven hypotheses are supported. The model demonstrates that perceived usefulness (PU), perception of cost (POC), and personal norms (PN) are positively associated with EV adoption intention (INT), with standardized path coefficients of 0.12, 0.11, and 0.44 respectively, all achieving statistically significant p-values. Both perception of cost and perceived behavioral control (PBC) show

Table 3.6: Structural model coefficient estimates and hypothesis testing results.

Hypothesis	Path	Std. Coefficient	p-value	Supported?
H1	PU → INT	0.12	0.00***	Yes
H2a	POC → INT	0.11	0.00***	Yes
H2b	POC → PU	0.85	0.00***	Yes
H3a	PBC → INT	-0.02	0.45	No
H3b	PBC → PU	0.83	0.00***	Yes
H4	PN → INT	0.44	0.00***	Yes
H5	EC → PN	0.87	0.00***	Yes
H6	RP → PN	0.79	0.00***	Yes
H7	PIC → INT	-0.06	0.03**	Yes
H8	PIR → INT	-0.49	0.00***	Yes
H9	PAM → INT	-0.05	0.00***	Yes
Variable	Type			
Gender	[= 1 if male]	0.01	0.69	
Age	[numeric]	-0.13	0.00***	
Location	[= 1 if city/urban]	0.18	0.00***	
Region	[=1 if Western Cape]	0.02	0.23	
Education	[= 1 if passed Grade 12+]	-0.10	0.00***	
Driver	[= 1 if driver]	-0.11	0.00***	
Owner	[= 1 if owner]	-0.01	0.67	

Notes: $**p < 0.05$; $***p < 0.01$.

positive relationships with the higher-order factor of perceived usefulness, with coefficients of 0.85 and 0.83. Environmental considerations (EC) and risk perceptions (RP) are also positively linked to personal norms, with coefficients of 0.87 and 0.79. On the other hand, perceptions of ICE costs (PIC), ICE reliability (PIR), and automobile market trends (PAM) are negatively related to EV adoption intention, with significant coefficients of -0.06, -0.49, and -0.05, respectively.

Hypothesis 3a, which posited a direct positive relationship between perceived behavioral control and EV adoption intention, was not supported (p = 0.858). However, perceived behavioral control does have an indirect influence on EV adoption intention through perceived usefulness. This suggests that perceived behavioral control's effect on EV adoption intention is fully mediated by perceived usefulness. This result may be due to paratransit owners and drivers being primarily concerned with their ability to operate an EV only insofar as it is deemed *useful* for their business, particularly regarding cost considerations, rather than the operation of the EV itself. In other words, their ability to operate the vehicle (behavioral control) is secondary to how the EV impacts their business's bottom line.

Since the coefficients are standardized, they allow for comparison of the relative strength of the relationships between the latent constructs and the target variable. For constructs mediated by higher-order factors, the indirect effect on EV adoption intention can be calculated by multiplying their path coefficients. For example, the total effect of perception of costs on EV adoption intention is the direct effect (0.12) plus the indirect effect (0.85×0.12), which equals 0.21. Based on the coefficients provided, the constructs with the most substantial positive effects on EV adoption intention are perception of costs, risk perceptions, and environmental considerations, with total standardized effects of 0.21, 0.35, and 0.38, respectively. These coefficients suggest that a 1 standard deviation increase in POC, RP, and EC is associated with 0.21, 0.35, and 0.38 standard deviation increases in EV adoption intention, respectively. The construct with the most substantial negative impact on EV adoption intention is PIR, with a standardized path coefficient of -0.49, representing the largest absolute effect on EV adoption intention in the model.

Regarding socio-demographic factors, living in a city/urban area and living in the Western Cape are positively and significantly related to EV adoption intention, while being older and being a driver are negatively associated with EV adoption intention. Gender and ownership status do not have a significant impact on EV adoption intention.

Overall, the hypothesis testing results suggest that interventions focused on improving paratransit owners' and drivers' perceptions of costs, safety compared to ICE vehicles, and environmental benefits are likely to have the greatest impact on boosting EV adoption intentions.

3.4 Key takeaways and discussion

This section summarizes the key findings of the chapter and discusses their implications for policy and future research. An example is provided to demonstrate how the results of the structural equation model can be used to simulate the effects of a potential intervention.

The descriptive statistics from the survey show that less than half (38.2%) of respondents agreed or strongly agreed that they would purchase an electric taxi when available, while 47% disagreed or strongly disagreed. This highlights a significant opportunity for interventions aimed at improving EV adoption intentions within this population.

Regarding the socio-demographic variables captured in the survey, a lower percentage of drivers (37.1%) expressed willingness to adopt an EV compared to owner-drivers (48.8%) and owners (43.8%). The structural model confirmed that drivers were significantly less likely to intend to adopt an EV, along with older respondents, those living in rural areas, and those residing outside of the Western Cape. When considering the relatively large effects of perception of ICE reliability (PIR) and risk perceptions (RP) in the structural model, the age effect suggests that older individuals may be less inclined to switch to EVs due to their familiarity and comfort with ICE vehicles. Drivers, who tend to be less affluent than owners, may be further discouraged by cost concerns (as indicated in Table 3.3). However, unlike age, perceptions of cost and reliability can change, particularly with more information or demonstrations of the safety and cost-saving benefits of EVs. Therefore, promoting EVs to younger drivers might be an effective approach based on these findings.

Although the hypotheses did not explicitly account for the magnitude of the coefficients, it was somewhat surprising that Environmental Concern (EC) and Risk Perceptions (RP) had the highest coefficients, considering the profit-driven nature of paratransit agents and their reputation for aggressive driving behavior [44, 158]. One might assume that the profit motive would outweigh personal ethical considerations when making business decisions, and that safety would not be a primary concern given their driving habits. However, these results make sense when considering the salience of these constructs in the drivers' day-to-day lives, along with the high mean scores for environmental considerations, risk perceptions, and ICE reliability in the measurement model. If drivers consistently expose themselves to risk and are comfortable with the safety of their current ICE vehicles, it follows that they would be more hesitant to switch to EVs. The strong trust in ICE vehicles is evident in the mean values for perception of ICE reliability, as seen in Table 3.3/Figure 3.3, which were the highest of all the constructs, followed by environmental considerations and risk perceptions.

One limitation of this survey is that it did not capture respondents' perceptions of EV safety, though the results suggest this as a topic ripe for future research. If paratransit owners and drivers perceive EVs to be less safe than ICE vehicles, targeted interventions aimed at raising awareness of EV safety may be necessary. Regarding environmental considerations, the median respondent Agreed (4) that electric taxis would benefit the environment, that the taxi industry should reduce its environmental impact, and that climate change is a serious concern. These scores are somewhat surprising, as environmental awareness is generally associated with more affluent groups. However, given these scores, it stands to reason that respondents with greater environmental consciousness would be more likely to favor adopting EV taxis, especially given the obvious environmental drawbacks of ageing paratransit fleets.

3.4.1 Simulating targeted interventions

Using the construct means and standard deviations from Table 3.3 and the factor loadings (λ) from Table 3.4, the effects of targeted interventions on each item related to EV adoption intention (INT) can be simulated. Based on established consumer behavior theories underlying this study's model, increases in INT are expected to lead to actual increases in EV adoption behavior. Before delving into the simulation results, it's important to acknowledge that coefficients in complex regression models, like the one used in this research, can be influenced by various factors, including sample size, measurement techniques, and the development of constructs. Therefore, the quantitative effects should be viewed as well-informed guidelines rather than fixed outcomes. With ten hypotheses showing significant results, the key takeaway is the necessity of a diverse set of approaches to improve EV adoption intention among paratransit owners and drivers.

Let's consider the simulated impact of interventions aimed at enhancing perception of cost (POC) and perceived behavioral control (PBC) of EVs. For instance, imagine an investment to introduce a few electric minibus taxis in the Western Cape, piloted along popular routes to showcase their performance. The promotional campaign could maximize exposure among taxi associations, highlighting the fuel savings and anticipated maintenance costs from these routes. This educational effort could shift the responses from many in the paratransit industry from "Disagree" to "Neutral" or "Agree" on questions like "Charging an electric taxi will be expensive" (POC-1) and "Servicing an electric taxi will be expensive" (POC-3). Assuming that responses for POC-1 and POC-3 both rise from 2.04 to 3.0, making the average response "Neutral," and using the factor loadings from Table 3.4 to create a weighted average, this would increase the mean of POC from 2.00 to 2.62 (with POC-1 = 3.0, POC-2 = 1.92, and POC-3 = 3.0). Given POC's standard deviation of 0.83 (calculated using weights from factor loadings), the mean of POC rises by $\frac{0.62}{0.83} = 0.75$ standard deviations. Referring to Table 3.6, where POC's total effect on INT is 0.21, this increase of 0.75 standard deviations in POC is expected to lead to a rise of $0.75 \times 0.21 = 0.16$ standard deviations in INT. Table 3.3 shows INT's standard deviation is 1.21, which translates to an expected increase of $0.16 \times 1.21 = 0.19$ points on the Likert scale for INT.

Now, suppose that due to the promotional campaigns, electric taxis attract significant attention from policymakers and city planners, leading to the development of a comprehensive network of charging stations that efficiently serve the paratransit routes. Additionally, off-grid solar and battery solutions are introduced to ensure charging is available even during load shedding. Such public investments in charging infrastructure could raise average responses for PBC-1 and PBC-2, which inquire about concerns regarding charging station availability and load shedding, to 2.50 (still relatively modest). Using the same methodology, this scenario would raise the mean score of INT by 0.10 points on the Likert scale.

In summary, the structural model results provide a means to assess the effects of changes in factors influencing EV adoption intention among paratransit owners and drivers. Conservative estimates from these simulations demonstrate that several well-designed and thoughtfully implemented interventions can make a noticeable difference. However, no single intervention will be sufficient on its own. The combined effect of the example simulations amounts to 0.29, which is a respectable change but not a game-changer on its own. Furthermore, although these estimates were intentionally conservative, if interventions are not carefully targeted or are poorly executed, the outcomes could easily be halved or worse, resulting in wasted resources and time, both of which are scarce in this context.

3.4.2 Implications for EV adoption policy

Overall, this study provides valuable insights into the factors that shape EV adoption intentions among paratransit owners and drivers in South Africa. These findings can inform the development of targeted interventions aimed at encouraging the adoption of electric minibus taxis within the paratransit industry. A key takeaway from the results is the need for a well-thought-out, scientifically grounded, and multifaceted approach to addressing concerns about EVs. A random or unfocused 'shotgun' approach is unlikely to be effective. The results clearly indicate that respondents prioritize both personal safety and their financial bottom line.

Educational and promotional campaigns can be most effective when they focus on informing paratransit owners and drivers about the safety and reliability of EVs, as well as their environmental benefits. These campaigns may also have positive spillover effects, encouraging other pro-environmental behaviors that benefit society as a whole [159]. Demonstrating the cost-saving potential of EVs could also play a crucial role in influencing their decision to switch to electric vehicles.

In addition, policies aimed at improving the availability and reliability of charging infrastructure, reducing the high upfront costs of EVs, and creating a supportive regulatory framework for the transition to electric vehicles could significantly boost EV adoption. Coordinating efforts to shift the Overton window for EV-related policies could shape perceptions of the automobile market and build early momentum for the transition. It is essential that these policies consider the unique cultural and social context of the South African paratransit industry and be developed in collaboration with industry stakeholders to ensure they are both effective and sustainable.

3.5 Summary and key insights

This chapter analyzes 4,452 survey responses from paratransit owners and drivers in South Africa, examining their intentions to adopt electric vehicles (EVs) as alternatives to their current internal combustion engine (ICE) vehicles when they become available. It also investigates the factors that influence these adoption intentions. The insights gained from this study help to understand what makes electric paratransit viable or attractive for key stakeholders in the industry, such as vehicle owners and drivers. By doing so, this chapter contributes to the development of targeted interventions that can facilitate the adoption of electric minibuses in the paratransit sector, ultimately supporting a more sustainable and environmentally friendly transportation system.

The survey findings revealed that 38% of respondents agreed or strongly agreed that they would purchase an EV once available, while 47% disagreed or strongly disagreed, highlighting the significant potential for targeted interventions. These results answer the chapter's first research question: *What are the intentions of paratransit owners and drivers to switch to EVs when they become available?*. With 38% user acceptance, the technology adoption curve places EV adoption within the "early majority" stage [143], which is promising. The early majority is typically the most challenging stage to reach, as it follows the early adopters at around 16% user acceptance. Future research can build on these findings as a baseline to evaluate the effectiveness of subsequent interventions.

For the second research question, *What are the factors that influence EV adoption intention for paratransit owners and drivers?*, a novel framework was created to analyze various factors influencing EV adoption intention among respondents. This framework integrates elements from three major consumer behavior theories—the Theory of Planned Behavior (TPB), the Norm Activation Model (NAM), and the Technology Acceptance Model (TAM)—and extends them with three additional constructs: perception of ICE vehicle costs, perception of ICE reliability, and perception of automobile market trends. Based on this framework, eleven hypotheses were developed and tested using structural equation modeling.

Ten of the eleven hypotheses were supported by significant p-values in the structural equation model, demonstrating the robustness of the findings. These results are critical for understanding the feasibility of electrifying paratransit fleets. Simulations of targeted interventions were conducted using the model's outcomes to predict their effects on EV adoption intention. The most influential factors on EV adoption intention were perceptions of operating costs, safety and reliability, and the environmental impact of the taxi industry. Thus, interventions or policies aimed at improving these factors are likely to be the most effective in promoting the viability of paratransit electrification for key industry agents. Given the importance of operating costs and environmental impact, these factors are explored further in the thesis, while safety and reliability are earmarked for future research. These latter aspects are dependent on the specific vehicle models available, and given the lack of electric vehicles currently in operation, these elements cannot be tested at this stage.

Overall, the results suggest that a multifaceted approach addressing various factors is most effective, as no single factor drives EV adoption intention independently. Moreover, any intervention must be carefully planned, as the simulations highlight that poorly targeted or randomly conducted interventions (a “shotgun" approach) could waste valuable resources and time.

The limitations and findings of this study provide several avenues for future research. First, the study's sample was largely drawn from the Western Cape province of South Africa, and further research is needed in other regions to determine whether the findings can be generalized. Second, follow-up studies are necessary to obtain a more objective understanding of how paratransit owners and operators perceive EV performance and their knowledge of EV technology. Lastly, given the current absence of electric paratransit vehicles in South Africa, future studies on the effects of EV experience, once these vehicles are available, will be crucial for ensuring the successful electrification of the paratransit sector.

Very little is known about the energy requirements of [minibus taxis], especially given their unique and mostly unknown mobility patterns.

— M.J. Booysen, C.J. Abraham, A.J. Rix, and J.H. Giliomee [34]

4

Constructing representative driving cycles for paratransit

Contents

Up to this point in the thesis, the feasibility of electric paratransit has been investigated from a market perspective. The preceding chapter uses a survey to measure the intentions of paratransit owners and drivers to adopt electric alternatives to their current combustion vehicles, and identify the key factors that influence these intentions. While calling for a holistic view on updating the body of knowledge of paratransit electrification and undertaking related educational campaigns, Chapter 3 highlighted cost, safety, and environmental concerns among the most important factors influencing EV adoption for paratransit owners and drivers.

Representative driving cycles offer a framework for understanding the costs, safety, and environmental impacts of a vehicle class from a certain region [77]. The literature review in Chapter 2 identifies several technical gaps in the existing literature relating to the construction of representative driving cycles. This chapter addresses **Research Gap 2**, which highlights a lack of methodologies suited for constructing representative driving cycles for paratransit vehicles. Previous driving cycle construction methodologies do not offer a robust way to capture the unique operating conditions of paratransit. Therefore this chapter sets out to address the research questions:

- *How can we construct representative driving cycles for paratransit?*
- *How well do international driving cycles represent paratransit mobility?*

To answer these questions, this chapter proposes a novel time series shape-based clustering methodology to develop representative driving cycles which includes transients from the measured data in cycle development. By reflecting these transients, the approach to cycle development demonstrated here is particularly suited for capturing the notoriously unconventional and aggressive driving style of paratransit. The methodology is then employed to construct the Paratransit Driving Cycle (PDC) from high-resolution GPS tracking data captured on minibus taxis in South Africa. Finally, the PDC and three standard international driving cycles are judged against a set of representative performance characteristics to compare how well they each represent paratransit mobility.

In tackling the above questions which directly relate to **Research Gap 2**, this chapter also takes a step toward addressing **Research Gap 3**, since driving cycles can be used to estimate energy consumption.

Driving cycles are vehicle speed-time series that simulate real-world driving patterns. They serve various purposes, from determining expected profiles of fuel consumption and emissions [49, 50, 51] to traffic control system design [52] and evaluating vehicle system performance [53, 54]. Essentially, driving cycles establish the protocol for measuring a vehicle's performance under typical driving conditions, often using equipment such as a chassis dynamometer. Engineers use driving cycles for vehicle technology research and development [67, 68], and policymakers or urban planners apply them in transportation planning [160]. As a result, an in-depth understanding of driving cycles aids long-term vehicle design decisions such as engine power, fuel type (e.g., diesel or electric), and vehicle size. They also help in crafting policies that manage congestion and emissions more efficiently [56, 57, 69, 70, 160], and are crucial for understanding the operation of transportation systems.

Over the past few decades, representative driving cycles have been developed for cities worldwide (e.g., [49, 50, 52, 76, 77]). However, a review of the driving cycle literature reveals that these cycles have mainly focused on the USA, Europe, South America, and Asia [71, 77, 78]. While there have been some isolated studies on energy consumption [29, 48, 161] and mobility [46, 59, 162] in paratransit systems in sub-Saharan Africa (SSA), there is a lack of research on the driving patterns of these systems. This gap is primarily due to a scarcity of data on actual driving patterns and a lack of standardized testing procedures. In contrast, the driving cycles of electric passenger vehicles and larger buses in developed regions have been thoroughly studied [41, 42, 64, 65, 66].

It is crucial that driving cycles accurately reflect the driving patterns of the specific vehicle type and region to ensure performance tests yield realistic results. However, well-known standard international driving cycles, such as the New European Driving Cycle (NEDC) and the Worldwide Harmonised Light Vehicle Procedure (WLTP), have been shown in several studies to inadequately represent local driving patterns in many developed economies [50, 52, 71, 72, 73]. Given the unique mobility patterns and unconventional driving styles of African paratransit systems [44, 59], these international driving cycles, developed for high-income countries, are often unsuitable in African contexts. The absence of accurate and representative driving cycles can hinder the effective design and operation of paratransit systems [3]. Therefore, the goal of this chapter is to propose a methodology for creating driving cycles specific to paratransit vehicles and to develop a representative paratransit driving cycle as a benchmark for future work. It also evaluates the extent to which standard international driving cycles represent paratransit operating conditions, further justifying the need for specialized paratransit driving cycles. Although the developed cycle is limited to Stellenbosch, the methodology is adaptable for other geographies and driving conditions.

The proposed methodology is based on “micro-trip" clustering, where micro-trips are defined as segments of a trip during which the vehicle moves from one stop to another. Dynamic time warping [163] is employed to measure the similarity between micro-trips of varying lengths based on their time series shapes, and mixed-integer programming is used to identify a globally optimal clustering solution. This method allows for the clustering of micro-trips of different lengths, a challenge that previous approaches to shape-based clustering of micro-trips have not addressed [73]. Additionally, the chapter introduces a parameter, $t_{\min}$, which imposes a minimum duration for micro-trips, preventing the inclusion of arbitrarily short or “spam" micro-trips in the clustering process. Micro-trips closest to the cluster centers are then used to form the basis of a representative cycle, and a maximum likelihood method ensures that these candidate micro-trips are sequenced in a way that reflects what would be expected on the road.

The use of unaltered micro-trips from real data ensures that the final cycle captures actual transients from the driving data, which are typically difficult to replicate using statistical driving cycle constructions. In this context, “data transients" refer to temporary, abrupt changes or irregularities in driving data collected from paratransit vehicles, such as rapid accelerations, decelerations, stops, or other unique patterns associated with the aggressive, stop-start nature of paratransit driving. Including these transients is essential for constructing a representative driving cycle that accurately reflects the real-world driving conditions and behaviors of paratransit drivers.

In addition to answering the stated research questions related to the planning of paratransit electrification, the novel contributions of this chapter to the driving cycle literature are as follows:

- Develops the first representative driving cycles for minibus taxi paratransit in sub-Saharan Africa.
- Presents a methodology to cluster micro-trips of varying lengths based on their time series shape. The clustering approach finds the globally optimal clustering solution.
- Introduces the parameter $t_{\min}$, which represents the minimum duration for a trip

segment to be considered a micro-trip.

Section 4.1 begins with an overview of driving cycle classification and the state-of-the-art in driving cycle construction. This review reveals a lack of approaches suitable for constructing representative driving cycles for paratransit. Section 4.2 steps through the proposed methodology for this study. Section 4.3 presents the developed cycles and assesses how well they represent the real-world measured data in comparison to several international cycles. Section 4.4 concludes the study and provides some research perspectives.

4.1 Driving cycle classification and construction

This section provides an overview of how driving cycles are typically classified, and a brief state of the art on methods for developing representative driving cycles. It elucidates how the methodology presented in this study is an improvement upon previous driving cycle development methodologies.

4.1.1 Driving cycle classification

It is common practice in vehicle design and regulatory frameworks to rely on standard international driving cycles, also referred to as “legislative" driving cycles. However, in reality, variations in infrastructure quality, traffic conditions, urban and geographical features, as well as economic, cultural contexts, and vehicle types lead to significant differences in real-world driving patterns and, consequently, driving cycles across different cities and regions [54, 164]. As a result, these standard international cycles often fail to accurately reflect the driving conditions experienced in real-world settings or capture region-specific driving patterns and transients [71, 165]. To truly evaluate the benefits of legislative, design, or engineering changes, it is essential to develop real-world representative driving cycles that are based on actual driving data from vehicles operating in the region of interest [166]. This need is especially relevant for paratransit vehicles, which are known for their distinctively aggressive driving style, marked by frequent rapid stop-start maneuvers [44, 59].

In addition to the distinction between legislative and non-legislative classifications, driving cycles can also be categorized as either “transient" or “modal," based on their development process. Transient cycles are derived from on-road driving data, while modal cycles are constructed from a sequence of steady speed and acceleration states, or “modes." Examples of transient cycles include the Worldwide Harmonized Light Vehicles Test Cycle (WLTC), the Hong Kong Driving Cycle, and the Standard Federal Test Procedure (SFTP-US06). Modal cycle examples include the New European Driving Cycle (NEDC) and Japan’s J10-J15 Driving Cycle [52].

The modal method has been widely recognized in the literature for its inability to accurately reflect real-world driving behavior, as the final aggregated speed-time series is artificially smoothed, and the effects of transient acceleration and deceleration events are lost [167, 168, 169]. In fact, it has been estimated that modal driving cycles can underestimate emissions by 30 – 50% [67, 170]. Generally, transient driving cycles, which are based on real-world data, are considered superior to modal cycles for real-world applications [73]. For instance, with the growing focus on electric vehicles (EVs), there has been an increased emphasis on the development of representative real-world driving cycles, which are critical for accurately predicting battery health [171] – a task that modal driving cycles would not effectively handle. Given that this study utilizes real-world on-road driving data for driving cycle construction, the representative driving cycles developed in this research are transient.

4.1.2 Cycle construction methodologies

In the literature, there are generally five main categories of methodologies for constructing transient driving cycles [172]. Many of these approaches involve the use of “micro-trips," which are typically defined as segments of a trip where the vehicle transitions from a complete stop to another stop. In some studies, micro-trips have been characterized as segments where engine RPM goes from zero to zero [73], a method particularly useful for evaluating a vehicle’s emissions performance based on the driving cycle. However, as engine RPM data was unavailable for this study, vehicle speed is used instead.

The five categories are: random selection-based methods (RS), segment-based (SB) methods, Monte Carlo-Markov Chain (MCMC) based methods, clustering analysis (CA) methods, and optimization-based (OB) methods. Other studies that fall outside these categories generally still incorporate the use of micro-trips and some form of statistical driving cycle construction [173].

1. Random selection-based methods (RS): These methods are straightforward and adaptable, making them applicable across various vehicle types and regions. The process involves breaking the dataset into a series of micro-trips and randomly selecting trips that meet specified criteria until the target cycle duration is achieved. Several studies have utilized this approach, such as Arun et al. [49], which develops driving cycles for passenger cars and motorcycles in Chennai, India. Similarly, Kamble et al. [54] create a representative driving cycle using data from major roads in Pune, India. Additionally, Tong [174] formulate driving cycles for diesel and super-capacitor electric buses in Hong Kong, while Ho et al. [52] construct a driving cycle for Singapore that more accurately reflected local emissions than a popular standard international cycle, the New European Driving Cycle (NEDC). In a comparative study, Saleh et al. [175] build driving cycles for both Edinburgh and Delhi, and Tong et al. [50] use RS to generate the first set of driving cycles for Hanoi, aligning with summary statistics. Although RS is widely studied and applied due to its simplicity and flexibility, it has limitations. One challenge is ensuring that all driving conditions are adequately represented, especially extreme events like sudden braking or rapid acceleration, which may not be captured well due to the randomness of the method. Moreover, this method can be computationally expensive when applied to large datasets.

2. Segment-based methods (SB): SB methods resemble micro-trip-based cycle construction but consider additional factors such as road type or Level of Service (LOS) instead of focusing only on adjacent stops. Since trip segments are divided based on traffic conditions and road characteristics, they may begin and end at different speeds. A crucial part of SB methods is aligning speed and acceleration between consecutive points within micro-trips. These methods are more suitable for constructing cycles for expressways with fewer stops. Using SB, Dai et al. [176] create a driving cycle for arterial driving in urban California, accurately capturing

high- and low-speed activities. Kivekäs et al. [177] apply this approach to analyze the effects of driving cycle variations on electric buses in Espoo, Finland, while Shen et al. [178] use it to build a driving cycle for hybrid electric buses in Shanghai, avoiding velocity fluctuations between segments and achieving error rates within 5%. SB methods excel at tailoring driving cycles to specific traffic conditions but are less effective for vehicles operating in unpredictable or complex driving environments.

3. Monte Carlo-Markov Chain (MCMC) methods: MCMC methods predict future vehicle states based on their current states. Using maximum likelihood estimation, velocity-time data are clustered into fragments characterized by parameters like speed and acceleration, which are then used to create modal bins. Transition probabilities between modes are calculated to establish a path between micro-segments. Bishop et al. [67] introduce a data-driven Markov chain approach for constructing driving cycles without segmenting raw speed-time sequences, while Gong et al. [179] use MCMC to generate a Beijing driving cycle for battery electric vehicles, showing better real-world consistency than international cycles. Li et al. [180] propose a method to improve prediction accuracy by 7.18%, and Liu et al. [181] use MCMC to develop a city bus driving cycle accounting for passenger load. While MCMC can glean insights from large datasets, a significant limitation is the need for large data volumes, and the results are not always consistent [172].

4. Clustering analysis (CA) methods: CA methods often employ dimensionality reduction techniques, such as principal component analysis (PCA), combined with clustering algorithms like k-means, hierarchical clustering, or c-fuzzy clustering to classify micro-trips based on their characteristics [182, 183, 184]. Dimensionality reduction highlights the most critical features, reduces noise, and allows for effective clustering. CA is well-supported in the literature [172] and has been widely used to address the limitations of RS in capturing real-world driving patterns. For example, Abas et al. [185] use a two-step clustering approach to develop an urban driving cycle in Malaysia, achieving energy consumption estimates within 10% of actual values. Jing et al. [186] build a Tianjin driving cycle using Fisher's two-class discrimination

method, achieving an average error of only 5.46%. Li et al. [187] proposed a two-level clustering approach to determine daily driving cycles for electric vehicles in China. Although CA is effective, the challenge lies in selecting the right features and the optimal number of clusters. While PCA helps reduce data dimensions, it can diminish the interpretability of clustered features. In this thesis, a variation of CA is implemented to avoid these issues by clustering based on time series shape.

5. Optimization-based (OB) methods: OB methods, a more recent addition to driving cycle construction literature, treat driving cycle creation as an optimization problem. These methods form an optimal combination of smaller segments to create a driving cycle that best matches real-world data. Chen et al. [188] use a genetic algorithm to construct an urban driving cycle in Shenyang, China, applying it to energy management systems and reducing energy costs under real driving conditions. Cui et al. [189] apply simulated annealing to a case study in Fujian Province, improving alignment between speed-acceleration patterns and real-world characteristics. Cui et al. [190] use a min-max ant colony optimization algorithm to develop driving cycles in Fuzhou under varying conditions. Although OB methods are generally more accurate than other methods, they are less consistent than CA, may miss data transients, and require large datasets to achieve optimal results.

4.1.3 Research gap

In the methods outlined above, the constructed driving cycles represent the average parameters of driver behavior observed in the measured data for the target cycle duration. However, such statistical approaches may *miss out on real-world transient features* present in the measured data [73]. To address this, Sundarkumar et al. [73] propose forming clusters of micro-trips based on their time-series shapes instead of their kinematic characteristics. This approach classifies micro-trips by the pattern of driving behavior they exhibit, rather than focusing solely on average features. By taking representative micro-trips from these clusters, the real-world transients are preserved in the final driving cycle.

Despite this improvement, previous time-series shape-based clustering methodologies are limited by their reliance on the k-means algorithm, which is unable to cluster micro-trips of varying lengths. This limitation forces all micro-trips to be truncated to the same length, distorting the driving patterns they represent. Additionally, previous approaches did not sequence the candidate micro-trips from the final clusters in a way that mirrors the order seen on the road. This study aims to address both of these gaps.

First, this research employs mixed integer programming (MIP) instead of k-means to cluster micro-trips. While k-means has certain advantages, such as ease of implementation and quick computation time, it also has known limitations. Chief among these is that k-means converges to locally optimal clustering solutions, which are rarely globally optimal. This is because centroids are often unable to move between clusters if large distances or stable clusters prevent centroid movement [191]. Another important limitation of k-means in time-series shape-based clustering is that it cannot minimize non-Euclidean distances like dynamic time warping (DTW) distances, which are crucial for comparing time series of different lengths.

DTW works by finding an optimal alignment between two time series by stretching or compressing their respective time axes, allowing for the comparison of sequences with varying speeds or timing discrepancies. Clustering based on DTW distances is the most effective method for grouping micro-trips by their shape, which is vital for capturing similar driving patterns. Alternative methods for measuring similarity between time series or real-number sequences include Longest Common Subsequence (LCSS) [192] and Edit Distance for Real Number Sequences (EDR) [193]. LCSS calculates similarity by finding the longest sub-sequence common to both series, while EDR measures similarity by calculating the minimum number of edits (insertions, deletions, substitutions) needed to transform one sequence into the other. While LCSS and EDR are computationally less intensive than DTW, DTW remains the most suitable choice for constructing representative driving cycles that closely mimic detailed driving patterns within micro-trips due to its ability to capture fine-grained shape similarities.

When clustering using arbitrary distances like DTW, k-means may fail to converge or yield suboptimal results, making it unsuitable for time-series shape-based clustering involving time series of different lengths. Previous research has attempted to address this by truncating all micro-trips to the same length before clustering, but this approach distorts their shapes and negatively affects the representation of driving patterns in the clustering process. Preserving the integrity of the time-series shapes would allow the benefits of time-series shape-based clustering to be fully realized, enabling the real-world transients in the data to be retained.

Options for clustering micro-trips of varying lengths by DTW distance include MIP and density-based algorithms like DBSCAN or OPTICS. Although density-based methods can effectively identify and separate noisy outliers, they require the minimum distance parameter ϵ, which may not translate easily to meaningful time-series distances for arbitrary DTW values. Additionally, these algorithms can be sensitive to initial conditions and may converge to local optima.

MIP, on the other hand, formulates the clustering problem as an optimization problem using a matrix of pair-wise DTW distances between micro-trips. This allows for the successful clustering of micro-trips of different lengths while reliably finding the globally optimal solution. In this study, a minimum micro-trip length parameter, $t_{\min}$, is implemented to avoid including micro-trips that are too short in duration. Only micro-trips with durations equal to or greater than $t_{\min}$ are selected for analysis.

Second, a simple maximum likelihood approach is used to sequence the micro-trips in the final driving cycle. Previous studies stitched together candidate micro-trips from clusters in a somewhat arbitrary order. By employing Viterbi programming to determine the most likely order of the micro-trips based on real-world driving sequences, the final driving cycle more accurately reflects the trips observed in the measured data. Further details on the MIP clustering algorithm and stitching approach are provided in Section 4.2.

4.2 Methodology

This section outlines the proposed methodology for driving cycle development. The steps involved in developing a driving cycle include route selection, data collection, cycle construction, and cycle assessment [77]. In this study, once the routes are selected and data is gathered, the construction of the driving cycle begins by applying a rolling window average of 3 seconds to smooth the data (thus normalizing GPS artefacts), followed by extracting micro-trips from the trip data. Dynamic Time Warping (DTW) is then utilized to compute the pairwise similarity between all micro-trips, and MIP is applied to cluster these micro-trips based on their DTW similarity. Afterward, representative micro-trips are selected from each cluster. These candidate micro-trips are ordered according to a transition probability matrix between the clusters and then combined to create the final driving cycle. Finally, eight target parameters are used to assess how well the constructed cycle represents the original measured data, ensuring its performance or 'representativeness' is evaluated. A flowchart outlining this proposed methodology can be found in Figure 4.1. Each of the steps is elaborated upon in the following sections.

The choice of target duration for the driving cycle varies considerably across the literature. For instance, driving cycles for buses in Delhi are only 170 s [51], while the Singapore Driving Cycle lasts 2400 s [52]. According to the findings of Giraldo et al. [194], cycles should last at least 1800 s to reliably represent real-world driving conditions. However, longer cycles tend to be more cumbersome for laboratory testing. As a result, the target driving cycle duration in this study is constrained to fall within the range of 1800 s to 2400 s.

4.2.1 Route selection

Selecting the right routes is essential for developing representative driving cycles. Traditionally, route selection has been somewhat subjective, relying on researchers' understanding of local traffic, topography, road types, and other factors [195]. However, more recent studies have taken a more systematic approach, using methods like Annual Average Daily Traffic (AADT) data [196] to identify the most frequently traveled routes. Other research focused on public transport driving cycles has employed different strategies, such as deploying surveyors to capture various activity patterns across urban districts and time periods [197, 198, 199], or choosing routes that are commonly used by typical commuters or target vehicles [71, 177, 181, 200].

In this study, data was gathered from three commonly used routes of different types in and around Stellenbosch, South Africa: urban, inter-urban, and hilly routes. Data was collected at three distinct times of day—morning, midday, and evening—to account

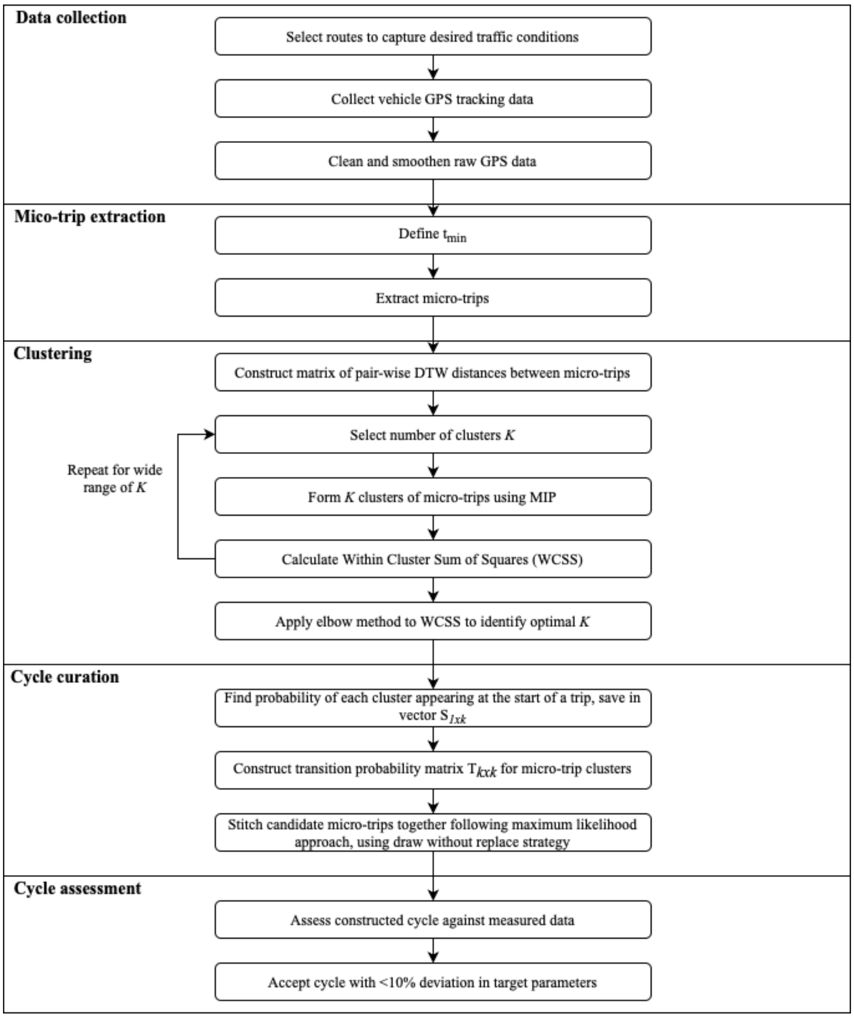

Figure 4.1: Driving cycle construction and assessment methodology flow chart.

for varying traffic conditions. While the taxis generally follow the same path for each route, occasional deviations occur to drop off passengers in nearby neighborhoods. These routes, all originating and terminating at the Bergzicht taxi rank in Stellenbosch, are shown in Figure 4.2.

The urban route connects Stellenbosch to the Kayamandi taxi rank (STB - KMNDI), which is located in a residential area of Stellenbosch that many taxi riders frequent. The roads between these taxi ranks have a speed limit of 60 km/h and consist solely of bidirectional roads. The route differs slightly on the return trip, as taxis circle through the Kayamandi neighborhood to drop passengers off closer to their homes before returning to the rank. The distances to and from Kayamandi taxi rank are 5 km and 2.6 km, respectively.

The hilly route extends from Stellenbosch to Pniel (STB - Pniel), crossing the Helshoogte

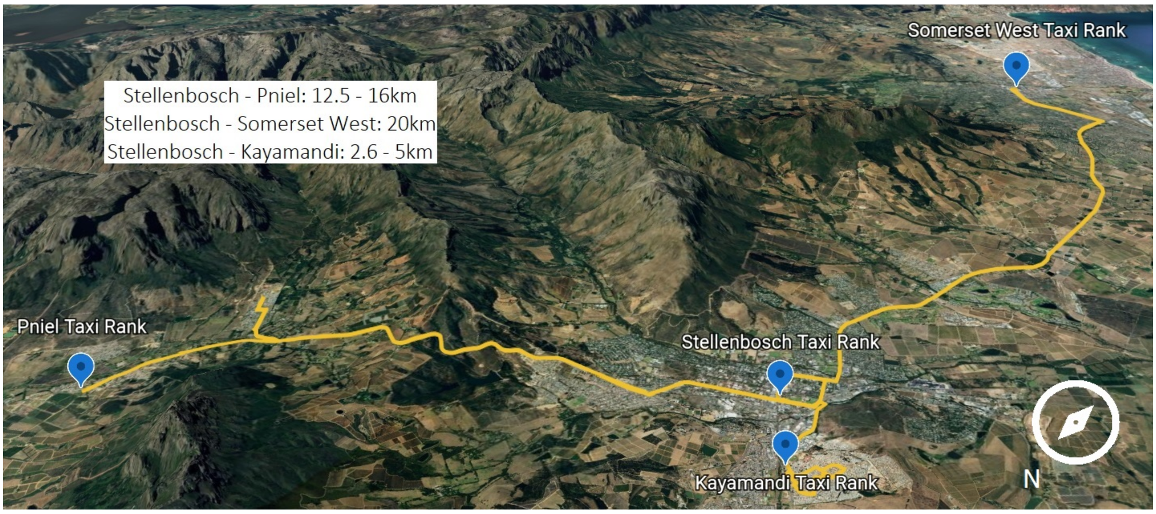

(a) Bird's eye view of the three routes selected for data capture [201].

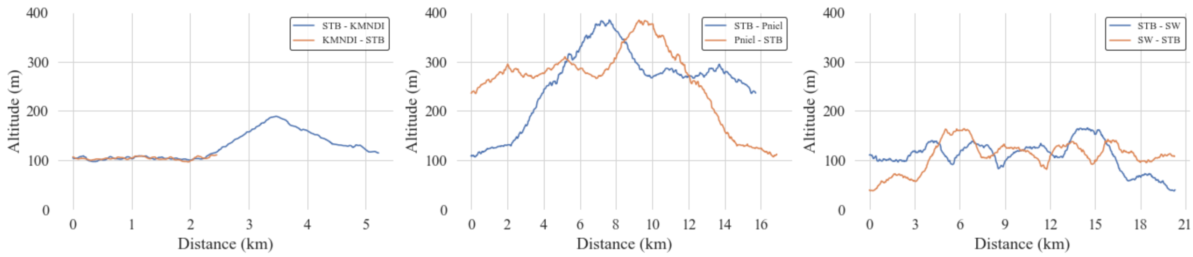

(b) Altitude plots for the three routes. Outbound trips are shown in orange, and inbound trips are shown in blue. The trip from Stellenbosch to Kayamandi includes an extra circular segment inside the township, making the trip roughly twice as long as its counterpart.

Figure 4.2: The routes used to assess vehicle mobility in and around Stellenbosch and their altitude profiles.

mountain pass, which involves a steady ascent of approximately 300 m over a distance of 7 km. This 12.5 km route, which occasionally includes a small detour, features a long uphill climb followed by a short descent, with a speed limit of 80 km/h.

The inter-urban route spans 20 km from Stellenbosch to Somerset West (STB - SW), primarily along a provincial road that is mostly a dual carriageway with a speed limit of 100 km/h.

4.2.2 Data collection

In the literature on driving cycle development, two main methods are employed to gather vehicle speed-time data during on-road testing: the chase car method and the on-board device method [50]. In the chase car method, a trained driver follows a designated target vehicle along a pre-determined route while equipped with GPS. Conversely, the on-board device method involves placing a GPS device directly inside the target vehicle to record its speed-time data.

The chase car method is more frequently used due to its lower resource demands. However, it is less precise than the on-board device approach, which captures the speed-time data directly from the target vehicle. Additionally, as noted by Galgamuwa et al. [77] in their review of driving cycle methodologies, the chase car method has limitations in environments where driving patterns are more aggressive.

This study opted for the on-board device approach for data collection. Six tracking devices were used to record GPS data at a frequency of 1 Hz, saving the data to an SD card. To mitigate GPS errors, the devices filtered the data in real-time, accepting only complete and accurate signals while discarding any erroneous data.

The six devices, built on the Arduino platform, were powered by alkaline battery packs, allowing them to function independently during testing. Once data collection was completed, the recorded data was processed separately. Fieldworkers, appointed as standardized passengers, initiated data capture by pressing a button when they boarded the minibus and stopped recording when the vehicle reached its destination. Each trip generated an individual file, allowing for the analysis of different routes and easy comparison between recordings made on the same route.

While designing the data collection approach, the use of smartphones as an alternative to Arduino-based GPS tracking was considered. Smartphones offer built-in GPS functionality and data logging capabilities, potentially reducing hardware requirements. However, safety considerations with having phones out in minibus taxis, their reliance on internal battery life, variable GPS accuracy across different models, and the need for additional application-based data handling were key limitations that led to their exclusion in favor of a dedicated GPS tracking setup.

The contributions of author of this thesis to the data collection for this chapter include conceptualization of gathering 1 Hz GPS data on minibus taxis for studying mobility patterns and energy consumption, as well as route selection. The co-authors of Hull et al. [202] and Hull et al. [203] from the University of Stellenbosch built the Arduino platforms and carried out data collection. As the data collection did not involve human subjects, it was determined by the University of Stellenbosch that ethical clearance for doing so was not necessary. For further details, the author refers the reader to the data-in-brief on this dataset published here: `https://www.sciencedirect.com/science/article/pii/S1361920923000925` [204].

The velocity, $v[n]$, was extracted from the GPS sample's speed data, while the elevation, $h[n]$, was derived from the GPS location data, which was then cross-referenced with the Earth Resources Observation and Science Center's dataset [205]. This approach was used because the GPS module's elevation data was less reliable compared to the location-based lookup. Displacement, $s[n]$, was calculated as the 3D geodesic distance between consecutive GPS locations. The slope angle, $\alpha[n]$ (positive for inclines and negative for declines), was derived from subsequent displacements, $s[n-1]$ and $s[n]$, and corresponding elevations, $h[n-1]$ and $h[n]$. However, only velocity is considered in this chapter, while the other measurements are discussed in Chapter 5, which focuses on energy consumption.

Table 4.1 provides a summary of the data collected after filtering out trips with missing or anomalous data. The goal was to gather at least three trips for each route and time-of-day combination, ensuring a sufficient dataset for each driving context. After data cleaning, this was achieved for all combinations except the Pniel - STB/'Evening' route, where only two trips were recorded. Ultimately, 62 trips were used for analysis.

Table 4.1: Summary of the number of trips recorded in data acquisition phase.

	Route						
From:	STB	KMNDI	STB	Pniel	STB	SW	
To:	KMNDI	STB	Pniel	STB	SW	STB	
Distance:	5 km	2.6 km	15 km	15 km	20 km	20 km	
Avg. Time:	18 min	6 min	28 min	23 min	29 min	27 min	
Speed Limit:	60 km/h	60 km/h	80 km/h	80 km/h	100 km/h	100 km/h	Total
Morning	4	4	3	3	3	3	20
Afternoon	3	5	4	4	4	4	24
Evening	3	3	3	2	4	3	18
Total	**10**	**12**	**10**	**9**	**11**	**10**	**62**

The dataset is publicly available in this repository at Mendeley data: `https://doi.org/10.17632/xt69cnwh56.1`. Further details on the data are available in this data-in-brief published in [204].

4.2.3 Micro-trip extraction

A micro-trip is defined as a segment of a trip that begins and ends when the vehicle comes to a stop. Vehicles are considered to be stopped when their speed is less than 2 km/h and their acceleration is within the range $-0\,10m/s^2 <$ acceleration $< 0\,10m/s^2$ [206]. Before analyzing the data, a 3 second rolling window average is applied to smooth the data, removing any outlier acceleration values caused by GPS noise. A rolling window average calculates the mean value of a set of data points within a sliding window that moves through the dataset from start to finish. Although windows of 4 and 5 seconds were also tested, the 3 second window was found to be sufficient to filter out outlier acceleration values above 4 seconds that might result from vibration, consistent with the WLTP standard. Extending the window further would reduce the sensitivity to sudden maneuvers, which is a crucial consideration for paratransit driving.

The algorithm used to extract micro-trips from the measured database is presented in the following algorithm:

1. Read in trip file, index $0.., i, .., T$.
2. Search for the index of the first GPS sample observation where the vehicle is stopped. i must be greater than $t_{\min}$ for $[0, i]$ to be a valid micro-trip.
3. Create a micro-trip by slicing trip file from index 0 to index i.
4. Save this slice in set of micro-trips.
5. **If** less than $t_{\min}$ seconds remain in the trip after this slice (i.e. $T - i < t_{\min}$), append remainder of trip to previous micro-trip. This avoids the issues of either creating a micro-trip with length less than $t_{\min}$, or cutting off data at the end of trips. **Else**, reindex the remainder of the trip (so the index starts from 0 again) and repeat steps 2 – 4.
6. Repeat Steps 1 – 5 until all trips in measured database are exhausted.

In this study, micro-trips are constrained to segments that last at least a minimum duration, $t_{\min}$. The $t_{\min}$ parameter ensures that each extracted micro-trip sufficiently captures a distinct driving pattern, which helps the clustering algorithm perform more effectively. Without enforcing $t_{\min}$, “spam" micro-trips, which do not accurately represent any real driving pattern, may be generated. These spam micro-trips could then be incorrectly clustered with valid micro-trips that do capture meaningful driving patterns. However, setting $t_{\min}$ too high can also be problematic, as it could group multiple shorter driving patterns into a single micro-trip, potentially losing important details during the clustering process. Therefore, the ideal $t_{\min}$ value should be the smallest possible duration that prevents the creation of spam micro-trips.

Since the ideal value for $t_{\min}$ is unknown and likely depends on the context, this study tests two values: $t_{\min} \in \{20, 180\}$. While the smallest $t_{\min}$ is preferable, a duration significantly shorter than 20 seconds might not provide enough data points, particularly given the 3-second rolling window average applied to smooth the data. Conversely, identifying a driving pattern may take longer, potentially requiring several minutes. This justifies the exploration of $t_{\min} = 180$.

Using $t_{\min} = 20$ resulted in 931 micro-trips, while $t_{\min} = 180$ yielded 232 micro-trips. Representative driving cycles are developed for both values and compared in Section 4.3.

Figure 4.3 provides an example of how a trip is segmented into micro-trips using $t_{\min} = 180s$. As discussed in the literature review, one of the contributions of this chapter is the development of a methodology that can cluster micro-trips of varying lengths. This variability in micro-trip length, ranging from 180 seconds (the enforced minimum) to over 200 seconds, can be observed in Figure 4.3. The raw and smoothed data are both visualized, and since only a 3-second rolling window average is used, the smooth data closely resembles the raw data, but with outlier acceleration values removed. The gray dashed line in the figure illustrates how a micro-trip continues until the first stop after $t_{\min}$ has been met.

The benefit of a larger $t_{\min}$ is particularly evident in the bottom chart in Figure 4.3. For example, the shorter duration segment at the end of the chart, between approximately 790 and 840 seconds, may not be of sufficient duration to capture a meaningful driving pattern. In such cases, increasing $t_{\min}$ to a value like 180s can improve the clustering algorithm's performance, ensuring more effective grouping of similar instances and preventing shorter

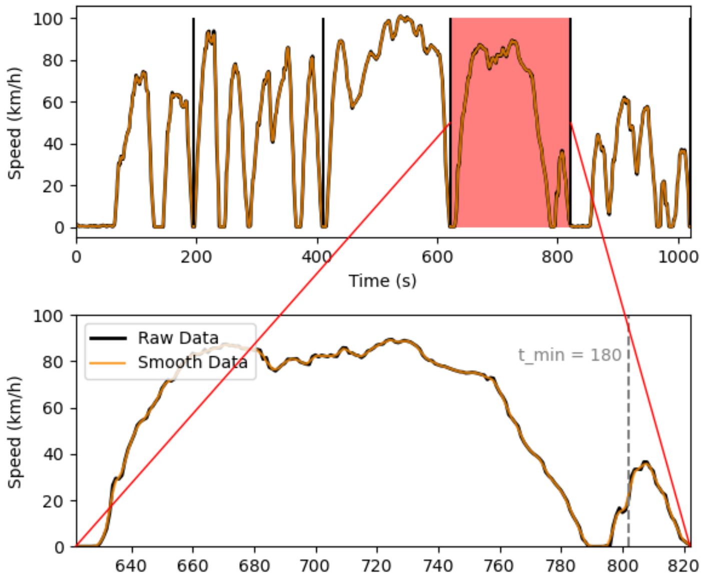

Figure 4.3: Sample trip comparing raw (black) vs smooth (orange) data. The bottom plot zooms in on a micro-trip extracted from the trip extracted using $t_{\mathrm{min}} = 180$. The gray dashed line at 180s shows how the micro-trip does not end at the first stop, but at the first stop after t_{min} is reached.

trips from being treated as independent micro-trips.

4.2.4 Clustering

Clustering involves organizing a set of p data points into k clusters according to their similarity. In this context, the purpose of clustering is to group micro-trips that exhibit distinct driving patterns. To determine the similarity between pairs of micro-trips, Dynamic Time Warping (DTW) is employed. DTW measures the similarity of micro-trips based on their shapes. One key advantage of DTW over simple Euclidean distance is its ability to compare time series of different lengths, something that Euclidean distance cannot handle effectively.

The clustering process can be broken down into two main steps. First, for a set of p micro-trips, a matrix of pair-wise DTW distances between every micro-trip is generated, denoted as $D_{p \times p}$. Next, a set of K clusters is formed based on these DTW distances, using Mixed Integer Programming (MIP). The use of MIP guarantees that the clustering solution is globally optimal [207].

Both the DTW distance calculations and MIP clustering are carried out using the

Table 4.2: DTW constraints.

Constraint	Description
Boundary	x_1 and y_1 must match, and x_n and y_m must match. This guarantees that the entirety of both sequences is used.
Monotonicity	If $x_j > x_k$, and $y_l > y_i$, then the algorithm cannot match x_j with y_i *and* x_k with y_l. This guarantees that observations are not repeated.
Continuity	There can be no jumps in time. The mapping between X and Y must transition along consecutive points in time. This guarantees that no observations are left out.

DTW-C++ package [207], which incorporates MIP with the Gurobi solver. The following section details the implementation of DTW and MIP clustering within the DTW-C++ package, as well as the methodology for selecting the optimal number of clusters, k. For further mathematical background, readers are referred to Kumtepeli et al. [207].

4.2.4.1 Dynamic Time Warping (DTW)

The formulation of DTW is detailed in the following algorithm, and the constraints are summarized in Table 4.2.

Consider two time series, X and Y, of length n and m respectively:

$$X = (x_1, x_2, ..., x_n)$$

$$Y = (y_1, y_2, ..., y_m)$$

1. Iterate along X, computing the Euclidean distance from each point in X to each point in Y.

2. Store the minimum distance calculated.

3. Switch to using Y as a reference series and repeat previous steps.

4. Add up minimum distances stored with objective of minimizing cumulative total distance, subject to the constraints in Table 4.2. This cumulative sum W is the DTW distance between the two time series.

To summarize the constraints in Table 4.2, the start and end points of the mapping between the two time series must align, no cross-matches are allowed, and all points from both series must be included in the mapping.

	j_1	j_2	j_3	j_4	j_5
i_1	0	0	0	0	0
i_2	1	1	0	0	1
i_3	0	0	0	0	0
i_4	0	0	1	1	0
i_5	0	0	0	0	0

A

Figure 4.4: Example matrix A. An entry of 1 indicates that micro-trip j belongs to cluster with centroid i. Cluster centers are non-zero rows (highlighted), where each cluster member is 1 and non-members are 0. (from [207]).

The DTW distance W is computed between every pair of micro-trips in the set. These distances are stored in matrix $D_{p\times p}$, where each element $d_{i,j}$ represents the distance between micro-trips i and j. Integer programming then uses the matrix D to partition the time series into k distinct clusters.

4.2.4.2 Mixed Integer Programming (MIP) clustering

This section describes how to divide matrix $D_{p\times p}$ into k clusters using MIP.

A binary square matrix $A_{p\times p}$ is constructed, where $A_{ij} = 1$ if micro-trip j belongs to the ith cluster centroid, and 0 otherwise, as illustrated in Figure 4.4. Cluster centroids are indicated by non-zero diagonal entries in A.

The optimization problem is then given by Equation4.1:

$$A^* = \min_A \sum_i \sum_j D_{ij} \times A_{ij} \tag{4.1}$$

The optimization is subject to the constraints in Equations 4.2, 4.3, and 4.4.

1. Only k series can be centroids

$$\sum_{i=1}^{p} A_{ii} = k \tag{4.2}$$

2. Each micro-trip time series can only exist in one cluster

$$\sum_{i=1}^{p} A_{ij} = 1 \; \forall j \in \boldsymbol{P} \tag{4.3}$$

with $\boldsymbol{P} = \{1, 2, ..., p\}$.

3. A row can only contain non-zero entries if the corresponding diagonal is non-zero, so a micro-trip time series can only be in a cluster where the row corresponds to a centroid micro-trip.

$$A_{ij} \leq A_{ii} \; \forall i, j \in \boldsymbol{P} \tag{4.4}$$

After solving this MIP problem, the cluster centroids are indicated by the non-zero diagonal entries in A, and the cluster members are represented by the corresponding non-zero columns in A.

In Figure 4.4, the clusters are 1,2,5 and 3,4 with 2 and 4 serving as the cluster centroids.

4.2.4.3 Choosing number of clusters

Selecting the appropriate number of clusters (k) is often the most challenging aspect of clustering problems. If k is too large, data points of the same type may be split into multiple clusters (overclustering). Conversely, if k is too small, important patterns in the data may be missed (underclustering).

The elbow method, commonly used to determine the optimal number of clusters, relies on plotting the Within-Cluster Sum of Squares (WCSS) against the number of clusters and identifying an "elbow" point on the curve. This method aims to balance simplicity (fewer clusters) with accuracy (capturing significant patterns in the data).

WCSS is the sum of squared distances between data points and their assigned cluster centers, or how tightly clustered the points are. A lower WCSS suggests that the data points are closer to their respective cluster centers. To compute WCSS, one must calculate the distance between each data point X_j and the cluster centroid. For the ith cluster χ_i with centroid $\chi_i^{centroid}$ and containing n data points, WCSS is given by Equation 4.5.

$$WCSS = \sum_{i}^{K} \sum_{j}^{n} (X_j - \chi_i^{centroid})^2 \tag{4.5}$$

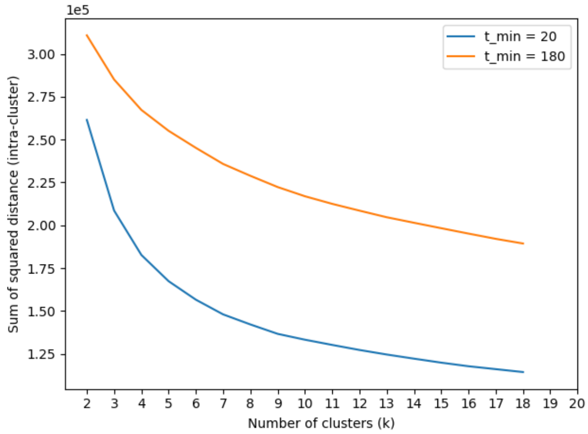

Figure 4.5: Within cluster sum of squares (WCSS) scores for clusters formed with $t_{\text{min}} = 20$ and $t_{\text{min}} = 180$.

The elbow method identifies the optimal number of clusters by looking for the point where the rate of WCSS reduction diminishes significantly. This is considered the ideal number of clusters, balancing the need to capture meaningful patterns while avoiding over-segmentation.

For micro-trips with a higher t_{min}, it is expected that fewer distinct driving patterns would be present, leading to a lower optimal number of clusters. This expectation is confirmed in Figure 4.5, which shows that the optimal k is eight for micro-trips with $t_{\text{min}} = 20$ and six for those with $t_{\text{min}} = 180$.

4.2.5 Candidate micro-trip selection

Following the clustering process, candidate micro-trips are chosen to be used in the final driving cycle. As seen in previous clustering-based methods in the literature, these micro-trips are selected by choosing those closest to the cluster centroids until the desired driving cycle duration is achieved [73, 182, 184, 206]. The target duration in this case ranges between 1800 and 2400 s. While the average trip length in the dataset slightly exceeds 20 minutes, real-world driving conditions and routes can differ substantially, meaning not every trip will follow a uniform pattern or duration. According to Giraldo et al. [194], driving cycles must be at least 1800 s long in order to reliably represent real-world driving behavior. As discussed in Section 4.2.1, this study collects data from three distinct route types (urban, inter-urban, and hilly) at three different times of day (morning, midday, and evening). Capturing this variability is crucial for evaluating vehicles and systems under various conditions. A longer driving cycle provides a more comprehensive depiction of real-world driving by encompassing a wider range of driving scenarios. However, [194] point out that cycles that are too long can become impractical to implement in a laboratory environment, such as running a vehicle on a chassis dynamometer to obtain an emissions or fuel consumption. For this reason, 2400 s is chosen as the upper limit, which is twice the average trip length and matches the duration of the longest cycle used in prior research [52].

The number of candidate micro-trips selected from each cluster is determined by the cluster weight χ_w, which is the size of the cluster in proportion to the smallest cluster, rounded to the nearest whole number (Equation 4.6).

$$\chi_w = round(\frac{len(C)}{len(C^{min})}) \tag{4.6}$$

where χ^{min} is the cluster containing the fewest micro-trips. This approach is motivated by the logic that the frequency of a cluster's appearance in the representative driving cycle should be proportional to the frequency of its appearances in real world data.

4.2.5.1 Stitching the driving cycle

After selecting the candidate micro-trips, they need to be combined to form the final representative driving cycle. This study utilizes a maximum likelihood method to determine the sequence of the micro-trips in the final cycle.

A transition probability matrix, $T_{k\times k}$, is constructed, where each element $T_{w,z}$ represents the probability that a micro-trip from cluster w is followed by a micro-trip from cluster z in the original dataset. Additionally, the likelihood of each cluster being the start of a trip is computed and stored in a vector $S_{1\times k}$. This probability is determined by dividing the number of times a micro-trip from a particular cluster appears at the start of a trip by the total number of trips.

Once the transition probability matrix T and the initial probability vector S are established, they are used to create the representative driving cycle. The cycle assembly begins with a “draw without replacement" strategy, starting with the cluster that has the highest probability of appearing at the beginning of a trip, as determined by the maximum value in S.

The next cluster in the sequence is determined by the maximum transition probability from the matrix T, meaning the cluster with the highest likelihood of following the current cluster is selected to continue the sequence.

In summary, this approach creates a representative driving cycle by modeling the transition probabilities between micro-trip clusters and factoring in the likelihood of a cluster appearing at the start of a trip. The aim is to generate a realistic sequence of clusters that mirrors the patterns observed in the original trip data. The complete procedure is detailed in the following algorithm.

Procedure: Stitching Representative Driving Cycle (RDC) from candidate micro-trips

1. Initialize Representative Driving Cycle (RDC) as an empty list.
2. Start with the cluster that has the highest probability of being seen at a trip's beginning by setting $\chi_{curr} = \arg\max S$.
3. Append the candidate micro-trips from χ_{curr} to RDC.
4. Look up the index of χ_{curr} in matrix T to find χ_{next}.
5. Remove χ_{curr} from T.
6. $\chi_{curr} = \chi_{next}$
7. Repeat steps 3-6 until T is empty. When T is empty it means all clusters are now present in the RDC.

Key:

RDC: Representative Driving Cycle (list)
χ_{curr}: Current cluster being considered (cluster)
χ_{next}: Next cluster to be considered (cluster)
S: Initial probability vector (vector)
T: Transition probability matrix between clusters (matrix)

4.2.6 Cycle Assessment

For cycle assessment, characteristic parameters of the constructed driving cycle are compared against the measured real world driving data. The relative error (RE_i) of characteristic parameter (x_i) in the driving cycle is the percentage difference from the value of that parameter in the measured database (x_i^*).

$$RE_i = \frac{x_i^* - x_i}{x_i^*} \tag{4.7}$$

Performance value (PV) for a cycle is the mean of the absolute values of the RE across all characteristic parameters.

$$PV = \frac{1}{N} \sum_{i=0}^{N} |RE_i| \tag{4.8}$$

where N is the number of characteristic parameters used for cycle assessment.

Numerous characteristic parameters have been proposed in the literature for evaluating driving cycles. These parameters generally fall into six main categories: distance, duration, speed, acceleration/deceleration, dynamics, and stop data. Berzi et al. [41] present a list of 40 parameters from these categories that have been commonly used.

However, utilizing an excessive number of parameters can be counterproductive. Many of these parameters are highly correlated, and including too many can lead to overemphasizing certain aspects in the final driving cycle [49, 206, 208]. As a result, most studies select a subset of these parameters.

This study identifies eight widely used parameters from the literature, which have been shown to significantly influence driving patterns while exhibiting minimal correlation with each other [172, 206]. These parameters, along with the formulas used to calculate them, are listed in Table 4.3. Typically, an acceptable threshold in driving cycle evaluation is set so that no individual parameter deviates by more than 10% from the target values [209].

Note: Speed is obtained from the GPS speed value, and acceleration is calculated using $\frac{dv}{dt}$ between speed samples.

4.3 Results

The RE of each characteristic parameter and final PV for the developed cycles are shown in Table 4.4. The cycle developed with $t_{\min} = 20$ had the better PV of 3.65%, versus

Table 4.3: characteristic parameters (CP) used for cycle assessment.

CP	Unit	Expression
Average speed	km/h	$V = \frac{\sum_{i=1}^{n} v_i}{n}$
Average running speed	km/h	$V_r = \frac{\sum_{i=1}^{n} v_i}{n} \forall\ [V > 2]$
Average acceleration	m/s^2	$a = \frac{\sum_{i=1}^{n} a_i}{n} \forall\ [a > 0.10]$
Average deceleration	m/s^2	$d = \frac{\sum_{i=1}^{n} a_i}{n} \forall\ [a < -0.10]$
Standard deviation acceleration	m/s^2	$\sigma_a = \sum_{i=1}^{n} \frac{(a_i - \overline{a})^2}{n}$
% time accelerating	%	$P_a = \frac{T_a}{T_{total}} \forall\ [a > 0.10]$
% time decelerating	%	$P_d = \frac{T_d}{T_{total}} \forall\ [a < -0.10]$
% time cruising	%	$P_{cr} = \frac{T_{cr}}{T_{total}} \forall\ [-0.10 \leq a \leq 0.10\ ]$

Table 4.4: Characteristic parameter (CP) values for the measured dataset and developed representative driving cycles, and performance values for the latter.

CP	Measured Data	$t_{\min} = 20$		$t_{\min} = 180$	
		Value	Relative Error (%)	Value	Relative Error (%)
Duration (s)	-	2077	-	2151	-
V (km/h)	35.30	35.87	1.62	34.03	-3.59
V_r (km/h)	43.18	44.19	1.29	44.29	2.56
a (m/s^2)	0.58	0.59	2.01	0.66	14.18
d (m/s^2)	-0.66	-0.71	-7.54	-0.70	-7.53
σ_a(m/s^2)	0.66	0.67	1.29	0.70	6.35
P_a (%)	37.79	36.69	-2.92	33.74	-10.72
P_d (%)	33.07	30.27	-8.49	31.30	-5.34
P_{cr} (%)	14.74	15.20	3.02	13.74	-6.85
PV (%)	-	-	3.65	-	7.14

7.14% for the cycle developed with $t_{\min} = 180$. The cycles are plotted in Figure 4.6.

The less restrictive value of $t_{\min}$ enabled the development of a driving cycle that was more representative, meaning it exhibited lower average deviation from the measured dataset across the eight key parameters. This outcome suggests the presence of distinct driving patterns lasting between 20 and 180s. By setting $t_{\min} = 180$, the clustering algorithm cannot effectively differentiate these shorter patterns from others.

This finding makes intuitive sense within the paratransit context. Given the aggressive driving behaviors often observed in paratransit systems, many maneuvers are brief yet distinct [44]. Micro-trips that are significantly longer than these short maneuvers would fail to capture these unique driving patterns.

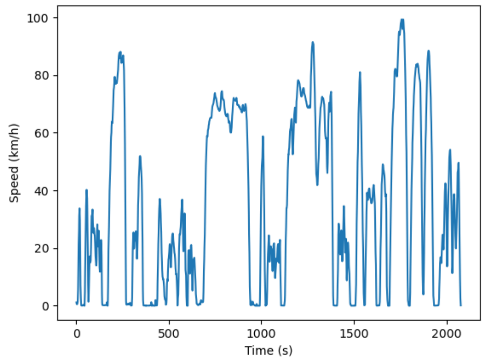

(a) $t_{\text{min}} = 20$

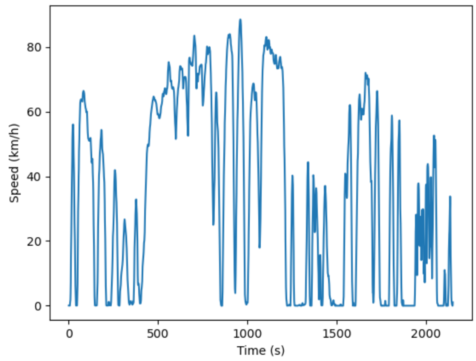

(b) $t_{\text{min}} = 180$

Figure 4.6: Developed representative driving cycles using $t_{\text{min}} = 20s$ (a) and $t_{\text{min}} = 180s$ (b).

4.3.1 Comparison with International Driving Cycles

A comparison between several international driving cycles and the Paratransit Driving Cycle (PDC) developed in this chapter reveals that the PDC most accurately reflects the real-world operating conditions of paratransit. Table 4.5 presents the characteristic parameters of the Worldwide Harmonized Light Vehicles Test Cycle (WLTC) [210], Federal Test Procedure 75 (FTP-75) [211], China Light-Duty Vehicle Test Cycle (CLTC) [212], the PDC, and the measured data. With a performance value (PV) of 3.65% for the PDC, compared to 33.87%, 23.36%, and 25.82% for the WLTC, FTP-75, and CLTC respectively, the PDC is shown to be a much closer match to the real-world conditions of paratransit vehicles. Additionally, unlike the other three cycles, the methodology used to construct the PDC ensures it includes transients derived from actual paratransit vehicle data. These transients, which are unique to paratransit driving behavior, are difficult to reproduce through statistical means and enhance the PDC's ability to represent real vehicle movements accurately.

It is notable that the average acceleration (a) and deceleration (d), along with the percentage of time spent accelerating (P_a) and decelerating (P_d), are significantly higher for both the PDC and the measured data compared to the three other driving cycles. In contrast, the percentage of time spent cruising (P_{cr}) is lower. This highlights the aggressive driving behavior typical of paratransit vehicles, which are known for their frequent rapid acceleration and deceleration maneuvers.

Table 4.5: Comparison of the characteristic parameters and performance value of the paratransit driving cycle (PDC) developed in this study versus several international driving cycles.

CP	Data	PDC		WLTC		FTP-75		CLTC	
		Val.	*RE* (%)	Val.	*RE* (%)	Val.	*RE* (%)	Val.	*RE*(%)
V (km/h)	35.30	35.87	1.62	46.50	31.73	33.89	-3.99	28.96	-17.69
V_r (km/h)	43.18	44.19	1.29	53.15	23.09	25.82	-40.20	37.15	-13.96
a (m/s^2)	0.58	0.59	2.01	0.42	-27.59	0.51	-12.07	0.45	-22.41
d (m/s^2)	-0.66	-0.71	-7.54	-0.44	33.33	-0.58	12.12	-0.49	25.76
σ_a(m/s^2)	0.66	0.67	1.29	0.43	-34.85	0.56	-15.15	0.48	-27.27
P_a (%)	37.79	36.69	-2.92	30.90	-18.23	31.1	-17.70	28.6	-24.32
P_d (%)	33.07	30.27	-8.49	28.60	-13.52	27.1	-18.05	26.4	-20.17
P_{cr} (%)	14.74	15.20	3.02	27.8	88.60	24.7	67.57	22.8	54.68
PV (%)	-	-	**3.65**	-	**33.87**		**23.36**	-	**25.82**

4.4 Summary and key insights

This chapter answers the research questions:

- *How can we construct representative driving cycles for paratransit?* and
- *How well do international driving cycles represent paratransit mobility?*

To address these questions, a novel time series shape-based clustering approach is applied to data collected from paratransit vehicles operating around Stellenbosch, South Africa. Dynamic time warping, combined with mixed integer programming, is used to cluster micro-trips of varying lengths based on the shapes of their time series. By framing the micro-trip clustering problem as an optimization challenge, the method identifies the globally optimal clustering solution. Micro-trips closest to the cluster centroids are then selected for inclusion in the final representative driving cycle. This approach, which incorporates original micro-trips in the cycle development process, ensures that a wide range of real-world transients from the driving data are retained. These transients capture micro-level mobility movements that are often difficult to capture using traditional driving cycle construction techniques.

The study explores the use of t_{min}, which defines the minimum allowable micro-trip length, as a way to modulate the driving patterns identified by the clustering algorithm. Driving cycles generated with different t_{min} values were compared. In this instance, a shorter t_{min} (20 seconds) produced a more representative cycle than the longer duration

$t_{\min}$ (180 seconds), though in other contexts a longer $t_{\min}$ may be more appropriate. Further research is needed to better understand which contexts favor shorter or longer minimum micro-trip lengths.

The Paratransit Driving Cycle (PDC) developed in this study deviated less than 10% from the measured data in all eight characteristic parameters, with an average deviance or "performance value" of 3.65%. This represents a significant improvement over several international comparison cycles, such as the WLTP, FTP-75, and CLTC, which show performance values between 23% and 34%. Additionally, compared to these cycles, the PDC demonstrates higher average acceleration and deceleration, a greater percentage of time spent accelerating and decelerating, and a lower percentage of time cruising. These characteristics align with the aggressive driving behavior often associated with paratransit vehicles, which are known for frequent acceleration and deceleration. The PDC speed-time data series can be accessed through this Mendeley repository: `https://data.mendeley.com/v1/datasets/j7c7gnby57/draft?preview=1`.

Although the specific findings are limited to minibus taxis operating in the Stellenbosch region, the methodology proposed in this study is adaptable and can be used to develop representative driving cycles for other cities and countries. These cycles can provide insight into the typical operating conditions faced by paratransit vehicles in various contexts. As global transportation continues to evolve and electrify, representative driving cycles will be essential for understanding vehicle operational requirements, shaping effective transport policies, and guiding long-term vehicle design decisions related to engine power, fuel type (e.g., diesel or electric), and vehicle size. While the cycles and methods developed here offer a foundation for understanding paratransit mobility, further investigation is needed to examine characteristics such as stop time distributions to provide more actionable insights for transportation system planning and to assess the feasibility of paratransit electrification.

The unique and unconventional driving patterns of paratransit, which have not been extensively studied, require more detailed analysis in different contexts across sub-Saharan Africa. This study marks a step in that direction, but additional efforts are needed to gather data and establish driving cycles for paratransit vehicles in both urban and peri-urban areas of the region.

Urgent action is needed to identify sustainable pathways for the decarbonisation of transport in sub-Saharan Africa, in line with the United Nations (UN) Sustainable Development Goals (SDGs) and the Paris Agreement [...] Yet, at present, [...] this investment is hindered in part by the inability to accurately forecast the likely EV demand for electricity, resulting in uncertain returns on investment.

— K.A. Collett and S. Hirmer [3]

5 Vehicle Energy Requirements and Payback Period

Contents

In the previous chapter, the application of driving cycle construction for paratransit was explored. One of the chief applications of driving cycles in a practical setting is their usage in estimating vehicle energy consumption. For example, driving cycles such as the WLTP or NEDC have been used to determine the mileage rating (e.g. mpg or km/L) of passenger cars in Europe. **Research Gap 3** highlights the need for better energy consumption estimates for paratransit vehicles. This chapter tackles **research**

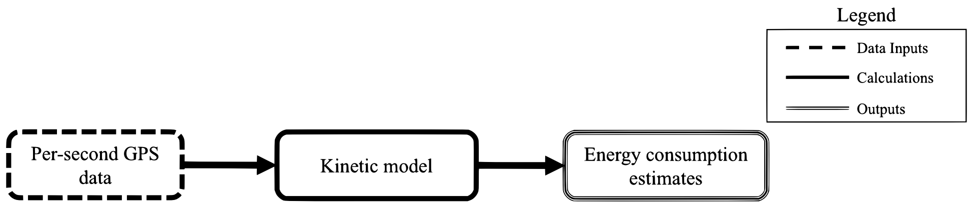

Figure 5.1: How per-second GPS data is used to estimate energy consumption via a kinetic model.

gap 3 by addressing the research questions:

- *What is the energy consumption of paratransit vehicles?*
- *Can per-minute GPS tracking data reliably determine the energy consumption of paratransit vehicles?*
- *What is the payback period of paratransit vehicles?*

In this chapter, the energy consumption of paratransit vehicles is first estimated directly by applying a physics-based kinetic model to the driving cycles developed in Chapter 4. Then, these estimates are validated by applying the kinetic model to the entire GPS dataset to gather a ground-truth and further validate the method of driving cycle construction in the previous chapter. Finally, the estimates here are compared to previous estimates which were based on per-minute data, and the differences are investigated and quantified.

5.1 Kinetic model

To construct high fidelity energy consumption estimates for minibus taxis: i) a kinetic model is required to establish energy demand from motion based on GPS data, and ii) granular GPS data from representative journeys is necessary. Figure 5.1 visualizes at a high level the process for using GPS data and a kinetic model to construct energy consumption estimates.

The purpose of the kinetic model is to estimate the energy consumed by a vehicle throughout the duration of a trip. This section provides background on kinetic models commonly found in the literature, justifies the principles underlying the construction of the kinetic model, and presents the mathematical formulation of the model.

All vehicle kinetic models are based on the fundamental principles of physics, which indicate that the instantaneous power output of an electric vehicle (EV) depends on its velocity, acceleration, and the slope it encounters. However, kinetic models in the literature often show slight variations, with different approaches being used to estimate EV energy consumption based on GPS travel data [213, 214, 215, 216, 217]. These variations arise not from the physical laws themselves, but from differences in assumptions drawn from empirical data or fitted model parameters. Validation using real-world data has shown that these differences can influence model accuracy [218].

For instance, Sagaama et al. [218] demonstrated that incorporating a dynamic regenerative braking formula into the micro-traffic simulator SUMO (Simulation Of Urban MObility) significantly improved the accuracy of its kinetic model, compared to using a static braking factor. This change reduced mean vehicle energy consumption across all trips by 15% (from 0.55 kWh/km to 0.47 kWh/km), a considerable margin. The dynamic formula assumes that drivers fully utilize regenerative braking whenever decelerating. However, in the context of paratransit, where drivers often engage in abrupt braking and make heavy use of brake pads, this formula would overestimate the energy recuperated into the battery. Therefore, this study employs a static regenerative braking factor to avoid overestimation caused by extreme deceleration events.

Sagaama et al. [218] also identified the impact of ambient air temperature on power offtake. While temperature data was unavailable in the dataset for this study, the authors argue that given the specific driving conditions in paratransit contexts and the limited use of low-voltage auxiliary power in these vehicles, this factor would likely have had minimal influence on the model's accuracy.

Though some kinetic models in developed countries have been validated using real-time EV energy consumption data [214, 215], these findings do not necessarily apply to sub-Saharan African paratransit driving conditions. Additionally, this chapter aims to provide high-fidelity estimates of vehicle energy consumption rather than to introduce a novel kinetic model. To minimize potential bias from empirical assumptions or fitted model parameters, the model presented here relies solely on fundamental physical principles.

While empirical assumptions are avoided, specific vehicle parameters must still be employed to estimate EV energy consumption. Table 5.1 lists these constant parameters and their sources. Some of these parameters, such as vehicle weight, rolling resistance coefficient, powertrain efficiency, regenerative braking efficiency, and power offtake, could vary over the course of a trip. However, as discussed earlier, dynamic calculations of regenerative braking efficiency and powertrain efficiency are avoided in this study. Further justification is required for keeping the first three parameters constant:

For vehicle weight, the model uses the fully-laden weight of an electric minibus. Since taxis tend to fill up with passengers at the start of their journey, they are typically operating at maximum capacity. The rolling resistance coefficient reflects the average resistance for car tires on tarred or asphalt roads, which is the typical surface these vehicles travel on. As for powertrain efficiency, dynamically modeling this would pose challenges similar to those encountered with regenerative braking efficiency, especially given the abrupt and inconsistent manoeuvering common in paratransit. Thus, an average powertrain efficiency value is used, based on the expected performance over the trip duration.

Recognizing that the model may be sensitive to these parameters, a sensitivity analysis is conducted, as detailed in Section 5.3.3.2. In the future, when electric taxis are introduced in South Africa and direct measurements become available, these parameters can be empirically fitted to improve the accuracy of electro-kinetic models.

To calculate energy consumption over the course of a trip, GPS data is used to compute the energy either drawn from the battery to power the wheels or auxiliary functions, or the energy recuperated through regenerative braking at each time step n, denoted as $E(n)$. The total energy consumption for a trip is then obtained by summing these values: $E_{\text{trip}} = \sum E(n)$.

To determine the energy flow at each time step, $E(n)$ in kWh, a five-step algorithm is applied, as described below:

1) Compute the sum of all external forces on the vehicle for sample n at a sample period of τ, $F_{\text{ext}}(n)$ in (N), using

$$F_{\text{ext}}(n) = -F_{\text{ad}}(n) - F_{\text{rs}}(n) - F_{\text{rr}}(n) \tag{5.1a}$$

Where $F_{\text{ad}}(n)$ is the aerodynamic drag, $F_{\text{rr}}(n)$ is the rolling resistance friction, and

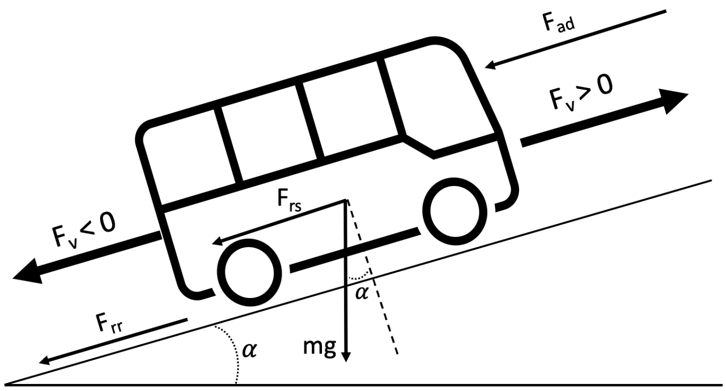

Figure 5.2: The forces acting on a vehicle driving on a slope: Aerodynamic drag (F_{ad}), rolling resistance (F_{rr}), slope drag (F_{sd}), and vehicle force (F_v) which can be either positive or negative depending on whether the vehicle is accelerating or decelerating. F_v is shown with thicker lines as it is usually the greatest force, since it must overcome other forces in order to accelerate or decelerate the vehicle.

Table 5.1: Constants and parameters used in kinetic model.

Parameter	Symbol	Value	Ref.
Gravitational acceleration	g	$9.81\,\mathrm{m/s^2}$	–
Density of air at 25°C	ρ	$1.184\,\mathrm{kg/m^3}$	[219]
Power offtake	p_0	$100\,\mathrm{W}$	[220]
Minibus weight	m_v	$3900\,\mathrm{kg}$	[221]
Roll drag coefficient	c_d	0.36	[222]
Rolling resistance coefficient	c_rr	0.02	[219]
Vehicle's front surface area	A	$4\,\mathrm{m^2}$	[17]
Powertrain efficiency	η_v	80%	[223, 224]
Regenerative braking efficiency	η_rg	65%	[225]

$F_\mathrm{rs}(n)$ is the slope drag force (positive for incline or negative for decline). The forces are shown in Figure 5.2.

The forces in Figure 5.2 are individually calculated from fundamental physics using the following equations and the constants listed in Table 5.1.

$$F_\mathrm{ad}(n) = \frac{1}{2}\rho c_d A(v(n))^2 \tag{5.1b}$$

$$F_\mathrm{rr}(n) = \begin{cases} m_\mathrm{v} g c_\mathrm{rr} cos(\theta(n)), & \text{if } v(n) > 0.3\,\mathrm{m/s} \text{ (GPS noise threshold)} \\ 0, & \text{otherwise} \end{cases} \tag{5.1c}$$

$$F_\mathrm{rs} = m_\mathrm{v} g sin(\theta_\mathrm{t}) \tag{5.1d}$$

where

$$\theta(n) = \begin{cases} \arcsin(\frac{h(n)-h[n-1]}{s(n)}) & \text{if } \mid h(n) - h[n-1] \mid > 0.1\,\text{m (GPS noise threshold)} \\ 0, & \text{otherwise} \end{cases}$$

2) Compute the net energy requirement as the sum of the energy needed to overcome the individual drag forces acting on the vehicle [1].

$$\begin{aligned} E_{\text{net}}(n) = \Delta E_{\text{kin}}(n) + \\ (F_{\text{ad}}(n) + F_{\text{rr}}(n) + F_{\text{rd}}(n) + F_{\text{rs}}(n))(x(n) - x[n-1])\tau \end{aligned} \tag{5.2}$$

3) When $E_{\text{net}}(n) > 0$, energy in (Ws) was **discharged from** the battery to apply propulsion to the vehicle.

$$E_{\text{prop}}(n) = \frac{E_{\text{net}}}{\eta_v} \tag{5.3a}$$

4) When $E_{\text{net}}(n) < 0$, energy in (Ws) was **charged into** the battery via regenerative braking:

$$E_{\text{regen}}(n) = \eta_{\text{rg}} E_{\text{net}}(n) \tag{5.3b}$$

The energy utilization to keep the vehicle running is called power offtake. For every measured time interval, the energy demanded by the power offtake systems in (Ws) is calculated by

$$E_0(n) = p_0\tau. \tag{5.4}$$

5) Compute the total energy flow in a given time-step $E(n)$ in (kWh) by summing the propulsive, regenerative, and constant off-take energies.

$$E(n) = \frac{E_{\text{prop}}(n) + E_{\text{regen}}(n) + E_0(n)}{3.6e+6} \tag{5.5}$$

The energy consumption over the whole trip in (kWh) can be computed by summing over the duration of the trip N.

$$E_{\text{trip}} = \sum_{0}^{N} E(n) \tag{5.6}$$

And finally, the per-distance energy consumption rate in kWh/km, η_{EV} is obtained by dividing E_{trip} by the distance covered during the trip.

[1]A small error was corrected from Step 3 in the kinetic model in the paper [202], which calculated E_{prop} by assuming the difference in measured and expected velocity was caused by F_{prop}.

5.2 Improvements to fidelity of kinetic model

Following the publication of Hull et al. [202] which developed the kinetic model presented above, updates were proposed to the kinetic model in a paper by Abraham et al. [161]. Specifically, rotational inertia and radial drag are added. Rotational inertia and radial drag are governed by equations 5.7 and 5.8 respectively.

$$\Delta E_{rot} = \frac{I \times \omega}{2} = \frac{I \times v^2}{2 \times r_{wheel}^2} \tag{5.7}$$

$$\Delta E_{rad} = c_{rad} \times \frac{m \times v^2}{r_{curve} \times \tau} \tag{5.8}$$

where I is the internal moment of inertia, ω is angular velocity, r_{wheel} is the radius of the vehicle's wheel, c_{rad} is the radial drag coefficient, and r_{curve} is the radius of the turning curve. Equation 5.2 from before is now updated with two additional phenomena, thus increasing the fidelity of the model.

$$\begin{aligned} E_{\text{net}}(n) = \Delta E_{\text{kin}}(n) + \Delta E_{\text{rad}}(n) + \Delta E_{\text{rot}}(n) + \\ (F_{\text{ad}}(n) + F_{\text{rr}}(n) + F_{\text{rd}}(n) + F_{\text{rs}}(n))(x(n) - x[n-1])\tau \end{aligned}$$

Rotary inertia was originally excluded because it was hypothesized to have an insignificant effect on energy consumption, and believed that there was no way to obtain an accurate value for the internal moment of inertia I. For this, an accurate estimation of the distribution of vehicle mass around the axis of rotation is required, and at the time was unavailable for the minibus taxis under investigation. Abraham et al. [161] get around this by using a suggested value for SUVs of 16 kgṁ^2 gathered from Eclipse SUMO [226]. To validate this value, they compute a rotational inertia of 5.5 kgṁ^2 for the minibus taxi based on wheel mass and radius, and assume the rest of the vehicle's rotary inertia comes from the other rotating components of the vehicle such as the gearbox, differential, and motor. There is likely some amount of error in this assumption, but it turns out to be irrelevant, as in their sensitivity testing they confirm the initial belief that rotary inertia does not significantly affect energy usage.

Radial drag was originally excluded because it was believed there was no reliable way to find r_{curve} for Equation 5.8. Abraham et al. [161] get around this by calculating $r_{curve} = \frac{\Delta s}{\Delta \theta}$, where $\Delta\theta$ is the change in the vehicle's heading angle. The radial drag coefficient used is 0.1, per the documentation of the urban fleet simulator SUMO [161, 226]. Abraham et al. [161] find that radial drag does have a meaningful effect on the energy consumption results.

Given these findings, and the more robust theoretical basis for a model which includes rotational inertia and radial drag, these components were added to the kinetic model. The results presented in the following section are obtained using the updated model including rotary inertia and rotational drag.

5.3 Results: Electric paratransit energy consumption

In this section, the *first research question* of the chapter is answered: *What is the energy consumption of paratransit vehicles?*. First, the energy consumption of paratransit vehicles (in kwh/km) is estimated using the representative driving cycle developed in Chapter 4, the Paratransit Driving Cycle (PDC). The PDC energy consumption estimates are then validated against the entire raw dataset. After the validation of results, a regression model is constructed to quantify the effects of net elevation, average speed, and average absolute acceleration on energy consumption. Finally, the section explores the energy consumption estimates from per-second data in comparison to energy consumption estimates from an equivalent per-minute dataset, which is the standard in previous literature. The results are compared to the values seen in previous publications, and the energy signal for different forces on the vehicle is decomposed for per-second and per-minute is decomposed and analysed.

5.3.1 Estimates from Paratransit Driving Cycle

After applying the kinetic model to the PDC, the paratransit vehicles are found to have an energy consumption η_{EV} of 0.55 kWh/km.

To validate these estimates, the kinetic model is applied to the entire dataset of raw GPS data gathered. The results from the entire dataset are shown in Figure 5.3.

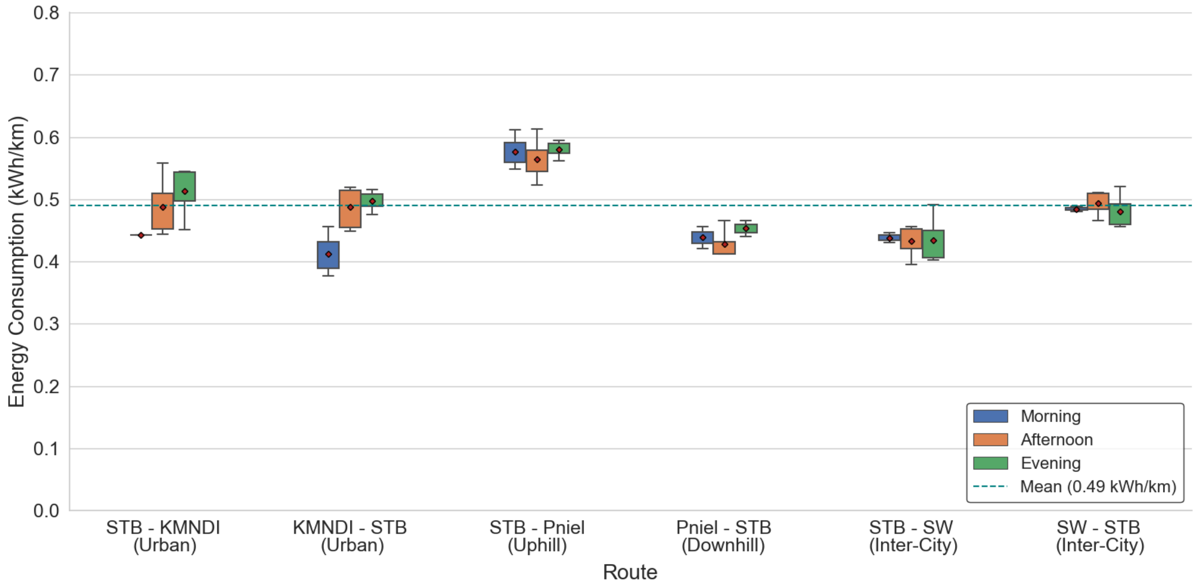

Figure 5.3: Distribution of energy consumption for each route in the morning, afternoon, and evening. The overall mean energy consumption of 0.49 kWh/km is indicated with a dashed teal line.

Specifically, Figure 5.3 shows the distributions of energy consumption estimates for the three routes considered, in both directions, for each time of day (yielding a total of 3 x 2 x 3 = 18 distributions). These are the first high fidelity estimates of paratransit energy consumption ever constructed. A dashed teal line indicates the overall mean of 0.49 kWh/km, which differs by 10% from the estimate derived from the PDC. This is an acceptable level of difference and validates the representativeness of the driving cycle construction method presented in Chapter 4 for usage in estimating paratransit energy consumption.

The figure demonstrates how energy consumption is largely determined by the characteristics of the route on which a minibus is driving. The route characteristic with the clearest effect is elevation change, as evidenced by the difference observed between the steep incline and steep decline directions of the hilly route (to/from Pniel).

Although distinctive patterns are observed between routes, the results do not show a consistent effect of time of day on energy consumption on any route. The estimates are within a fairly tight range for each route, with a mean inter-route standard deviation of 0.02 kWh/km, which supports the hypothesis the per-second sampling strategy leads to high fidelity estimates.

Table 5.2 provides a summary of the average energy consumption along with key mobility characteristics for each route. It highlights differences in the physical attributes of the routes and factors related to traffic flow, such as speed and stop frequency. The urban route exhibited the highest average absolute acceleration and the lowest speeds, reflecting the stop-and-go nature of urban travel. The impact of this driving pattern on energy consumption is discussed in subsequent sections. The average absolute acceleration is used to consider both acceleration and deceleration.

Table 5.2: Breakdown of average energy consumption, net elevation change, average speed, maximum speed, and average absolute acceleration by route.

Route	Energy Consumption (kWh/km)	Net Elevation Change (m)	Average Speed (km/h)	Maximum Speed (km/h)	Average Acceleration (absolute) (m/s^2)
STB - KMNDI	0.50	12.7	15.9	64.2	0.52
KMNDI - STB	0.47	1.3	26.1	70.7	0.57
STB - SW	0.44	-68.1	42.5	101.4	0.50
SW - STB	0.49	67.5	44.2	98.5	0.49
STB - Pniel	0.57	126.7	33.3	84.0	0.48
Pniel - STB	0.44	-127.2	40.4	90.2	0.52

5.3.2 Results in context

This section contextualizes energy consumption results by comparing them to values reported in the literature and the manufacturer-stated kWh/km metrics for similar vehicles in real-world conditions. Table 5.3 outlines these values along with their sources. Although some vehicles lack data for certain parameters in Table 5.1, they have comparable physical and mechanical characteristics to the minibus taxis under study, making them appropriate for comparison.

Figure 5.4 presents the energy consumption distributions for each route alongside the values from Table 5.3. Since Section 5.3.1 found no effect of time of day on energy consumption, data are aggregated by route for a clearer comparison.

The results are slightly higher than the energy consumption values for small passenger vans on the market, which typically range between 0.20 and 0.36 kWh/km. This difference is reasonable given that taxi drivers are known for aggressive driving, which tends to increase energy usage [227, 228, 229, 230]. The similarity to manufacturer values provides confidence in the accuracy of these estimates.

However, the mean estimate is lower than the values from the literature, which range from 0.50 to 0.93 kWh/km. The 0.50 kWh/km figure from Collett and Hirmer [3] was an informed guess by the researchers, reasonably accurate but not supported by data or modeling. Notably, the highest values from Abraham et al. [29], despite being based on GPS tracking data, were the most distant from the estimates. Their method involved using the EV fleet simulator "ev-fleet-sim," which relies on the Simulation of Urban MObility (SUMO) micro-traffic simulator and an EV kinetic model developed by Kurczveil et al. [213]. The EV fleet simulator works by processing GPS waypoints per minute and uses SUMO's routing function to simulate per-second mobility data on a virtualized road infrastructure in Open Street Maps. This data is then run through a kinetic model to estimate energy consumption.

As noted in Section 2.2.2, an initial evaluation of their method pointed to inaccuracies in the physical infrastructure virtualization and per-second driving simulation as potential reasons for the high consumption rates. After identifying these issues, Giliomee et al. [63] attempted to correct the flaws in ev-fleet-sim and integrate the kinetic-energetic model developed by Hull et al. [231], aiming to provide accurate estimates of paratransit vehicle energy requirements using only per-minute GPS data. This approach is promising because it could reduce the data required to estimate energy consumption for paratransit fleets across Sub-Saharan Africa. Significant progress was made, with initial overestimations of nearly 240% reduced to around 10% [63]. However, the fixes involved many manual steps which could not feasibly be implemented at scale, and even with the improved simulator, the research suggests that per-minute data may not achieve the accuracy and reliability of per-second data for energy consumption estimates in the near future.

5.3.3 Effect of mobility characteristics and physical constants on energy consumption

This analysis of this section aims to 1) generalize the energy consumption estimates for contexts not explicitly represented in the dataset and 2) do so for different sets of vehicle physical parameters.

Table 5.3: Comparative energy consumption (kWh/km) values seen in the literature and from real-world OEM vehicle specs.

Source		Energy Consumption (kWh/km)
Literature	Abraham et al. [29]	0.93
	Cignini et al. [43]	0.70
	Collett et al. [1]	0.50
OEM	Higer H5C EV [221]	0.36
	Dongfeng E-Mini Van [232]	0.27
	Ruivii Toano [233]	0.26

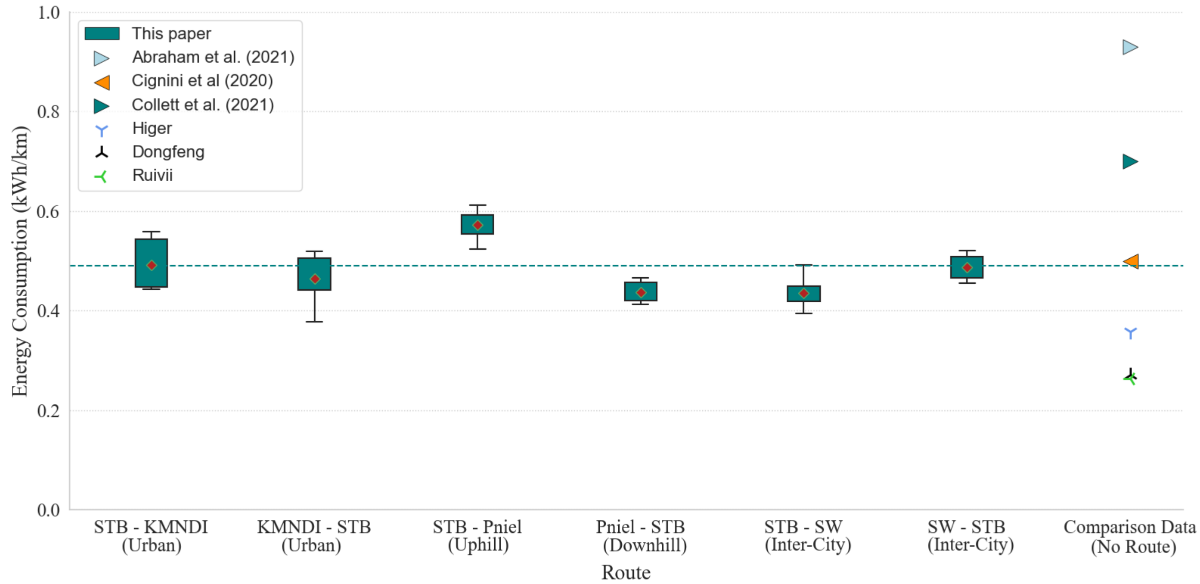

Figure 5.4: Distributions of energy consumption, compared to state-of-the-art from literature and real world vehicle specs. The dashed teal line represents the mean of the estimates constructed from the per-second data (0.49 kWh/km).

To address the first objective, the effects of net elevation change (m), average speed (m/s), and average absolute acceleration (m/s^2) on energy consumption are quantified with Ordinary Least Squares (OLS) regression. Absolute acceleration is used to account for the combined effect of both acceleration and deceleration. For the second objective, the sensitivity of the kinetic model to each vehicle parameter listed in Table 5.1 is calculated.

Elevation change, speed, and acceleration were chosen as key factors because they correspond to forces in the kinetic model and are also easily measurable in real-world scenarios. Respectively, they relate to slope drag, aerodynamic drag, and vehicle force. Elevation change is factored into slope drag via the slope angle (Equation 5.1d), speed directly affects aerodynamic drag (Equation 5.1b), and acceleration is derived as the change in vehicle velocity between timesteps. [2].

Although slope angle directly enters the slope drag equation, net elevation change was chosen instead of average slope angle because it is a more practical measurement. It is easier to obtain net elevation change than average slope angle for global routes, and net elevation change was found to approximate slope angle effectively. Quantifying the effects of these factors on energy consumption is valuable only if the results can be applied by stakeholders. Net elevation change and speed limits are easily accessible for any route through a simple online search. Including average absolute acceleration in the regression controls for the impact of driver behavior and micro-traffic flows on energy consumption, factors that are otherwise difficult to predict without GPS data.

In addition to corresponding to forces in the kinetic model, elevation change, speed, and acceleration are the only measured factors that do so, ensuring that the regression model captures most of the variation in energy consumption. This confidence is supported by the OLS regression's R-squared value of 0.98, which indicates that 98% of the variation in energy consumption is explained by the variables included in the model.

5.3.3.1 Effects of Elevation Change, Speed, and Acceleration

An OLS regression model is used to quantify the effects of net elevation, average speed, and average absolute acceleration on energy consumption. OLS regressions estimate model parameters by minimizing the sum of the squared differences between the observed outcome variable (energy consumption in this case), and the outcome predicted by a linear function of the explanatory variables. The OLS regression results are presented in Table 5.4.

The coefficients in a regression specify how much the outcome variable changes for a 1 unit increase in each factor:

$$\text{coeff} = \frac{d_{\text{outcome}}}{d_{\text{factor}}}$$

Specifically, the regression in Table 5.4 shows that an increase of 1 m in net elevation change is predicted to increase energy consumption for a trip by 0.0007 kWh/km, an increase in average speed of 1 km/h is predicted to increase the average energy consumption

[2]The last force in the model, rolling resistance (equation 5.1c), does not have a direct mobility characteristic analog in the model. While slope angle does enter into the rolling resistance equation, this force is primarily a consequence of the physical parameters of mass and rolling resistance coefficient.

for a trip by 0.0042 kWh/km, and an increase of 1 m/s^2 in average acceleration during a trip is predicted to increase energy consumption by 0.4540 kWh/km. These coefficients on net elevation change and average speed are the most useful because they are the two factors that would be easiest to ascertain in the absence of GPS tracking data, and thus most likely to of use for extrapolating an energy consumption estimate in another area.

One potentially confusing aspect of these results is the high coefficient for acceleration compared to the other two factors, which is due to differences in units. While net elevation change and average speed vary by tens or hundreds, average acceleration typically falls between 0 and 1 m/s^2.

To better understand the relative impact of each factor on energy consumption, a standardized OLS regression model is created using the same variables as in the previous section. The standardized regression results are displayed in Table 5.5. In a standardized regression, the coefficients indicate how many standard deviations (σ) the outcome variable changes for a 1 σ change in an explanatory variable.

The asterisks next to the regression coefficients represent the p-value of the coefficient. A p-value below 0.05 is considered statistically significant, with ***, **, and * indicating p < 0.001, p < 0.01, and p < 0.05, respectively. All four factors are statistically significant at p < 0.001. The number in parentheses beneath each coefficient represents the standard deviation of that coefficient. The R-squared value of 0.98 shows that this linear model with the four variables captures almost all the variation in energy consumption in the dataset.

These regression results, even in the non-standardized model, provide useful insights for anyone planning to deploy electric minibuses in different regions with varying mobility characteristics. While high-frequency GPS data would be ideal for analyzing energy consumption, obtaining such data can be challenging or impossible in certain situations.

One noticeable difference between the results of the two regression models is the significance level of the coefficient for acceleration. In the non-standardized model, it is marked with ***, indicating $p < 0.001$, while in the standardized model it is marked with **, indicating $p < 0.01$. This discrepancy arises from the difference in units between the models. Specifically, the non-standardized model predicts that energy consumption will change by 0.4540 kWh/km for each 1 m/s^2 change in average absolute acceleration,

Table 5.4: OLS Regression model of average speed, net elevation change, and average absolute acceleration on energy consumption. The units on each coefficient are a ratio of the units of the corresponding factor (m, m/s, and m/s^3) to the units on energy consumption (kWh/km). The standard deviation of each coefficient is shown in brackets beneath the coefficient. The percentage of the variation in the data captured by the model is shown in the R-squared statistic. The *** indicates 99.9% confidence that the coefficient is statistically significant.

	Average Trip Energy Consumption (kWh/km)
Net Elevation Change (m)	0.0007*** (kWh/km per m)
	[0.0001]
Average Speed (m/s)	0.0042*** (kWh/km per m/s)
	[0.0006]
Average (absolute) Acceleration (m/s^2)	0.4540*** (kWh/km per m/s^2)
	[0.0395]
R-squared	0.9780
R-squared Adj.	0.9769

Table 5.5: Standardized OLS Regression model of net elevation change, average speed, and average absolute acceleration on energy consumption. Each coefficient represents how many standard deviations (σ) energy consumption changes for a 1 standard deviation change in the corresponding factor. The standard deviation of each coefficient is shown in brackets beneath the coefficient. The ** and *** indicate 99% and 99.9% confidence in the statistical significance of the coefficients respectively.

	Average Trip Energy Consumption (σ)
Net Elevation Change (σ)	0.9037*** (σ kWh/km per σ m)
	[0.0543]
Average Speed (σ)	0.3735*** (σ kWh/km per σ m/s)
	[0.0542]
Average (absolute) Acceleration (σ)	0.1229** (σ kWh/km per σ m/s^2)
	[0.0536]

whereas the standardized model estimates a change of 0.1229 σ in energy consumption for a 1 σ change in acceleration.

5.3.3.2 Sensitivity of kinetic model parameters

Next, the sensitivity of the kinetic model to various vehicle physical parameters is examined. Table 5.6 summarizes the results of the sensitivity analysis. The first column indicates the relative sensitivity of energy consumption as the percentage change in consumption for a 1% change in a given parameter. The second column presents the absolute change in energy consumption in kWh/km for a 1% change in a parameter.

Table 5.6: Sensitivity of kinetic model to physical parameters.

Parameter	Sensitivity ($\frac{\text{\% change output}}{\text{\% change input}}$)	Sensitivity ($\frac{\text{absolute change output}}{\text{\% change input}}$) (kWh/km)
Minibus weight (m_{v})	0.84	0.004
Rolling resistance coefficient (c_{rr})	0.48	0.002
Roll drag coefficient (c_{d})	0.15	0.001
Vehicle's front surface area (A)	0.15	0.001
Radial drag coefficient (c_{rad})	0.15	0.001
Regenerative braking efficiency (η_{rg})	-0.50	-0.002
Powertrain efficiency (η_{v})	-1.48	-0.006

The results reveal that the model is most sensitive to powertrain efficiency, followed by vehicle weight, regenerative braking efficiency, and rolling resistance coefficient, with drag coefficient and frontal surface area having the least impact.

The parameters used for the estimates in this chapter, listed in Table 5.1, were selected from various literature sources, although alternative values could be justified, as they vary across studies [29]. Similar to the OLS regression findings, the sensitivity analysis results are helpful in assessing how changes in individual parameters affect energy consumption in taxis. For instance, the weight of a taxi can fluctuate by several hundred kilograms based on passenger load and luggage. If the minibus weight were increased by 10% (i.e., by 390 kg), raising the total weight to 4.290 kg, the mean energy consumption would be expected to rise by 8.4%, or 0.03 kWh/km, resulting in a total energy consumption of 0.42 kWh/km.

To generate Table 5.6, the overall mean energy consumption was simulated using three different input values for each parameter. The central value for each parameter correspond to the values from Table 5.1. Sensitivities were determined by running the model twice for each parameter. Once with the parameter varying above the central value, and once below, while holding all other parameters equal. The sensitivity reported in Table 5.6 is the average of these two values. The input values are given in Table 5.7. The values are chosen based on a range of likely operating conditions and values seen in the literature.

Table 5.7: Values used to compute sensitivities of the physical parameters of the kinetic model.

Parameter	Values		
Minibus weight (kg)	2900	3900	4900
Rolling resistance coefficient	0.01	0.02	0.03
Roll drag coefficient	0.24	0.36	0.48
Frontal Area (m^3)	3.50	4.00	4.50
Radial drag coefficient	0.05	0.1	0.15
Regenerative braking efficiency(%)	0.50	0.65	0.80
Powertrain efficiency (%)	0.85	0.90	0.95

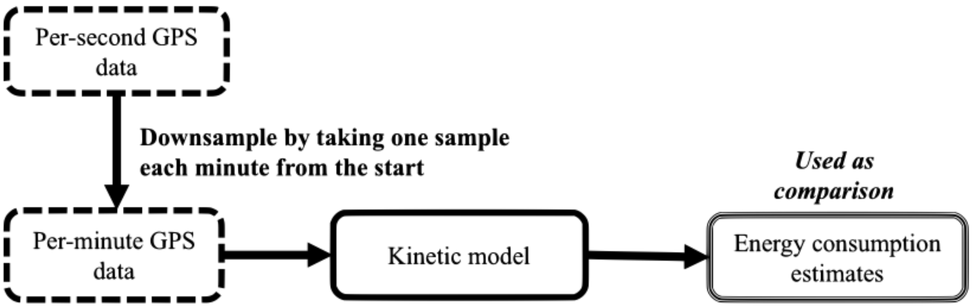

Figure 5.5: How an equivalent per-minute dataset created from the raw per-second data and used to construct energy consumption results. These results are then compared with the results generated by the process in Figure 5.1.

5.4 Evaluation of sampling frequency: Per-second vs per-minute data input

This section evaluates the energy consumption estimates derived from per-second data compared to those from an equivalent per-minute dataset, addressing the chapter's second research question: Can per-minute GPS tracking data reliably estimate the energy consumption of paratransit vehicles? To assess the model's performance with per-second versus per-minute data, an equivalent per-minute dataset was created by downsampling the per-second data to one GPS observation per minute using the Python pandas resample function. Starting from the first sample, subsequent samples are taken at one-minute intervals. The per-minute data is then input into the kinetic model to generate energy consumption estimates, which are compared to the original results. This process is depicted in Figure 5.5.

Throughout the section, per-second data and results are shown in teal, while the per-minute data is represented in orange.

The differences between the per-second and per-minute datasets are illustrated in

Figure 5.6, which shows the elevation change (m), speed (km/h), and acceleration (m/s^2) profiles for an example trip from Pniel to STB. Each plot is paired with a chart that quantifies the percentage of each mobility characteristic's signal captured by the per-minute sampling frequency. To construct these charts, a Fast Fourier Transformation (FFT) of the per-second data is performed, the corresponding power spectral density is retrieved, and the percentage of the signal captured at sampling frequencies up to $\frac{1}{60}$Hz (orange bars) is calculated. The teal bars represent the percentage of the signal captured by higher frequencies, up to $\frac{1}{2}$Hz, which is the Nyquist frequency for per-second data [80].

These plots demonstrate that, compared to per-second data, the per-minute data captures 28.4% of the elevation change, 83.4% of the speed, and only 8.6% of the acceleration data. While speed is well represented in the per-minute data, both elevation change and acceleration are much noisier, requiring a higher sampling frequency for more accurate capture. As a result, the driving cycle in the per-minute dataset is much smoother and fails to account for the vehicle's micro-mobility movements.

Although data for all trips are available in the Mendeley repository, the specific trip used in Figure 5.6 is included as an addendum along with the kinetic model code at: `https://github.com/ChullEPG/Bumpy-Ride`, allowing readers to explore the example trip at their convenience.

Table 5.8 compares the net elevation change, total absolute elevation change, average speed, and average acceleration profiles by route for the per-minute data versus the per-second data. While average speed and net elevation change are reasonably captured in the per-minute data, average absolute acceleration and total absolute elevation change are consistently underestimated. Total absolute elevation change was included because, while per-minute data captures general trends in elevation change, it misses the smaller ascents and descents occurring between minutes that contribute to the total absolute elevation change. The impact of these omissions on vehicle energy consumption is discussed later in the section.

Together, Figure 5.6 and Table 5.8 support the hypothesis that per-minute data fails to capture micro-mobility patterns.

The comparison of energy consumption estimates derived from per-minute and per-

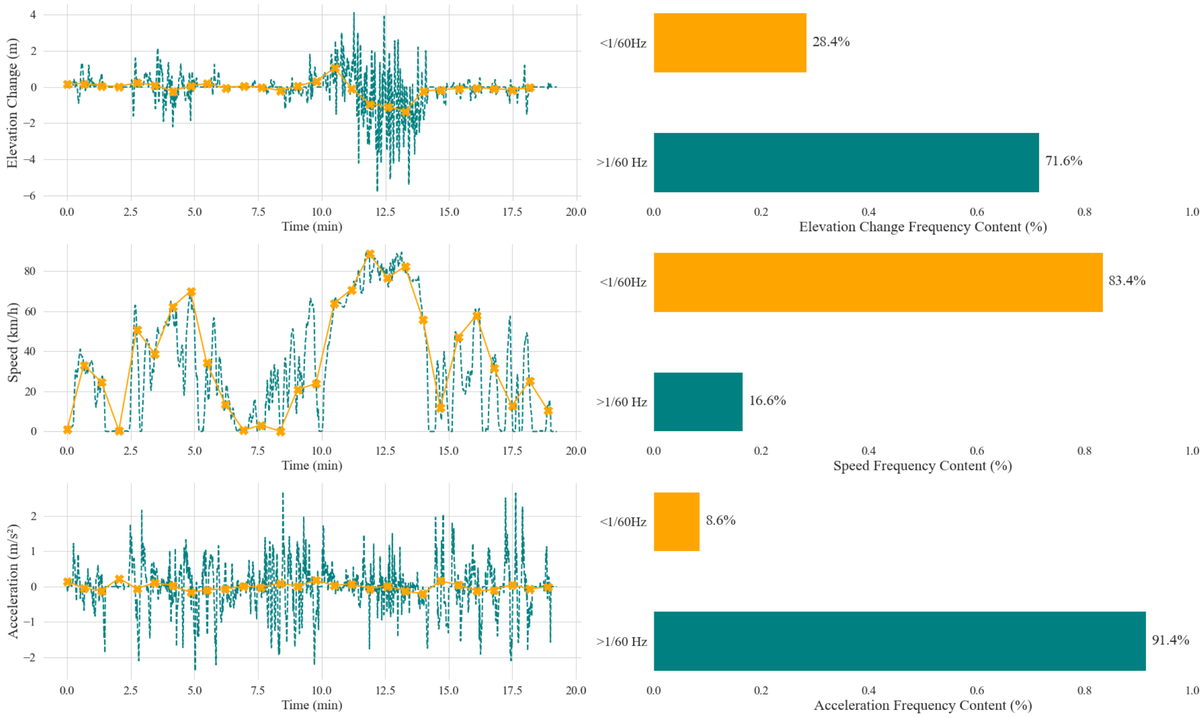

Figure 5.6: Comparison of the elevation change, speed, and acceleration profiles in the per-second data (dashed teal lines) and per-minute data (solid orange lines) for an example route from Pniel - STB. Each minutely sample on the orange lines is marked with an marked with an X. The bar charts show the portion of signal that is captured in the per-minute sampling frequency (<1/60Hz), and the portion of signal that it misses (>1/60Hz) for each factor.

Table 5.8: Characteristics of factors known to influence efficiency in per-minute dataset (orange), compared to the analogous measurements in the per-second dataset (teal) from 5.2.

Route	Net Elevation Change (m)	Total Elevation Change (absolute) (m)	Average Speed (km/h)	Average Acceleration (absolute) (m/s^2)
STB - KMNDI	17.5 (12.7)	25.2 (92.8)	14.0 (15.9)	0.07 (0.52)
KMNDI - STB	-3.5 (1.3)	169.7 (230.8)	24.4 (26.1)	0.09 (0.57)
STB - SW	-70.5 (-68.1)	423.3 (736.4)	40.3 (42.5)	0.14 (0.50)
SW - STB	67.7 (67.5)	409.6 (755.0)	43.1 (44.2)	0.11 (0.49)
STB - Pniel	126.9 (126.7)	481.2 (797.6)	32.6 (33.2)	0.10 (0.48)
Pniel - STB	-127.2 (-127.2)	457.4 (793.2)	40.6 (40.4)	0.10 (0.52)

second data is presented in Figure 5.7. This figure illustrates that, compared to the per-second data, the per-minute data a) consistently underestimates energy consumption and b) exhibits greater variance in its estimates. On average, the overall energy consumption is 31% lower in the per-minute estimates—0.27 vs. 0.49 kWh/km—and the average inter-route standard deviation is 0.13 kWh/km, over six times higher than the 0.02 kWh/km seen in the per-second estimates. The coefficient of variation for the per-minute estimates across all trips is 0.29, nearly triple the 0.13 observed in the per-second data.

However, the per-minute data does retain the relative effect of elevation change, as seen in the higher energy consumption for the uphill route (STB to Pniel) and lower consumption for the downhill route (Pniel to STB). This is because, while the per-minute data accurately captures the net elevation change for the route, it misses the small dips and climbs that contribute to total elevation change and, subsequently, to overall energy consumption.

The main shortcoming of the per-minute dataset—its inability to capture micro-mobility patterns—is most pronounced in urban environments, where trips are shorter and driver behavior has a greater impact on energy consumption relative to environmental factors. As shown in Figure 5.7, the short urban trips to and from Kayamandi (KMNDI) have the greatest variance, largely due to the relatively small sample size. Additionally, the urban route features lower elevation change and speed limits compared to the hilly or inter-city routes, coupled with higher average absolute acceleration. As discussed in Section 5.3.3, micro-mobility patterns, such as frequent acceleration and deceleration, have a more significant effect on energy consumption on these routes. An analysis of jerk (m/s^3) and the number of stops per kilometer across all routes also showed that the urban environment had the highest jerk and the most stop-start driving cycles. These findings indicate that per-minute data is least reliable for estimating vehicle energy consumption in urban or residential settings, which tend to have low elevation changes, low speed limits, and a higher number of acceleration/deceleration events (i.e., aggressive driving behaviors).

One key question remains: where does the energy consumption underestimate in the per-minute data originate? To answer this, we must revisit the physics of the kinetic model.

The model incorporates eight distinct physical forces, six of which are external or “environmental forces," and two that are generated by the vehicle, known as “vehicle forces." The breakdown is as follows:

- Environmental forces: Propulsive slope drag (downhill), resistive slope drag (uphill), propulsive rotational inertia (accel), resistive rotational inertia (decel), aerodynamic drag, rolling resistance, radial drag.

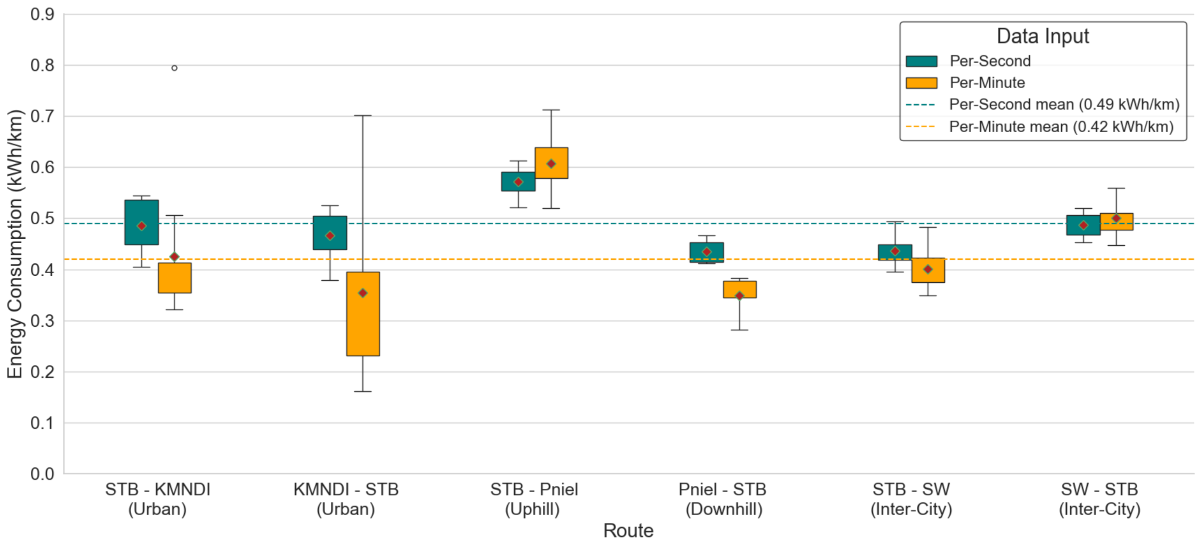

Figure 5.7: Distribution of energy consumption estimates for each route when the kinetic model is inputted with per-second data versus per-minute data. The dark red diamond in each box represents the mean for that route. The teal and orange dashed lines represent the mean across all trips for the per-second and per-minute inputs respectively. There is one outlier trip at 0.83 kWh/km in STB - KMNDI.

- Vehicle forces: Propulsive (motor to wheels), braking (wheels to motor)

At a basic level, the vehicle needs to generate enough propulsive or braking force to overcome the environmental forces and achieve the driver's desired acceleration or deceleration. The energy expended by the battery to counteract the environmental forces and achieve this acceleration or deceleration can be attributed to environmental factors and driver behavior. If the per-minute data underestimates either the environmental forces or the driver's intended acceleration, it will lead to an underestimation of energy consumption.

To pinpoint the source of the underestimation in the per-minute model, the contributions of each environmental and vehicle force to energy consumption (in kWh/km) are analyzed, and a Fast Fourier Transform (FFT) is used to determine how much of this energy is captured by the per-minute sampling frequency. These results are shown in Figure 5.8. The top bars represent the amount of energy (in kWh/km) captured in the per-minute data for each force, while the bottom bars show the amount of energy missed. The substantial size of the bottom bars highlights the source of the underestimation in the per-minute dataset, as seen in Figure 5.7.

Table 5.9 further decomposes the energy contribution of each force for each dataset, categorized by route. The most significant discrepancies are observed primarily in the two vehicle forces and the slope drags. This reflects how the per-minute dataset underestimates average absolute acceleration and total absolute elevation change, as indicated in Table 5.8. Net elevation change is accurately captured, as evidenced by its preserved effect in Figure 5.7, particularly in the difference between uphill and downhill routes. However, the omission of some total absolute elevation change results in an underestimation of the total contribution of slope drag to energy consumption. Although radial drag and rotational inertia are poorly represented in the minutely data, their overall contribution to energy consumption is relatively minor, resulting in a negligible net effect.

Table 5.9 further breaks down the energy contribution of each force by dataset and route. The largest discrepancies are primarily observed in the two vehicle forces and slope drag. This reflects how the per-minute data underestimates both average absolute acceleration and total absolute elevation change, as noted in Table 5.8. While net elevation change is captured accurately, as demonstrated by its preserved effect in Figure 5.7 – especially in the difference between uphill and downhill routes—the omission of some total absolute elevation change results in an underestimation of slope drag's contribution to energy consumption. Though radial drag and rotational inertia are poorly represented in the per-minute data, their overall contribution to energy consumption is minor, leading to a negligible net effect.

In summary, this section illustrates that per-minute data fails to capture vehicle micro-mobility patterns, leading to underestimates in energy consumption. Additionally, the variance in the per-minute estimates is higher, supporting the initial hypothesis that per-second GPS data would provide a more accurate representation of paratransit micro-mobility patterns.

5.5 Implementation of results: Modelling with energy consumption

Energy consumption is a crucial input parameter in various downstream models that are essential for assessing the technical and financial viability of vehicle electrification

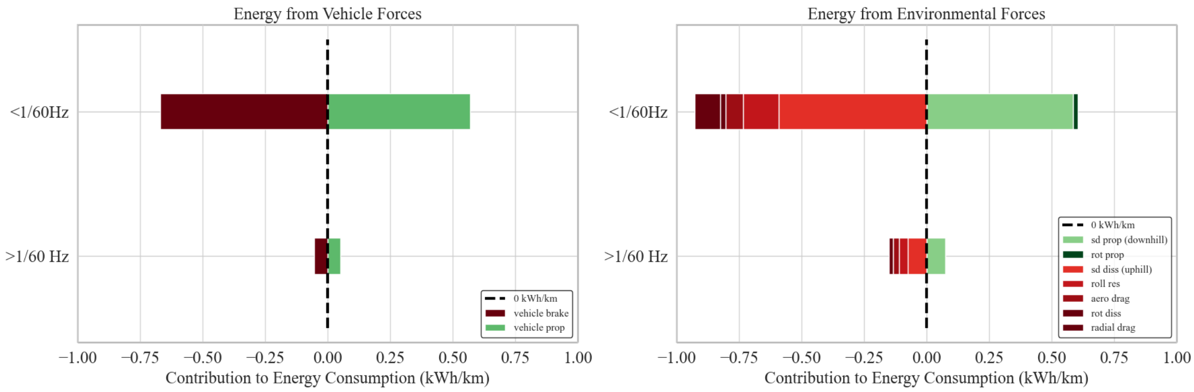

Figure 5.8: FFT analysis disaggregated by force type. Shows how much energy for each force is captured by sampling frequencies up to once per-minute (<1/60Hz) and greater than once per-minute (>1/60Hz), for all trips. The bottom bar in each graph represents the amount of energy not captured in the per-minute data.

Table 5.9: Percentage difference between energy captured in per-minute and per-second datasets for each vehicle and environmental force.

Route	Vehicle Braking	Vehicle Propulsive	Propulsive Slope Drag (downhill)	Dissipative Slope Drag (uphill)	Aerodynamic Drag	Rolling Resistance
KMNDI - STB	-83.5	-61.8	-51.8	-78.5	6.2	12.2
STB - KMNDI	-52.4	-28.7	8.0	9.9	-1.6	10.0
STB - Pniel	-70.1	-25.9	-34.5	-14.6	15.3	12.3
Pniel - STB	-51.7	-46.8	0.1	-43.7	30.0	22.3
STB - SW	-64.8	-51.1	-28.8	-48.8	1.8	0.6
SW - STB	-75.5	-42.0	-37.0	-46.4	6.4	3.0
Mean	-66.3	-42.7	-24.0	-37.0	9.7	10.1

for fleet owners. To illustrate this, the energy consumption estimates developed earlier in this chapter are employed in three distinct ways. Firstly, these estimates are used to calculate vehicle range based on different battery sizes in Section 5.5.1 to ascertain the likely battery size necessary for vehicle operation. Then, given the emphasis that survey respondents in Chapter 3 placed on environmental impact of the taxi industry, GhG and emissions impact of paratransit electrification are briefly assessed in Section 5.5.2. Finally, Section 5.5.3 addresses the third research question of the chapter: *What is the payback period of paratransit vehicles?*.

5.5.1 Battery sizing

Since energy demands for EVs are known to vary depending on driving conditions [227], this chapter provides recommendations for multiple scenarios. Specifically, values are suggested for urban, inter-city, and hilly (uphill and downhill) conditions. Uphill and downhill routes are treated separately because if a taxi ascends before a charge and descends afterward, different energy consumption figures are required for accurate planning, as the energy demands vary significantly between the two directions.

Electric minibus taxis in South Africa often cover over 200 km daily, needing to travel at least 100 km before the opportunity to stop and recharge [29]. Typically, taxis operate continuously during rush hours—roughly 6 AM to 10 AM and 5 PM to 9 PM—and at a slower pace throughout the middle of the day [29, 48]. An electric taxi must sustain operations during rush hour without stopping for a charge; otherwise, the driver and owner could lose profits, discouraging the adoption of electric taxis and hindering the electrification transition. Therefore, the highest estimated energy consumption values should be used for operational planning to ensure continuous operation.

However, it is not economical to equip every electric taxi with the largest possible battery pack. An overly large battery would be unnecessarily expensive and heavy. A taxi traveling long distances in hilly terrain will have different battery needs than one covering short distances in an urban environment. With this in mind, Table 5.10 provides recommendations for battery sizes tailored to specific conditions and range requirements. The ranges are calculated as 85% of the battery's physical capacity, since discharging too deeply or charging to the maximum can negatively impact battery health.

Based on the results in the table and known taxi mobility requirements [29, 48], a battery size of approximately 70 kWh should meet most operational needs without being excessively large. From a design perspective, this is technically feasible, as minibuses in similar global markets use comparably sized batteries [221].

5.5.2 Emissions and grid impact

Chapter 3 highlighted that the environmental impact of the taxi industry is one of the most significant factors influencing paratransit owners' and drivers' intentions to adopt

Table 5.10: Recommended energy consumption (kWh/km) for calculating range in different driving conditions, based on highest energy consumption observed in each condition. Example ranges (km) using different battery sizes (kWh) are given. Ranges are calculated as 85% of the physical limit that a battery would be able to provide at the given energy consumption.

	Urban	Uphill	Downhill	Inter-city
Energy Consumption (kWh/km)	0.49	0.57	0.44	0.47
Range (km) - 50 kWh battery	87	75	97	90
Range (km) - 70 kWh battery	121	104	135	127
Range (km) - 90 kWh battery	156	134	174	163

EVs. Additionally, policymakers are often concerned with the emissions savings of EVs compared to internal combustion engine (ICE) vehicles, so it's useful for stakeholders to use these estimates to model the greenhouse gas (GhG) emissions impact of transitioning to an electric fleet.

A diesel minibus taxi with a fuel consumption rate of 13L/100km [234] and a diesel emissions factor of 2.6 kg CO2/L [235] emits 0.325 kg CO2 per km driven. According to historical data from Eskom [236], the average CO2 emissions intensity of the South African electricity grid between March 31, 2021, and March 31, 2022, was 0.95 kg CO2/kWh, aligning with public estimates by the Institute for Global Environmental Strategies [237]. Using this emissions intensity, a vehicle energy consumption rate of 0.55 km/kWh, and a charging efficiency of 90%, the per-distance emissions intensity for electric minibus taxis operating in South Africa is 0.58 kg CO2/km. For electric minibus taxis to achieve GhG emissions parity with ICE vehicles, the emissions intensity of the South African grid would need to decrease by at least 44%, falling below 0.53 kg CO2/kWh. Given the findings related to environmental concerns in Chapter 3, this is an essential consideration.

Moreover, in an energy-constrained and coal-dependent context, the interactions between EVs and the electricity grid must be carefully considered when planning fleet electrification. Adequate charging infrastructure and clean energy generation are crucial to sustain the fleet, as EV charging can significantly impact the grid [238].

In contrast to battery sizing, where high energy consumption estimates are used for operational planning, using the average recommended energy consumption is appropriate for fleet-wide energy demand and grid impact assessments. With approximately 300,000 minibus taxis in South Africa [239], traveling an average daily range of $100 - 200\,\text{km}$, an energy consumption of 0.55 kWh/km and a charging efficiency of 90% would result in an additional electricity demand of $18.3 - 36.7$ GWh per day, and $6.4 - 12.8$ TWh annually (assuming a 50-week work year). This accounts for roughly 2.5 to 5% of the country's annual electricity consumption [240].

Even a local fleet of just 20 taxis traveling 200 km daily, typical for the region [29], would require 1.96 MWh per day and 0.72 GWh per year. Such additional loads could place significant strain on both local grids and the national electricity supply, which is a concern given the frequent blackouts and power shortages many cities in sub-Saharan Africa already experience. This may impact the technical and financial feasibility of switching to electric vehicles for paratransit fleet owners. Fleet operators must consider electricity availability in their area, as well as the frequency and severity of load shedding, to determine how it could affect the profitability and reliability of EV investments and charging infrastructure.

The research in Chapter 6 builds on the values provided in this chapter to explore how investments in renewables at charging stations can be optimized considering grid constraints. Hybrid renewable charging stations can help alleviate grid constraints, but further work to solve the fundamental electricity supply constraints in South Africa will be needed regardless.

5.5.3 Payback period

As revealed by the survey analysis in Chapter 3, a significant portion of paratransit fleet owners and drivers may not fully understand the value of an electric power source for their vehicles, and may need to be shown evidence of the potential financial benefits of EVs before buying into the transition.

A key metric in understanding the financial viability of EV adoption is the vehicle payback period. The payback period measures the time taken for the operational savings of an EV (from its comparatively advantageous fuel economy) to offset the greater initial purchase price it faces compared equivalent ICE vehicles (from its expensive battery and electric traction system). Since cash flow estimates and predictions of market indicators are relatively accurate in the near future and uncertain in the long term, payback period can be considered an indicator of investment risk. In the paratransit sector, fleet owners face capital and infrastructure constraints, as well as a degree of regulatory uncertainty, political instability, and economic volatility. Therefore, understanding the risks inherent in payback period is especially critical as compared to fleet owners in public transportation industries in developed countries with more stable operating environments. A sensitivity analysis is conducted after the payback period is calculated to ascertain the parameters which carry the greatest risk.

To ascertain payback period, a model for the cumulative costs of ownership for electric and ICE minibus taxis is established. The parameters for this model include the energy consumption estimates derived earlier in this chapter from the PDC developed in Chapter 4, and a set of representative South African paratransit vehicle usage and market parameters. The model itself comprises fixed expenditures associated with its acquisition, along with the variable costs for its operation. The acquisition cost is financed with a loan that is paid back in monthly installments over time. The variable costs include fuel, maintenance, insurance, and taxes. Fuel and maintenance costs occur based on vehicle usage, and insurance and taxes are charged on an annual basis. All future payments (loan installments and variable costs) are discounted by a discount rate so as to be represented in year 0 currency. In the analysis, sensitivities are conducted on several parameters which express higher uncertainty and have a greater effect on the results.

The cumulative cost of ownership for each vehicle is then compared over a 10-year period, a time frame selected to accommodate the evaluation of battery replacement costs and incentives. Prior research and reports have estimated the average age of minibus taxis in South Africa to be anywhere from 5 [239] to over 10 years old [19, 241]. It is possible that the average age of the national fleet is coming down due to South Africa's Taxi Recapitalisation Programme, which incentivizes taxi owners to voluntarily surrender their old vehicles for scrapping in exchange for compensation towards purchasing new ones. Therefore, while acknowledging that some responsible fleet owners may retire their taxis before a decade's end, the 10-year benchmark is reasonable given historical data on taxi usage and is helpful for drawing conclusions regarding the cost competitiveness of EVs against ICE counterparts.

The cost of ownership (O) model can be summarized by the following equation:

$$O = D + \sum_{t=1}^{T} [P_t + F_t + M_t + N_t + B_t - \lambda_t] * (\frac{1}{1+\delta})^t \tag{5.9}$$

where D is the down payment in year 0, and in year t, F_t is the fuel cost, P_t is the loan payment, M_t is the maintenance and repair cost, N_t is the insurance cost, B_t is the battery replacement cost, λ_t is a government incentive, and δ represents the discount rate. This equation is the same for the EV and ICE vehicles, but B_t and I_t are always set to 0 for the ICE vehicle.

Loan model

The largest seller and financier of minibus taxis in South Africa is SA Taxi, SA Taxi, a subsidiary of a large multinational holding company called Transaction Capital. Approximately 80,000 of the nation's 300,000 minibus taxis have been financed or insured by SA Taxi [239, 242]. Under the National Credit Act (NCA), SA Taxi can charge interest rates up to 2.2 times the repo rate plus 20%. Since 2020, the repo rate in South Africa has risen from 3.5% to over 8.25% [243], leading to SA taxi charging vehicle owners an interest rate range of 12 – 26%, with an average rate of 19% [239, 242]. Compared to typical car finance rates in countries such as the UK and USA (3–10%), a rate of 19% is exorbitant. Considering the recent fluctuations in interest rates and the inherent uncertainties in the minibus taxi industry, particularly regarding financing rates for EVs, a sensitivity analysis on the interest rate is conducted to better understand the financial potential of EVs in this context.

Charging infrastructure

Paratransit fleet owners will need to invest in charging infrastructure to support their vehicles' energy requirements. EV Company [244], a South African firm specializing in charging solutions, provides clients with a 22kW AC charger priced between R10,000 and R25,000 ($540 to $1,350). Including installation costs, which range from R15,000 to R40,000 ($800 to $2,260), fleet owners can expect to spend a maximum of R65,000 per charger ($3,510). This investment in charging infrastructure is distributed across each vehicle. For this analysis, a conservative stance is adopted, and fleet owners are assumed to purchase a charger for every vehicle, to ensure a charger is available whenever a vehicle needs it. Along with the vehicle purchase cost, this capital cost is assumed to be financed by a loan and is included in the loan model.

Fuel costs

Diesel prices are based on diesel prices reported by the Automobile Association of South Africa [245] in Jan 2023. In South Africa, electricity prices are subject to time-of-use tariffs, meaning that the user pays a different amount per unit of energy obtained from the grid depending on what time of day/time of year they are plugged in [246, 247]. Therefore, the cost of electricity for an electric minibus taxi will depend on its charging schedule, which depends on a fleet operational schedule, which will vary based on time of week as well as what proportion of the fleet is electrified. For this analysis, charging schedules are simulated for electric minibus taxis which belong to a fleet that is 100% electrified. To simulate charging schedules, operational data from traditional ICE vehicles is inputted into a bespoke electric paratransit operations planning tool developed by Wust et al. [248]. This tool leverages ICE vehicle schedules to devise feasible schedules adaptable to EVs with specific characteristics. One notable advantage is the tool's ability to enforce zero lateness, ensuring punctuality for all passengers. The vehicle parameters used for generating the schedule are listed in Table 5.11. A weekly operational schedule is generated and repeated 52 times to create a year's worth of e-paratransit operational data, which yields an annual charging load profile. The charging load profile is multiplied by Eskom time of use tariffs, which vary by time of day and season [246], to get an average price of electricity from the grid, which is the price reported in Table 5.12.

While diesel and electricity prices rise throughout the vehicle lifetime, it should be noted that no attempt is made to made to predict future diesel and electricity prices. The former is notoriously volatile due to global events, and the latter, while more stable, is still difficult to predict into the future, especially in a place with unstable electricity supply such as South Africa. In order to account for this uncertainty, three scenarios are included in the analysis. The first scenario assumes that both electricity and diesel prices rise by 5% per annum. The second scenario assumes that diesel prices rise by 10% per annum and electricity prices rise by 5% per annum. The third scenario assumes that electricity prices rise by 10% per annum and diesel prices by 5% per annum.

Battery replacement

Many experts agree that lithium-ion batteries are likely to achieve 3,000 cycles [249, 250]. Following this amount they are likely to require replacement due to degradation and diminishing capacity. Given the driving behavior and battery size of the vehicle modelled in this section, this leads to battery replacement occurring in year 7 of vehicle lifetime. This means that replacement of the battery is likely to occur during the economic lifetime of an electric minibus taxi in South Africa – that is, before the rest of the vehicle falls out of operational capability. Given the high cost of batteries, this is likely to have a significant effect on the payback period and financial viability of the investment. Some published reviews of battery cost forecasting [251, 252], along with reports by Bloomberg [253] and McKinsey & Company [254] project that battery costs will reach approximately USD $100/kWh, with some estimates suggesting a decline to as low as $70/kWh by 2030 or the early 2030s if not earlier. However, there are different estimations due to the uncertainty inherent in techno-economic predictions associated with technological advancement and volume of production. Further supply chain uncertainties exist for the yet-to-be-established electric paratransit market in South Africa. Based on the reports above the analysis assumes a central estimate for the battery replacement cost of $125/kWh. To capture the uncertainty in future battery prices, a sensitivity analysis is included which varies the battery price by 20% in each direction.

Maintenance and repair cost

Minibus taxi vehicle owners typically pay approximately R600 per month, or R7,200 per annum, to city authorities for routine maintenance and the right to operate in the city [46]. Maintenance and repair costs are assumed to be 2 – 6x greater for ICE than equivalent EV [255, 256]. This is due to several key factors. First, EVs have fewer moving parts compared to ICE vehicles, which inherently reduces the potential points of failure and the need for regular maintenance. Without complex components like fuel systems, exhaust systems, and transmissions found in traditional vehicles, EVs experience less wear and tear over time. They also do not require oil changes, transmission fluid replacements, or exhaust system repairs. Moreover, regenerative braking systems in EVs help extend the lifespan of brake pads and rotors by harnessing kinetic energy during deceleration, thereby reducing the frequency of brake replacements. Overall, the simplified design and absence of conventional engine components make EVs inherently cheaper to maintain compared to ICE vehicles. They require maintenance less frequently, and unless something happens to the battery, are typically cheaper to fix. For this analysis, a conservative assumption is made that EV maintenance costs are half that of the equivalent ICE vehicle.

Non-cash expenses

A significant ongoing non-cash expense not factored into the assessment is vehicle depreciation. Depreciation calculations involve intricate forecasting and assumptions, and depreciation rates can also vary significantly based on factors such as geographic location and individual driving habits. While depreciation patterns for ICE vehicles are well-established, those for EVs remain relatively nascent due to their relatively recent introduction to the vehicle market. Given the uncertainties surrounding EV resale values and battery longevity, attempting to accurately predict depreciation can introduce significant complexity and potential inaccuracies in the assessment. Furthermore, the primary focus of payback period assessments is typically on direct costs (e.g. purchase price, fuel expense, maintenance costs), which are more directly relevant to the decision making process and offer a clearer picture of the immediate financial implications of choosing between EV and ICE vehicles. By excluding depreciation and resale value, the analysis retains a higher degree of simplicity and transparency and better captures the holistic value proposition of EVs.

Table 5.12 gives the parameters for the cost of ownership model in the base scenario. The original numbers for the analysis were in South African Rand (ZAR), but for the presentation of the thesis the numbers have been changed to USD. The exchange rate of 1 ZAR = 0.0539983 USD was found using `https://www.xe.com` on May

Table 5.11: Input parameters for scheduling EV fleet.

Parameter	Value	Source
Vehicle battery capacity	70 kWh	[161]
Energy consumption	0.55 kWh/km	This chapter
Charger rating	22 kW	
Charging outlets	1 per vehicle	

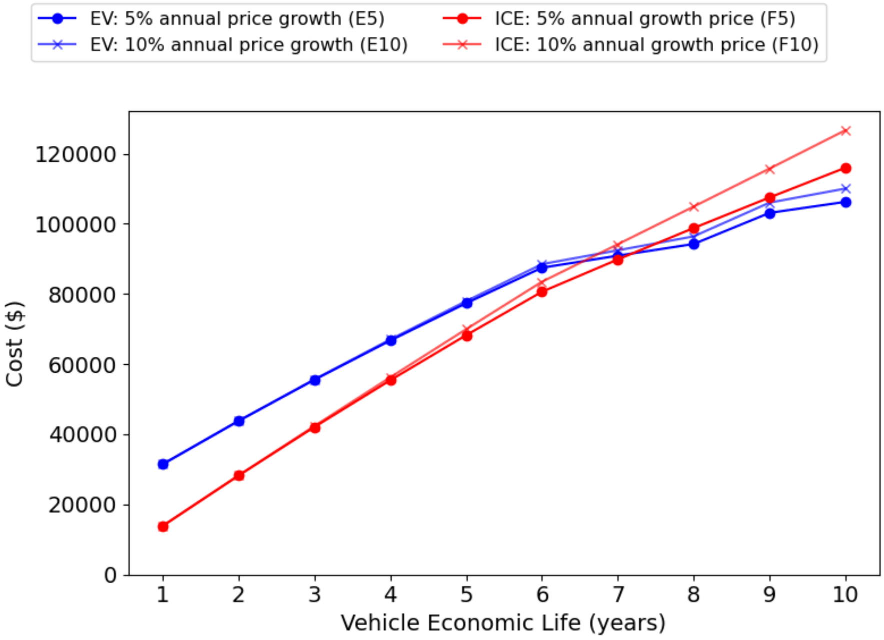

Figure 5.9: EV vs. ICE lifetime cumulative total cost of ownership with varied annual growth rates for electricity and diesel prices.

9, 2024 at 12:00 UTC.

Figure 5.9 shows the cumulative costs of owning an electric paratransit vehicle versus a comparable ICE vehicle. The figure encapsulates essentially four scenarios: 1) base case electricity and diesel price growth rate (E5/F5), 2) high electricity and diesel price growth rate (E10/F10), 3) high electricity and base diesel price growth rate (E10/F5), and 4) base electricity and high diesel price growth rate (E5/F10). At the current prices and market environment, the electric minibus taxi achieves cost parity with the comparative ICE vehicle after 8 years in scenarios 1 and 3, and after 7 years in scenarios 2 and 4. Notably, in this case there are two kinks in the figure which clearly significantly affect the payback period outcome. These kinks come from 1) the loan being fully paid off (year 6), and 2) the battery replacement (year 8).

Table 5.12: Parameters for calculating vehicle cost of ownership (values represent the base case).

Parameter	Value	Source
Financing model		
Loan lifetime	72 months	[257]
Interest rate	19.00%	[243]
Inflation rate	7.00%	[258]
Discount rate	6.00%	[259]
Down payment	50%	Assumption
Fuel prices		
Diesel price	1.21 $/L	[245]
Electricity price	0.11 $/kWh	[246]
Diesel price growth rate	5 %/yr	Assumption
Electricity price growth rate	5 %/yr	Assumption
Vehicle usage		
Annual mileage	52,500 km	[85]
ICE Fuel efficiency	13 L/100km	[260]
EV energy consumption	0.55 kWh/km	Chapter 5.3
EV battery life	3,000 cycles	[250]
Battery size	70 kWh	[161]
Acquisition costs		
ICE purchase price	27.72 k $	[257]
EV purchase price	59.94 k $	Assumption[a]
Maintenance and repair costs		
ICE maintenance	388 $/yr	[46]
EV maintenance	194 $/yr	Assumption ([255, 256])
EV battery replacement cost	128 k $/kWh	Assumption ([251, 252, 253, 254])
Charging infrastructure		
Rating	22 kW	
Efficiency	90%	
Capital cost	32,500 R	[244]
Vehicle-to-charger ratio	1:1	

[a] Based on Rham Equipment (`https://rhamequipment.co.za`) bill of materials for electric minibus taxi retrofit with a 78 kWh/km battery, 09/2023.

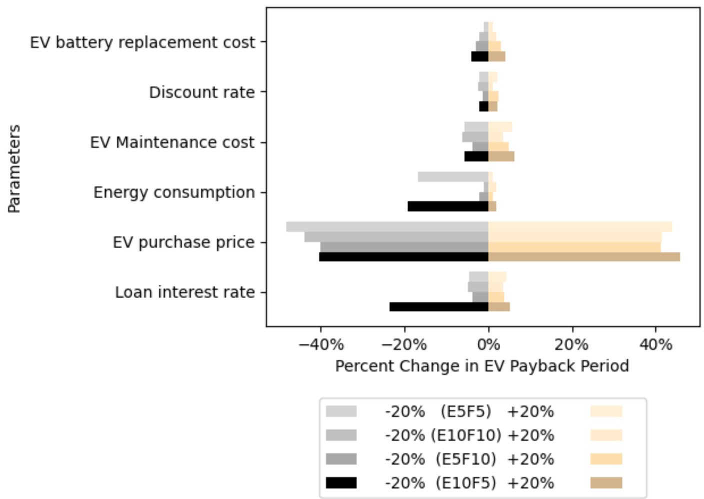

Figure 5.10: Sensitivity of the electric minibus taxi payback period to cost of ownership model parameters. The x-axis represents the percent change in EV payback period given a plus (light bars) or minus (dark bars) 20% change in a given parameter.

As noted in previous techno-economic analyses of ICE vehicle alternatives [259], the cumulative cost of ownership of a vehicle can be highly sensitive to the initial parameters. There is naturally a level of uncertainty in the model proportional to uncertainty inherent in the model input parameters. A sensitivity analysis is performed in an attempt to capture the uncertainty in the model. For the sensitivity analysis, six parameters that are uncertain due to lack of real in-region electric minibus taxis are varied from their baseline values by 20% in both directions.

Figure 5.10 shows the results of the sensitivity analysis.

These results show that a change in purchase price has the greatest influence on the payback period, followed by loan interest rate and EV maintenance cost. Thus, reducing uncertainty in the cost of ownership model is largely a question of reducing uncertainty in these parameters. Loan interest rate and vehicle energy consumption have noticeably larger effects in E5F5 and E10F5 than in the other scenarios. This is because adjustments in those parameters directly affect when the loan is paid off and when the battery is replaced respectively, which are the two conditions that determine the timing of the kinks noted above. Because of the proximity of the kinks to the overlap in cumulative costs, shifting the timing of the kinks leads to a step change in payback period.

Overall, this section demonstrates that one can determine the financial viability of electrifying paratransit from the fleet owner perspective, including the accompanying charging equipment. The results show that with conservative estimates, a payback period of approximately seven to eight years can be expected.

5.6 Summary and key insights

This chapter has investigated the research questions:

- *What is the energy consumption of electric paratransit?*,
- *Can per-minute GPS tracking data reliably determine the energy consumption of paratransit vehicles?* and
- *What is the payback period of electric paratransit?*

By applying a kinetic model to the Paratransit Driving Cycle (PDC) developed in Chapter 4, a general estimate for electric paratransit energy consumption of 0.55 kWh is found. This estimate is validated by comparing it with the first high-fidelity estimates of paratransit energy consumption, which are gathered from the entire raw 1 Hz GPS mobility dataset from which the PDC is constructed. The difference of 10% is within an acceptable margin for validation.

In context, the energy consumption estimates here are lower than in previous literature, which provided average estimates ranging from 0.50 – 093kWh/km. Results in previous literature were based on per-minute data. Fast Fourier transformations of the per-second data show that although per-minute data captures the environmental characteristics of a trip, it misses out on the micro-mobility patterns of a vehicle, leading to imprecise estimates. These results imply that the estimated battery capacity requirements and thus cost and grid impact of electric minibus taxis are less than previously suggested, an encouraging result for paratransit fleet owners. Given the estimated level of energy consumption and paratransit operational requirements, minimum viable battery size is likely to be in the 70 – 80 kWh range, which is reasonable for the typical 9- to 16-seater minibus taxi.

Energy consumption estimates may be required for dozens or even hundreds of different driving conditions across sub-Saharan Africa when planning the transition to electric paratransit. It is impractical to capture every possible combination of these factors in a single dataset; however, by using high-resolution GPS data to capture variations in environmental and mobility profiles, the effects of different mobility characteristics on energy consumption can be quantified. The coefficients from the non-standardized regression model in Section 5.3.3.1 can be applied to extrapolate these results to routes not included in the dataset that may have different elevation and speed profiles. Similarly, a range of likely operating conditions for e-taxis can be modeled, with various parameter values found in the literature for vehicle kinetic models. To support this, the sensitivity of the model to each parameter is measured, allowing for the assessment of how adjustments to each parameter affect the overall model.

The per-distance emissions intensity for electric minibus taxis is estimated to be 0.58 kgCO2/km, significantly higher than the estimated 0.32 kgCO2/km for the equivalent ICE minibus taxi. Given the importance of environmental impact of the taxi industry to owners and drivers found in Chapter 3, ensuring the taxis can refuel from cleaner electricity sources by cleaning up grid electricity production or installing distributed renewables-powered charging stations may influence future EV adoption in the paratransit industry.

The energy consumption estimates are then used in a payback period model, and after a sensitivity analysis, it is found that in most scenarios, an electric paratransit vehicle would be likely to pay itself back in seven to eight years. These result suggest that on the vehicle level, an electric version of current combustion-powered paratransit vehicles is at the edge of financial feasibility. Given the absence of in-region electric vehicles, there is an inherent level of uncertainty in the model which is quantified in a sensitivity analysis. The sensitivity analysis reveals that the payback period is most sensitive to the initial purchase price, followed by loan interest rate, energy consumption, and maintenance cost. These are therefore the parameters that fleet owners must be aware of as the greatest sources of uncertainty in electric paratransit payback period.

In sub-Saharan Africa, the transition to electric vehicles continues to be painstakingly slow [...]
This uncertainty on the vehicle side of this revolution is further overshadowed by the looming threat of energy scarcity on the electricity supply side.

— M.J. Booysen, C.J. Abraham, A.J. Rix, and J.H. Giliomee [34]

6

Technoeconomic Optimization of Solar-Storage System at Paratransit Charging Stations Considering Grid Constraints

Contents

Up to this point in the thesis, the focus has been on the the vehicle side of paratransit fleet operations. However, assessing the technical and financial viability of electrification for paratransit fleet owners requires a comprehensive evaluation of how electric fleets will integrate with the necessary electric infrastructure installations. In the contemporary landscape of sustainable energy systems guided by the United Nations Sustainable Development Goals (SDG), the intersection of renewable energy and EV technology stands as a pivotal frontier in the pursuit of economic and low carbon mobility [261]. The confluence of these two domains has given rise to the concept of solar-storage integration at EV charging stations, presenting an innovative solution to the challenges of grid reliability, energy efficiency, and carbon emissions reduction. As the global transition toward renewable energy intensifies, the deployment of photovoltaic (PV) arrays coupled with energy storage (ES) systems at EV charging stations (CS) not only promises to augment the resilience of the power grid but also provides a pathway to economically viable electric transportation networks.

Against this backdrop and the central research question of the thesis, this chapter aims to address the questions:

- *How can we optimize the size of PV and energy storage at paratransit charging stations to maximize economic gain, considering electricity supply constraints?*
- *What are the effects of varying electricity demand (as fleet size) on the economic performance of the PV-ES-CS system?*

To address these questions, this chapter develops a novel methodology which integrates grid constraints into a PV-ES capacity optimization model that maximizes the net present value (NPV) of the investment. Through a case study on a paratransit fleet in Dobsonville, South Africa, it examines the effects of optimistic and conservative grid constraint scenarios, as well as varying degrees of fleet EV penetration, on the system's techno-economic performance. The case study utilizes the recommended vehicle energy consumption rate and battery size established in the previous chapters.

By addressing these questions, this chapter provides paratransit fleet owners with a methodology to understand not only how much PV-ES capacity to build out given their particular grid constraint circumstances, but also a framework for understanding when to invest in PV-ES-CS systems given their fleet electrification plans. In doing so, the chapter fills **Research Gaps 4 and 5** as presented in Chapter 2.

The insights gleaned from the analysis and methodology developed herein are of significant value to paratransit fleet owners and operators, especially those in regions with grid or capital-constraints. Furthermore, while achieving the stated objectives of answering the above research questions, this thesis also establishes benchmarks of the feasibility and performance of these systems for sub-Saharan African (SSA) paratransit. Given that paratransit is SSA's dominant road transport modality and is in urgent need of decarbonization solutions and attention from investors [3, 79, 262], the findings presented here hold considerable external relevance and potential impact.

6.1 Modelling hybrid renewable-charging stations

This section reviews the literature on modelling grid constraints in PV-ES-CS systems, analyzing PV-ES-CS systems for mixed fleets, and the mathematical modelling of PV-ES-CS systems.

6.1.1 Grid constraints and mixed fleets

In Chapter 2, the literature review explored the infrastructural challenges and opportunities associated with supporting an electrified paratransit system, particularly in the context of SSA's unstable energy landscape. A major focus of the review was on the integration of PV and ES systems at charging stations, which can help mitigate the impact of load shedding and ensure continuous electric vehicle (EV) operations. While studies like those of Collett and Hirmer [3] and Giliomee and Booysen [85] emphasized the potential of PV-ES systems to enhance energy resilience and reduce grid dependence, they also pointed to a significant gap in the literature: the lack of methodologies to maximize the economic benefits of these systems under conditions of frequent grid instability.

Additionally, various approaches to designing PV-ES charging station systems were reviewed, highlighting insights into reducing grid strain and improving energy independence. However, many studies, such as those by Singh et al. [86] and Hassoune et al. [88], did not fully address the unique challenges posed by load shedding or how to optimize system configurations for economic viability in grid-constrained regions. This underscored the need for more comprehensive models that incorporate grid reliability and resilience into the design of PV-ES systems for EV charging stations, particularly in SSA.

Furthermore, while some studies examined the impact of fleet electrification on charging infrastructure, they often assumed static or fully electrified fleets, as seen in Ullah et al. [93] and Ampah et al. [94]. This assumption overlooks the realities of staged fleet electrification in developing regions. The literature, therefore, lacks studies that explore how varying levels of EV penetration affect the feasibility and performance of PV-ES charging systems, presenting a clear research gap in assessing the impact of partial fleet electrification on system design.

In summary, the literature points to two major research gaps: **Research Gap 4: the need for optimization approaches that account for grid instability** and **Research Gap 5: the lack of analysis on the effects of different levels of EV penetration on the techno-economic performance of PV-ES charging station systems.**

6.1.2 Mathematical modeling

Two primary research methods are commonly used to study the integration of renewable energy into energy systems: mathematical modeling and integrated computer-based optimization software [263]. Mathematical modeling involves representing a real-world system through mathematical equations, enabling simulations of system behavior and performance optimization. On the other hand, integrated computer-based optimization software combines mathematical modeling with optimization algorithms, allowing researchers to solve complex problems that would be difficult or impossible to address manually.

The most widely used tool in the literature for these optimization problems is Hybrid Optimization of Multiple Energy Resources (HOMER) [264], developed by the U.S. National Renewable Energy Laboratory. HOMER is popular for modeling hybrid renewable energy systems because it eliminates the need for developing custom tools for analysis. Thirunavukkarasu et al. [265] provide a thorough review of studies applying HOMER to optimize hybrid renewable systems. Although HOMER is user-friendly, it has limitations, including its financial cost and closed-source nature, which restrict users from adapting it for specific features, such as variable load shedding. Other tools like HYBRID2, HYBRIDS, TRYNSY, GAMS, and RETSCREEN have also been used for system optimization [264], but in addition to their financial barriers, recent reviews have found these traditional methods unsuitable for addressing complex, novel problems [264]. To overcome these limitations, an open-source model has been developed that can be customized for specific use cases and continuously improved upon (link to GitHub repo here: `https://github.com/ChullEPG/PV-ES-CS-Sizer`).

6.2 Methodology

This section introduces a techno-economic model designed to determine the optimal size of the PV and ES components that will maximize the net present value (NPV) of the PV-ES-CS system. The development of this model and the accompanying case study analysis address **research gaps 4 and 5**. A visual summary of the capacity optimization process is shown in Fig. 6.1.

At a high level, the optimization seeks to balance the cost savings from the PV and ES systems with their associated capital and operational expenses. Specifically, solar PV is used to offset EV charging loads at no marginal cost when solar resources are available, with any excess solar energy directed to charge an external stationary battery storage system, assuming the battery has available capacity. The battery is then discharged to meet EV charging demands when solar resources are insufficient. These energy-saving benefits are weighed against the total cost of ownership for the PV and battery storage systems.

6.2.1 System setup

A schematic of the PV-ES-CS system is depicted in Fig. 6.2. EVs charge directly from solar power when it is available and from the grid when neither solar nor battery energy can meet the load demand. Any excess electricity generated by the solar panels is either

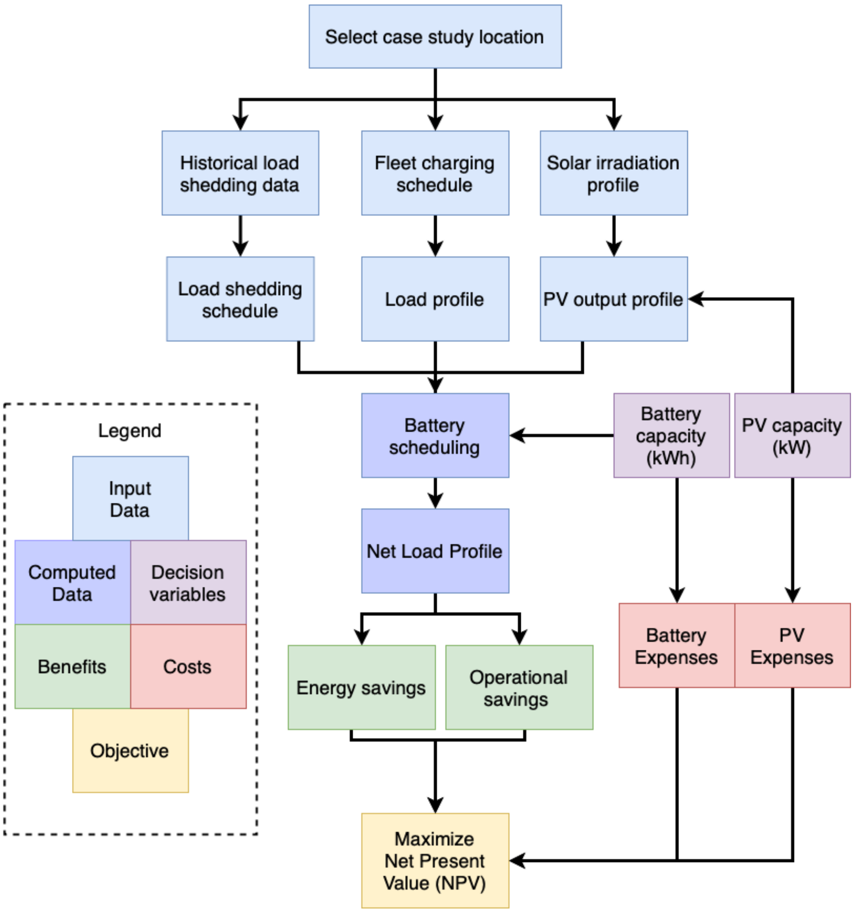

Figure 6.1: Flow chart of optimization model to determine the PV and battery sizes that maximize net present value.

stored in the battery, subject to its capacity limits, or curtailed. The battery can also discharge to meet positive net load, constrained by its physical discharge limits.

6.2.1.1 Solar PV

The solar capacity factor represents the ratio of the actual energy output to the rated energy output of the PV panel. The solar capacity factor profile is calculated using Pfenninger and Staffell's Renewables.ninja service [266], which incorporates weather data from global reanalysis models and satellite observations [267, 268, 269]. This service converts solar irradiance data into power output using the Global Solar Energy Estimator [270].

Within Renewables.ninja, hourly capacity factors are computed as a five-year average from 2015 to 2019 to reduce the impact of outliers. Using this capacity factor profile, the solar PV output for hour h $E_{PV}(h)$ is determined by Eq. 6.1.

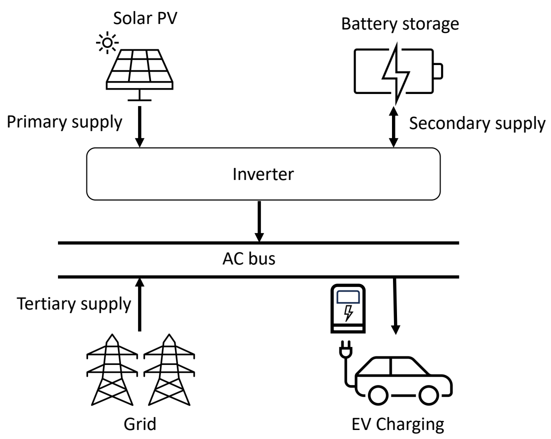

Figure 6.2: Schematic of the grid-tied solar PV and energy storage-powered EV charging station.

$$E_{\mathrm{PV}}(h) = Y_{\mathrm{PV}}(h) \times P_{\mathrm{PV\text{-}rated}} \tag{6.1}$$

where $Y_{\mathrm{PV}}(h)$ is the capacity factor in hour h, and $P_{\mathrm{PV\text{-}rated}}$ is the installed PV capacity in $\mathrm{kW_{pk}}$.

6.2.1.2 Grid constraints

In this chapter, the impacts of both planned and unplanned grid constraints on the value of PV-ES-CS systems are modelled. Grid constraints, such as load shedding or power outages, prevent electric vehicles (EVs) from drawing power from the grid, thereby affecting their charging schedules and overall operational profile.

The study examines how grid constraints influence EV charging and the economic performance of the PV-ES-CS system by considering various scenarios: no grid constraints, planned grid constraints, and unplanned grid constraints.

- **No Grid Constraints**: In scenarios with no grid constraints, EVs are able to charge exactly as they are scheduled.
- **Planned Grid Constraints**: Events with at least 24 hours of forewarning, allowing fleet operators to adjust charging schedules.
- **Unplanned Grid Constraints**: Sudden events without prior notice, causing immediate operational impacts.

Planned Grid Constraints Planned grid constraints occur due to foreseen issues such as scheduled maintenance, environmental factors, or network capacity limits. When a planned constraint is anticipated:

- **Notification**: Fleet operators receive at least 24 hours' notice.
- **Schedule adjustment**: EV charging schedules are modified to avoid constrained hours while maintaining a zero lateness condition to meet passenger demand.
- **Economic impact**: The only change is the timing of EV charging, potentially affecting electricity prices or solar resource availability.

For instance, if a maintenance event is scheduled between 2 PM and 4 PM, EVs will be rescheduled to charge either before or after this time to ensure all trips are completed on schedule. In creating these new operational schedules, a zero lateness condition is enforced to guarantee passenger demand is still met satisfactorily despite the shift. The primary difference between planned grid constraints and no grid constraints is *when* the EV charging occurs, which could be significant if charging is shifted to hours with different electricity prices or solar availability.

Unplanned Grid Constraints Unplanned grid constraints arise suddenly from issues like unscheduled maintenance, natural disasters, or accidents. In these cases:

- **Notification**: There is no forewarning and fleet operators are unable to reschedule EV charging schedules in advance.
- **Schedule adjustment**: EV charging schedules are not modified.
- **Economic impact:** Costs are incurred due to missed trips, calculated based on the mileage and kWh that could have been charged during the outage. However, the PV-ES-CS system can mitigate these costs by providing backup power during outages.

As an example, if the fleet intended to draw 20 kWh from the grid between 2 PM and 4 PM but is prevented by an unexpected outage, the operational cost of missed trips

Table 6.1: How grid constraints (GC) affect the EV charging schedules and economics of PV-ES-CS optimization.

GC Schedule Type	New EV charging schedule required?	Operational cost from missing charging opportunity?	Opportunity for PV-ES-CS system to provide resiliency?
No GC	✗	✗	✗
Planned GC	✓	✗	✗
Unplanned GC	✗	✓	✓

is calculated based on the mileage the EVs would have covered using the energy they would have charged during those hours. However, if the PV-ES-CS system can fully or partially compensate for the outage, the operational cost is reduced proportionally based on the energy provided. The detailed calculation method is outlined in Section 6.2.5. Notably, this represents an economic advantage for the PV-ES-CS system, as it reduces operational costs by offering resiliency during these constrained hours.

The differences between the scenarios are summarized in Table 6.1.

6.2.1.3 EV charging load

The EV charging load profiles are generated using the tool developed by Wust et al. [248], which takes the operational schedule of a fleet of internal combustion engine (ICE) minibus taxis and produces a feasible operational schedule for an equivalent fleet of EVs, including individual vehicle charging schedules. Given the current absence of electric minibus taxis in sub-Saharan Africa, this step is crucial for creating a realistic charging profile for such a fleet.

The tool derives passenger demand from measured tracking and validated rank-observed data. The vehicle schedules and charging demand profiles are generated through an algorithm that matches passenger demand to a reduced vehicle supply and charging schedules using an optimization heuristic. The tool ensures that all passenger demand is met with zero lateness and that the EVs operate within their battery capacity and energy consumption rates (kWh/km), confirming the fleet's operational feasibility.

As outlined in Section 6.2.1.2, the charging schedules adjust according to different load shedding scenarios. They also vary based on the proportion of the fleet that is electrified. In this chapter, four levels of EV fleet penetration are modelled: low (25%), medium

(50%), high (75%), and full (100%), each with its own charging schedule.

From a simulated schedule, the total EV load during hour h, $D_{load}(h)$, is determined by Eq. 6.2, which calculates the total EV load at the charging station as the sum of the loads from individual vehicles.

$$D_{\mathrm{load}}(h) = \sum_{\mathrm{i=1}}^{\mathrm{N}} D_{\mathrm{veh}}(i,h)\ \forall i \in [1,N] \tag{6.2}$$

where N is the number of vehicles charging.

6.2.2 Energy dispatch strategy

A conventional rule/logic-based strategy is adopted for energy storage (ES) charge and discharge management. This approach is commonly selected for techno-economic assessments of hybrid solar and storage systems [90, 271, 272, 273]. While various energy dispatch and control strategies have been proposed in the literature for similar capacity sizing problems (e.g. [274, 275, 276, 277]), the conventional rule/logic-based strategy is chosen for its advantages, including low computational requirements and robustness to hyperparameter initialization. Since this method is not guided by an optimization function, the resulting ES size in the overall system optimization is conservative compared to more sophisticated usage strategies. In other words, if the system achieves feasibility with the conventional rule/logic-based approach, it will do so with any further optimized ES usage.

The conventional rule/logic-based energy storage and dispatch algorithm follows specific steps. First, the load is met by the PV system. Any excess PV energy is charged into the battery, up to its charging limits. If there is unmet load, the ES discharges as much as possible, constrained by its maximum depth of discharge. If any load remains after the ES discharge, it is imported from the grid. This process is visually summarized in Fig. 6.3.

Following Figs. 6.2 and 6.3, load served by PV production $D_{PV}(h)$ can be derived via Eq. 6.3, and load served by the ES $D_{ES}(h)$ with Eq. 6.4.

$$D_{\mathrm{PV}}(h) = \min(E_{\mathrm{PV}}(h), D_{\mathrm{load}}(h)) \tag{6.3}$$

$$D_{\mathrm{ES}}(h) = \min(D_{\mathrm{load}}(h) - D_{\mathrm{PV}}(h), E_{\mathrm{ES}}(h) \times \eta_{\mathrm{ES}}^{\mathrm{DC}}) \tag{6.4}$$

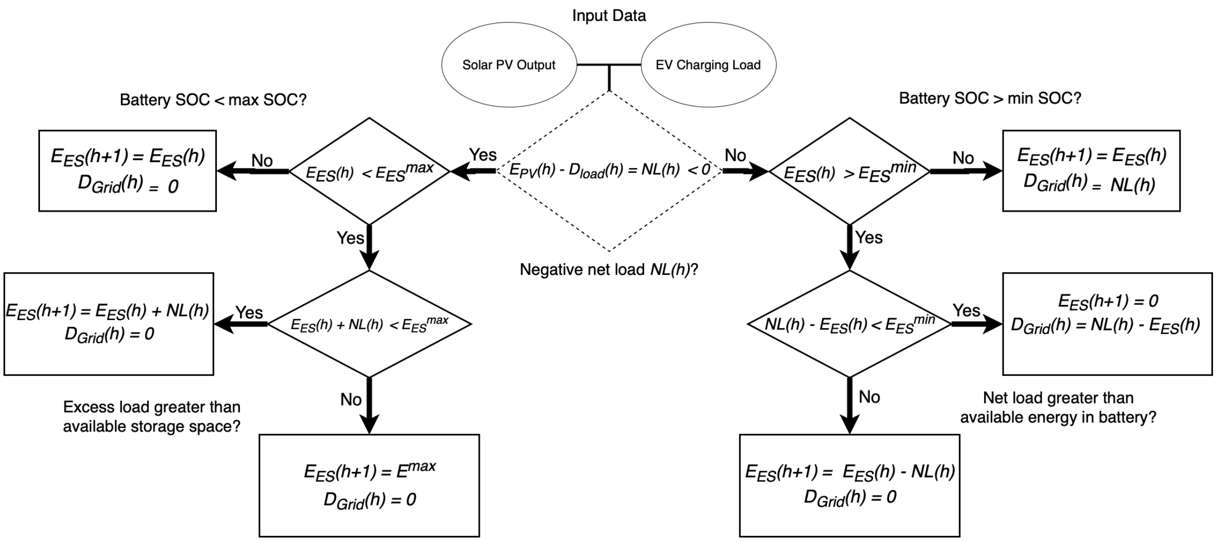

Figure 6.3: Conventional rule/logic-based strategy for managing the ES system. the reader is referred to the nomenclature table for complete index of variable meanings.

where $E_{\mathrm{ES}}(h)$ is the energy available in the ES in hour h and $\eta_{\mathrm{ES}}^{\mathrm{DC}}$ is its discharging efficiency.

Given the above, Eq. 6.5 models the demand met by the PV-ES-CS $D_{\mathrm{sys}}(h)$, and Eq. 6.6 finds the resulting energy imported from the grid $D_{\mathrm{grid}}(h)$.

$$D_{\mathrm{sys}}(h) = D_{\mathrm{PV}}(h) + D_{\mathrm{ES}}(h) \tag{6.5}$$

$$D_{\mathrm{grid}}(h) = D_{\mathrm{load}}(h) - D_{\mathrm{sys}}(h) \tag{6.6}$$

To contextualize the benefits of the PV-ES-CS system, the EV load demand met by the system, $D_{\mathrm{sys}}(h)$, incurs a marginal cost of zero, whereas the marginal cost of $D_{\mathrm{grid}}(h)$ is determined by the electricity price during hour P_{grid}. This serves as the link between the technical and economic models, and all prior equations have been aimed at solving for $D_{\mathrm{sys}}(h)$ and $D_{\mathrm{grid}}(h)$. The next section delves into the economic aspects of the system modeling.

6.2.3 System economic model

The economic model of the proposed system consists of the investment and maintenance costs of the components, component degradation, and residual and replacement value.

6.2.3.1 Component costs

The investment cost for the solar PV (I_{PV}) covers the PV and inverter modules, installation and commissioning costs, peripherals, and vendor markup, while the investment for the ES is simply the battery. The total system investment cost is expressed by Eq. 6.7, where the costs are split between the PV (I_{PV}) and the battery (C_{ES}).

$$I_{\mathrm{sys}} = I_{\mathrm{PV}} + I_{\mathrm{ES}} \tag{6.7}$$

The investment cost is repaid through annual payments (α), which are calculated by multiplying the initial investment by the Capital Recovery Factor (CRF). The CRF is a financial formula used to determine the annual payment needed to recover the initial capital investment over a specified time period, typically with interest. Equations for the CRF and α are provided in Eq. 6.8 and 6.9,

$$CRF = \frac{\phi(1+\phi)^{\mathrm{T}}}{(1+\phi)^{\mathrm{T}} - 1} \tag{6.8}$$

where ϕ represents the interest rate per period and T is the number of periods over which the capital is recovered. For the battery, which may need to be replaced before the end of T periods, the repurchase costs are amortized over the remaining life of the project.

$$\alpha = CRF \times I_{\mathrm{sys}} \tag{6.9}$$

Each component also incurs a maintenance cost (M_{t}) in every time period t, which remains constant each year but scales with inflation. The total maintenance cost for the system, $M_{\mathrm{sys}}(h)$, is given by Eq. 6.10.

$$M^{\mathrm{t}}_{\mathrm{sys}} = (M^{\mathrm{t}}_{\mathrm{PV}} + M^{\mathrm{t}}_{\mathrm{ES}}) \times (1+\pi)^{\mathrm{t}} \tag{6.10}$$

where π is the inflation rate in time t.

6.2.3.2 Component degradation

PV system performance degrades over time due to factors such as oxidation, temperature, thermal stresses, weather conditions, and mechanical wear. Jordan et al. [278] conducted a statistical analysis of over 11,000 solar systems in 40 countries, finding a median degradation rate of 0.5% to 0.6% per year. In this study, a degradation rate of $\delta^{PV} = 0.6\%$ is used, meaning PV output decreases by 0.6% annually.

The battery is considered to have reached end of life once its capacity falls to 80% of its original rating. For a lithium-ion battery with a 20-year calendar life [279], this translates to a 1% reduction in usable capacity per year until replacement becomes necessary.

Although cycle life offers valuable insights into how usage patterns and depth of discharge contribute to battery degradation, the calendar life metric frequently provides a more suitable basis for planning and evaluation – particularly when charging schedules are irregular, as they may be under load-shedding conditions. For practical purposes, therefore, calendar life is adopted as the primary indicator of battery longevity in the following study.

In the context of EV charging stations, operational profiles can involve sporadic or moderate cycling, meaning the cumulative effects of physical and chemical aging may outweigh the impact of high-intensity cycling. Factors like ambient temperature and the state-of-charge during storage are key drivers of calendar aging, making it the principal determinant of capacity loss. Emphasizing calendar life thereby streamlines cost projections and reliability assessments.

Nonetheless, it is crucial to recognize that this approach may underestimate the effects of extreme or frequent cycling, which can accelerate capacity fade beyond what a simple calendar-based model would predict. Real-world aging also depends on temperature fluctuations, charge rates, and usage patterns that can interact in complex ways. Despite these caveats, prioritizing calendar life provides a pragmatic framework for system-wide planning, which is the intention in this chapter of the thesis.

Ultimately, while energy throughput can shed additional light on day-to-day efficiency, in the paratransit context calendar life serves as a more practical measure for gauging long-term performance and economic viability in the context of an EV charging station.

6.2.3.3 Residual and replacement value

Residual value (R) is the estimated worth of an asset at the end of its useful life, typically expressed as a percentage of the initial investment cost [89, 90]. The residual value is recouped in the final year of the system's operation and is added to the last cash flow, subject to the applicable discount rate.

Replacement cost (ϱ^{t}) represents the cost of replacing an asset in a specific time period t. The replacement cost for a given component is assumed to be equal to its initial investment cost plus any inflation that has occurred up to that point.

6.2.4 Net Present Value

The goal of the optimization is to maximize the net present value (NPV) of all cash flows related to the system over its lifetime. NPV is a financial metric that evaluates the profitability of an investment by comparing the present value of expected cash inflows to the present value of cash outflows. It incorporates a discount rate (Γ) to account for the time value of money, meaning that a dollar received in the future is worth less than one received today. A positive NPV suggests that the project is expected to generate more value than the initial investment, making it attractive, while a negative NPV indicates that the investment may not be financially viable.

NPV (\$) is calculated using Eq. 6.11, where T represents the number of periods over the project's lifespan, and RV is the residual value in the final year, added to the cash flow in the last period.

$$NPV = \sum_{\mathrm{t=1}}^{\mathrm{T\,-\,1}} \frac{NCF^{\mathrm{t}}}{(1+\Gamma)^{\mathrm{t}}} + \frac{NCF^{\mathrm{T}} + R}{(1+\Gamma)^{\mathrm{T}}} \tag{6.11}$$

Net cash flow in a given time period (NCF^{t}) is determined by subtracting the annual capital payments $\alpha^{\mathrm{t}}_{\mathrm{sys}}$, maintenance costs $M^{\mathrm{t}}_{\mathrm{sys}}$, and replacement costs $RC^{\mathrm{t}}_{\mathrm{sys}}$ from the savings in marginal energy costs provided by the PV-ES-CS system S^{t} (Eq. 6.12).

$$NCF^{\mathrm{t}} = S^{\mathrm{t}} - M^{\mathrm{t}}_{sys} - \varrho^{\mathrm{t}}_{sys} - \alpha^{\mathrm{t}}_{\mathrm{sys}} \tag{6.12}$$

Energy savings (\$) are defined as the difference between the energy costs at the charging station without the system in place (C^t) and the energy costs with the system in place ($C^{\mathrm{t}}_{\mathrm{sys}}$), as shown in Eq. 6.13.

$$S^{\mathrm{t}} = C^{\mathrm{t}}_{\mathrm{base}} - C^{\mathrm{t}}_{\mathrm{sys}} \tag{6.13}$$

$C^{\mathrm{t}}_{\mathrm{base}}$ refers to the total cost of electricity from the grid in time period t. According to Eq. 6.14, it is calculated as the sum of all energy drawn from the grid during the time period $D^{\mathrm{grid}}(\mathrm{h})$, multiplied by the energy tariffs for that hour $P^{\mathrm{grid}}(\mathrm{h})$.

$$C^{\mathrm{t}}_{\mathrm{base}} = \sum_{\mathrm{h}=1}^{\mathrm{H}} D_{\mathrm{grid}}(h) \times P_{\mathrm{grid}}(h) \times (1+\pi)^{\mathrm{t}} \tag{6.14}$$

where H is the number of hours in time period t.

6.2.5 Value of resiliency

The value of resiliency (Λ) represents the operational savings that the PV-ES-CS system provides during unplanned grid constraints, such as load shedding. This value is calculated by determining the operational savings associated with mitigating the energy loss due to load shedding (E_{LS}) with the help of the PV-ES system.

Assuming that fleet operators will deploy internal combustion engine (ICE) vehicles to cover trips that cannot be fulfilled by EVs during load shedding, the value of E_{LS} is determined as the difference between the operational costs of an EV and an equivalent ICE vehicle. The operational cost of an EV for a trip is based on the electricity cost required to cover the trip's distance, while the operational cost of an ICE vehicle is calculated using the fuel cost needed to travel the same distance that E_{LS} would have enabled for the EV. This cost can be expressed as the product of the fuel consumption rate in L/km (η_{ICE}) and the fuel price (P_{fuel}) for the distance that could have been covered by the EV ($E_{\mathrm{LS}} \times \frac{1}{\eta_{EV}}$).

Therefore, the value of resiliency is the additional cost incurred when operational demand is met by an ICE vehicle instead of an EV, which is represented mathematically by Equation 6.15.

$$\Lambda^{\mathrm{t}} = E^{\mathrm{t}}_{\mathrm{LS}} \times \frac{1}{\eta_{EV}} \times \eta_{ICE} \times P_{fuel} - C^{\mathrm{t}} \tag{6.15}$$

In the optimization problem, Λ is added to the NPV of the system whenever the system provides electricity to vehicles during an unplanned load shedding event.

The assumption that ICE vehicles will take over operational duties from EVs during load shedding is supported by several factors. First, the transition from ICE to EV fleets is gradual, meaning that many fleets will continue to operate ICE vehicles for some time. Second, even after replacing most ICE vehicles with EVs, fleets are likely to retain some ICE vehicles for operational flexibility. Finally, given that load shedding is a well-known challenge, fleet owners are expected to anticipate such events and develop contingency plans to ensure continuous operations. These factors suggest that fleet owners are aware of the potential for load shedding and will take steps to maintain operational continuity during such interruptions.

6.2.6 Economic evaluation

The levelized cost of electricity (LCOE) is a classical metric used to understand how expensive the electricity from a given generation asset is over its lifetime. It expresses the total cost of an electricity supply asset per unit of electricity it provides over its lifespan. To estimate LCOE, net present cost of the investment is divided by the quantity of electricity it serves:

$$LCOE = \frac{\sum_{\mathrm{t=1}}^{\mathrm{T}} \frac{\alpha_{\mathrm{sys}}^{\mathrm{t}} + M_{\mathrm{sys}}^{\mathrm{t}} + \varrho_{\mathrm{sys}}^{\mathrm{t}} - R_{\mathrm{sys}}^{\mathrm{t}}}{(1+\Gamma)^{\mathrm{t}}}}{\sum_{\mathrm{t=1}}^{\mathrm{T}} \frac{D_{\mathrm{sys}}^{\mathrm{t}}}{(1+\Gamma)^{\mathrm{t}}}} \tag{6.16}$$

LCOE is typically most valuable when comparing two different investments to determine which one will generate cheaper energy over its lifespan, taking into account capital costs. In this study, however, the PV-ES-CS is being compared to a CS without PV-ES, rather than to an alternative investment at the same CS. Since the charging station exists in both cases, the comparison of LCOE to the average cost of energy without the system is not a direct one. The LCOE accounts for full lifecycle costs, including maintenance and investment, while the average energy cost reflects only the marginal cost of producing electricity at a given moment. In practice, when the PV-ES-CS cannot cover the entire EV load, the grid supplies the remaining load at the prevailing tariff, which affects the overall cost of electricity for the PV-ES-CS. As a result, a normalized cost of electricity

Table 6.2: Geographical coordinates and elevation of selected case study location.

Province	City	Latitude (°N)	Longitude (°E)	Elevation (m)
Gauteng	Dobsonville	-26.21	27.87	1,650m

(COE) is used as a more accurate measure of economic performance:

$$COE = \frac{LCOE \times \sum_{\mathrm{t=1}}^{\mathrm{T}} \frac{D_{\mathrm{sys}}^{\mathrm{t}}}{(1+\Gamma)^{\mathrm{t}}} + \sum_{\mathrm{t=1}}^{\mathrm{T}} \sum_{\mathrm{h=1}}^{\mathrm{H}} \frac{(P_{\mathrm{grid}}(h) \times D_{\mathrm{grid}}^{\mathrm{t}}(h))}{(1+\Gamma)^{\mathrm{t}}}}{\sum_{\mathrm{t=1}}^{\mathrm{T}} \frac{D_{\mathrm{load}}^{\mathrm{t}}}{(1+\Gamma)^{\mathrm{t}}}} \tag{6.17}$$

which simplifies to

$$COE = \frac{\sum_{\mathrm{t=1}}^{\mathrm{T}} \frac{\alpha_{\mathrm{sys}}^{\mathrm{t}} + M_{\mathrm{sys}}^{\mathrm{t}} + \varrho_{\mathrm{sys}}^{\mathrm{t}} - R_{\mathrm{sys}}^{\mathrm{t}} + C_{\mathrm{grid}}^{\mathrm{t}}}{(1+\Gamma)^{\mathrm{t}}}}{\sum_{\mathrm{t=1}}^{\mathrm{T}} \frac{D_{\mathrm{load}}^{\mathrm{t}}}{(1+\Gamma)^{\mathrm{t}}}}, \tag{6.18}$$

where $C_{\mathrm{grid}}^{\mathrm{t}} = \sum_{\mathrm{h=1}}^{\mathrm{H}} (P_{\mathrm{grid}}(h) \times D_{\mathrm{grid}}^{\mathrm{t}}(h))$.

6.3 Case study

In this section, the technical specifications of the system components and relevant economic indicators are presented in the context of a case study. The estimated project lifetime T is 25 years. A time period t of one year is used for this analysis, so $H = 8760$.

6.3.1 Study area

A minibus taxi fleet operating out of the Dobsonville Mall taxi rank (terminus) is selected as a research object. Dobsonville is a township in greater Soweto, Johannesburg, South Africa. The location is presented in Table 6.2 and Fig. 6.4.

6.3.2 Solar PV output profile

The simulation in renewables.ninja is set at Dobsonville Mall taxi rank at -26.2139°N, 27.8705E°, with system efficiency loss set at 10%. The panel tilt is set at 30 degrees facing North, which is suitable for South Africa [282]. Fig. 6.5 displays the resulting capacity factor profile.

As expected, the capacity is highest in the summer months (Nov - Feb) aside from a slight dip from Dec. 5 - Dec. 9, and lowest in the winter months (Jun - Aug).

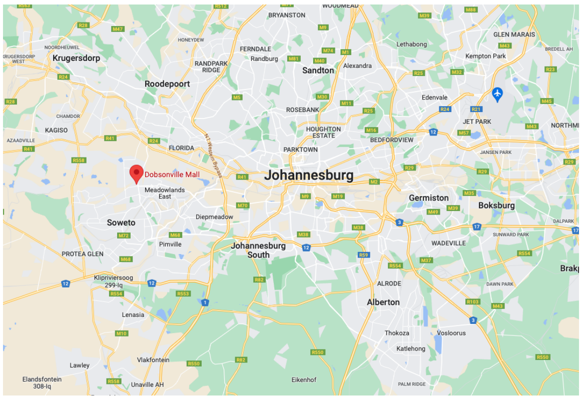

(a) Location of case study within Johannesburg [280].

(b) Satellite image of Dobsonville Mall taxi rank (terminus) [281].

Figure 6.4: Case study location.

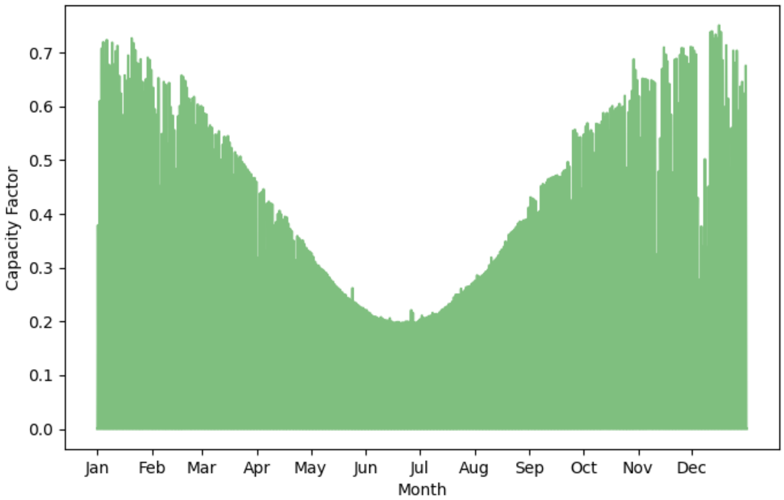

Figure 6.5: Annual solar profile at the selected case study location, the Dobsonville Mall Taxi Rank in Dobsonville, Greater Soweto, Johannesburg. The data underpinning this profile are from 2019 [270].

As mentioned in the caption, the data in this figure come from a single year, 2019, which means that the capacity factor is more susceptible to anomalies as compared to using a multi-year average. The visible dip in mid-December is an example of such an anomaly which likely does not persist across years, and must be regarded as a slight limitation of the dataset.

Table 6.3: Eskom seasonal time of use electricity tariffs for large users medium voltage [246]. [a]

Month	High/Low	Off-peak ($/kWh)	Standard ($/kWh)	High ($/kWh)
Jan	L	0.08	0.11	0.15
Feb	L	0.08	0.11	0.15
Mar	L	0.08	0.11	0.15
Apr	L	0.08	0.11	0.15
May	L	0.08	0.11	0.15
Jun	H	0.09	0.13	0.34
Jul	H	0.09	0.13	0.34
Aug	H	0.09	0.13	0.34
Sep	L	0.08	0.11	0.15
Oct	L	0.08	0.11	0.15
Nov	L	0.08	0.11	0.15
Dec	L	0.08	0.11	0.15

[a] Converted from South African Rand to US Dollar using a conversion rate of R0.054 to 1 USD, the average conversion rate in 2023 as of August, 2023.

6.3.3 Electricity pricing

The electricity price schedule for the first year of the optimization simulation is given in Table 6.3. These prices are based on the City of Johannesburg three-part time-of-use tariff rates for medium voltage users [246], and serve as a proxy for electricity prices for businesses in South Africa (prices in other large cities such as Cape Town are similar [247]). Prices in subsequent years are subject to inflation.

On weekdays, the hours for off-peak energy tariff are 22:00 - 05:00. The hours for standard energy tariff are 6:00, 10:00 - 17:00, and 20:00 - 21:00. The hours for peak energy tariff are 07:00 - 09:00 and 18:00 - 19:00. All hours on weekends are charged the off-peak tariff [247].

6.3.4 Load shedding schedule

To account for the grid constraints due to load shedding, load shedding schedules are simulated from historical load shedding data from Eskom [283], which holds a monopoly on electricity supply in South Africa.

In South Africa, Eskom implements load shedding in stages, ranging from Stage 1 to Stage 8, with higher stages indicating more severe power cuts. For example, during Stage 1, Eskom enforces either three two-hour outages over four days or three four-hour

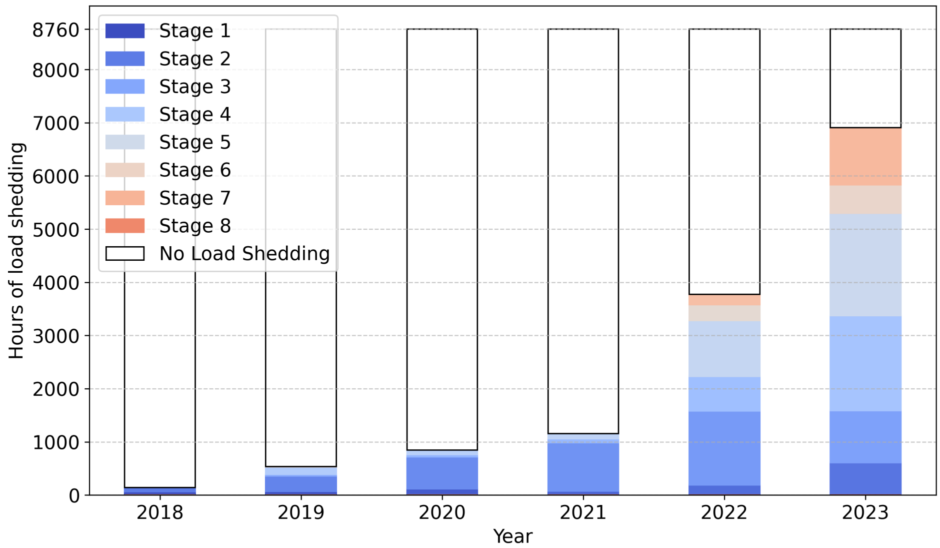

Figure 6.6: Trend of hours spent in each load shedding stage over the past several years [283].

outages over eight days. In Stage 8, power cuts can occur up to six times per day, with electricity being unavailable for up to 12 hours daily. Detailed definitions for all eight load shedding stages are provided in Table A1 in Appendix A.

An analysis of Eskom's historical data shows a clear upward trend in load shedding over the past several years [283]. Fig. 6.6 illustrates the monthly load shedding trends over recent years. Detailed values for stages and months are available in Appendix A, Tables A2 and A3. From 2018 to 2023, the total number of load shedding hours increased from 141 to 6,908 annually, with the median load shedding stage rising from none to Stage 3.

There are mixed predictions about the future of load shedding in South Africa. Some reports suggest a worsening outlook with ongoing energy supply shortfalls [284, 285], while others foresee a surge in private sector power generation in the coming years [286, 287]. Given the root causes of the crisis—such as Eskom's management challenges, aging infrastructure, and regulatory complexities—and the necessary solutions, which include infrastructure upgrades, distributed renewable energy, energy efficiency improvements, and market-driven pricing [288], it is unlikely that load shedding will be resolved in the near future.

The extent of load shedding will depend on several external factors. For fleet owners, it is reasonable to expect some degree of load shedding to persist, even if improvements

Table 6.4: Sample Stage 2 and Stage 4 load shedding day schedules, with the starting and ending hour of each event. Vehicles cannot charge while load shedding is active.

		First Event		Second Event		Third Event	
Daily Schedule ID		Start	End	Start	End	Start	End
Stage 4	ST4-D0	0:00	2:00	8:00	10:00	16:00	18:00
	ST4-D1	2:00	4:00	10:00	12:00	18:00	20:00
	ST4-D2	4:00	6:00	12:00	14:00	20:00	22:00
	ST4-D3	6:00	8:00	14:00	16:00	22:00	0:00
Stage 2	ST2-D0	0:00	2:00	-	-	-	-
	ST2-D1	0:00	2:00	8:00	10:00	-	-
	ST2-D2	8:00	10:00	16:00	18:00	-	-
	ST2-D3	16:00	18:00	-	-	-	-
	ST2-D4	22:00	24:00	-	-	-	-
	ST2-D5	6:00	8:00	-	-	-	-
	ST2-D6	6:00	8:00	14:00	16:00	-	-

occur in the future. In this case study, both conservative and optimistic scenarios are simulated. Based on historical trends, the conservative scenario assumes an average of Stage 4 load shedding over the lifespan of the PV-ES-CS project, reflecting a slightly worse situation than 2023. The optimistic scenario assumes an average of Stage 2 load shedding over the same period. These two scenarios are referred to as ST4 and ST2, respectively, in the results section. The load shedding definitions outlined by Eskom in Table A1 of Appendix A.1 are used to simulate both Stage 4 and Stage 2 load shedding.

Simulating a week of load shedding involves two steps. First, a set of daily load shedding schedules is generated that, when combined in certain patterns, meet the definition of the specified load shedding stage. These daily schedules are listed in Table 6.4. The second step is to combine these daily schedules into a weekly pattern that aligns with the desired load shedding stage.

The daily schedules are then stitched together in a specific order to create a weekly load shedding schedule (starting from Monday):

Weekly load shedding schedules (using daily schedule IDs from Table 6.4)

– **Stage 4:** ST4-D0, ST4-D1, ST4-D2, ST4-D3, ST4-D0, ST4-D1, ST4-D2

– **Stage 2:** ST2-D0, ST2-D1, ST2-D2, ST2-D3, ST2-D4, ST2-D5, ST2-D6

This schedule indicates that the Stage 4 load shedding schedule starts with daily schedule 0 (ST4-D0) on Monday, which according to Table 6.4 has load shedding events

Table 6.5: Input parameters for scheduling EV fleet.

Parameter	Value	Source
Vehicle battery capacity	70 kWh	[161]
Energy consumption	0.55 kWh/km	Chapter 5 (PDC)
Charger rating	22 kW	
Charging outlets	1 per vehicle	

from 00:00 - 02:00, 08:00 - 10:00, and 16:00 - 18:00. On Tuesday, S4T-D2 happens, meaning load shedding events occur from 02:00 - 04:00, 10:00 - 12:00, and 18:00 - 20:00. And so on for the rest of the week. Similarly, the Stage 2 schedule, starts with ST-D0 on Monday, and so on.

As detailed in Section 6.2.1.2, load shedding can be either planned or unplanned. These two situations require different modeling approaches: when load shedding is planned, fleet owners can schedule their EV charging around the outage hours, whereas unplanned outages prevent recharging, disrupting the ability to meet operational demand. Based on data from Eskom's Weekly Unplanned Outages portal [289] and their historical load shedding records [283], it is assumed that two-thirds of outages are planned and one-third are unplanned.

6.3.5 EV charging load profiles

EV charging load profiles are simulated using real-world origin-destination data from a fleet of minibus taxis operating at the Dobsonville Mall taxi rank. Since electric paratransit services are currently unavailable in the region, this study utilizes advanced tools to generate operational schedules EVs from this taxi rank. As electric paratransit becomes more widely adopted, the model and insights can be refined through feedback loops based on empirical data.

To create these profiles, operational data from traditional internal combustion engine (ICE) vehicles is fed into an electric paratransit operations planning tool developed by [248]. This tool uses ICE vehicle schedules to generate feasible schedules that are adaptable for EVs with specific parameters. A key feature of the tool is its ability to enforce zero lateness, ensuring all passengers are served punctually. The vehicle parameters used for this scheduling process are detailed in Table 6.5.

To model the PV-ES-CS system at different levels of EV penetration, load profiles are simulated for 25%, 50%, 75%, and 100% EV penetration in the fleet. These scenarios are referred to as “low," “medium," “high," and “full" penetration, respectively. In each case, zero lateness is enforced to ensure that the operational schedule remains feasible. It is assumed that each vehicle has its own charger, ensuring a charger is always available when needed at the station.

The weekly load profiles for each level of EV penetration within each load shedding schedule scenario are visualized in Fig. 6.7. The three scenarios are:

1. No load shedding (No LS): Base case (this scenario serves as a reference point).
2. Stage 2 load shedding (ST2): Optimistic scenario.
3. Stage 4 load shedding (ST4): Conservative scenario.

In the visual representation, grey bars indicate periods when load shedding restricts vehicle charging activities. A key observation from these energy demand profiles is that the EV fleet typically requires more energy on weekends than on weekdays, with peak daily load generally occurring in the evening and peak weekly load on Saturdays. These trends are consistent with most urban minibus taxi fleets in the Global South [29], supporting the external validity of the findings.

Table 6.6 presents summary statistics for the different fleets shown in Fig. 6.7. The “per vehicle load" column shows a peak in vehicle load between 50% and 75% EV penetration, followed by a decline as EV penetration reaches 100%. This reflects vehicle utilization rates, indicating that beyond a certain point of EV saturation, each individual EV is used less frequently.

Fig. 6.7 also highlights that although peak load is high, there is potential to spread charging throughout the night, particularly during the early morning hours between midnight and 5:00 am when little charging occurs. This suggests the possibility of reducing the number of chargers, thereby lowering charge point investment costs—a topic not covered in this thesis. Future research could explore the potential for peak shaving in electric minibus taxi operational schedules to minimize the number of charge points or maximize solar energy utilization.

Table 6.6: Summary of fleet mobility, power, and economic characteristics under the different levels of EV penetration load shedding schedule scenarios. The load values are calculated on a weekly basis.

	EV Pen	# EVs	Total (per-vehicle) Load (kWh)	Peak Load (kW)	Peak hourly average (kW)	Cost of Electricity ($/kWh)
No LS	25%	19	6,522 (343)	420	7.0	0.119
	50%	38	22,756 (599)	768	12.8	0.118
	75%	57	33,745 (592)	1,164	19.4	0.115
	100%	76	35,637 (469)	1,542	25.7	0.113
ST2	25%	19	6,271 (330)	396	6.6	0.115
	50%	38	21,233 (559)	768	12.8	0.118
	75%	57	32,346 (567)	1,164	19.4	0.115
	100%	76	35,583 (468)	1,452	24.2	0.112
ST4	25%	19	6,465 (340)	396	6.6	0.113
	50%	38	21,871 (576)	834	13.9	0.112
	75%	57	32,724 (574)	1,188	19.8	0.110
	100%	76	35,128 (462)	1,542	25.7	0.110

Lastly, the cost of electricity (COE) varies across the different load shedding scenarios, largely due to adjustments in EV charging profiles triggered by the load shedding schedules, which, in turn, affect the time-of-use tariffs they incur.

6.3.5.1 Incremental fleet electrification scenarios

In addition to evaluating the low (25%), medium (50%), high (75%), and full (100%) fleet electrification scenarios discussed earlier, this study also examines the viability and performance of the PV-ES-CS system under incremental fleet electrification conditions. These scenarios represent increasing levels of EV penetration over the lifespan of the PV-ES-CS project.

Two incremental fleet electrification scenarios are modeled: one fast (INC-F) and one slow (INC-S), as outlined in Table 6.7. In the fast scenario, the fleet begins with 25% electrification, reaches 50% in five years, progresses to 75% in another five years, and achieves full electrification in 15 years. In the slow scenario, the fleet starts at 25% electrification, reaches 50% in 10 years, 75% after another eight years, and 100% after an additional four years, resulting in a total of 22 years to full electrification.

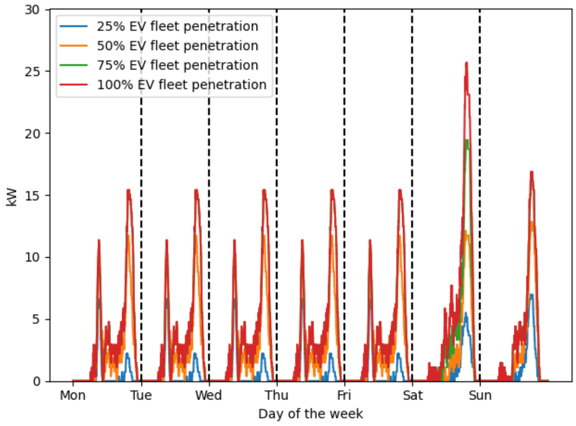

(a) Weekly EV fleet load profile – No load shedding (No LS).

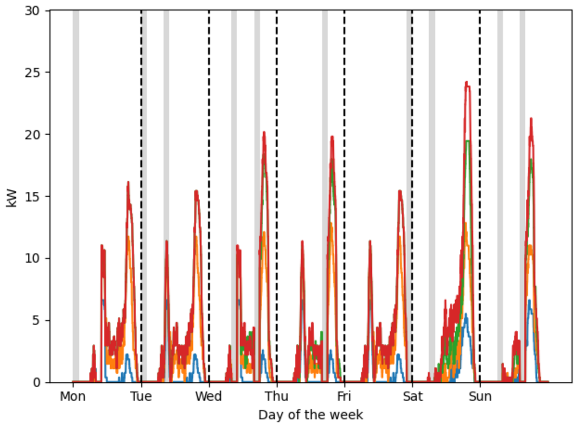

(b) Weekly EV fleet load profile – Stage 2 load shedding (ST2).

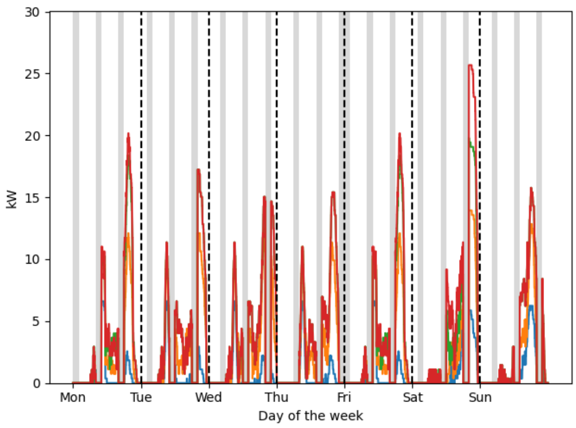

(c) Weekly EV fleet load profile – Stage 4 load shedding (ST4).

Figure 6.7: Weekly charging load profiles at the Dobsonville taxi rank for varying levels of EV penetration and load shedding schedules (either no load shedding or stage 4). The gray shaded areas on the ST4 graph indicate times when load shedding is active and the EVs cannot charge. The dashed black lines demarcate midnight between each day.

Table 6.7: The year in which each level of EV fleet penetration is reached during each of the two incremental fleet electrification scenarios (INC-F(ast) and INC-S(low)).

	Level of EV fleet penetration			
Scenario	25%	50%	75%	100%
INC-F (year)	0	3	7	10
INC-S (year)	0	10	18	22

6.3.6 Timed slow charging

By applying the conventional rule/logic-based energy dispatch strategy, this thesis assesses the system under a “worst-case" usage scenario for the energy storage (ES). Additionally, a scenario featuring a basic timed slow charging (TC) heuristic is introduced to demonstrate the advantages of marginally improved ES utilization, highlighting the potential for future research to further optimize the energy dispatch strategy for better economic or technical performance.

In the TC scenario, the ES is permitted to charge at 2.2 kW from the grid overnight. Charging during the night ensures a positive economic outcome for timed slow charging, as it draws electricity from the grid when prices are lowest and serves the load during the morning when electricity is more expensive (see Section 6.3.3 for details on hourly pricing).

6.3.7 System specifications

A summary of the technical specifications, relevant economic indicators, and energy market parameters that go into the techno-economic optimization model are given in Table 6.8.

6.4 Simulation, results and discussion

In this section, the optimal sizing results for the PV-ES-CS system are evaluated under the following scenarios: no load shedding (No LS), Stage 4 load shedding (LS-ST4), Stage 2 load shedding (LS-ST2), and each of these scenarios with timed slow charging (No LS + TC, LS-ST4 + TC, and LS-ST2 + TC).

Each scenario is assessed across the four fleet EV penetration levels: low (25%), medium (50%), high (75%), and full (100%), as well as the two incremental electrification cases, INC-F (fast) and INC-S (slow). The analysis is conducted according to the case

Table 6.8: Summary of the PV-ES-CS capacity optimization model input parameters.

Specification	Value	Source
PV module		
Panel cost	\$500/kW	[290]
O&M cost	\$25/kW/year	[291]
Inverter Cost	\$140/kW	[292]
Lifetime	25 years	[290]
System efficiency	90%	[293]
Degradation rate	0.6%/year	[278]
Energy storage		
Pack cost	\$300/kWh	[292, 294]
O&M cost	10/kWh-year	[294]
Roundtrip efficiency	95%	[279]
Depth of discharge	90%	[279]
Lifetime	20 years	[279]
Degradation rate	1%/year	[279]
C-rating	0.5C	
Economic indicators		
Inflation rate	7.04%/year	[258]
Discount rate	5%/year	[271]
Interest rate	13.75%/year	[243, 295]
Residual value	10% investment cost	[89]
Vehicle parameters		
Energy consumption	0.55kWh/km	[161]
Fuel consumption	13.8L/100km	[296]
Diesel fuel cost	\$1.05/L	[245]

study described in Section 6.3, and is then revisited with minor adjustments in Sections 6.4.2.1 and 6.4.2.2. In Section 6.4.2.1, the ratio of planned to unplanned grid constraint events is adjusted from 1:2 to 2:1 to explore different mixes of planned and unplanned load shedding. In Section 6.4.2.2, a feed-in tariff is introduced to evaluate the impact of financial incentives for solar PV panels. The key findings from these results are discussed in detail in Section 3.4.

6.4.1 Main results

The primary techno-economic characteristics for each scenario are presented side-by-side in Fig. 6.8, and the cost of electricity (COE) for each scenario with and without the system is presented in Table 6.9.

Summary: System feasibility

Overall, Fig. 6.8 demonstrates that the PV-ES-CS system is economically viable (i.e.,

(a) PV rating (kW). **(b)** ES capacity (kWh).

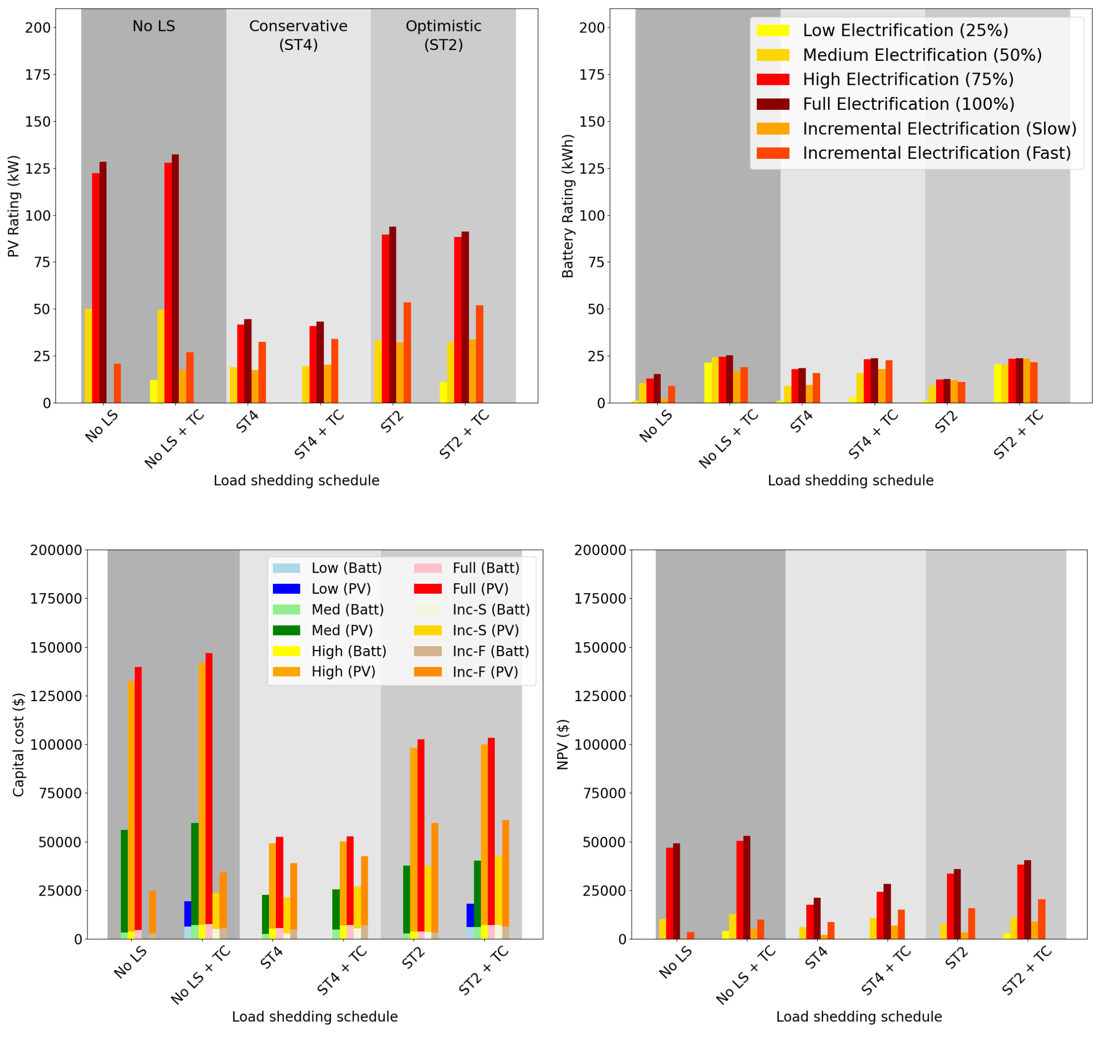

(c) Investment cost ($). Separated by PV (darker shades) and ES (lighter shades). **(d)** Net Present Value ($).

Figure 6.8: Techno-economic characteristics of the optimally configured PV-ES-CS in each scenario. For each scenario, low (25%), medium (50%), high (75%), and full (100%) fleet EV penetration are assessed. Scenarios are color grouped by the no load shedding, optimistic load shedding outlook, and conservative load shedding outlooks.

Table 6.9: Cost of electricity (COE) adjusted for inflation without the PV-ES system and with the PV-ES system over the lifetime of the project, and the percentage change in COE from the former to the latter.

Scenario	EV Pen	COE without [with] system ($/kWh)	Change (%)
No LS	25%	0.1191 [-]	-
	50%	0.1181 [0.1166]	-1.27
	75%	0.1152 [0.1124]	-2.43
	100%	0.1132 [0.1105]	-2.39
	INC-S	0.1148 [0.1146]	-0.17
	INC-F	0.1140 [0.1137]	-0.26
No LS + TC	25%	0.1191 [0.1175]	-1.33
	50%	0.1181 [0.1165]	-1.35
	75%	0.1152 [0.1122]	-2.60
	100%	0.1132 [0.1103]	-2.57
	INC-S	0.1148 [0.1144]	-0.35
	INC-F	0.1140 [0.1134]	-0.53
ST4	25%	0.1132 [-]	-
	50%	0.1115 [0.1103]	-1.05
	75%	0.1102 [0.1078]	-2.17
	100%	0.1090 [0.1065]	-2.25
	INC-S	0.1108 [0.1100]	-0.68
	INC-F	0.1104 [0.1083]	-1.56
ST4 + TC	25%	0.1132 [0.1120]	-1.05
	50%	0.1115 [0.1100]	-1.34
	75%	0.1102 [0.1076]	-2.34
	100%	0.1090 [0.1064]	-2.40
	INC-S	0.1108 [0.1096]	-1.11
	INC-F	0.1104 [0.1079]	-1.90
ST2	25%	0.1184 [-]	-
	50%	0.1171 [0.1156]	-1.27
	75%	0.1145 [0.1118]	-2.38
	100%	0.1132 [0.1105]	-2.39
	INC-S	0.1144 [0.1143]	-0.07
	INC-F	0.1137 [0.1134]	-0.30
ST2 + TC	25%	0.1184 [0.1168]	-1.33
	50%	0.1171 [0.1155]	-1.34
	75%	0.1145 [0.1116]	-2.54
	100%	0.1132 [0.1103]	-2.56
	INC-S	0.1144 [0.1140]	-0.33
	INC-F	0.1137 [0.1131]	-0.50

Table 6.10: Summary of fleet mobility, power, and economic characteristics under the different levels of EV penetration load shedding schedule scenarios. Same as Table 6.6 with 58% and 65% scenarios now included in red to highlight the effects of per vehicle load.

	EV. Pen	# EVs	Total (per vehicle) Load (kWh)	Peak Load (kW)	Peak hourly average (kW)	COE ($/kWh)
No LS	25%	19	6,522 (343)	420	7.0	0.119
	50%	38	22,756 (599)	768	12.8	0.118
	58%	44	28,273 (643)	900	15.0	0.116
	66%	50	32,932 (658)	1,014	16.9	0.115
	75%	57	33,745 (592)	1,164	19.4	0.115
	100%	76	35,637 (469)	1,542	25.7	0.113
ST2	25%	19	6,271 (330)	396	6.6	0.115
	50%	38	21,233 (559)	768	12.8	0.118
	58%	44	25,623 (582)	900	15.0	0.116
	66%	50	30,022 (600)	990	16.5	0.116
	75%	57	32,346 (567)	1,164	19.4	0.115
	100%	76	35,583 (468)	1,452	24.2	0.112
ST4	25%	19	6,465 (340)	396	6.6	0.113
	50%	38	21,871 (576)	834	13.9	0.112
	58%	44	25,643 (583)	966	16.1	0.111
	66%	50	29,732 (594)	1,014	16.9	0.111
	75%	57	32,724 (574)	1,188	19.8	0.110
	100%	76	35,128 (462)	1,542	25.7	0.110

positive NPV) in all scenarios with at least 50% EV penetration, with NPVs ranging from $2,427 in LS-ST4/Inc-S to $52,832 in No LS + TC/100%. The system remains feasible, though smaller and less economically advantageous, in the incremental fleet electrification scenarios, as most savings are realized in the future when they are discounted.

One notable aspect of the figure is the relatively small increase in system size and NPV between 75% and 100% EV penetration compared to the larger jumps observed between 25%, 50%, and 75%. This suggests diminishing returns for system performance as EV fleet saturation increases, likely due to the reduction in per-vehicle load once the fleet becomes heavily electrified. To test this hypothesis, fleet penetration levels of 58% and 66% (the tertile values between 50% and 75%) were added to the simulation. The results, including the 58% and 66% cases, are shown in Figure 6.9. Summary statistics for the 58% and 66% fleets are provided in Table 6.10, highlighting the trends in per-vehicle load.

As hypothesized, system size and performance increase significantly with per-vehicle load (a proxy for vehicle utilization). In both the No LS and ST2 scenarios, per-vehicle load increases sharply up to 66% EV penetration, after which it stabilizes. However,

(a) PV rating (kW). **(b)** ES capacity (kWh).

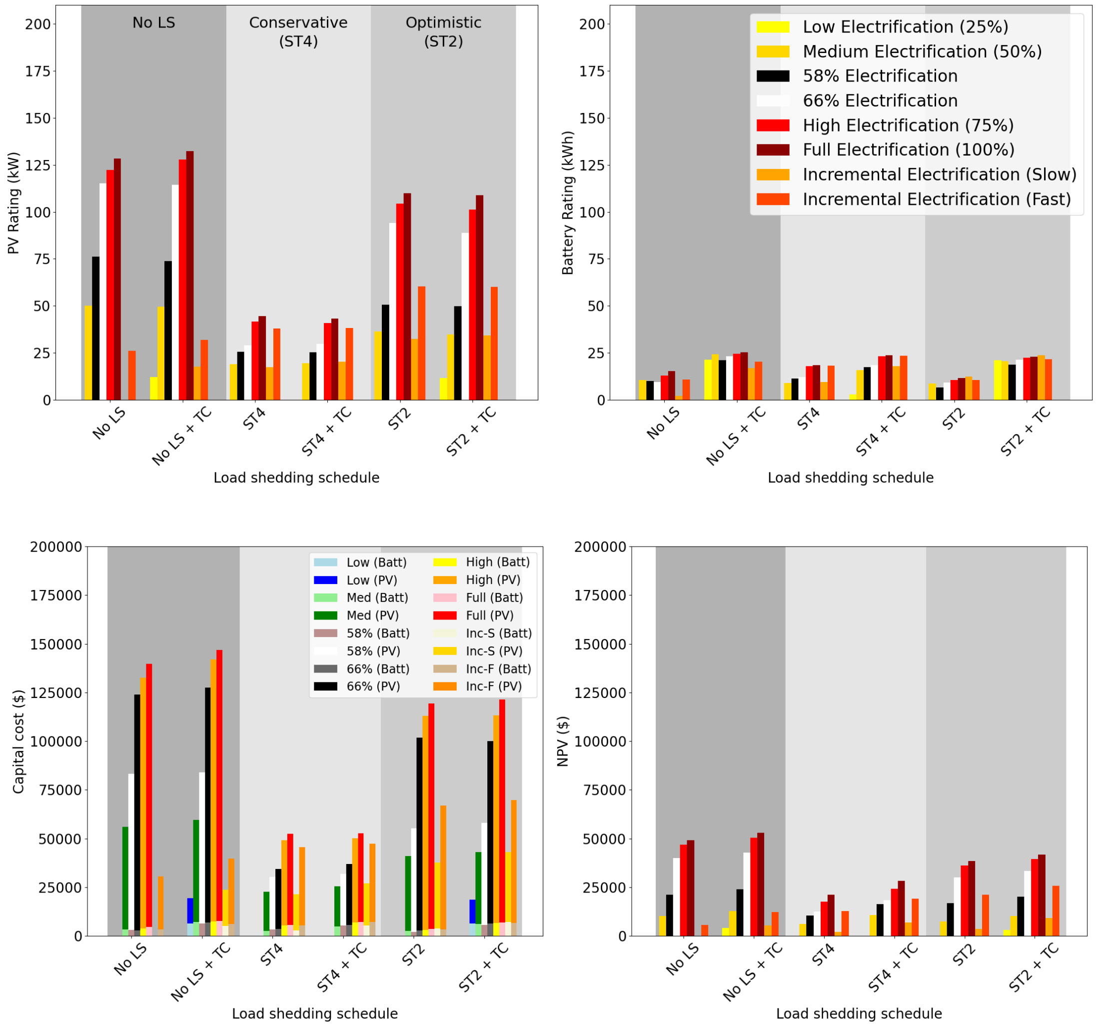

(c) Investment cost ($). Separated by PV (darker shades) and ES (lighter shades).

(d) Net Present Value ($).

Figure 6.9: Techno-economic characteristics of the optimally configured PV-ES-CS in each scenario. Same as Figure 6.8, but now including 58% and 66% EV fleet penetration scenarios (black and white respectively)

the ST4 scenario behaves slightly differently, as the system size does not experience the same pronounced jump between 50% and 58% EV penetration. This is likely due to the smaller increase in per-vehicle load (from 576 to 583, or 1.1%) between 50% and 58% EV penetration, compared to the increases seen in No LS (7.3%) and ST2 (4.1%). The effects of this difference are reflected in Fig. 6.9, which shows a less steep gradient in system sizing results for the ST4 and ST4 + TC scenarios.

6.4.2 Sensitivity of results to real-world uncertainty

This section explores the sensitivity of results to a greater proportion of unplanned load shedding events as well as a feed-in-tariff.

6.4.2.1 Greater proportion of unplanned load shedding events

The primary results are based on a planned-to-unplanned load shedding event ratio of 2:1, derived from Eskom's historical data (see Section 6.3.4). However, this ratio may change or vary by region, and the value of resiliency provided by the system could make the results sensitive to this ratio. To explore this, the results were also run with a ratio of planned to unplanned load shedding events of 1:2.

The results, shown in Figure 6.10, reveal only a slight improvement in the system's techno-economic performance. System sizes and NPVs increased by about 5%, due to the additional value of resiliency provided by the system during unplanned outages.

6.4.2.2 Feed-in tariff

The environmental and cost-saving benefits of solar PV and energy storage technologies, combined with their high capital costs, make them ideal candidates for government subsidies and incentives. One common financial incentive for solar PV, available in many countries, is a feed-in tariff. This allows PV system owners to sell excess electricity back to the grid.

Fig 6.11 presents the outcomes of the techno-economic analysis when a feed-in tariff of \$0.05/kWh is introduced, starting ten years after project implementation. The choice of a ten-year delay is based on South Africa's five-year political cycles, under the assumption that such a policy would require at least two cycles to be enacted.

With the introduction of the feed-in tariff, the system's techno-economic performance improves, though the overall trends remain consistent with previous results. On average, across all scenarios, PV and ES system sizes increase by 57% and 10%, respectively, while the investment cost and NPV grow by 50% and 78%, respectively.

(a) PV rating (kW). **(b)** ES capacity (kWh).

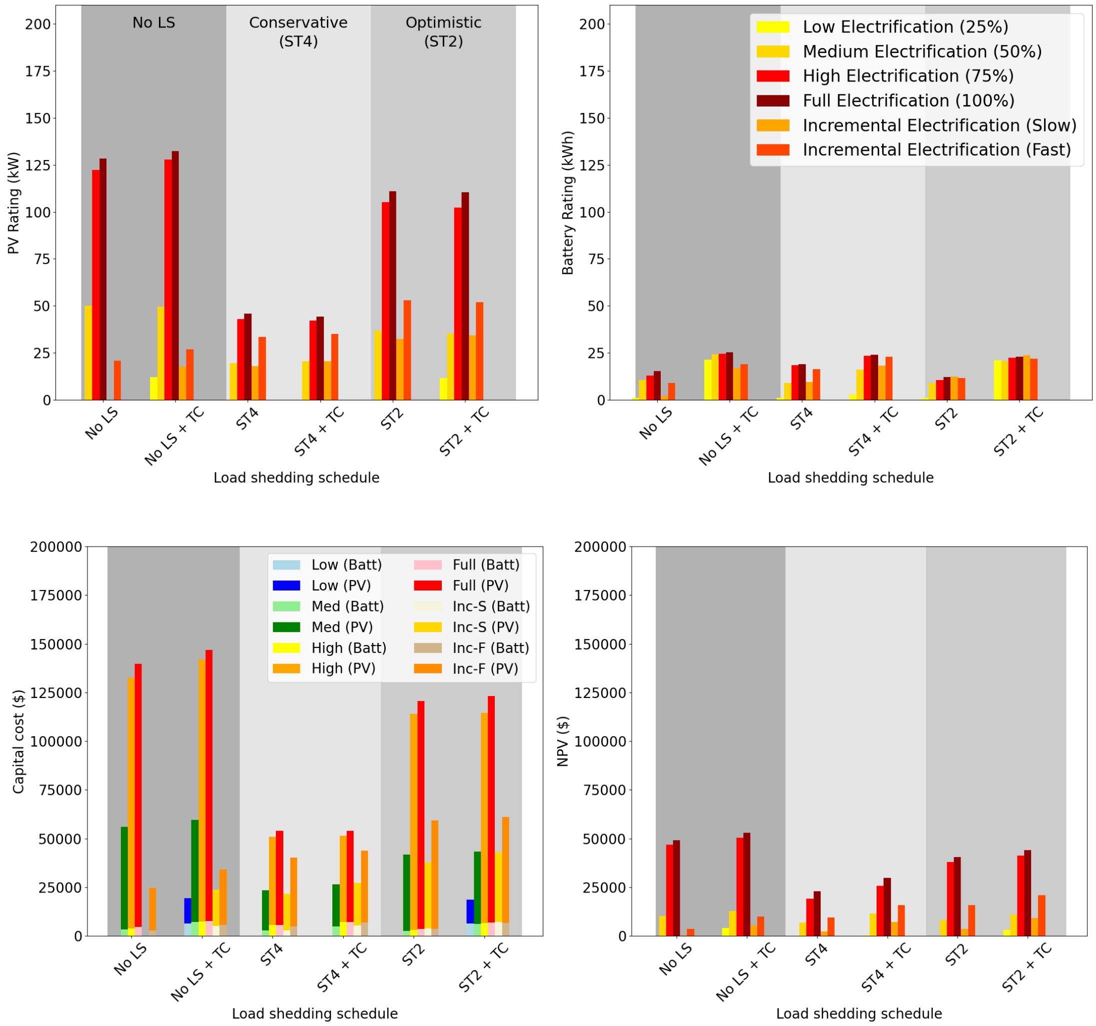

(c) Investment cost ($). Separated by PV (darker shades) and ES (lighter shades). **(d)** Net Present Value ($).

Figure 6.10: Same as Figure 6.8 but with the ratio of planned to unplanned load shedding events adjusted from 2:1 to 1:2.

6.4.3 Key insights

Key insight 1: Diminishing marginal returns

A key insight from these results is the highly non-linear increase in PV system size and NPV as EV fleet penetration rises. In all scenarios, there is a significant jump in system size and NPV from low to medium EV penetration, and again from medium to high penetration (dark yellow to light red bars), with a smaller increase from high to full penetration (light red to dark red bars). On average, across all scenarios, the

(a) PV rating (kW). **(b)** ES capacity (kWh).

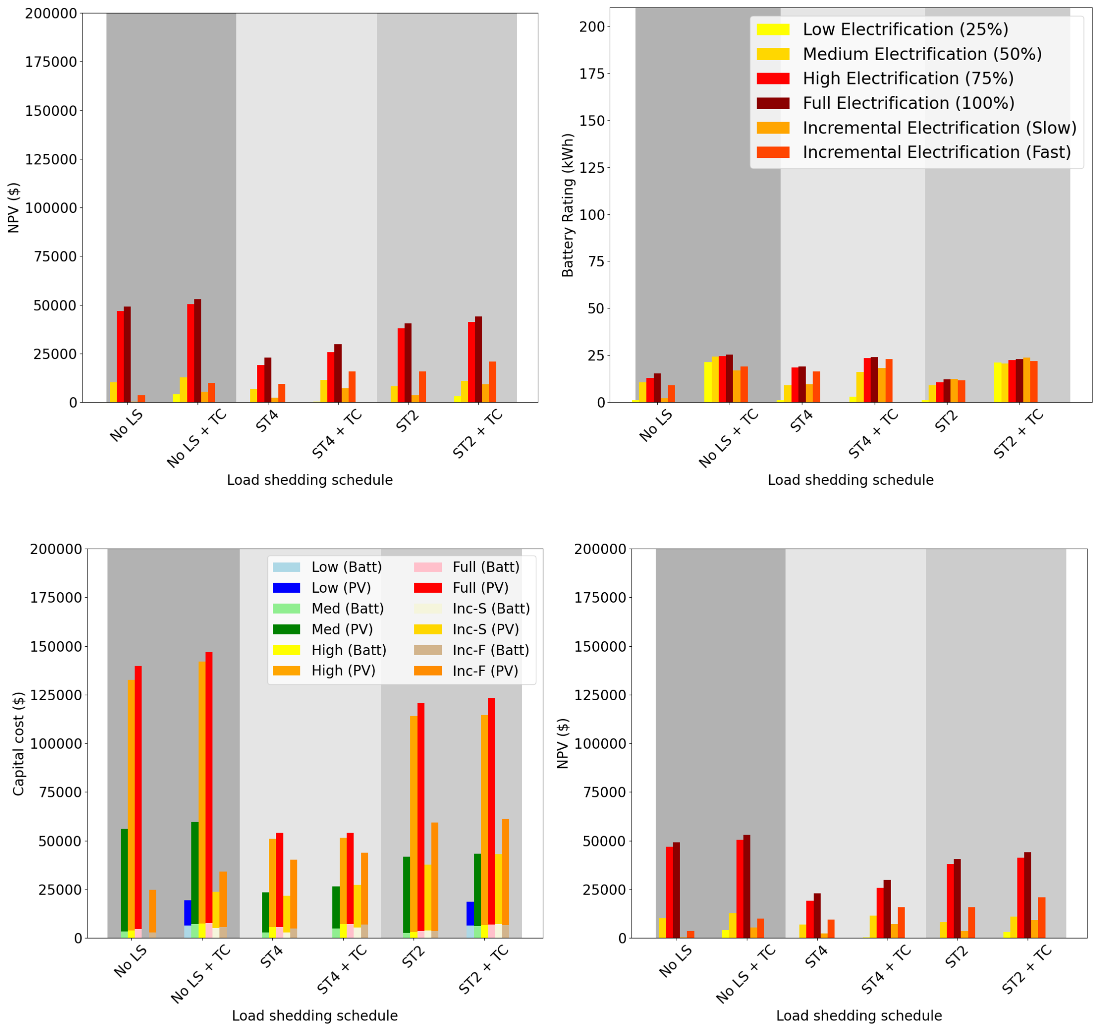

(c) Investment cost ($). Broken down by PV (darker shades) and ES (lighter shades).

(d) Net Present Value ($).

Figure 6.11: Same as Figure 6.8 but with a feed-in-tariff implemented in year 10 onwards.

increases in PV capacity, ES capacity, investment cost, and NPV between 50% and 75% EV penetration are 145%, 37%, 133%, and 258%, respectively. In contrast, the average increases of these factors when EV penetration increases from 75% to 100% are only 4%, 5%, 5%, and 10%.

These diminishing returns are due to a reduction in per-vehicle usage as EVs saturate the fleet. Table 6.10 shows that per-vehicle load increases up to 66% EV fleet penetration before tapering off. There are only two days (Saturday and Sunday) where 50 EVs cannot meet all trip demands, and only Saturday sees unmet demand with 57 EVs. As a result, the energy demand differences between the 66%, 75%, and 100% penetration scenarios are confined to these one or two days, leading to minimal overall system utilization differences.

This trend has broader implications for public transport fleets, especially those with peak demand on weekends. Understanding how EV fleet saturation impacts per-vehicle usage can aid strategic planning and resource allocation. By analyzing how trip distribution across days influences energy demand, transportation authorities can optimize fleet management strategies to meet peak demands efficiently, maximizing PV-ES investments while minimizing vehicle costs.

Although system NPV continues to increase slightly beyond the saturation point as total load rises, the benefits are negated when ICE vehicles are needed to cover operations during unplanned grid constraints. Additional simulations that include an extra hiring cost of $0.015/km for ICE vehicles in the 100% EV penetration scenarios, reveal that this cost entirely negates the benefits of the PV-ES-CS system in every scenario.

Key insight 1b: Sensitivity to incremental fleet electrification

Alongside the previous insights, it becomes clear that the returns with incremental fleet electrification are significantly lower than returns with an established level of fleet electrification. This is true even when the incremental strategy eventually achieves a higher level of fleet EV penetration by the end of the PV-ES investment's lifespan. Both the fast and slow incremental fleet electrification scenarios underperform compared to the 50% fleet electrification scenario. The discrepancy arises due to the time value of money—savings realized earlier in the system's lifetime hold much greater value. Therefore, the potential financial benefit of installing a PV-ES system is substantially higher when fleet electrification is already in place. This suggests that for fleet owners, investing in a PV-ES system prematurely could be financially risky, and delaying investment until a significant portion of the fleet is electrified may be a wiser strategy.

In summary, the diminishing marginal returns on system performance and the sensitivity to fleet size indicate that, under grid and capital constraints, fleet owners are likely to achieve better financial outcomes with partial fleet electrification rather than full electrification. Additionally, waiting to invest in a PV-ES system until a substantial portion of the fleet is electrified proves to be financially advantageous.

Key insight 2: Sensitivity to load shedding frequency and forecasting

The second key insight highlights the sensitivity of system economic performance to grid constraints. Load shedding impacts PV-ES system performance in two ways: (1) by necessitating charging schedule adjustments during planned outages, and (2) by providing resiliency during unplanned outages. The analysis shows that system NPV is higher in scenarios with less load shedding, indicating that the negative effects of (1) outweigh the positive effects of (2).

The negative effect of (1) is evident in Table 6.9, where the cost of electricity (COE) without the PV-ES system is lower in the ST4 scenario than in the No LS or ST2 scenarios, demonstrating how shifting charging schedules around planned load shedding events pushed charging into cheaper hours. As a result, the economic potential of the PV-ES system, which offers energy at zero marginal cost, is reduced. The sensitivity to the positive effects of (2) is explored in Section 6.4.2.1, where the ratio of planned to unplanned load shedding events is adjusted from 2:1 to 1:2. The results show minimal changes, with system size and NPV increasing by about 5% in load shedding scenarios. [1].

For regions experiencing frequent grid constraints, fleet owners can significantly benefit from the methodologies proposed here to assess and plan PV-ES investments. This emphasizes the practical value of these findings for guiding decisions toward more resilient and economically viable renewable energy solutions for fleet operations.

Key insight 3: Effects of intelligent energy storage management

The third key insight concerns the impact of timed slow charging (TC) on system feasibility and performance. TC has its greatest effect at lower levels of EV penetration, where its inclusion helps make the PV-ES system feasible. However, beyond 25% fleet penetration, the incremental benefits of TC on system size and economic performance become marginal.

The relatively consistent impact of TC across scenarios can be attributed to the presence of both morning and evening peak loads at all EV penetration levels (see Fig. 6.7). Because solar energy is not available during the evening peak (see Fig. 6.12), the

[1] In addition to the analysis in Section 6.4.2.1, to confirm that (2) yields positive economic effects, simulations were run with entirely unplanned load shedding schedules (unrealistic), and system sizes and economic performance were greater than in the No LS scenario, confirming that the value of resiliency offered by the exceeds the operational cost of running an EV.

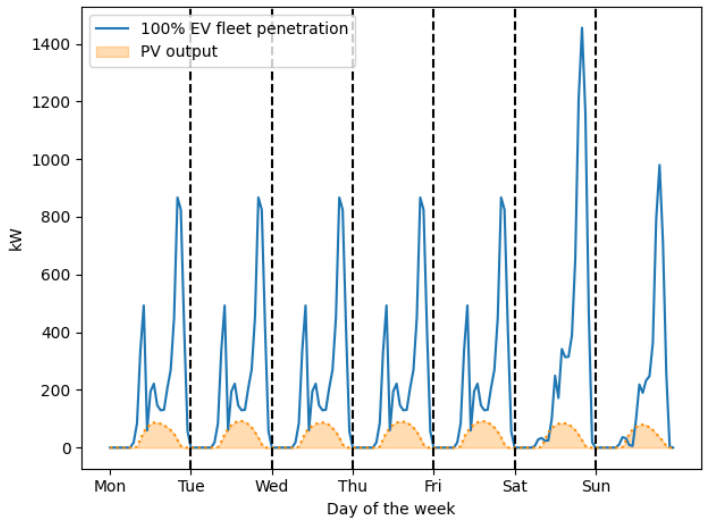

Figure 6.12: Weekly charging load profile for the 100% EV fleet (No LS) with example week of solar output overlaid to exemplify when solar resource is available compared to when energy is demanded.

battery is depleted by nightfall. It is then recharged overnight at the lower timed slow charging rate and helps offset the morning peak demand.

This benefit is sufficient to make a 25% electrified fleet feasible in the No LS and ST2 scenarios, but it only marginally increases system size and performance at higher EV penetration levels. For instance, the COE reduction in the ST4, 50% scenario is -1.05, while in the ST4 + TC, 50% scenario, it is -1.34. Figure 6.13 illustrates the impact of TC on COE in each EV penetration scenario. As TC's contribution remains relatively constant across EV penetration levels, its effect diminishes at higher penetration rates, where the overall benefits of the system are greater.

This insight is especially relevant for fleets with morning and evening peak demand, which is common among commercial fleets. For such fleets, the findings indicate that improved energy storage management, such as timed slow charging, will be most beneficial at lower levels of EV penetration. Enhancements like TC can make a PV-ES-CS system feasible when it might not otherwise be. Future research could explore whether more sophisticated battery dispatch strategies or daytime timed slow charging could yield better economic results for larger EV fleets.

Limitations and generalizability

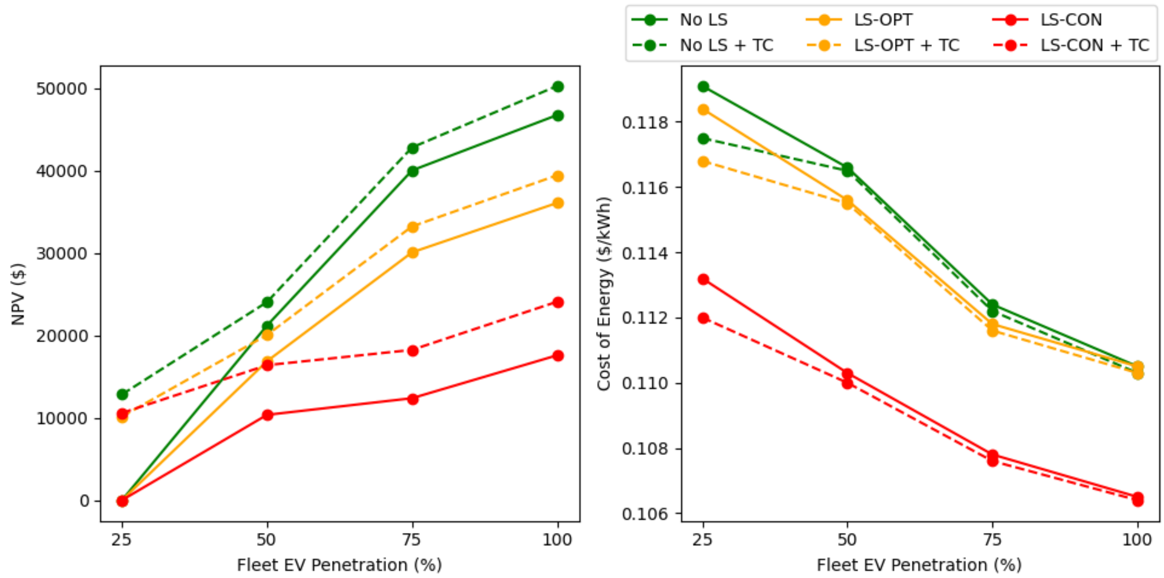

Figure 6.13: Impact of timed slow charging on NPV and COE in the 25%, 50%, 75%, and 100% cases for the No LS, ST4, and ST2 scenarios.

The geographic specificity of this case study means that the system sizing results, investment costs, and economic returns detailed in Section 6.4 are tailored to the paratransit fleet operating from Dobsonville taxi rank in Johannesburg, South Africa. While similar paratransit fleets within South Africa may expect comparable outcomes, these specific results do not extend beyond this context.

However, the three key insights derived from this study have broader applicability because their underlying drivers are relevant to electric fleets in various settings, particularly commercial and public transport fleets. Key insights 1 and 1b, namely *diminishing marginal returns* and *sensitivity to incremental fleet electrification*, stem from the dynamics of EV fleet saturation and its effect on per-vehicle usage. Key insight 2, *sensitivity to load shedding frequency and forecasting*, relates to the economic value of resiliency provided by the PV-ES system during power outages. Finally, key insight 3, *effects of intelligent energy storage management*, is influenced by the common presence of morning and evening peak loads in commercial fleets.

6.5 Summary

This chapter presents a methodology for techno-economic optimization and assessment of co-located photovoltaic-energy storage-charging station (PV-ES-CS) systems under a range of grid constraint scenarios with varying degrees of fleet EV penetration. In doing so, it answers the questions:

- *How can we optimize the size of PV and energy storage at paratransit charging stations to maximize economic gain, considering electricity supply constraints?* and
- *What are the effects of varying electricity demand (as fleet size) on the economic performance of the PV-ES-CS system?*

Comprehensive scenario simulation and analysis revealed three key insights that contribute to the understanding of PV-ES system dynamics and their implications for fleet owners and policymakers:

The first key insight highlights the diminishing marginal returns on system performance and the sensitivity to fleet size. The results show that under grid and capital constraints, fleet owners are more likely to achieve optimal financial results by partially electrifying their fleets and delaying PV-ES system investments until a substantial portion of the fleet has been electrified. This emphasizes the importance of strategic planning and resource allocation to maximize the economic benefits of PV-ES systems.

Building on this, the second insight underscores the significant impact of load shedding scenarios on the value of PV-ES systems. The economic feasibility and performance of these systems are highly sensitive to the frequency of grid constraint events. Fleet owners in regions with frequent grid disruptions can benefit greatly from the methodology proposed for assessing and planning PV-ES investments, guiding them toward more resilient and cost-effective renewable energy solutions.

The third key insight examines the influence of timed slow charging (TC) on system feasibility and performance. While TC integration helps improve the viability of PV-ES systems, its impact diminishes as EV penetration increases. This is particularly relevant for fleets with morning and evening peak loads, suggesting that optimizing the energy storage component, such as through timed slow charging, is most effective at lower levels of EV penetration.

Together, these insights contribute to the growing body of knowledge on integrating renewable energy solutions in commercial fleet operations. The methodology and findings presented here offer valuable guidance to fleet operators navigating the transition to electrified transportation, assessing the financial viability of fleet electrification, and implementing optimal strategies for PV-ES investments. Additionally, this chapter lays the groundwork for future research, encouraging further exploration of advanced battery dispatch strategies and optimizations that could improve economic outcomes at higher levels of EV penetration.

7
Conclusions

Contents

7.1 Concluding Discussion

The motivation of this thesis is to address the core research question:

Given the absence of electric paratransit vehicles in sub-Saharan Africa, is it possible to model the market perception, as well as the technical and financial viability, of electrifying the region's paratransit systems from the perspective of fleet owners?

The scope of this question demanded a comprehensive review of the literature on paratransit electrification to focus the research, out of which five main research lacunae were identified. Accordingly, the overarching question is broken down into the following sub-questions:

Sub-question 1a: ***What are the intentions of paratransit owners and drivers to switch to EVs when they become available?***

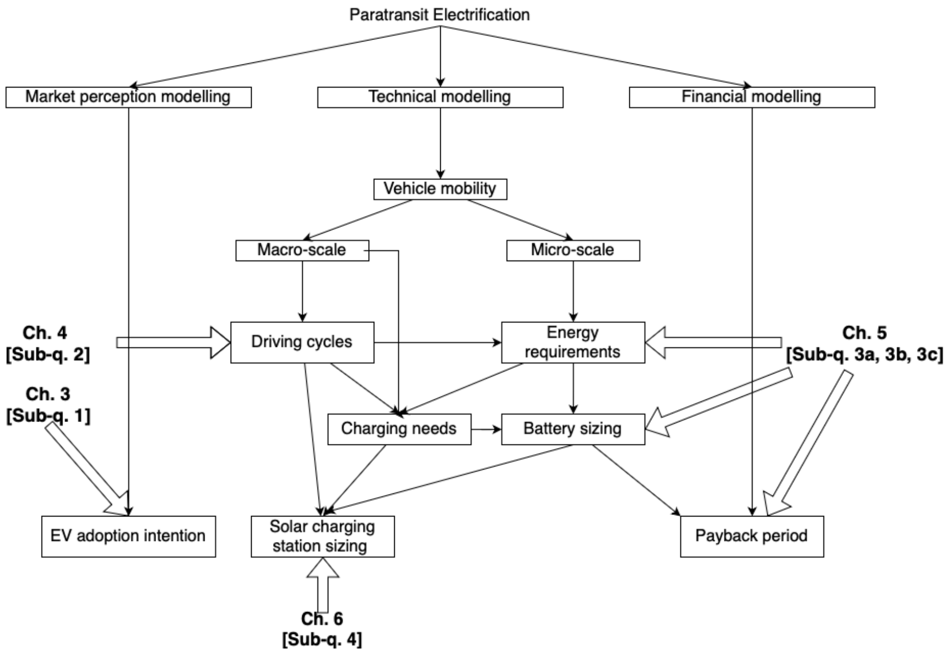

Figure 7.1: For clarity, this is a repeat of Figure 1.3. This figure is included again here to remind the reader how the key insights of this thesis fit into the pertinent body of literature.

Through a survey of 4,452 paratransit owners and drivers, Chapter 3 shows a user acceptance rate of 38%, indicating that this percentage of paratransit owners and drivers intend to adopt an electric vehicle when available. This result is significant as it indicates that the early majority segment of the technology adoption curve is ready to engage with EV technology. However, while this is already a promising number, the result indicates significant potential improvements from targeted interventions designed to raise this number. Widespread trust and acceptance of new technology in a market is key to accelerating its adoption, thus leading to question 1b, which is intended to help us design effective interventions:

Sub-question 1b: ***What are the factors that influence EV adoption intention for paratransit owners and drivers?***

The investigation of market perception and user acceptance is extended in Chapter 3 through the development of a structural equation model to investigate the factors influencing EV adoption intention for paratransit owners and drivers. The model is based on a novel integrated theory of consumer behavior developed specifically to understand EV adoption intention among paratransit owners and drivers. Existing models of consumer behavior were not appropriate for the problem of modelling EV adoption intention on their own. Therefore, behavioral constructs from three established theories of consumer behavior – Theory of Planned Behavior, Technology Acceptance Model, and Norm Acceptance Model – are integrated and extended with three additional constructs – Perception of ICE Costs, Perception of ICE Reliability, and Perception of Automobile Market Trends – leading to a novel integrated framework of consumer behavior. Eleven hypothesis are constructed within the integrated framework and related to EV adoption intention via a structural equation model. When applied to the survey data, the structural equation model indicates that targeted interventions aimed at improving EV adoption intention among paratransit owners and drivers would benefit most by focusing on improving perception of EV operating cost, environmental impact of the taxi industry, and safety and reliability. Safety and reliability are particular to the vehicle model used, but that as there are no extant vehicles on the road this cannot be tested at this stage. So this question is left for future work. To understand operational cost and environmental impact within the context of paratransit, and assess technical and financial viability, and assess technical and financial viability, accurate models to assess vehicle design are required. A key component which is unique to this problem are representative driving cycles, thus leading to the questions which govern Chapter 4:

Sub-question 2a: ***How can we construct representative driving cycles for paratransit?***

Representative driving cycles are key for modelling vehicle performance, which in turn influences vehicle design and hence technical and financial viability. The difficulty in constructing driving cycles for paratransit lies in capturing their unique driving style, characterized by many sharp acceleration and deceleration manoeuvres that only last a few seconds and are difficult to replicate through any sort of statistical construct. Consequently, in order to address sub-question 2a and construct a representative driving cycle for paratransit, Chapter 4 applies a novel time series shape-based clustering methodology to 1 Hz GPS tracking data gathered on combustion engine paratransit vehicles. This methodology is novel because it includes measured transients from the raw data in the final cycle, which are typically difficult to replicate in traditional methods.

The constructed paratransit driving cycle (PDC) is validated against the initial raw dataset to judge its representativeness and found to deviate by an average of only 3.65%, which meets the acceptable threshold of 5%, a commonly used threshold in driving cycle performance assessment.

Importantly, the PDC is only really useful if it represents paratransit driving better than existing standard international driving cycles, leading to sub-question 2b:

Sub-question 2b: ***How well do international driving cycles represent paratransit mobility?***

Modelling the technical and financial viability of paratransit has been assumed to be an inherently different problem than transportation systems in the developed world because of the subjective differences in operational patterns. Chapter 4 tests this assumption by using comparing the ability of several widely used international driving cycles – namely the WLTC, FTP-75, and CLTC – to represent paratransit driving against that of the PDC. The PDC is found to outperform these cycles by 20 – 30% in essential characteristic mobility parameters, which include average speed, average running speed, average acceleration, average deceleration, standard deviation of acceleration, % time accelerating, % time decelerating, and % time cruising. The superior performance of the PDC indicates that it is a substantially better fit for representing the real-world operating conditions faced by paratransit vehicles. Furthermore, the international driving cycles are shown to fail to capture the idiosyncratic, jerky movements of paratransit mobility.

Perhaps the most common applications of representative driving cycles is to establish the typical energy consumption of the subject vehicle. One of the most critical parameters in modeling technical and financial viability is vehicle energy consumption. Energy consumption will determine the required battery size for paratransit vehicles to satisfy their operational demands, and the battery is the most expensive component of an EV. It will also play a significant role in determining battery size (which plays significantly into acquisition cost), operational emissions intensity, and operational cost. This leads to the sub-questions which govern Chapter 5:

Sub-question 3a: ***What are the per-distance energy requirements of electric***

paratransit?

Chapter 5 presents a physics-based electro-kinetic vehicle model and applies it to the PDC developed in Chapter 4 to estimate per-distance energy consumption. It is found that paratransit vehicles consume energy at an average rate of 0.55 kWh/km. This PDC-based estimate is validated against the entire dataset of raw GPS data and found to satisfactorily meet the acceptable threshold of less than 10% different.

From a technical design standpoint, an energy consumption of 0.55 kWh/km is a very feasible level of energy consumption. Given the operational needs of paratransit, this estimate leads to likely battery sizes in the range of 70 – 80 kWh, which can easily fit in a minibus taxi sized vehicle.

Prior to the work of this thesis, estimates of paratransit energy consumption in the literature had been based on data captured at a frequency of $\frac{1}{60}$ Hz. This low resolution was hypothesized to be unsatisfactory for capturing the aggressive manoeuvres for which paratransit is notorious. However, $\frac{1}{60}$ Hz GPS data is significantly easier and cheaper to collect than 1 Hz data, and therefore of interest to modellers if it can be accurate enough to be useful, thus leading to sub-question 3b:

Sub-question 3b: ***Can per-minute GPS tracking data reliably determine the energy consumption of paratransit vehicles?***

To understand how useful minute-by-minute GPS tracking data is for estimating energy consumption, fast fourier transforms are employed to evaluate the percentage of energy signal it captures versus the 1 Hz data. The minutely data is found to underestimate energy consumption by an average of 31%, and have six times greater standard deviation. The latter feature explains the great variation in previous energy consumption estimates in the literature. Overall, while per-minute samples may offer some insights into minibus taxi operations in some cases, it is not suitable for detailed modelling of technical and financial viability based on energy use.

With this analysis of vehicle energy consumption, we can now examine the financial viability of electric vehicles compared to traditional gasoline-powered taxis. This brings us to the next sub-question:

Sub-question 3c: ***What is the payback period of an electric minibus taxi?***

Chapter 5 finds the payback period for an electric minibus taxi to be seven to eight years in most scenarios for fleet owners. This result includes the price of purchasing and installing charging equipment for the vehicle. In summary, the electric minibus taxi is likely to be a financially viable investment. However, given the absence of vehicles in-region, there are some significant uncertainties around key parameters, including EV purchase price, EV maintenance cost, and loan interest rate. The uncertainty in the techno-economic model of vehicle ownership cost is captured in a sensitivity analysis. EV purchase price is found to have the greatest influence on the payback period outcome – a 20% increase or decrease in EV purchase price could increase or decrease payback period by 40% – followed by EV maintenance cost and loan interest rate. Reducing uncertainty in the cost of ownership model is largely a question of reducing uncertainty in these parameters.

Following the investigation of energy consumption requirements, which inform both the technical and financial viability of paratransit vehicles, Chapter 6 shifts focus to infrastructure optimization, developing a methodology and tool for fleet owners to explore the potential value proposition of integrated solar PV-energy storage assets at charging stations. This leads to the final two sub-questions:

Sub-question 4a: ***How can we optimize the size of PV and energy storage at paratransit charging stations to maximize economic gain, considering electricity supply constraints?***

Sub-question 4b: ***What are the effects of varying electricity demand (as fleet size) on the economic performance of the PV-ES-CS system?***

To tackle these questions, Chapter 6 develops an open-source techno-economic capacity optimization model that maximizes the net present value of hybrid solar-storage systems at charging stations in the face of grid constraints. Unlike other standard models for sizing hybrid renewables systems, this model is customizable for specific use cases, free to use, and prices in the value of resilience that the renewables system provides during hours when the grid is constrained. The model is applied to a case study in Dobsonville, South Africa, where a plethora of electricity supply and demand scenarios are considered and three key insights about system performance under different technical and market conditions are gathered. First, there are diminishing marginal returns on system performance with increasing fleet size. Second, the value of the system is highly sensitive to the frequency and intensity of grid constraint events. Third, timed reduced-rate charging facilitates the feasibility of PV-ES systems at low levels of EV penetration, but has little effect at high levels of EV penetration. Overall, the chapters show that the integration of a PV-ES system at an EV charging station could be highly profitable and thus have a significant effect on the financial viability of fleet electrification for a paratransit fleet owner, but that detailed high-fidelity modeling is required to navigate the transition.

Conclusion and policy implications

In conclusion, this thesis demonstrates that, despite the absence of in-region electric vehicles, it is possible to model the market perception, technical feasibility, and financial viability of electrifying paratransit in sub-Saharan Africa from a fleet owner's perspective. However, the lack of in-region electric paratransit, the distinct operational characteristics of paratransit, and the constrained financial context of the developing world imply that existing tools and knowledge from developed countries are not directly transferable to these challenges. Consequently, there is a need to develop contextually appropriate, bespoke tools and knowledge that address critical gaps in the current literature on paratransit electrification. By addressing these gaps and devising new methodologies to model the market perception, technical feasibility, and financial viability of paratransit electrification from a fleet owner's perspective, this thesis provides a robust foundation for understanding and facilitating the transition towards more economically sustainable and environmentally friendly transportation options for paratransit in sub-Saharan Africa.

The findings of this thesis highlight several critical policy interventions that could facilitate the electrification of paratransit systems in sub-Saharan Africa. Given the significant role of fleet owners in adoption decisions, policies should prioritize financial mechanisms such as targeted subsidies, low-interest financing, or leasing models to mitigate the high upfront costs of electric vehicles (EVs). Additionally, public awareness campaigns and pilot programs demonstrating the economic and operational benefits of EVs could play a pivotal role in addressing concerns about reliability, cost savings, and environmental impact, thereby enhancing market perception and accelerating adoption.

Infrastructure development is another key policy area, particularly the strategic deployment of charging stations integrated with solar photovoltaic (PV) and energy storage systems. Policymakers should explore incentives and regulatory frameworks that support public-private partnerships in building resilient charging networks, especially in areas with unreliable grid access. Furthermore, given the sensitivity of electrification viability to operational factors such as energy consumption patterns, policies should encourage the standardization and collection of high-resolution mobility data to improve the accuracy of techno-economic models used in planning and decision-making.

Overall, a coordinated policy approach that addresses financial barriers, infrastructure constraints, and market perceptions – while leveraging context-specific modeling tools developed in this research – can significantly accelerate the transition toward a more sustainable and economically viable electric paratransit ecosystem in sub-Saharan Africa.

7.2 Contributions to knowledge

This thesis provides four main contributions to knowledge, each one corresponding to one of Chapters 3, 4, 5, and 6:

1. **An understanding of paratransit owner and driver perception of EVs.** Chapter 3 enriches our understanding of the perceptions held by paratransit owners and drivers towards EVs. The chapter provides insights into their current intentions towards adoption, their attitudes, the barriers they anticipate in transitioning to EVs, and the factors that could potentially incentivize a shift from conventional vehicles to electric alternatives.

2. **Development of a methodology to construct representative driving cycles for paratransit**. Chapter 4 introduces a novel methodology to construct

representative driving cycles for paratransit. The methodology provides a more accurate basis for assessing vehicle performance and energy requirements in real-world operating conditions, reflecting the unique driving behaviours associated with paratransit services.

3. **High-fidelity estimates of electric paratransit energy consumption**. Chapter 5 provides credible estimates of energy consumption for electric paratransit and uses them to calculates the vehicle payback period. These high-fidelity estimates are instrumental in conducting economic evaluations and enabling stakeholders to make informed decisions concerning the adoption of electric paratransit solutions.

4. **Framework for techno-economic optimization and assessment of solar PV-energy storage systems at EV charging stations considering grid constraints**. Chapter 6 establishes a techno-economic capacity optimization model for hybrid solar PV-energy storage systems that considers electricity supply constraints. The chapter analyzes how variations in energy demand impact the feasibility and performance of these systems, providing practical guidance for the design and implementation of effective and sustainable energy solutions in electric paratransit infrastructure.

7.2.1 Contributing publications

The list of published journal articles contributing to this thesis, and the chapters and sections which they inform, is presented in Table 7.1. The list of published data-in-brief articles, which thoroughly describe and provide access to research data used in the thesis, is presented in Table 7.2.

7.3 Future work

Incentivizing market actors

Despite comprehensive modeling efforts, the acceleration of paratransit electrification remains contingent upon the willingness of industry stakeholders to adopt EVs. Chapter 3 introduces a novel dataset and analytical method to examine the perceptions of paratran-

Table 7.1: Contributing journal articles.

Citation	Type	Section
Hull, C., Giliomee, J. H., Visser, M., & Booysen, M. J. (2024). Electric vehicle adoption intention among paratransit owners and drivers in South Africa. *Transport Policy*, 146, 137–149.	Journal Article	Chapter 3
Hull, C., Giliomee, J. H., Collett, K. A., McCulloch, M., & Booysen, M. J. (2024). Developing a representative driving cycle for paratransit that reflects measured data transients: Case study in Stellenbosch, South Africa. *Transportation Research Part A: Policy and Practice*, 181, 103987.	Journal Article	Chapters 4 & 5
Hull, C., Giliomee, J. H., Collett, K. A., McCulloch, M. D., & Booysen, M. J. (2023). High fidelity estimates of paratransit energy consumption from per-second GPS tracking data. *Transportation Research Part D: Transport and Environment*, 118, 103695.	Journal Article	Chapter 5
Giliomee, J. H., Hull, C., Collett, K. A., McCulloch, M., & Booysen, M. J. (2023). Simulating mobility to plan for electric minibus taxis in Sub-Saharan Africa's paratransit. *Transportation Research Part D: Transport and Environment*, 118, 103728.	Journal Article	Section 5.3
Hull, C., Wust, J., Booysen, M. J., & McCulloch, M. D. (2024). Techno-economic optimization and assessment of solar-battery charging station under grid constraints with varying levels of fleet EV penetration. *Applied Energy*, 374, 123990.	Journal Article	Chapter 6

Table 7.2: Contributing Data in Brief publications.

Citation	Type	Section
Hull, C., Giliomee, J. H., Visser, M., & Booysen, M. T. (2024). Survey data on the socio-economic characteristics and electric vehicle perceptions of paratransit owners and drivers in and around the Cape Town Metropole of South Africa. *Data in Brief*, 110126.	Data-in-brief	Chapter 3
Hull, C., Giliomee, J. H., Collett, K. A., McCulloch, M., & Booysen, M. J. (2024). High-fidelity tracking data gathered on minibus taxis in Stellenbosch, South Africa. *Data in Brief*, 55, 110732.	Data-in-brief	Chapters 4 & 5

sit owners and drivers towards EVs and the determinants influencing these attitudes. It is imperative that this exploration be considered a continuous process. Initially, the analytical framework should be extended to additional regions where paratransit is prevalent. Subsequently, based on the insights garnered from this thesis, targeted interventions such as educational initiatives and strategic marketing should be devised and implemented to positively influence paratransit stakeholders. Moreover, the impact of these interventions should be assessed through longitudinal studies to measure changes against the established baselines.

Expanding representative driving cycles

Chapter 4 establishes a robust methodology for the creation of driving cycles, tailored to the aggressive driving patterns typical of paratransit services. Nevertheless, there may be valid concerns regarding the external validity of these representative driving cycles. Additional GPS tracking data across diverse paratransit-active locales are required to develop driving cycles that accurately reflect the varied operational environments. These newly formed cycles should then be juxtaposed with the Paratransit Driving Cycles (PDC) established in this thesis, to scrutinize the similarities and differences in driving behaviors across different sub-Saharan regions.

Ground-truthing of energy consumption estimates

Chapter 5 employs a first-principles physics based model to estimate paratransit energy consumption from mobility data gathered on combustion-powered vehicles. This approach is necessitated by the absence of empirical data from electric minibus taxis in the region. However, the acquisition of real-world data from electric vehicles will be crucial for validating the energy consumption models and findings presented in this thesis. Upcoming collaborations with the MTN Mobile Intelligence Lab led by Prof. Booysen at Stellenbosch University are expected to bridge this gap.

Electricity grid impact

An initial assessment of the national grid impact of a fully electrified paratransit fleet in South Africa is outlined in Chapter 5. Further research should focus on a more detailed analysis for specific fleets within the region to elucidate their energy demands and peak power requirements in relation to the existing electrical infrastructure. This investigation will guide the sizing of fleets that current utilities can support and identify necessary infrastructure upgrades for future electrification efforts.

Payback period

The payback period analysis described in Chapter 5 exhibits high sensitivity to certain parameters. Given the profit-driven nature of fleet operators, the payback period for transitioning to electric minibus taxis is a critical factor influencing adoption. Future studies should continuously update model parameters as new data becomes available, and should also consider longitudinal surveys to monitor changes in public perception, alongside ongoing payback period modeling and marketing strategies.

Charging station siting

While taxi ranks present logical venues for the establishment of charging stations, the disparate range capabilities and refueling demands of electric vehicles (EVs) compared to internal combustion engine (ICE) vehicles may necessitate the installation of additional charging facilities to accommodate all passengers effectively. Charging stations are situated at the nexus of the mobility and electricity sectors, each characterized by distinct constraints. Rigorous computational modeling is essential to ascertain optimal locations for new sites. This ensures that the sites are strategically positioned to avoid excessive distance from electrical substations—thereby preventing escalated costs and diminished efficiency of the electrical infrastructure—as well as to minimize deviation from established mobility routes, thus reducing time and financial losses for drivers and passengers.

Appendices

A

Eskom load shedding definitions and data

Contents

A.1 Appendix 1: Information on Load Shedding

Table A1: Definition of Eskom load shedding stages. [297].

Stage	Energy shed (MW)	Definition
1	1,000	Up to 3 times over a four-day period for two hours at a time, or 3 times over an eight-day period for four hours at a time.
2	2,000	Up to 6 times over a four-day period for two hours at a time, or 6 times over an eight-day period for four hours at a time.
3	3,000	Up to 9 times over a four-day period for two hours at a time, or 9 times over an eight-day period for four hours at a time.
4	4,000	Up to 12 times over a four-day period for two hours at a time, or 12 times over an eight-day period for four hours at a time.
5	5,000	Up to 12 times over a four-day period: 9 times for 2 hours plus 3 times for 4 hours.
6	6,000	Up to 12 times over a four-day period: 6 times for 2 hours plus 6 times for 4 hours.
7	7,000	Up to 12 times over a four-day period: 3 times for 2 hours plus 9 times for 4 hours.
8	8,000	Up to 12 times over a four-day period for four hours at a time.

Table A2: Number of hours in each load shedding stage over the past several years [283].

	Number of load shedding hours					
Stage	2018	2019	2020	2021	2022	2023
1	62	67	119	72	190	611
2	79	290	597	915	1393	975
3	0	32	46	70	645	1786
4	0	141	83	96	1051	1926
5	0	0	0	0	298	536
6	0	0	0	0	199	1074
7	0	0	0	0	0	0
8	0	0	0	0	0	0
Total	141	534	845	1153	3776	6908

Table A3: Trends in load shedding over the past several years [283].

	Number of load shedding hours					
Month	2018	2019	2020	2021	2022	2023
Jan	0	0	104	121	0	744
Feb	0	66	342	66	114	661
Mar	0	210	127	207	147	667
Apr	0	0	0	8	197	690
May	0	0	0	54	215	737
Jun	14	0	0	185	185	377
Jul	0	0	89	5	5	606
Aug	0	0	60	0	0	690
Sep	0	0	92	0	0	583
Oct	0	56	0	262	521	263
Nov	29	7	0	220	642	630
Dec	97	195	31	24	698	260
Total	141	534	844	1153	3776	6908

References

[1] K. A. Collett et al. “Can electric vehicles be good for Sub-Saharan Africa?” In: *Energy Strategy Reviews* 38 (2021), p. 100722. ISSN: 2211-467X. DOI: 10.1016/j.esr.2021.100722 (cit. on pp. 1, 5, 6, 103).

[2] R. Behrens, D. McCormick, and D. Mfinanga. *Paratransit in African cities: Operations, regulation and reform*. Routledge, 2015, pp. 1–311. DOI: 10.4324/9781315849515 (cit. on pp. 1–6, 30).

[3] K. A. Collett and S. A. Hirmer. “Data needed to decarbonize paratransit in Sub-Saharan Africa”. In: *Nature Sustainability* 4.7 (2021), pp. 562–564. ISSN: 2398-9629. DOI: 10.1038/s41893-021-00721-7. URL: https://rdcu.be/ckzez (cit. on pp. 1, 4, 5, 19, 21, 22, 24, 63, 92, 102, 130).

[4] J Teter. *Tracking Transport 2020*. Tech. rep. IEA, 2020. URL: https://www.iea.org/reports/tracking-transport-2020 (cit. on p. 2).

[5] *Do you know all 17 SDGs?* 2022. URL: https://sdgs.un.org/goals. (accessed: 08.07.2022) (cit. on pp. 2, 4, 5).

[6] J. Motavalli. *Every Automaker’s EV Plans Through 2035 and Beyond*. 2021. URL: https://www.forbes.com/wheels/news/automaker-ev-plans/. (accessed: 27.04.2022) (cit. on pp. 2, 5).

[7] J. Conzade et al. *Power to move: Accelerating the electric transport transition in sub-Saharan Africa*. Feb. 2022. URL: https://www.mckinsey.com/industries/automotive-and-assembly/our-insights/power-to-move-accelerating-the-electric-transport-transition-in-sub-saharan-africa. (accessed: 30.08.2022) (cit. on pp. 2, 6).

[8] E. Odhiambo et al. “The potential for minibus electrification in three African cities: Cairo, Nairobi, and Cape Town”. In: *Volvo Research and Educational Foundations* (2021) (cit. on p. 2).

[9] R. Behrens, D. McCormick, and D. Mfinanga. *Paratransit in African cities: Operations, regulation and reform*. 1st ed. London: Routledge, 2015, pp. 1–311. ISBN: 9781315849515. DOI: 10.4324/9781315849515. URL: https://doi.org/10.4324/9781315849515 (cit. on p. 2).

[10] G. Jennings and R. Behrens. *The Case for Investing in Paratransit: Strategies for regulation and reform*. Jan. 2017 (cit. on pp. 3, 6).

[11] J. Evans, J. O'Brien, and B. Ch Ng. "Towards a geography of informal transport: Mobility, infrastructure and urban sustainability from the back of a motorbike". In: *Transactions of the Institute of British Geographers* 43.4 (2018), pp. 674–688. DOI: 10.1111/tran.12239. URL: https://rgs-ibg.onlinelibrary.wiley.com/doi/abs/10.1111/tran.12239 (cit. on p. 3).

[12] M. J. Booysen, S. J. Andersen, and A. S. Zeeman. "Informal public transport in Sub-Saharan Africa as a vessel for novel Intelligent Transport Systems". In: *16th International IEEE Conference on Intelligent Transportation Systems (ITSC 2013)*. Oct. 2013, pp. 767–772. DOI: 10.1109/ITSC.2013.6728324 (cit. on p. 3).

[13] L. Diaz Olvera, D. Plat, and P. Pochet. "Looking for the obvious: Motorcycle taxi services in Sub-Saharan African cities". In: *Journal of Transport Geography* (July 2019), p. 102476. ISSN: 0966-6923. DOI: 10.1016/J.JTRANGEO.2019.102476. URL: https://www.sciencedirect.com/science/article/pii/S0966692317306269 (cit. on p. 3).

[14] W. Mutiso and R. Behrens. "'Boda Boda' bicycle taxis and their role in urban transport systems: case studies of Kisumu and Nakura, Kenya". In: *30th Annual Southern African Transport Conference 11-14 July 2011 "Africa on the Move", CSIR International Convention Centre*. Pretoria, South Africa, 2011, pp. 430–444. URL: http://hdl.handle.net/2263/17308 (cit. on p. 3).

[15] D. McCormick, H. Schalekamp, and D. Mfinanga. "The nature of paratransit operations". In: *Paratransit in African Cities: Operations, Regulation and Reform*. Ed. by R. Behrens, D. McCormick, and D. Mfinanga. 1st ed. New York: Routledge, 2016. Chap. 3, pp. 59–78. ISBN: 9781315849515 (cit. on pp. 3, 5).

[16] KCCA. *Multimodal Urban Transport Master Plan for Greater Kampala Metropolitan Area*. Tech. rep. Kampala: Kampala Capital City Authority (KCCA), 2016 (cit. on p. 3).

[17] Toyota. *Hiace Ses'fikile Specfications*. URL: https://www.toyota.co.za/specs-compare/hiace-sesfikile?model=CY2. (accessed: 01.04.2022) (cit. on pp. 4, 96).

[18] R. Cervigni. *Assessing low-carbon development in Nigeria: an analysis of four sectors*. World Bank Publications, 2013 (cit. on p. 4).

[19] A. Mahaputra Kumar, V. Foster, and F. Barrett. *Stuck in traffic : urban transport in Africa*. Tech. rep. Washington, DC: World Bank, 2008. URL: http://siteresources.worldbank.org/EXTAFRSUBSAHTRA/Resources/Stuck-in-Traffic.pdf (cit. on pp. 4, 118).

[20] A. van Benthem. *Arthur van Benthem on new cars, old cars, and air pollution today*. 2021. URL: https://penntoday.upenn.edu/news/wharton-arthur-van-benthem-new-cars-old-cars-and-air-pollution-today#:~:text=While%5C%20federal%5C%20emissions%5C%20standards%5C%20have,of%5C%20total%5C%20pollution%5C%2C%5C%E2%5C%80%5C%9D%5C%20says%5C%20van. (accessed: 13.07.2022) (cit. on p. 4).

[21] A. Amegah and S. Agyei-Mensah. "Urban air pollution in Sub-Saharan Africa: Time for action". In: *Environmental Pollution* 220 (2017), pp. 738–743. ISSN: 0269-7491. DOI: https://doi.org/10.1016/j.envpol.2016.09.042. URL: https://www.sciencedirect.com/science/article/pii/S0269749116312933 (cit. on p. 5).

[22] S. Dalal et al. "Non-communicable diseases in sub-Saharan Africa: what we know now". In: *International Journal of Epidemiology* 40.4 (Mar. 2011), pp. 885–901. ISSN: 0300-5771. DOI: 10.1093/ije/dyr050. URL: https://doi.org/10.1093/ije/dyr050 (cit. on p. 5).

[23] W. H. Organization et al. *Indicator 3.9. 1: Mortality rate attributed to household and ambient air pollution (per 100 000 population).* 2018 (cit. on p. 5).

[24] U. Nations. "World population prospects 2019, custom data acquired via website". In: (2019) (cit. on p. 5).

[25] S. (2021). *Tracking Trends in a Time of Change: The Need for Radical Action Towards Sustainable Transport Decarbonisation - Transport and Climate Change Global Status Report – 2nd edition.* Tech. rep. Transport and Climate Change Global Status Report – 2nd edition. URL: www.tcc-gsr.com (cit. on p. 5).

[26] H. Ritche and M. Roser. *CO2 and greenhouse gas emissions. Our world in data in.* 2018 (cit. on p. 5).

[27] D. Ehebrecht, D. Heinrichs, and B. Lenz. "Motorcycle-taxis in sub-Saharan Africa: Current knowledge, implications for the debate on "informal" transport and research needs". In: *Journal of Transport Geography* 69 (2018), pp. 242–256. ISSN: 0966-6923. DOI: https://doi.org/10.1016/j.jtrangeo.2018.05.006. URL: http://www.sciencedirect.com/science/article/pii/S0966692317303344 (cit. on p. 5).

[28] S. C. et. al. *Power sector accelerating e-mobility.* 2022 (cit. on p. 5).

[29] C. J. Abraham et al. "Ray of hope for sub-Saharan Africa's paratransit: Solar charging of urban electric minibus taxis in South Africa". In: *Energy for Sustainable Development* 64 (2021), pp. 118–127. ISSN: 0973-0826. DOI: https://doi.org/10.1016/j.esd.2021.08.003 (cit. on pp. 5, 14, 17–19, 21, 22, 63, 102, 103, 107, 115, 117, 150).

[30] E. Bruun et al. "The state of public transport systems in three Sub-Saharan African cities". In: *Paratransit in African Cities: Operations, Regulation and Reform.* Ed. by R. Behrens, D. McCormick, and D. Mfinaga. 1st ed. New York: Routledge, 2016. Chap. 2. ISBN: 9781315849515. DOI: 10.4324/9781315849515 (cit. on p. 6).

[31] C. Corradi, E. Sica, and P. Morone. "What drives electric vehicle adoption? Insights from a systematic review on European transport actors and behaviours". In: *Energy Research & Social Science* 95 (2023), p. 102908 (cit. on pp. 6, 16, 30, 35).

[32] J. Plananska. "Touchpoints for electric mobility: Investigating the purchase process for promoting sales of electric vehicles in Switzerland". In: *Energy Research & Social Science* 69 (2020), p. 101745 (cit. on pp. 15, 29).

[33] N. DellaValle and A. Zubaryeva. "Can we hope for a collective shift in electric vehicle adoption? Testing salience and norm-based interventions in South Tyrol, Italy". In: *Energy Research & Social Science* 55 (2019), pp. 46–61 (cit. on pp. 15, 29, 36).

[34] M. Booysen et al. "e-Quantum leap on a data highway: Planning for electric minibus taxis in sub-Saharan Africa's paratransit system". In: (Nov. 2021). DOI: `10.31224/osf.io/2hkdv`. URL: `https://doi.org/10.31224%5C%2Fosf.io%5C%2F2hkdv` (cit. on pp. 16, 61, 128).

[35] N. Adnan et al. "What make consumer sign up to PHEVs? Predicting Malaysian consumer behavior in adoption of PHEVs". In: *Transportation Research Part A: Policy and Practice* 113 (2018), pp. 259–278 (cit. on pp. 16, 33, 36).

[36] S. Asadi et al. "Factors impacting consumers' intention toward adoption of electric vehicles in Malaysia". In: *Journal of Cleaner Production* 282 (2021), p. 124474 (cit. on pp. 16, 32, 33, 36).

[37] S. Priye, M. Manoj, and R. Ranjan. "Understanding the socioeconomic characteristics of paratransit drivers and their perceptions toward electric three-wheeled rickshaws in Delhi, India". In: *IATSS research* 45.3 (2021), pp. 357–370 (cit. on p. 16).

[38] R. Chakraborty and S. Chakravarty. "Factors affecting acceptance of electric two-wheelers in India: A discrete choice survey". In: *Transport Policy* 132 (2023), pp. 27–41 (cit. on pp. 16, 32, 35).

[39] P. Van Tuan et al. "Factors Influencing Purchasing Intention Toward Electric Vehicle in Vietnam". In: *Journal of Social Commerce* 2.2 (2022), pp. 82–99 (cit. on p. 16).

[40] P. Bryła, S. Chatterjee, and B. Ciabiada-Bryła. "Consumer Adoption of Electric Vehicles: A Systematic Literature Review". In: *Energies* 16.1 (2023), p. 205 (cit. on pp. 16, 32, 41, 42).

[41] L. Berzi, M. Delogu, and M. Pierini. "Development of driving cycles for electric vehicles in the context of the city of Florence". In: *Transportation Research Part D: Transport and Environment* 47 (2016), pp. 299–322. ISSN: 1361-9209. DOI: `https://doi.org/10.1016/j.trd.2016.05.010`. URL: `https://www.sciencedirect.com/science/article/pii/S1361920916303017` (cit. on pp. 17, 20, 63, 86).

[42] Q. Wang et al. "Characterization of vehicle driving patterns and development of driving cycles in Chinese cities". In: *Transportation Research Part D: Transport and Environment* 13.5 (2008), pp. 289–297 (cit. on pp. 17, 20, 63).

[43] F. Cignini et al. "Experimental Data Comparison of an Electric Minibus Equipped with Different Energy Storage Systems". In: *Batteries* 6.2 (2020). ISSN: 2313-0105. DOI: `10.3390/batteries6020026`. URL: `https://www.mdpi.com/2313-0105/6/2/26` (cit. on pp. 17, 103).

[44] A. Zeeman and M. J. Booysen. "Public transport sector driver behaviour: measuring recklessness using speed and acceleration". In: *Southern African Transport Conference* (2014). URL: `http://hdl.handle.net/2263/45581` (cit. on pp. 17–19, 21, 55, 63, 65, 87).

[45] I. Ndibatya, M. J. Booysen, and J. Quinn. "An adaptive transportation prediction model for the informal public transport sector in Africa". In: *17th International IEEE Conference on Intelligent Transportation Systems (ITSC)*. 2014, pp. 2572–2577 (cit. on pp. 17, 18).

[46] I. Ndibatya and M. J. Booysen. "Minibus taxis in Kampala's paratransit system: Operations, economics and efficiency". In: *Journal of Transport Geography* 88 (2020). ISSN: 09666923. DOI: `10.1016/j.jtrangeo.2020.102853` (cit. on pp. 17–19, 23, 63, 121, 124).

[47] I. Ndibatya, J. Coetzee, and M. J. Booysen. "Mapping the informal public transport network in Kampala with smartphones: Making sense of an organically evolved chaotic system in an emerging city in sub-Saharan Africa". In: *Proc. 35th Southern African Transport Conference, Pretoria.* July 2016, pp. 4–7 (cit. on pp. 17, 18).

[48] M. J. Booysen et al. "Walking on sunshine: Pairing electric vehicles with solar energy for sustainable informal public transport in Uganda". In: *Energy Research & Social Science* 85 (2022), p. 102403. ISSN: 2214-6296. DOI: `https://doi.org/10.1016/j.erss.2021.102403`. URL: `https://www.sciencedirect.com/science/article/pii/S2214629621004904` (cit. on pp. 17–19, 22, 63, 115).

[49] N. Arun et al. "Development of driving cycles for passenger cars and motorcycles in Chennai, India". In: *Sustainable Cities and Society* 32 (2017), pp. 508–512. DOI: `https://doi.org/10.1016/j.scs.2017.05.001` (cit. on pp. 17, 18, 20, 21, 62, 63, 67, 86).

[50] H. Tong et al. "Development of driving cycles for motorcycles and light-duty vehicles in Vietnam". In: *Atmospheric Environment* 45.29 (2011), pp. 5191–5199 (cit. on pp. 17, 20, 21, 62, 63, 67, 74).

[51] A. A. Badusha and B. Ghosh. *Driving cycle for buses in Delhi city*. Tech. rep. SAE Technical Paper, 1999 (cit. on pp. 17, 62, 72).

[52] S.-H. Ho, Y.-D. Wong, and V. W.-C. Chang. "Developing Singapore driving cycle for passenger cars to estimate fuel consumption and vehicular emissions". In: *Atmospheric Environment* 97 (2014), pp. 353–362 (cit. on pp. 17, 18, 20, 62, 63, 66, 67, 72, 84).

[53] S. K. Mayakuntla and A. Verma. "A novel methodology for construction of driving cycles for Indian cities". In: *Transportation Research Part D: Transport and Environment* 65 (2018), pp. 725–735 (cit. on pp. 17, 18, 20, 62).

[54] S. H. Kamble, T. V. Mathew, and G. K. Sharma. "Development of real-world driving cycle: Case study of Pune, India". In: *Transportation Research Part D: Transport and Environment* 14.2 (2009), pp. 132–140 (cit. on pp. 17, 62, 65, 67).

[55] J. S. C. Herrera, K. MacAskill, and S. Haigh. “Identifying interactions between policy, accountability and outcomes for adaptation of urban roads”. In: *Transportation Research Part D: Transport and Environment* 88 (2020), p. 102595 (cit. on p. 17).

[56] M. Kim and H. K. Kim. “Investigation of environmental benefits of traffic signal countdown timers”. In: *Transportation research part D: transport and environment* 85 (2020), p. 102464 (cit. on pp. 17, 20, 63).

[57] R. Jaikumar, S. S. Nagendra, and R. Sivanandan. “Modal analysis of real-time, real world vehicular exhaust emissions under heterogeneous traffic conditions”. In: *Transportation Research Part D: Transport and Environment* 54 (2017), pp. 397–409 (cit. on pp. 17, 63).

[58] H. Tong and W. Hung. “A framework for developing driving cycles with on-road driving data”. In: *Transport reviews* 30.5 (2010), pp. 589–615 (cit. on p. 17).

[59] I. Ndibatya and M. J. Booysen. “Characterizing the movement patterns of minibus taxis in Kampala’s paratransit system”. In: *Journal of Transport Geography* 92 (2021), p. 103001. ISSN: 0966-6923. DOI: https://doi.org/10.1016/j.jtrangeo.2021.103001. URL: https://www.sciencedirect.com/science/article/pii/S0966692321000545 (cit. on pp. 17, 18, 21, 63, 65).

[60] G. Jennings and R. Behrens. “The case for investing in paratransit: Strategies for regulation and reform”. In: (2017) (cit. on p. 18).

[61] K. Lucas et al. *Transport Social Exclusion in Five African Cities*. Tech. rep. Leeds,UK: International Network for Transport and Accessibility in Low Income Communities, 2019. URL: http://www.vref.se/download/18.45182a5f16a84e95fac8b2b5/1561370471910/Transport%20and%20Social%20Exclusion%20in%20five%20African%20Cities%20-%20June%202019.pdf (cit. on p. 18).

[62] T. Goodfellow. “‘Double Capture’ and De-Democratisation: Interest Group Politics and Uganda’s ‘Transport Mafia’”. In: *The Journal of Development Studies* 53.10 (2017), pp. 1568–1583. DOI: 10.1080/00220388.2016.1214722. URL: https://doi.org/10.1080/00220388.2016.1214722 (cit. on p. 18).

[63] J. Giliomee et al. “Simulating mobility to plan for electric minibus taxis in Sub-Saharan Africa’s paratransit”. In: *Transportation Research Part D: Transport and Environment* 118 (2023), p. 103728 (cit. on pp. 19, 102).

[64] J. Brady and M. O’Mahony. “Development of a driving cycle to evaluate the energy economy of electric vehicles in urban areas”. In: *Applied Energy* 177 (2016), pp. 165–178. ISSN: 0306-2619. DOI: https://doi.org/10.1016/j.apenergy.2016.05.094. URL: https://www.sciencedirect.com/science/article/pii/S0306261916306924 (cit. on pp. 20, 63).

[65] K. Kivekäs, J. VepsäläInen, and K. Tammi. “Stochastic Driving Cycle Synthesis for Analyzing the Energy Consumption of a Battery Electric Bus”. In: *IEEE Access* 6 (2018), pp. 55586–55598. DOI: 10.1109/ACCESS.2018.2871574 (cit. on pp. 20, 63).

[66] R. Smith et al. "Characterization of urban commuter driving profiles to optimize battery size in light-duty plug-in electric vehicles". In: *Transportation Research Part D: Transport and Environment* 16.3 (2011), pp. 218–224 (cit. on pp. 20, 63).

[67] J. D. Bishop, C. J. Axon, and M. D. McCulloch. "A robust, data-driven methodology for real-world driving cycle development". In: *Transportation Research Part D: Transport and Environment* 17.5 (2012), pp. 389–397 (cit. on pp. 20, 63, 66, 68).

[68] P. B. Wangsness, S. Proost, and K. L. Rødseth. "Vehicle choices and urban transport externalities. Are Norwegian policy makers getting it right?" In: *Transportation Research Part D: Transport and Environment* 86 (2020), p. 102384 (cit. on pp. 20, 63).

[69] M. Dixit and A. Sivakumar. "Capturing the impact of individual characteristics on transport accessibility and equity analysis". In: *Transportation Research Part D: Transport and Environment* 87 (2020), p. 102473 (cit. on pp. 20, 63).

[70] D. Gupta and A. Garg. "Sustainable development and carbon neutrality: Integrated assessment of transport transitions in India". In: *Transportation Research Part D: Transport and Environment* 85 (2020), p. 102474 (cit. on pp. 20, 63).

[71] H. Y. Tong and K. W. Ng. "Developing electric bus driving cycles with significant road gradient changes: A case study in Hong Kong". In: *Sustainable Cities and Society* 98 (2023), p. 104819 (cit. on pp. 20, 21, 63, 65, 72).

[72] C. Chandrashekar et al. "Development of E-rickshaw driving cycle (ERDC) based on micro-trip segments using random selection and K-means clustering techniques". In: *IATSS research* 45.4 (2021), pp. 551–560 (cit. on pp. 20, 63).

[73] G. G. Sundarkumar et al. "A time series clustering based approach for construction of real-world drive cycles". In: *Transportation Research Part D: Transport and Environment* 97 (2021), p. 102896. ISSN: 1361-9209. DOI: `https://doi.org/10.1016/j.trd.2021.102896`. URL: `https://www.sciencedirect.com/science/article/pii/S1361920921001966` (cit. on pp. 20, 63, 64, 66, 69, 83).

[74] A. Sheykhfard et al. "How do driving behavior and attitudes toward road safety vary between developed and developing countries? Evidence from Iran and the Netherlands". In: *Journal of safety research* 85 (2023), pp. 210–221 (cit. on p. 21).

[75] A. Gebisa et al. "Driving cycles for estimating vehicle emission levels and energy consumption". In: *Future transportation* 1.3 (2021), pp. 615–638 (cit. on p. 21).

[76] R. A. Rodríguez et al. "Influence of driving patterns on vehicle emissions: A case study for Latin American cities". In: *Transportation Research Part D: Transport and Environment* 43 (2016), pp. 192–206 (cit. on pp. 21, 63).

[77] U. Galgamuwa, L. Perera, and S. Bandara. "Developing a general methodology for driving cycle construction: comparison of various established driving cycles in the world to propose a Ggeneral approach". In: *Journal of Transportation Technologies* 05 (Jan. 2015), pp. 191–203. DOI: `10.4236/jtts.2015.54018` (cit. on pp. 21, 62, 63, 71, 75).

[78] L. F. Quirama et al. "Driving cycles that reproduce driving patterns, energy consumptions and tailpipe emissions". In: *Transportation Research Part D: Transport and Environment* 82 (2020), p. 102294 (cit. on pp. 21, 63).

[79] M. Booysen et al. "Walking on sunshine: Pairing electric vehicles with solar energy for sustainable informal public transport in Uganda". In: *Energy Research & Social Science* 85 (2022), p. 102403 (cit. on pp. 21, 130).

[80] C. Shannon. "Communication in the Presence of Noise". In: *Proceedings of the IRE* 37.1 (1949), pp. 10–21. DOI: `10.1109/jrproc.1949.232969`. URL: `https://doi.org/10.1109/jrproc.1949.232969` (cit. on pp. 22, 109).

[81] P. A. Lopez et al. "Microscopic Traffic Simulation using SUMO". In: *2019 IEEE Intelligent Transportation Systems Conference (ITSC)*. IEEE, Nov. 2018, pp. 2575–2582. URL: `https://elib.dlr.de/127994/` (cit. on p. 22).

[82] T. Kurczveil, P. Á. López, and E. Schnieder. "Implementation of an Energy Model and a Charging Infrastructure in SUMO". In: *Simulation of Urban Mobility*. Ed. by M. Behrisch, D. Krajzewicz, and M. Weber. Berlin, Heidelberg: Springer Berlin Heidelberg, 2014, pp. 33–43. ISBN: 978-3-662-45079-6 (cit. on p. 22).

[83] BusinessTech. *One year later: Load shedding in South Africa hits bleak milestone*. URL: `https://businesstech.co.za/news/energy/715776/one-year-later-load-shedding-in-south-africa-hits-bleak-milestone/#:~:text=Tuesday%2C%206%20September%202022%2C%20was,October%202022%20and%20March%202023.` (cit. on p. 24).

[84] K. Gubangxa. *Major Countries with Load Shedding*. URL: `https://elum-energy.com/blog/major-countries-with-load-shedding/` (cit. on p. 24).

[85] J. H. Giliomee and M. J. Booysen. "Grid-Sim: Simulating Electric Fleet Charging with Renewable Generation and Battery Storage". In: *World Electric Vehicle Journal* 14.10 (2023), p. 274 (cit. on pp. 24, 124, 130).

[86] S. Singh, P. Chauhan, and N. J. Singh. "Feasibility of grid-connected solar-wind hybrid system with electric vehicle charging station". In: *Journal of Modern Power Systems and Clean Energy* 9.2 (2020), pp. 295–306 (cit. on pp. 24, 131).

[87] B. Singh et al. "Implementation of solar PV-battery and diesel generator based electric vehicle charging station". In: *IEEE Transactions on Industry Applications* 56.4 (2020), pp. 4007–4016 (cit. on pp. 24, 25).

[88] A. Hassoune et al. "Power management strategies of electric vehicle charging station based grid tied PV-battery system". In: *International Journal of Renewable Energy Research* 8.2 (2018), pp. 851–860 (cit. on pp. 25, 131).

[89] M. H. Amrollahi and S. M. T. Bathaee. "Techno-economic optimization of hybrid photovoltaic/wind generation together with energy storage system in a stand-alone micro-grid subjected to demand response". In: *Applied Energy* 202 (2017), pp. 66–77 (cit. on pp. 25, 141, 154).

[90] Y. Amry et al. "Optimal sizing and energy management strategy for EV workplace charging station considering PV and flywheel energy storage system". In: *Journal of Energy Storage* 62 (2023), p. 106937 (cit. on pp. 25, 137, 141).

[91] M. P. Bakht et al. "Techno-economic modelling of hybrid energy system to overcome the load shedding problem: A case study of Pakistan". In: *PloS one* 17.4 (2022), e0266660 (cit. on p. 25).

[92] R. Zieba Falama et al. "A solution to the problem of electrical load shedding using hybrid PV/battery/grid-connected system: The case of households' energy supply of the Northern Part of Cameroon". In: *Energies* 14.10 (2021), p. 2836 (cit. on p. 26).

[93] Z. Ullah et al. "Optimal scheduling and techno-economic analysis of electric vehicles by implementing solar-based grid-tied charging station". In: *Energy* 267 (2023), p. 126560 (cit. on pp. 26, 131).

[94] J. D. Ampah et al. "Electric vehicles development in Sub-Saharan Africa: Performance assessment of standalone renewable energy systems for hydrogen refuelling and electricity charging stations (HRECS)". In: *Journal of Cleaner Production* 376 (2022), p. 134238 (cit. on pp. 26, 131).

[95] Z. Rezvani, J. Jansson, and J. Bodin. "Advances in consumer electric vehicle adoption research: A review and research agenda". In: *Transportation research part D: transport and environment* 34 (2015), pp. 122–136 (cit. on pp. 30, 37, 38).

[96] V. Singh, V. Singh, and S. Vaibhav. "A review and simple meta-analysis of factors influencing adoption of electric vehicles". In: *Transportation Research Part D: Transport and Environment* 86 (2020), p. 102436 (cit. on p. 32).

[97] J. Urry. "The 'system'of automobility". In: *Theory, culture & society* 21.4-5 (2004), pp. 25–39 (cit. on p. 32).

[98] J. Law and J. Hassard. "Actor network theory and after". In: *The Sociological Review* (1999) (cit. on p. 32).

[99] V. Venkatesh and C. Speier. "Computer technology training in the workplace: A longitudinal investigation of the effect of mood". In: *Organizational behavior and human decision processes* 79.1 (1999), pp. 1–28 (cit. on p. 32).

[100] I. Ajzen. "The theory of planned behavior". In: *Organizational behavior and human decision processes* 50.2 (1991), pp. 179–211 (cit. on pp. 32, 33, 35).

[101] S. H. Schwartz. "Normative influences on altruism". In: *Advances in experimental social psychology*. Vol. 10. Elsevier, 1977, pp. 221–279 (cit. on pp. 32, 36).

[102] F. D. Davis. "Perceived usefulness, perceived ease of use, and user acceptance of information technology". In: *MIS quarterly* (1989), pp. 319–340 (cit. on pp. 32, 35).

[103] V. Venkatesh et al. "User acceptance of information technology: Toward a unified view". In: *MIS quarterly* (2003), pp. 425–478 (cit. on p. 32).

[104] B. K. Sovacool. "Experts, theories, and electric mobility transitions: Toward an integrated conceptual framework for the adoption of electric vehicles". In: *Energy Research & Social Science* 27 (2017), pp. 78–95 (cit. on p. 32).

[105] B. Lane and S. Potter. “The adoption of cleaner vehicles in the UK: exploring the consumer attitude–action gap”. In: *Journal of cleaner production* 15.11-12 (2007), pp. 1085–1092 (cit. on pp. 32, 35).

[106] K. Degirmenci and M. H. Breitner. “Consumer purchase intentions for electric vehicles: Is green more important than price and range?” In: *Transportation Research Part D: Transport and Environment* 51 (2017), pp. 250–260 (cit. on pp. 32, 35, 36).

[107] S. Haustein and A. F. Jensen. “Factors of electric vehicle adoption: A comparison of conventional and electric car users based on an extended theory of planned behavior”. In: *International Journal of Sustainable Transportation* 12.7 (2018), pp. 484–496 (cit. on pp. 32, 35).

[108] L. Li, Z. Wang, and Q. Wang. “Do policy mix characteristics matter for electric vehicle adoption? A survey-based exploration”. In: *Transportation Research Part D: Transport and Environment* 87 (2020), p. 102488 (cit. on pp. 32, 34, 35).

[109] S. Hasan. “Assessment of electric vehicle repurchase intention: A survey-based study on the Norwegian EV market”. In: *Transportation Research Interdisciplinary Perspectives* 11 (2021), p. 100439 (cit. on pp. 32, 35, 38, 51).

[110] B. Wang et al. “Analysis of factors influencing residents’ habitual energy-saving behaviour based on NAM and TPB models: Egoism or altruism?” In: *Energy policy* 116 (2018), pp. 68–77 (cit. on pp. 32, 33).

[111] C. Zhao, M. Zhang, and W. Wang. “Exploring the influence of severe haze pollution on residents’ intention to purchase energy-saving appliances”. In: *Journal of Cleaner Production* 212 (2019), pp. 1536–1543 (cit. on p. 32).

[112] P. Goel et al. “Understanding transport users’ preferences for adopting electric vehicle based mobility for sustainable city: A moderated moderated-mediation model”. In: *Journal of Transport Geography* 106 (2023), p. 103520 (cit. on p. 32).

[113] S. Bamberg, M. Hunecke, and A. Blöbaum. “Social context, personal norms and the use of public transportation: Two field studies”. In: *Journal of environmental psychology* 27.3 (2007), pp. 190–203 (cit. on p. 33).

[114] X. Zhang, G. Geng, and P. Sun. “Determinants and implications of citizens’ environmental complaint in China: Integrating theory of planned behavior and norm activation model”. In: *Journal of Cleaner Production* 166 (2017), pp. 148–156 (cit. on p. 33).

[115] R. Rezaei et al. “Drivers of farmers’ intention to use integrated pest management: Integrating theory of planned behavior and norm activation model”. In: *Journal of Environmental Management* 236 (2019), pp. 328–339 (cit. on p. 33).

[116] S. Wang et al. “Policy implications for promoting the adoption of electric vehicles: do consumer’s knowledge, perceived risk and financial incentive policy matter?” In: *Transportation Research Part A: Policy and Practice* 117 (2018), pp. 58–69 (cit. on p. 33).

[117] D. Jaiswal et al. “Consumer adoption intention for electric vehicles: Insights and evidence from Indian sustainable transportation”. In: *Technological Forecasting and Social Change* 173 (2021), p. 121089 (cit. on pp. 33, 35).

[118] M. Zhou et al. “Characterizing the motivational mechanism behind taxi driver’s adoption of electric vehicles for living: Insights from China”. In: *Transportation Research Part A: Policy and Practice* 144 (2021), pp. 134–152 (cit. on p. 33).

[119] S. Taylor and P. Todd. “Assessing IT usage: The role of prior experience”. In: *MIS quarterly* (1995), pp. 561–570 (cit. on p. 33).

[120] A. Vafaei-Zadeh et al. “Modelling electric vehicle purchase intention among generation Y consumers in Malaysia”. In: *Research in Transportation Business & Management* 43 (2022), p. 100784 (cit. on p. 34).

[121] M. Moslehpour et al. “E-purchase intention of Taiwanese consumers: Sustainable mediation of perceived usefulness and perceived ease of use”. In: *Sustainability* 10.1 (2018), p. 234 (cit. on p. 35).

[122] N. Shanmugavel, C. Alagappan, and J. Balakrishnan. “Acceptance of electric vehicles: A dual-factor approach using social comparison theory and technology acceptance model”. In: *Research in Transportation Business & Management* 45 (2022), p. 100842 (cit. on p. 35).

[123] M. Barth, P. Jugert, and I. Fritsche. “Still underdetected–Social norms and collective efficacy predict the acceptance of electric vehicles in Germany”. In: *Transportation Research Part F: traffic psychology and behaviour* 37 (2016), pp. 64–77 (cit. on p. 35).

[124] G. L. Paradies et al. “Falling short in 2030: Simulating battery-electric vehicle adoption behaviour in the Netherlands”. In: *Energy Research & Social Science* 97 (2023), p. 102968 (cit. on pp. 35, 36).

[125] N. Berkeley, D. Jarvis, and A. Jones. “Analysing the take up of battery electric vehicles: An investigation of barriers amongst drivers in the UK”. In: *Transportation Research Part D: Transport and Environment* 63 (2018), pp. 466–481 (cit. on p. 35).

[126] G. Cecere, N. Corrocher, and M. Guerzoni. “Price or performance? A probabilistic choice analysis of the intention to buy electric vehicles in European countries”. In: *Energy policy* 118 (2018), pp. 19–32 (cit. on p. 35).

[127] X. He and W. Zhan. “How to activate moral norm to adopt electric vehicles in China? An empirical study based on extended norm activation theory”. In: *Journal of Cleaner Production* 172 (2018), pp. 3546–3556 (cit. on p. 36).

[128] I. K. Lai et al. “Factors influencing the behavioural intention towards full electric vehicles: An empirical study in Macau”. In: *Sustainability* 7.9 (2015), pp. 12564–12585 (cit. on p. 36).

[129] Y.-N. Sang and H. A. Bekhet. “Modelling electric vehicle usage intentions: an empirical study in Malaysia”. In: *Journal of Cleaner Production* 92 (2015), pp. 75–83 (cit. on p. 36).

[130] M. Ng, M. Law, and S. Zhang. “Predicting purchase intention of electric vehicles in Hong Kong”. In: *Australasian Marketing Journal (AMJ)* 26.3 (2018), pp. 272–280 (cit. on p. 36).

[131] J. Wu et al. “The role of environmental concern in the public acceptance of autonomous electric vehicles: A survey from China”. In: *Transportation Research Part F: Traffic Psychology and Behaviour* 60 (2019), pp. 37–46 (cit. on p. 36).

[132] J. Lee et al. “Public intentions to purchase electric vehicles in Pakistan”. In: *Sustainability* 13.10 (2021), p. 5523 (cit. on p. 36).

[133] B. Dutta and H.-G. Hwang. “Consumers purchase intentions of green electric vehicles: The influence of consumers technological and environmental considerations”. In: *Sustainability* 13.21 (2021), p. 12025 (cit. on pp. 36, 37).

[134] K. Alzahrani, A. Hall-Phillips, and A. Z. Zeng. “Applying the theory of reasoned action to understanding consumers’ intention to adopt hybrid electric vehicles in Saudi Arabia”. In: *Transportation* 46 (2019), pp. 199–215 (cit. on p. 36).

[135] D. L. Greene, S. Park, and C. Liu. “Public policy and the transition to electric drive vehicles in the US: The role of the zero emission vehicles mandates”. In: *Energy Strategy Reviews* 5 (2014), pp. 66–77 (cit. on p. 36).

[136] J. Li, J. Jiao, and Y. Tang. “Analysis of the impact of policies intervention on electric vehicles adoption considering information transmission—based on consumer network model”. In: *Energy Policy* 144 (2020), p. 111560 (cit. on p. 36).

[137] R. Inkpen and B. Baily. “Environmental beliefs and their role in environmental behaviours of undergraduate students”. In: *Journal of Environmental Studies and Sciences* 10 (2020), pp. 57–67 (cit. on p. 37).

[138] A. Amin et al. “A review of optimal charging strategy for electric vehicles under dynamic pricing schemes in the distribution charging network”. In: *Sustainability* 12.23 (2020), p. 10160 (cit. on p. 37).

[139] F. Bühler et al. “Is EV experience related to EV acceptance? Results from a German field study”. In: *Transportation Research Part F: traffic psychology and behaviour* 25 (2014), pp. 34–49 (cit. on p. 38).

[140] C. Hull et al. “Survey data on the socio-economic characteristics and electric vehicle perceptions of paratransit owners and drivers in and around the Cape Town Metropole of South Africa”. In: *Data in Brief* (2024), p. 110126 (cit. on p. 39).

[141] B. K. Sovacool, J. Axsen, and S. Sorrell. “Promoting novelty, rigor, and style in energy social science: Towards codes of practice for appropriate methods and research design”. In: *Energy Research & Social Science* 45 (2018), pp. 12–42 (cit. on p. 42).

[142] C.-f. Chen et al. “Assessing the socio-demographic, technical, economic and behavioral factors of Nordic electric vehicle adoption and the influence of vehicle-to-grid preferences”. In: *Renewable and Sustainable Energy Reviews* 121 (2020), p. 109692 (cit. on p. 42).

[143] V. Carr Jr. “Technology adoption and diffusion”. In: *The Learning Center for Interactive Technology* (1999) (cit. on pp. 44, 59).

[144] H. F. Kaiser. “A second generation little jiffy.” In: *Psychometrika* 35 (1970) (cit. on p. 48).

[145] L. Guttman. “Some necessary conditions for common-factor analysis”. In: *Psychometrika* 19.2 (1954), pp. 149–161 (cit. on p. 48).

[146] J. F. Hair Jr et al. *A primer on partial least squares structural equation modeling (PLS-SEM)*. Sage publications, 2021 (cit. on pp. 48–50).

[147] C. Fornell and D. F. Larcker. “Evaluating structural equation models with unobservable variables and measurement error”. In: *Journal of marketing research* 18.1 (1981), pp. 39–50 (cit. on pp. 49, 50).

[148] J. F. Hair Jr et al. *Advanced issues in partial least squares structural equation modeling*. saGe publications, 2017 (cit. on pp. 49, 50).

[149] R. B. Kline. *Principles and practice of structural equation modeling*. Guilford publications, 2015 (cit. on p. 50).

[150] A. A. Igolkina and G. Meshcheryakov. “semopy: A python package for structural equation modeling”. In: *Structural Equation Modeling: A Multidisciplinary Journal* 27.6 (2020), pp. 952–963 (cit. on p. 51).

[151] R. H. Hoyle. *Handbook of structural equation modeling*. Guilford press, 2012 (cit. on pp. 51, 52).

[152] J. C. Anderson and D. W. Gerbing. “Structural equation modeling in practice: A review and recommended two-step approach.” In: *Psychological bulletin* 103.3 (1988), p. 411 (cit. on p. 51).

[153] K. G. Jöreskog and D. Sörbom. “Recent developments in structural equation modeling”. In: *Journal of marketing research* 19.4 (1982), pp. 404–416 (cit. on p. 51).

[154] J. H. Steiger. “Structural model evaluation and modification: An interval estimation approach”. In: *Multivariate behavioral research* 25.2 (1990), pp. 173–180 (cit. on p. 51).

[155] R. Cudeck and S. J. Henly. “Model selection in covariance structures analysis and the" problem" of sample size: a clarification.” In: *Psychological bulletin* 109.3 (1991), p. 512 (cit. on p. 51).

[156] P. E. Meehl. “Theory-testing in psychology and physics: A methodological paradox”. In: *Philosophy of science* 34.2 (1967), pp. 103–115 (cit. on p. 51).

[157] P. M. Bentler and D. G. Bonett. “Significance tests and goodness of fit in the analysis of covariance structures.” In: *Psychological bulletin* 88.3 (1980), p. 588 (cit. on p. 51).

[158] I. Ndibatya and M. Booysen. “Characterizing the movement patterns of minibus taxis in Kampala’s paratransit system”. In: *Journal of Transport Geography* 92 (2021), p. 103001 (cit. on p. 55).

[159] A. M. Peters, E. van der Werff, and L. Steg. “Beyond purchasing: Electric vehicle adoption motivation and consistent sustainable energy behaviour in The Netherlands”. In: *Energy Research & Social Science* 39 (2018), pp. 234–247 (cit. on p. 58).

[160] J. Axsen, P. Plötz, and M. Wolinetz. “Crafting strong, integrated policy mixes for deep CO2 mitigation in road transport”. In: *Nature Climate Change* 10.9 (2020), pp. 809–818. DOI: `https://doi.org/10.1038/s41558-020-0877-y` (cit. on p. 63).

[161] C. J. Abraham, A. Rix, and M. J. Booysen. *Aligned simulation models for simulating Africa’s electric minibus taxis*. TechRxiv. Preprint. 2023. URL: `https://doi.org/10.36227/techrxiv.23376311.v1` (cit. on pp. 63, 98, 99, 123, 124, 149, 154).

[162] I. Ndibatya and M. Booysen. “Transforming Paratransit in Africa’s congested Cities: An ICT- enabled Integrated Demand Responsive Transport (iDRT) approach”. In: *IST-Africa 2020 Conference Proceedings*. Ed. by C. Miriam and C. Paul. Kampala, Uganda: IST-Africa Institute and IIMC, May 2020, pp. 1–10. URL: `www.IST-Africa.org/Conference2020` (cit. on p. 63).

[163] H. Sakoe. “Dynamic-programming approach to continuous speech recognition”. In: *1971 Proc. the International Congress of Acoustics, Budapest*. 1971 (cit. on p. 64).

[164] X. Zhao et al. “Development of a representative EV urban driving cycle based on a k-means and SVM hybrid clustering algorithm”. In: *Journal of Advanced Transportation* 2018 (2018), pp. 1–18 (cit. on p. 65).

[165] B. Degraeuwe and M. Weiss. “Does the New European Driving Cycle (NEDC) really fail to capture the NOX emissions of diesel cars in Europe?” In: *Environmental Pollution* 222 (2017), pp. 234–241 (cit. on p. 65).

[166] A. Vámosi, L. Czégé, and I. Kocsis. “Development of bus driving cycle for Debrecen on the basis of real-traffic data”. In: *Periodica Polytechnica Transportation Engineering* 50.2 (2022), pp. 184–190 (cit. on p. 65).

[167] A. Esteves-Booth et al. “The measurement of vehicular driving cycle within the city of Edinburgh”. In: *Transportation Research Part D: Transport and Environment* 6.3 (2001), pp. 209–220 (cit. on p. 66).

[168] J.-H. Tsai et al. “Development of a local real world driving cycle for motorcycles for emission factor measurements”. In: *Atmospheric Environment* 39.35 (2005), pp. 6631–6641 (cit. on p. 66).

[169] N. Nylund et al. *Evaluation of duty cycles for heavy-duty urban vehicles : final report of IEA AMF Annex 29*. July 2007 (cit. on p. 66).

[170] A. Michel. “The ARTEMIS European driving cycles for measuring car pollutant emissions”. In: *Science of The Total Environment* 334 (2004), pp. 73–84. DOI: `https://doi.org/10.1016/j.scitotenv.2004.04.070` (cit. on p. 66).

[171] M. Pfriem and F. Gauterin. “Development of real-world driving cycles for battery electric vehicles”. In: *World Electric Vehicle Journal* 8.1 (2016), pp. 14–24 (cit. on p. 66).

[172] Z. Chen et al. “Constructing the real-world driving cycle for electric vehicle applications: A comparative study”. In: *Transactions of the Institute of Measurement and Control* (2022), p. 01423312221094384 (cit. on pp. 66, 68, 86).

[173] H. Kaymaz, H. Korkmaz, and H. Erdal. “Development of a driving cycle for Istanbul bus rapid transit based on real-world data using stratified sampling method”. In: *Transportation Research Part D: Transport and Environment* 75 (2019), pp. 123–135 (cit. on p. 67).

[174] H. Tong. “Development of a driving cycle for a supercapacitor electric bus route in Hong Kong”. In: *Sustainable Cities and Society* 48 (2019), p. 101588 (cit. on p. 67).

[175] W. Saleh, R. Kumar, and A. Sharma. “Driving cycle for motorcycles in modern cities: case studies of Edinburgh and Delhi”. In: *World Journal of Science, Technology and Sustainable Development* (2010) (cit. on p. 67).

[176] Z. Dai, D. Niemeier, and D. Eisinger. “Driving cycles: a new cycle-building method that better represents real-world emissions”. In: *Department of Civil and Environmental Engineering, University of California, Davis* 570 (2008) (cit. on p. 67).

[177] K. Kivekäs, J. VepsäläInen, and K. Tammi. “Stochastic driving cycle synthesis for analyzing the energy consumption of a battery electric bus”. In: *IEEE Access* 6 (2018), pp. 55586–55598 (cit. on pp. 68, 72).

[178] P. Shen et al. “Development of a typical driving cycle for an intra-city hybrid electric bus with a fixed route”. In: *Transportation Research Part D: Transport and Environment* 59 (2018), pp. 346–360 (cit. on p. 68).

[179] H. Gong et al. “Generation of a driving cycle for battery electric vehicles: A case study of Beijing”. In: *Energy* 150 (2018), pp. 901–912 (cit. on p. 68).

[180] Y. Li et al. “The study on multi-scale prediction of future driving cycle based on Markov chain”. In: *Energy Procedia* 105 (2017), pp. 3219–3224 (cit. on p. 68).

[181] X. Liu et al. “Study on driving cycle synthesis method for city buses considering random passenger load”. In: *Journal of Advanced Transportation* 2020 (2020), pp. 1–21 (cit. on pp. 68, 72).

[182] Y. Peng, Y. Zhuang, and Y. Yang. “A driving cycle construction methodology combining k-means clustering and markov model for urban mixed roads”. In: *Proceedings of the Institution of Mechanical Engineers, Part D: Journal of Automobile Engineering* 234.2-3 (2020), pp. 714–724 (cit. on pp. 68, 83).

[183] Y. Yang et al. “Time dimension analysis: Comparison of Nanjing local driving cycles in 2009 and 2017”. In: *Sustainable Cities and Society* 53 (2020), p. 101949 (cit. on p. 68).

[184] A. Fotouhi and M. Montazeri-Gh. “Tehran driving cycle development using the k-means clustering method”. In: *Scientia Iranica* 20.2 (2013), pp. 286–293 (cit. on pp. 68, 83).

[185] M. A. Abas, S. Rajoo, and S. F. Z. Abidin. “Development of Malaysian urban drive cycle using vehicle and engine parameters”. In: *Transportation Research Part D: Transport and Environment* 63 (2018), pp. 388–403 (cit. on p. 68).

[186] Z. Jing et al. “Building Tianjin driving cycle based on linear discriminant analysis”. In: *Transportation Research Part D: Transport and Environment* 53 (2017), pp. 78–87 (cit. on p. 68).

[187] X. Li et al. “A data-driven two-level clustering model for driving pattern analysis of electric vehicles and a case study”. In: *Journal of Cleaner Production* 206 (2019), pp. 827–837 (cit. on p. 69).

[188] Z. Chen et al. “Optimization-based method to develop practical driving cycle for application in electric vehicle power management: A case study in Shenyang, China”. In: *Energy* 186 (2019), p. 115766 (cit. on p. 69).

[189] Y. Cui et al. “Optimization based method to develop representative driving cycle for real-world fuel consumption estimation”. In: *Energy* 235 (2021), p. 121434 (cit. on p. 69).

[190] Y. Cui et al. “A novel optimization-based method to develop representative driving cycle in various driving conditions”. In: *Energy* 247 (2022), p. 123455 (cit. on p. 69).

[191] P. Fränti and S. Sieranoja. “How much can k-means be improved by using better initialization and repeats?” In: *Pattern Recognition* 93 (2019), pp. 95–112 (cit. on p. 70).

[192] M. Vlachos, G. Kollios, and D. Gunopulos. “Discovering similar multidimensional trajectories”. In: *Proceedings 18th international conference on data engineering*. IEEE. 2002, pp. 673–684 (cit. on p. 70).

[193] L. Chen, M. T. Özsu, and V. Oria. “Robust and fast similarity search for moving object trajectories”. In: *Proceedings of the 2005 ACM SIGMOD international conference on Management of data*. 2005, pp. 491–502 (cit. on p. 70).

[194] M. Giraldo et al. “The effect of driving cycle duration on its representativeness”. In: *World Electric Vehicle Journal* 12.4 (2021), p. 212 (cit. on pp. 72, 83, 84).

[195] H. Tong, W. Hung, and C. S. Cheung. “Development of a driving cycle for Hong Kong”. In: *Atmospheric Environment* 33.15 (1999), pp. 2323–2335 (cit. on p. 72).

[196] W. T. Hung et al. “Development of a practical driving cycle construction methodology: A case study in Hong Kong”. In: *Transportation Research Part D: Transport and Environment* 12.2 (2007), pp. 115–128 (cit. on p. 72).

[197] H. Y. Tong and K. W. Ng. “A bottom-up clustering approach to identify bus driving patterns and to develop bus driving cycles for Hong Kong”. In: *Environmental Science and Pollution Research* 28 (2021), pp. 14343–14357 (cit. on p. 72).

[198] H. Y. Tong and K. Ng. “Development of bus driving cycles using a cost effective data collection approach”. In: *Sustainable Cities and Society* 69 (2021), p. 102854 (cit. on p. 72).

[199] K. Nesamani and K. Subramanian. “Development of a driving cycle for intra-city buses in Chennai, India”. In: *Atmospheric Environment* 45.31 (2011), pp. 5469–5476 (cit. on p. 72).

[200] J. Norbakyah et al. “myBas driving cycle for Kuala Terengganu city”. In: *Int. J. Electr. Comput. Eng* 11 (2021), p. 2054 (cit. on p. 72).

[201] Google. *Google Earth*. URL: https://earth.google.com/web/@-33.88614835,18.82391936,130.63246104a,12436.34033288d,35y,350.20430081h,0t,0r. (accessed: 11.04.2022) (cit. on p. 74).

[202] C. Hull et al. "High fidelity estimates of paratransit energy consumption from per-second GPS tracking data". In: *Transportation Research Part D: Transport and Environment* 118 (2023), p. 103695 (cit. on pp. 75, 97, 98).

[203] C. Hull, M. McCulloch, and K. A. Collett. "Developing a Representative Driving Cycle for Paratransit that Reflects Measured Data Transients: Case Study in Stellenbosch, South Africa". In: *SSRN Electronic Journal* (2023) (cit. on p. 75).

[204] C. Hull et al. "High-fidelity tracking data gathered on minibus taxis in Stellenbosch, South Africa". In: *Data in Brief* 55 (2024), p. 110732 (cit. on p. 76).

[205] USGS. *Earth Resources Observation and Science (EROS) Center*. URL: https://www.usgs.gov/centers/eros. (accessed: 06.05.2022) (cit. on p. 76).

[206] X. Zhao et al. "Development of a representative urban driving cycle construction methodology for electric vehicles: A case study in Xi'an". In: *Transportation Research Part D: Transport and Environment* 81 (2020), p. 102279 (cit. on pp. 77, 83, 86).

[207] V. Kumtepeli, R. Perriment, and D. A. Howey. "Fast dynamic time warping and clustering in C++". In: *arXiv preprint arXiv:2307.04904* (2023) (cit. on pp. 79–81).

[208] M. A. Pouresmaeili, I. Aghayan, and S. A. Taghizadeh. "Development of Mashhad driving cycle for passenger car to model vehicle exhaust emissions calibrated using on-board measurements". In: *Sustainable Cities and Society* 36 (2018), pp. 12–20 (cit. on p. 86).

[209] J. D. Bishop, C. J. Axon, and M. D. McCulloch. "A robust, data-driven methodology for real-world driving cycle development". In: *Transportation Research Part D: Transport and Environment* 17.5 (2012), pp. 389–397. ISSN: 1361-9209. DOI: https://doi.org/10.1016/j.trd.2012.03.003. URL: https://www.sciencedirect.com/science/article/pii/S136192091200034X (cit. on p. 86).

[210] DieselNet. *Worldwide Harmonized Light Vehicles Test Cycle (WLTC)*. 2019. URL: https://dieselnet.com/standards/cycles/wltp.php (cit. on p. 88).

[211] DieselNet. *FTP-75*. 2014. URL: https://dieselnet.com/standards/cycles/ftp75.php (cit. on p. 88).

[212] DieselNet. *China Light-Duty Vehicle Test Cycle (CLTC)*. 2020. URL: https://dieselnet.com/standards/cycles/cltc.php (cit. on p. 88).

[213] T. Kurczveil, P. Álvarez López, and E. Schnieder. "Implementation of an Energy Model and a Charging Infrastructure in SUMO". In: Springer Berlin Heidelberg, Nov. 2014, pp. 33–43. ISBN: 9783662450789. DOI: 10.1007/978-3-662-45079-6_3 (cit. on pp. 94, 102).

[214] X. Wu et al. "Electric vehicles' energy consumption measurement and estimation". In: *Transportation Research Part D: Transport and Environment* 34 (2015), pp. 52–67. ISSN: 1361-9209. DOI: `https://doi.org/10.1016/j.trd.2014.10.007`. URL: `https://www.sciencedirect.com/science/article/pii/S1361920914001485` (cit. on p. 94).

[215] C. Fiori, K. Ahn, and H. A. Rakha. "Power-based electric vehicle energy consumption model: Model development and validation". In: *Applied Energy* 168 (2016), pp. 257–268. DOI: `https://doi.org/10.1016/j.apenergy.2016.01.097`. URL: `https://www.sciencedirect.com/science/article/pii/S030626191630085X` (cit. on p. 94).

[216] R. Maia et al. "Electric vehicle simulator for energy consumption studies in electric mobility systems". In: *2011 IEEE Forum on Integrated and Sustainable Transportation Systems*. 2011, pp. 227–232. DOI: `10.1109/FISTS.2011.5973655` (cit. on p. 94).

[217] M. Ilyès, A. Fotouhi, and N. Ewin. "Electric vehicle energy consumption modelling and estimation - A case study". In: *International Journal of Energy Research* 45.1 (2020), pp. 501–520. DOI: `https://doi.org/10.1002/er.5700` (cit. on p. 94).

[218] I. Sagaama et al. "Evaluation of the Energy Consumption Model Performance for Electric Vehicles in SUMO". In: *2019 IEEE/ACM 23rd International Symposium on Distributed Simulation and Real Time Applications (DS-RT)*. 2019, pp. 1–8. DOI: `10.1109/DS-RT47707.2019.8958704` (cit. on p. 94).

[219] Engineering Toolbox. *Rolling Resistance*. URL: `https://www.engineeringtoolbox.com/rolling-friction-resistance-d_1303.html`. (accessed: 01.04.2022) (cit. on p. 96).

[220] J. Fridlund and O. Wilen. *Parameter Guidelines for Electric Vehicle Route Planning*. 2020 (cit. on p. 96).

[221] Higer. *Higer H5C EV specifications*. URL: `https://en.higer.com/NewEnergy/info.aspx?itemid=6851`. (accessed: 22.04.2022) (cit. on pp. 96, 103, 115).

[222] Toyota. *Toyota Hi'ace Specifications*. URL: `https://toyota.dreamhosters.com/pages/hiace-tmc/spec.php`. (accessed: 01.04.2022) (cit. on p. 96).

[223] S. Lacock, A. A. du Plessis, and M. J. Booysen. "Electric Vehicle Drivetrain Efficiency and the Multi-Speed Transmission Question". In: *World Electric Vehicle Journal* 14.12 (2023), p. 342 (cit. on p. 96).

[224] S. Lacock et al. "Simulating Electric Vehicle Powertrain Efficiency with Driving Cycle Data and Electric Motor Efficiency Maps". In: *2024 32nd Southern African Universities Power Engineering Conference (SAUPEC)*. 2024, pp. 1–6. DOI: `10.1109/SAUPEC60914.2024.10445072` (cit. on p. 96).

[225] Tesla. *The Magic of Tesla Roadster Regenerative Braking*. URL: `https://www.tesla.com/blog/magic-tesla-roadster-regenerative-braking`. (accessed: 01.04.2022) (cit. on p. 96).

[226] *Koch, L and Buse, D.S. and Wegener, M. and Schoenberg, S. and Badalian, K. and Dressler, F. and Andert, J.* 2021. URL: https://github.com/mechatronics-RWTH/sumo/tree/ev_powertrain_device (cit. on pp. 98, 99).

[227] Y. Al-Wreikat, C. Serrano, and J. R. Sodré. "Driving behaviour and trip condition effects on the energy consumption of an electric vehicle under real-world driving". In: *Applied Energy* 297 (2021), p. 117096. ISSN: 0306-2619. DOI: 10.1016/j.apenergy.2021.117096. URL: https://www.sciencedirect.com/science/article/pii/S0306261921005444 (cit. on pp. 101, 115).

[228] M. V. Faria et al. "Driving for decarbonization: Assessing the energy, environmental, and economic benefits of less aggressive driving in Lisbon, Portugal". In: *Energy Research & Social Science* 47 (2019), pp. 113–127. DOI: https://doi.org/10.1016/j.erss.2018.09.006 (cit. on p. 101).

[229] Y. L. Murphey, R. Milton, and L. Kiliaris. "Driver's style classification using jerk analysis". In: *2009 IEEE Workshop on Computational Intelligence in Vehicles and Vehicular Systems*. 2009, pp. 23–28. DOI: 10.1109/CIVVS.2009.4938719 (cit. on p. 101).

[230] N. E. Eno Akpa, M. Booysen, and M. Sinclair. "Fuel savings as an incentive for speed compliance in the informal public transport industry in South Africa". In: *2019 IEEE Intelligent Transportation Systems Conference (ITSC)*. 2019, pp. 492–496. DOI: 10.1109/ITSC.2019.8917491 (cit. on p. 101).

[231] C. Hull et al. "Using High Resolution GPS Data to Plan the Electrification of Paratransit: A Case Study in South Africa". In: *Submitted for review, Energy (Elsevier)* (2022) (cit. on p. 102).

[232] T. Dongfeng. *Dongfeng Electric 15 Seater Mini Van (RHD)*. URL: https://tara-dongfeng.co.uk/listings/dongfeng-ev-15seat-2-2/. (accessed: 22.04.2022) (cit. on p. 103).

[233] Ruivii. *Toano 15 Seats Electric Minibus*. URL: https://www.ruviivehicle.com/products/minibus/toano-15-seats-electric-minibus/. (accessed: 22.04.2022) (cit. on p. 103).

[234] *GoMetro DORLJOTA Fuel Survey*. Oct. 2021 (cit. on p. 116).

[235] *Emissions Factors for Greenhouse Gas Inventories*. Apr. 2014. URL: https://www.epa.gov/sites/default/files/2015-%2007/documents/emission-factors_2014.pdf (cit. on p. 116).

[236] Eskom. *Eskom Data Portal, Data Request Form*. 2022. URL: https://www.eskom.co.za/dataportal/ (cit. on p. 116).

[237] *IGES List of Grid Emission Factors*. 2022. URL: https://www.iges.or.jp/en/pub/list-grid-emission-factor/en (cit. on p. 116).

[238] K. M. Buresh, M. D. Apperley, and M. J. Booysen. "Three shades of green: Perspectives on at-work charging of electric vehicles using photovoltaic carports". In: *Energy for Sustainable Development* 57 (2020), pp. 132–140. ISSN: 0973-0826. DOI: 10.1016/j.esd.2020.05.007. URL: https://www.sciencedirect.com/science/article/pii/S0973082620302441 (cit. on p. 116).

[239] Transaction Capital. *Transaction Capital Results Presentation.* 2021. URL: https://thevault.exchange/?get_group_doc=305/1637037219-TCFY21AnalystBooklet.pdf. (accessed: 15.06.2022) (cit. on pp. 116, 118, 119).

[240] IEA. [Online; accessed 20 Jan. 2023]. 2021. URL: https://www.iea.org/countries/south-africa/electricity (cit. on p. 117).

[241] R. Govender and D. Allopi. "Towards a safer minibus taxi industry in South Africa". In: *SATC 2006* (2006) (cit. on p. 118).

[242] TransactionCapital. *Half-Year Funder Prospectus 2022.* 2022. URL: https://www.transactioncapital.co.za/wp-content/uploads/Transaction-Capital-HY22-SA-Taxi-Funding-Prospectus.pdf. accessed: 21.01.2024 (cit. on p. 119).

[243] T. S. A. R. Bank. *Selected Historical Rates.* 2023. URL: https://www.resbank.co.za/en/home/what-we-do/statistics/key-statistics/selected-historical-rates (cit. on pp. 119, 124, 154).

[244] *What Does It Cost To Install An Electric Vehicle Charger At Your Home In South Africa.* 2024. URL: https://evcompany.co.za/what-does-it-cost-to-install-an-electric-vehicle-charger-at-your-home-in-south-africa/ (cit. on pp. 119, 124).

[245] Automobile Association of South Africa. *Fuel Pricing.* 2023. URL: https://aa.co.za/fuel-pricing/ (cit. on pp. 120, 124, 154).

[246] City of Johannesburg. *Electricity Tariff - City of Johannesburg.* 2023. URL: https://www.joburg.org.za/Documents/2023%20Notices/2023-24%20FINAL%20TARIFFS.pdf (cit. on pp. 120, 124, 146).

[247] City of Cape Town. *ENERGY - ELECTRICITY GENERATION AND DISTRIBUTION (CONSUMPTION AND GENERATION TARIFFS).* 2023. URL: https://resource.capetown.gov.za/documentcentre/Documents/Financial%20documents/Electricity%20Consumptive%20Tariffs.pdf (cit. on pp. 120, 146).

[248] J. Wust, J. Bekker, and M. Booysen. "Scheduling tool for electric paratransit". In: *submission in progress* (2024) (cit. on pp. 120, 136, 149).

[249] E. Baker, H. Chon, and J. Keisler. "Battery technology for electric and hybrid vehicles: Expert views about prospects for advancement". In: *Technological Forecasting and Social Change* 77.7 (2010), pp. 1139–1146 (cit. on p. 121).

[250] P. Weldon, P. Morrissey, and M. O'Mahony. "Long-term cost of ownership comparative analysis between electric vehicles and internal combustion engine vehicles". In: *Sustainable Cities and Society* 39 (2018), pp. 578–591 (cit. on pp. 121, 124).

[251] L. Mauler et al. "Battery cost forecasting: a review of methods and results with an outlook to 2050". In: *Energy & Environmental Science* 14.9 (2021), pp. 4712–4739 (cit. on pp. 121, 124).

[252] G. Berckmans et al. "Cost projection of state of the art lithium-ion batteries for electric vehicles up to 2030". In: *Energies* 10.9 (2017), p. 1314 (cit. on pp. 121, 124).

[253] O. Catsaros. *Lithium-Ion Battery Pack Prices Hit Record Low of* 139/kWh. Nov. 2023. URL: https://about.bnef.com/blog/lithium-ion-battery-pack-prices-hit-record-low-of-139-kwh/#:~:text=Given%20this%2C%20BNEF%20expects%20average,and%20%2480%2FkWh%20in%202030. (cit. on pp. 121, 124).

[254] N. Campagnol, A. Pfeiffer, and C. Tryggestad. "Capturing the battery value-chain opportunity". In: *McKinsey & Company* (2022) (cit. on pp. 121, 124).

[255] Z. Liu et al. "Comparing total cost of ownership of battery electric vehicles and internal combustion engine vehicles". In: *Energy Policy* 158 (2021), p. 112564 (cit. on pp. 121, 124).

[256] I. Veza et al. "Electric vehicle (EV) and driving towards sustainability: Comparison between EV, HEV, PHEV, and ICE vehicles to achieve net zero emissions by 2050 from EV". In: *Alexandria Engineering Journal* 82 (2023), pp. 459–467 (cit. on pp. 121, 124).

[257] Transaction Capital. *Half-Year Funder Prospectus 2022*. 2022. URL: https://www.transactioncapital.co.za/wp-content/uploads/Transaction-Capital-HY22_SA-Taxi_FP_FINAL.pdf (cit. on p. 124).

[258] Macrotrends LLC. *South Africa Inflation Rate 1960 - 2023*. 2023. URL: https://www.macrotrends.net/countries/ZAF/south-africa/inflation-rate-cpi (cit. on pp. 124, 154).

[259] B. M. Al-Alawi and T. H. Bradley. "Total cost of ownership, payback, and consumer preference modeling of plug-in hybrid electric vehicles". In: *Applied Energy* 103 (2013), pp. 488–506 (cit. on pp. 124, 125).

[260] Toyota. *2024 Toyota Quantum 2.5 D-4D Sesfikile 16-seat*. 2024. URL: https://www.cars.co.za/for-sale/new/2024-Toyota-Quantum-2.5-D-4D-Sesfikile-16-seat-Gauteng-Centurion/9087744/ (cit. on p. 124).

[261] K. Y. Yap, H. H. Chin, and J. J. Klemeš. "Solar Energy-Powered Battery Electric Vehicle charging stations: Current development and future prospect review". In: *Renewable and Sustainable Energy Reviews* 169 (2022), p. 112862 (cit. on p. 129).

[262] C. Abraham et al. "Decarbonising South Africa's paratransit with hydrogen: a simulated case study". In: Southern African Transport Conference. 2023 (cit. on p. 130).

[263] R. P. Narasipuram and S. Mopidevi. "A technological overview & design considerations for developing electric vehicle charging stations". In: *Journal of Energy Storage* 43 (2021), p. 103225 (cit. on p. 131).

[264] J. Lian et al. "A review on recent sizing methodologies of hybrid renewable energy systems". In: *Energy Conversion and Management* 199 (2019), p. 112027 (cit. on pp. 131, 132).

[265] M. Thirunavukkarasu, Y. Sawle, and H. Lala. "A comprehensive review on optimization of hybrid renewable energy systems using various optimization techniques". In: *Renewable and Sustainable Energy Reviews* 176 (2023), p. 113192 (cit. on p. 132).

[266] I. Staffell and S. Pfenninger. "Using bias-corrected reanalysis to simulate current and future wind power output". In: *Energy* 114 (2016), pp. 1224–1239 (cit. on p. 133).

[267] M. M. Rienecker et al. "MERRA: NASA's modern-era retrospective analysis for research and applications". In: *Journal of climate* 24.14 (2011), pp. 3624–3648 (cit. on p. 133).

[268] R. Müller et al. "Digging the METEOSAT treasure—3 decades of solar surface radiation". In: *Remote Sensing* 7.6 (2015), pp. 8067–8101 (cit. on p. 133).

[269] R. Müller et al. "Surface solar radiation data set-Heliosat (SARAH)-". In: *Climate Monitoring Satellite Application Facility: Darmstadt, Germany* (2015) (cit. on p. 133).

[270] S. Pfenninger and I. Staffell. "Long-term patterns of European PV output using 30 years of validated hourly reanalysis and satellite data". In: *Energy* 114 (2016), pp. 1251–1265 (cit. on pp. 133, 145).

[271] L. Al-Ghussain et al. "Techno-economic assessment of photovoltaic-based charging stations for electric vehicles in developing countries". In: *Energy Sources, Part A: Recovery, Utilization, and Environmental Effects* 45.1 (2023), pp. 523–541 (cit. on pp. 137, 154).

[272] H. K. Ren, M. McCulloch, and D. Wallom. "Optimal sizing of solar photovoltaic and lithium battery storage to reduce grid electricity reliance in buildings". In: *arXiv preprint arXiv:2306.03581* (2023) (cit. on p. 137).

[273] L. Al-Ghussain, A. M. Abubaker, and A. D. Ahmad. "Superposition of renewable-energy supply from multiple sites maximizes demand-matching: Towards 100% renewable grids in 2050". In: *Applied Energy* 284 (2021), p. 116402 (cit. on p. 137).

[274] M. F. Ishraque et al. "Optimization of load dispatch strategies for an islanded microgrid connected with renewable energy sources". In: *Applied Energy* 292 (2021), p. 116879 (cit. on p. 137).

[275] M. F. Ishraque et al. "Techno-economic and power system optimization of a renewable rich islanded microgrid considering different dispatch strategies". In: *IEEE Access* 9 (2021), pp. 77325–77340 (cit. on p. 137).

[276] Y. Yang et al. "Modelling and optimal energy management for battery energy storage systems in renewable energy systems: A review". In: *Renewable and Sustainable Energy Reviews* 167 (2022), p. 112671 (cit. on p. 137).

[277] T. Yang et al. "Dynamic energy dispatch strategy for integrated energy system based on improved deep reinforcement learning". In: *Energy* 235 (2021), p. 121377 (cit. on p. 137).

[278] D. C. Jordan et al. "Compendium of photovoltaic degradation rates". In: *Progress in Photovoltaics: Research and Applications* 24.7 (2016), pp. 978–989 (cit. on pp. 139, 154).

[279] S. Funke et al. "Fast charging stations with stationary batteries: A techno-economic comparison of fast charging along highways and in cities". In: *Transportation Research Procedia* 48 (2020), pp. 3832–3849 (cit. on pp. 140, 154).

[280] Google. *[Pin of township Dobsonville within Johannesburg, South Africa]*. URL: https://www.google.com/maps. (accessed: 20.08.2023) (cit. on p. 145).

[281] Google. *[Satellite image of Dobsonville mall taxi rank]*. URL: https://www.google.com/maps. (accessed: 20.08.2023) (cit. on p. 145).

[282] B. Bekker. "Irradiation and PV array energy output, cost, and optimal positioning estimation for South Africa". In: *Journal of Energy in Southern Africa* 18.2 (2007), pp. 16–25 (cit. on p. 144).

[283] Eskom. 2023. URL: https://docs.google.com/spreadsheets/d/1ZpX_twP8sFBOAU6t--Vvh1pWMYSvs60UXINuD5n-K08/edit#gid=863218371 (cit. on pp. 146, 147, 149, 183, 184).

[284] *Bleak outlook for load shedding in South Africa*. Business Tech, Nov. 2023. URL: https://businesstech.co.za/news/energy/731057/bleak-outlook-for-load-shedding-in-south-africa/ (cit. on p. 147).

[285] *Eskomw warns to expect an even darker 2024 after South Africa's worst year of load-shedding in 2023*. BizNews. URL: https://www.biznews.com/energy/2024/01/08/eskom-warns-darker-2024-after-worst-year-2023#:~:text=Compared%20to%20the%20previous%20year,outlook%20for%202024%20appears%20grim.. (accessed: 25.01.2023) (cit. on p. 147).

[286] W. Kelly. *Load shedding is not forever*. Daily Maverick, Sept. 2023. URL: https://www.dailymaverick.co.za/article/2023-08-17-loadshedding-is-not-forever/ (cit. on p. 147).

[287] *Massive shift for load shedding in South Africa*. Business Tech, Dec. 2023. URL: https://businesstech.co.za/news/business-opinion/735779/massive-shift-for-load-shedding-in-south-africa/ (cit. on p. 147).

[288] C. Naidoo. "The Impact of Load Shedding on the South Africa Economy". In: *Journal of Public Administration* 58.1 (2023), pp. 7–16 (cit. on p. 147).

[289] Eskom. *Weekly unplanned outages*. Eskom. URL: https://www.eskom.co.za/dataportal/outage-performance/weekly-unplanned-outages/. (accessed: 25.01.2023) (cit. on p. 149).

[290] S. W. Coast. *Solar Panels in South Africa*. 2020. URL: https://solarwc.co.za/product/solar-panels/#:~:text=Prices%20range%20between%20R1800%20for,%2C000%20to%20R110%2C000. (cit. on p. 154).

[291] S. Hasan et al. "Techno-economic feasibility analysis of an electric vehicle charging station for an International Airport in Chattogram, Bangladesh". In: *Energy Conversion and Management* 293 (2023), p. 117501 (cit. on p. 154).

[292] M. Maas. *Zimi - Empower your electric fleet*. 2023. URL: http://www.zimicharge.com (cit. on p. 154).

[293] X. Han et al. "A review on the key issues of the lithium ion battery degradation among the whole life cycle". In: *ETransportation* 1 (2019), p. 100005 (cit. on p. 154).

[294] P. Ralon et al. “Electricity storage and renewables: Costs and markets to 2030”. In: *International Renewable Energy Agency: Abu Dhabi, United Arab Emirates* 164 (2017) (cit. on p. 154).

[295] Business Tech. *Your guide to solar financing*. 2023. URL: `https://businesstech.co.za/news/industry-news/676865/your-guide-to-solar-financing/` (cit. on p. 154).

[296] Toyota. *Toyota Quantum 2.7 14-seater bus*. 2023. URL: `https://www.cardealer.co.za/new-cars/Toyota/Quantum/Quantum-2-7-14-seater-bus/2010-2014/r198613` (cit. on p. 154).

[297] Eskom. *Interpreting Eskom load-shedding stages*. URL: `https://loadshedding.eskom.co.za/LoadShedding/ScheduleInterpretation#:~:text=Stage%201%20allows%20for%20up,national%20load%20to%20be%20shed.` (cit. on p. 183).